Universitat Ramon Llull

C.I.F. G: 59069740 Universitat Ramon Lull Fundació Privada. Rgtre. Fund. Generalitat de Catalunya núm. 472 (28-02-90)

DOCTORAL THESIS

Title	Development of 3D cancer models to obtain mechanistic insights into disease progression
Presented by	Mireia Alemany Ribes
Centre	IQS School of Engineering
Department	Bioengineering
Directed by	Dr. Carlos E. Semino

C. Claravall, 1-3
08022 Barcelona
Tel. 936 022 200
Fax 936 022 249
E-mail: urlsc@sec.url.es
www.url.es

A la meva família

“The important thing is not to stop questioning”

“L’important és no deixar de fer-se preguntes”

Albert Einstein (1879-1955)

ACKNOWLEDGEMENTS

En primer lloc, m'agradaria agrair al Dr. Carlos Semino l'oportunitat de realitzar la tesis doctoral al laboratori d'Enginyeria de Teixits. *Carlos me has transmitido la pasión por el mundo de la biología celular y la medicina regenerativa. Me has dado la confianza y libertad para ir aprendiendo a llevar un proyecto de investigación. Me has animado para superar las etapas sin resultados, repensando los objetivos y experimentos. Has compartido conmigo muchas ideas locas e inspiradoras. Muchas gracias por todo!*

I am very grateful to Dr. Bianca M. Bussmann from Translationzentrum für Regenerative Medizin in Leipzig. During my stage, you taught me several techniques in cellular and molecular biology. You transmitted me you german touch, being very strict in the laboratory and critic when analyzing the obtained results. Moltíssimes gràcies a la Dra. Maria Pilar Armengol i al Dr. Marco Antonio Fernández, responsables dels serveis de genòmica i citometria de flux de l'IGTP de l'Hospital Germans Tries i Pujol a Badalona. Sempre que he vingut a utilitzar els equips heu tingut molta paciència ajudant-me i responent-me tots els dubtes. Al món de la ciència li falta gent com vosaltres: generosos, propers, amb ganes d'ensenyar tot el que sabeu i sempre posant facilitats. De veritat que ha sigut un plaer treballar amb vosaltres i teniu tot el laboratori d'Enginyeria de Teixits igual d'encantat! A la Dra. Marta Vives de l'IGTP per proporcionar-nos mostres de teixit pancreàtic. *Agradecer al Dr. Jesús Otero del Hospital Universitario de Asturias por darnos los fibroblastos humanos. Al Dr. Ángel Raya del Instituto de Bioingeniería de Catalunya por darnos los fibroblastos marcados fluorescentemente con GFP. A Ana Sancho y Elena de Juan Pardo del CEIT y TECNUN en la Universidad de Navarra por el análisis de FEG-SEM.* Al Dr. Salvador Borrós i la Dr. Núria Agulló del laboratori de Materials de l'IQS per deixar-nos utilitzar els equips de reometria i ajudar-nos a trobar el millor protocol per mesurar les nostres mostres. M'agradaria donar-li les gràcies al Salvador per tota la confiança que m'ha donat durant tots aquests anys a l'IQS. Al Dr. Iñaki Borrell del laboratori de Síntesis de l'IQS per sintetitzar els inhibidors de tirosina quinases. Al Dr. Santi Nonell del laboratori de Fotoquímica de l'IQS i la Dra. Ángeles Villanueva de la Universitat Autònoma de Madrid per la col·laboració amb els experiments sobre teràpia fotodinàmica. Aquesta etapa l'he compartit amb la María García, la Pilar Acedo i l'Ester Boix, que m'han ensenyat moltes tècniques de fotoquímica i s'han convertit en bones amigues.

La millor etapa del doctorat ha sigut quan l'he compartit amb la Caterina, l'Alex i el Javi. Aquesta tesis us pertany també a vosaltres! M'heu ensenyat moltíssim: totes les vostres ganes d'aprendre han suposat una gran motivació per mi, tots els dubtes que no sabia resoldre han sigut reptes i totes les vostres idees han ajudat a millorar el projecte. El treball en equip és sempre millor.

Aquests anys han sigut molt feliços gràcies a tots els amics que he conegut al laboratori i m'emporto per sempre. Sento una gran melancolia per haver de posar punt i final a aquesta etapa i si pogués l'allargaria. Són moltes les aventures viscudes fins ara i espero que no s'acabin: innumerables viatges (des de Bor fins a Riba-roja d'Ebre, passant per Madrid, Villaoscura, Sant Carles de la Ràpita, etc.), *destructions parties*, carnavals *biofrikis* i un llarg etcètera. En primer lloc, m'agradaria donar les gràcies al laboratori d'Enginyeria de Teixits. Els començaments amb la Cris, la Tere, la Vero i la Núria van ser un aprenentatge constant. Amb elles vaig descobrir la passió pel món de la investigació. Núria quanta paciència vas haver de tenir durant el nostre primer any! Però en cap moment vas perdre el somriure i les ganes d'ensenyar. Cris, Tere i Vero vam començar aquesta aventura juntes i us asseguro que no hi havia tres millors doctorasses per compartir camí. Cris hem fet la carrera, el màster i el doctorat juntes, fins i tot hem viscut 6 anys juntes, així que enyoraré molt no veure't cada dia. *Tere me encanta tu exigencia y meticulosidad a la hora de trabajar junto con tus ganas de orchatitas y afters, es una combinación perfecta*. *Te tendremos que venir a visitar a Tui.* Vero encara enyoro les teves bromes i la teva energia al laboratori, Califòrnia queda massa lluny! Després van arribar la Lourdes, la Caterina, la Patri, l'Àlex i el Javi i amb tots ells un laboratori cada cop més organitzat i professional. Lourdes t'asseguro que tens màgia, em fas riure tant que el Robert es pensa que ens passem el dia borratxes, però també em reconfortes tant que els teus consells i ànims s'han convertit en una necessitat per mi. Cate quantes confidències i filosofades entre robots i *Real Times*, a partir d'ara espero que només siguin entre cerveses i riures. Patri m'has demostrat que el camí no és sempre fàcil, però que val la pena perseverar fins aconseguir el que vols, ets una gran lluitadora. *Álex sacaste mi lado más bromista y desenfadado que tenía un poco olvidado y me encantó ver tu lado más profesional y serio, apasionándote con el proyecto y llevando la iniciativa. Fue un año increíble y te aseguro que se te echa muchísimo de menos en el laboratorio…nos falta un menudo. Javi tus ideas me han ayudado a avanzar con el proyecto, gracias por todas las correcciones.* I el laboratori continua creixent: Anna, Òscar, Juli, Ana i Silvia. M'ha encantat poder coincidir amb vosaltres durant aquesta etapa de redacció. Anna queda pendent anar a algun festivalet!

No m'imagino el laboratori d'Enginyeria de Teixits sense el laboratori de Materials. Tots junts formem un gran equip! Pere hem desenvolupat un llenguatge propi, una barreja entre lleidatà i gallec que només nosaltres entenem. Tu sempre tan *agusto* y *cogiéndotelo todo con calma*, que *dejadita* em quedaré sense tu...tot i que jo crec que després de tants moments compartits no ens fan falta paraules per comunicar-nos. *Leti nos hemos ganado a pulso el nombre de Zipi y Zape y espero que así continúe siempre, yo vendré en auto donde haga falta…pero no te vayas muy lejos Carballito! Sejin me encanta tu espontaneidad y simpatía, eres un ángel! Ya sabes que siempre puedes contar conmigo.* Pam com s'enyoren les festes i els caps de setmana amb tu, gaudeix d'aquesta nova aventura americana. *Nathaly quedan pendientes muchas meriendas, gimnasios y sobretodo el viaje a Ecuador.* Pau poses la melodia del laboratori. Estela sempre tens un somriure per tothom, així que és genial veure't. *Djamila transmites dulzura y paz, me ha encantado coincidir contigo*. Joan quins formats més macos te aquesta tesis gràcies a tu. Els nous fitxatges de materials continuen el bon nivell o fins i tot el

milloren;) Sara, Robert, Gemma, Cris, Mariana, Ingrid….quin bon grup que feu, segur que ens anirem veient. Finalment, gràcies al Pol, al Miquel i al Miguel per uns dinars memorables i unes tardes/nits de divendres apoteòsiques. Us asseguro a tots que encara no m'imagino arribar a un lloc on no hi hagi totes les vostres bromes i confidències. Gràcies per tots aquests anys, us trobaré moltíssim a faltar!

Durant aquesta etapa també m'han acompanyat tots els amics de Tàrrega i Barcelona. Victoria, Mireia i Albert, moltes gràcies per les incursions muntanyenques que sempre em fan oblidar tots els problemes. Al Fredy, Moles, Ignasi, Rubén, Elias, Victor i un llarg etcètera gràcies per la diversió desenfrenada per Barcelona. A l'Alex que sempre està al meu costat i em dóna els millors consells, sento una connexió brutal amb tu, deu ser l'efecte de les terres de Ponent. A la Jordina i l'Eli perquè ens coneixem des de petites i sou els meus pilars en un món que constantment està canviant. Jordina no podia faltar el teu toc artístic en aquesta tesis, quines cèl·lules tan precioses que m'has dibuixat. A l'Edu perquè m'has fet creure en mi i m'has donat l'autoestima i energia necessàries per tirar endavant aquest doctorat. *Només s'hi veu bé amb el cor, l'essencial és invisible als ulls*: aquesta frase del Petit Príncep m'ha acompanyat durant els últims 8 anys, moltíssimes gràcies per tot.

A la meva família, que m'ho ha donat tot. Tant els meus avis com els meus pares són un model per mi: la seva bondat, humilitat i generositat són infinites. Admiro el sacrifici que heu fet perquè les tres germanes poguéssim estudiar, la fe cega que heu tingut quan les coses no han sortit com esperàvem i els ànims que ens heu donat perquè ens seguíssim superant a nosaltres mateixes sense tenir por a res i sense autoimposar-nos límits. A les meves germanes Ingrid i Alba, que les necessito al meu costat. Sou el meu gran tresor, sempre tant rialleres i optimistes. M'ajudeu a relativitzar els problemes i concentrar-me en els petits plaers d'aquesta vida. Amb tots vosaltres sento casa. Us dedico aquesta tesis doctoral.

Mireia
22 d'agost del 2014

This thesis has been possible thanks to a predoctoral FI fellowship (2012 FI_B2 00151) from DURSI (Generalitat de Catalunya), as well as to IQS School of Engineering.

SUMMARY

Cancer is a dynamic disease in which cells proliferate, differentiate and migrate by accessing to reminiscent genetic and epigenetic programs of embryogenesis. This process is driven by the crosstalk between cancer cells and tumor microenvironment, which comprises a three-dimensional (3D) extracellular matrix (ECM) together with stromal cells (fibroblasts, cells from vasculature system and cells from immune system). Effector biomolecules and enzymes (e.g. cytokines, growth factors and proteases) are continuously secreted by cancer and stroma cells, influencing phenotypically each other and modifying the structure and composition of ECM. These environmental changes lead to cell plasticity and heterogeneity during cancer. In tissue engineering field, researchers try to deconstruct this complex tumor microenvironment into simpler and predictable 3D cell models in order to analyze the role of specific chemical, mechanical and/or physical signals in disease progression.

The most critical tumor stage is local invasion and metastasis, which accounts for approximately 90% of all cancer deaths. In the present thesis, 3D cell models were developed to recapitulate the transition from a 2D to a 3D milieu that cancer cells experience when they escape from epithelial layer and invade mesenchymal connective tissue. Experiments revealed that 3D cultures compromised epithelial organization, inducing different mesenchymal-like phenotypes depending on composition and stiffness of scaffold. Therefore, cells showed the capacity to adapt to changing microenvironmental conditions. Moreover, 3D cultures induced E-cadherin downregulation, suggesting the disruption of epithelial cell-cell adhesions and the activation of early stages of epithelial to mesenchymal transition. Its expression pattern was influenced by the presence and concentration of ECM binding motifs. E-cadherin regulatory mechanisms were characterized at epigenetic and transcriptional level.

3D cell models can also help in the discovery and therapeutic assessment of cancer medicines. Part of this thesis work was focused on photodynamic therapy research. 3D cultures emerged as powerful platforms for photosensitizers screening processes since they could recreate molecular gradients for drug and oxygen. These conditions induced the development of a protective microenvironment for cells located in the core of the culture, accounting for the low therapeutic efficacy found in clinical practice. In a different part of the thesis, cancer drugs targeting receptor tyrosine kinases activity were studied. Results evidenced that cells developed different survival strategies to evade or escape from drugs action depending on the composition of scaffold. We hypothesized that ECM could provide cells with access to a large and redundant spectrum of signaling pathways, complementing the activity of the blocked cellular receptors. Therefore, cancer cells presented an adaptive behavior supported by the dynamic and complex tumor microenvironment. These findings reinforced the necessity to develop 3D cultures to study cell resistance mechanisms.

RESUMEN

El cáncer es una enfermedad dinámica en la cual las células proliferan, se diferencian y migran accediendo a programas genéticos y epigenéticos reminiscentes de la embriogénesis. Este proceso está dirigido por la comunicación bidireccional entre las células cancerígenas y el microambiente tumoral que está formado por una matriz extracelular (ECM) tridimensional (3D) y células del estroma (fibroblastos, células del sistema inmune y células del sistema vascular). Muchas biomoléculas y enzimas (ej. citoquinas, factores de crecimiento y proteasas) son continuamente secretadas por las células cancerígenas y del estroma, influenciando fenotípicamente ambos tipos celulares y modificando la estructura y composición de la ECM. Esta serie de cambios ambientales provocan plasticidad y heterogeneidad celular durante el cáncer. En el campo de la ingeniería de tejidos, los investigadores intentan deconstruir el complejo microambiente tumoral en modelos celulares 3D más simples y predictivos con el objetivo de analizar el papel específico de señales químicas, mecánicas y/o físicas en la progresión de la enfermedad.

La etapa más crítica del cáncer es la invasión y metástasis, la cual provoca aproximadamente el 90% de muertes. Durante la presente tesis, se desarrollaron modelos 3D para recapitular la transición del microambiente 2D al 3D que experimentan las células cancerígenas cuando se escapan de la monocapa epitelial e invaden el tejido conectivo mesenquimal. Los experimentos demostraron que los cultivos 3D eran capaces de romper la organización epitelial, induciendo diferentes fenotipos tipo-mesenquimales dependiendo de la composición y rigidez de la matriz. Por lo tanto, las células mostraban capacidad para adaptarse a entornos cambiantes. Además, los cultivos 3D provocaban la disminución de la expresión de la E-cadherina, sugiriendo la disociación de las adhesiones epiteliales célula-célula y la activación de los primeros estadios de la transición epitelial-mesenquimal. Este patrón de expresión estaba influenciado por la presencia y concentración de motivos de unión de la ECM. Los mecanismos de regulación de E-cadherina se caracterizaron a nivel epigenético y transcripcional.

Los cultivos 3D también pueden contribuir al descubrimiento y evaluación terapéutica de nuevos tratamientos contra el cáncer. Parte de esta tesis se focalizó en investigar la terapia fotodinámica. Los cultivos 3D emergieron como valiosas plataformas en procesos de cribado de fotosensibilizadores ya que pudieron recrear los gradientes moleculares de fármaco y oxígeno. Estas condiciones crearon un microambiente protector para las células localizadas en la parte interior del cultivo, causando una baja eficacia terapéutica y, por lo tanto, mimetizando las limitaciones actuales de la práctica clínica. En otra parte de la tesis, se estudió la actividad de fármacos anticancerígenos dirigidos a inhibir receptores de tirosina quinasas. Los resultados evidenciaron que las células desarrollaron distintas estrategias de supervivencia para escaparse o evadir el efecto de los fármacos dependiendo de la composición de la matriz. Se formuló la hipótesis que la ECM podía proporcionar a las células acceso a una gran y redundante red de cascadas de señalización que complementaban la actividad de los receptores bloqueados. Por lo tanto, las células cancerígenas presentaron un comportamiento adaptativo sostenido gracias al dinámico y complejo microambiente tumoral. Estos descubrimientos reforzaban la necesidad de desarrollar cultivos 3D para estudiar los mecanismos de resistencia a los fármacos.

RESUM

El càncer és una malaltia dinàmica durant la qual les cèl·lules proliferen, es diferencien i migren accedint a programes genètics i epigenètics reminiscents de l'embriogènesis. Aquest procés està dirigit per la comunicació bidireccional entre les cèl·lules cancerígenes i el microambient tumoral que està format per una matriu extracel·lular (ECM) tridimensional (3D) i cèl·lules de l'estroma (fibroblasts, cèl·lules del sistema immune i cèl·lules del sistema vascular). Moltes biomolècules i enzims (p. ex. citoquines, factors de creixement i proteases) són contínuament secretats per les cèl·lules cancerígenes i de l'estroma, influenciant fenotípicament ambdós tipus cel·lulars i modificant l'estructura i composició de l'ECM. Aquests canvis ambientals provoquen plasticitat i heterogeneïtat cel·lular durant el càncer. En el camp d'enginyeria de teixits, els investigadors intenten deconstruir el microambient tumoral en models cel·lulars 3D més simples i predictius que permetin analitzar el paper de senyals químics, mecànics i/o físics en la progressió de la malaltia.

L'etapa més crítica del càncer és la invasió i metàstasis, la qual provoca aproximadament el 90% de morts. Durant la present tesis, es van desenvolupar models 3D per recapitular la transició del microambient 2D al 3D que experimenten les cèl·lules cancerígenes quan s'escapen de la monocapa epitelial i envaeixen el teixit connectiu mesenquimal. Els experiments van demostrar que els cultius 3D van ser capaços de trencar l'organització epitelial, induint diferents fenotips tipus-mesenquimal dependent de la composició i rigidesa de la matriu. Per tant, les cèl·lules mostraven capacitat per adaptar-se a entorns canviants. A més, els cultius 3D provocaven la disminució de l'expressió de l'E-cadherina, suggerint la dissociació de les adhesions epitelials cèl·lula-cèl·lula i la conseqüent activació dels primers estadis de la transició epitelial-mesenquimal. Aquest patró d'expressió estava molt influenciat per la presència i concentració dels motius d'unió de la ECM. Els mecanismes de regulació d'E-cadherina es van caracteritzar a nivell epigenètic i transcripcional.

Els cultius 3D també poden contribuir al descobriment i avaluació terapèutica de nous tractaments contra el càncer. Part d'aquesta tesis es va focalitzar en investigar la teràpia fotodinàmica. Els cultius 3D van emergir com valuoses plataformes per processos de cribratge de fotosensibilitzadors ja que van aconseguir recrear els gradients moleculars de fàrmac i oxigen. Aquestes condicions van crear un microambient protector per les cèl·lules localitzades en la part interior del cultiu, causant una baixa eficàcia terapèutica i, per tant, mimetitzant les limitacions actuals de la pràctica clínica. En una altra part de la tesis, es va estudiar l'activitat de fàrmacs anti-cancerígens dirigits a inhibir receptors de tirosina quinases. Els resultats van evidenciar que les cèl·lules desenvolupaven diferents estratègies de supervivència per escapar-se o evadir de l'efecte d'aquests fàrmacs depenent de la composició de la matriu. Es va formular la hipòtesis que la ECM podia proporcionar a les cèl·lules accés a una gran i redundant xarxa de cascades de senyalització que complementaven l'activitat dels receptors bloquejats. Per tant, les cèl·lules cancerígenes presentaven un comportament adaptatiu sostingut gràcies al dinàmic i complex microambient tumoral. Aquesta sèrie de descobriments reforçava la necessitat de desenvolupar cultius 3D per estudiar els mecanismes de resistència dels fàrmacs.

LIST OF CONTENTS

LIST OF FIGURES

LIST OF TABLES

LIST OF ABBREVIATIONS

2D Two-dimensional
3D Three-dimensional
$^1O_2$ Singlet oxygen
ABC ATP-binding cassette
AMF Autocrine mobility factor
ATCC American type culture collection
ATP Adenosine triphosphate
BCA Bicinchoninic acid
bHLH Basic helix-loop-helix
BM Basement membrane
BMP Bone morphogenetic protein
BSA Bovine serum albumin
CA Co-activator protein
CAFs Cancer-associated fibroblasts
Calcein AM Calcein acetoxymethyl
cDNA Complementary DNA
CMT Center for molecular therapeutics
CO_2 Carbon dioxide
COX cyclooxygenase
CSC Cancer stem cells
DAPI 4',6-diamidino-2-phenylindole
DAMP damage-associated molecular pattern
DC Dendritic cells
DMA Dynamic mechanical assay
DMEM Dulbecco's modified Eagle medium
DMSO Dimethyl sulfoxide
DNA Deoxyribonucleic acid
DN-LPR5 Dominant negative low-density lipoprotein receptor-related protein
DNMT DNA methyltransferase
dNTP Deoxynucleoside triphosphate
DR Desmoplastic reaction
E-cadherin Epithelial-cadherin
ECM Extracellular matrix
EGF Epithelial growth factor
EGFR EGF receptor
EMT Epithelial to mesenchymal transition
EtBr Ethidium bromide
FA Focal adhesion
FAK FA kinase
FBS Fetal bovine serum
FEG-SEM Field emission gun–scanning electron microscopy
FGF Fibroblast growth factor
FGFR Fibroblast growth factor receptor
FITC Fluorescein isothiocyanate
FSH Follicle stimulating hormone
GAG Glycosaminoglycans
GFP Green fluorescent protein
HA Hydroxyapatite

HAT Histone acetyltransferase
HDAC Histone deacetylases
HeLa Human cervical adenocarcinoma
HER human epidermal growth factor receptor
HFF Human foreskin fibroblasts
HGF Hepatocyte growth factor
HMG High mobility group
hNDF Human normal dermal fibroblasts
HRP Horseradish peroxidase
IGF Insulin-like growth factor
IGFR IGF receptor
mAb monoclonal antibody
MAPK Mitogen-activated protein kinase
MBP methyl-CpG-binding protein
MET mesenchymal to epithelial transition
MMP Metalloproteinases
MTA Metastasis-associated gene
MTT 3-[4,5-dimethylthiazol-2-yl]-2,5- diphenyl tetrazolium bromide
NCBI National center for biotechnology information
NCI National cancer institute
NFκB Nuclear factor κB
NRTK Non-receptor tyrosine kinase
OOPS 1,2-dioleoyl-*sn*-glycer-3-[phosphor-*L*-serine]
PAGE Polyacrylamide gel
PANC-1 Pancreatic ductal adenocarcinoma cells
PBS phosphate buffered saline
PCR Polymerase chain reaction
PDAC Pancreatic ductal adenocarcinoma
PDGF Platelet derived growth factor
PDT Photodynamic therapy
PEG Polyethylene glycol
PFA *p*-formaldehyde
PGI Phosphoglucose isomerase
Phalloidin Phalloidin-tetramethylrhodamine B isothiocyanate
PKA Protein kinase A
PLA Polylactid acid
PLG Poly(lactide-co-glycolide)
PLGA Poly(lactide-co-glycolacid)
POPC 1-palmitoyl-2-oleoyl-*sn*-glycero-3-phosphocoline
PS Photosensitizer
RGD Arginine-glycine-aspartate
RIPA Radioimmunoprecipitation assay
RNA Ribonucleic acid
ROCK Rho-associated coiled-coil containing protein kinase
ROS Reactive oxygen species
RPL27 Ribosomal protein 27L
RTK Receptor tyrosine kinase
RT-PCR Reverse-transcriptase polymerase chain reaction
SAM S-adenosyl-l-methionine
SC Stem cells
SDS Sodium dodecyl sulphate
sFRP secreted frizzled-related protein
SNP Single nucleotide polymorphism

TE Tissue engineering
TF Transcription factor
TGF Transforming growth factor
TK Tyrosine kinase
TKI TK inhibitor
TMPyP 5,10,15,20-tetrakis(N-methyl-4-pyridyl)-21H,23H-porphine
TRITC Tetramethylrhodamine B isothiocyanate
TSS Transcription start site
VEGF Vascular endothelial growth factor
VEGFR VEGF receptor
X-gal 5-bromo-4-chloro-3-indolyl-β-D-galactopyranoside
ZEB Zinc finger E-box-binding homeobox
ZnPc Zinc(II)-phthalocyanine

Chapter 1

Introduction to 3D cancer models

1.1 BACKGROUND

1.1.1 HALLMARKS OF CANCER

Cancer is a major devastating disease, being a public health problem that involves more than 14 million of new cases[1] and 8 million of deaths[2] per year worldwide. Cancer is a multistep process characterized by a sustained proliferative signaling, growth suppressors evasion, cell death resistance, immortal replication, angiogenesis induction and invasion and metastasis activation. Therefore, the hallmarks of cancer comprise a minimum of six biological capabilities, which organize and rationalize disease complexity[3].

From the 1990s, pioneering experiments have revealed that the biology of cancer cannot be understood by simply enumerating the genetic alterations accumulated in cells. Instead, it must encompass the evolving crosstalk with the microenvironment[4,5], which is the compartment that provides the connective tissue framework. Tumor microenvironment comprises the extracellular matrix (ECM), an intricate network of fibrous proteins (e.g. collagen, elastin, laminin and fibronectin) and proteoglycans (e.g. hyaluronic acid and heparin sulphate). It also contains a wide variety of non-epithelial cells including fibroblasts, cells from inflammatory system (lymphocytes, macrophages and mast cells) and cells from vasculature system (endothelial cells, pericytes and smooth muscle cells), which are known as stromal cells[6]. This complex milieu provides multiple signaling to cancer cells (**Figure 1.1**), being classified as chemical, mechanical and physical cues[7,8]. Some relevant examples are cited:

1. Chemical cues: recognition and binding of growth factors, cytokines, proteases, ECM adhesion motifs, etc.

2. Mechanical cues: crosslinking and remodeling of the ECM that modifies its stiffness value and cell cytoskeleton dynamics.

3. Physical cues: three-dimensionality experienced by cells, establishment of molecular gradients that cause hypoxia and necrosis within the core of the tumor.

Cancer cells respond to these chemical, mechanical and physical stimuli by activating a series of epigenetic and transcriptional events that change their phenotype. In parallel, they reorganize the structure and composition of the ECM and release diffusible molecules, establishing a bidirectional communication network with the microenvironment[5]. Indeed, experimental evidence has demonstrated that the reintroduction of a normal physiological stroma context can phenotypically revert tumors *in vitro*[9,10]. Therefore, microenvironment steers plasticity to cancer cells.

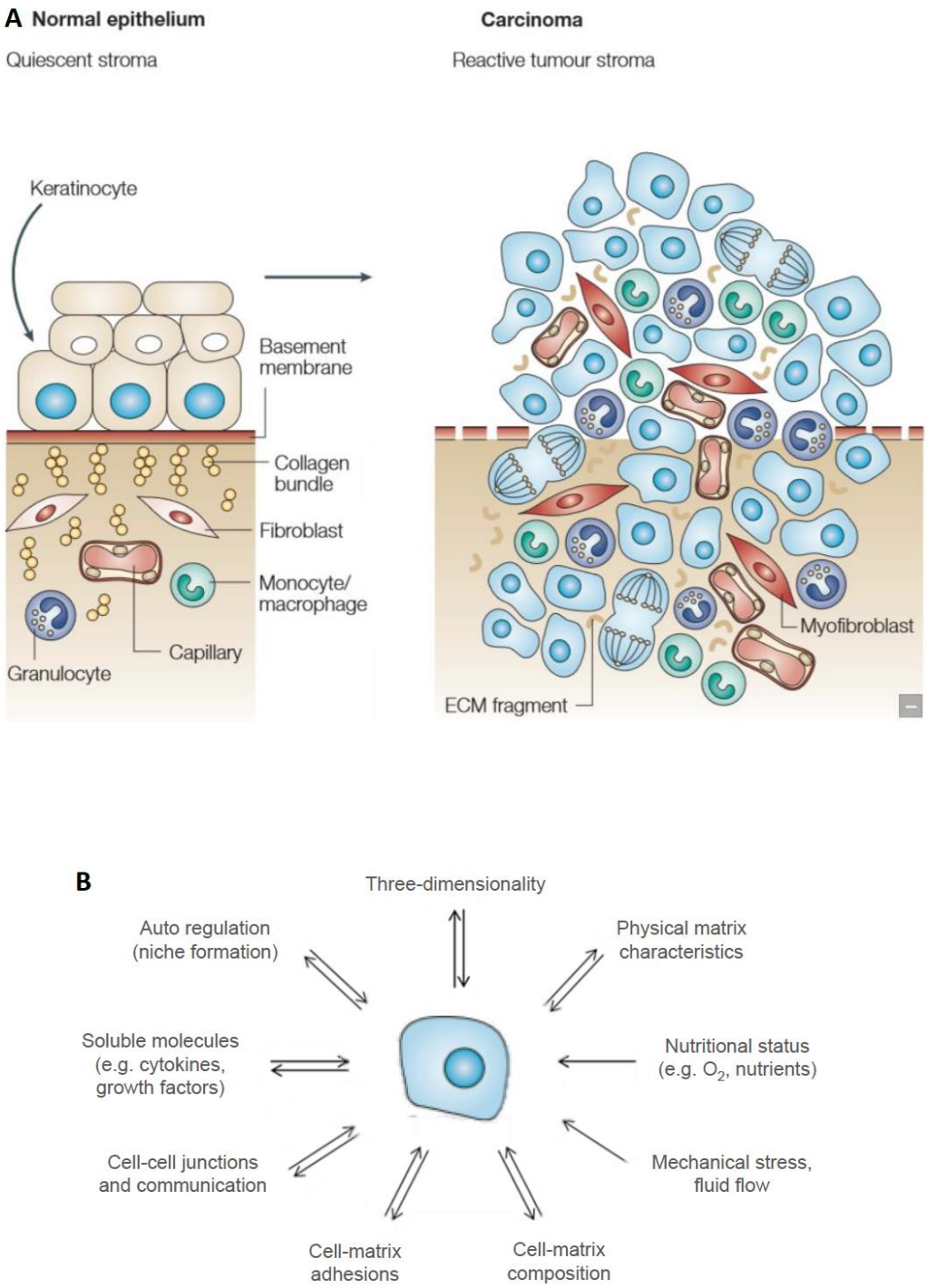

Figure 1.1. Microenvironment contributes to tumor progression. (A) In a normal stage, a well-differentiated stratified epithelium is separated by a basement membrane from the stromal compartment. During transition to a tumor stage, epithelium becomes hyperplastic (abnormal proliferation) and disrupts basement membrane. Then, cancer cells produce a wide range of proteases and growth factors that modify their surrounding milieu. Consequently, the number of inflammatory cells increases. Moreover, fibroblasts differentiate into myofibroblasts, resulting in the expression of specific pro-migratory ECM components and the secretion of additional proteases and growth factors to amplify signaling in the proliferative and invasive cascade. **(B)** At the molecular level, multiple physical, mechanical and chemical factors of the microenvironment modulate cell biology. Cells, in turn, modify their local milieu to form a permissive and supportive framework for disease progression, enabling processes such as angiogenesis, invasion and metastasis. Therefore, there is a bidirectional communication between cells and microenvironment. Adapted from Mueller *et al*.[5] and Yamada *et al*.[7]

1.1.2 CANCER CELL MODELS

The development of *in vitro* cell models is essential for understanding cancer biology. Their main function consists in deconstructing the tumor in simpler and more predictive systems in order to identify both intrinsic genomic signature and extrinsic chemical, mechanical and/or physical factors that drive human pathophysiology.

Following this paradigm, cancer research has traditionally relied on two-dimensional (2D) cultures, also known as monolayer[11]. They are based on growing cells on rigid and flat substrates (e.g. Petri dishes and culture flasks). 2D cultures have provided valuable information concerning the identification of many oncogenes and tumor-suppressor genes, being genome-centered models[5]. However, it is commonly accepted that cells are cultured in physiologically constrained conditions on these substrates.

Cells are attached to substrates that force them to polarize and increase their exchange area to the culture media. As a result, they are exposed to an excessive nutrition and oxygenation and molecular gradients cannot be reproduced. Furthermore, production of ECM proteins is strongly modified –in composition, configuration and amount- due to differences in the surface receptors orientation and clustering, preventing cells from receiving the proper signals that arise from the ECM[8]. Specifically in the field of cancer, poorly adherent cells (metastatic cells) cannot form tight focal adhesions to plastic and, therefore, cannot be cultured properly in monolayer. Thus, the most aggressive cells are excluded from classical molecular characterization and drug screening processes[12]. 2D cultures also activate an immortalization process through multiple passages, which result in the selection of cancer cells that rapidly proliferate. These cells misrepresent the whole tumor, since they are specifically susceptible to therapies that target rapidly dividing cells[13].

To avoid these experimental inconsistencies, *in vitro* cell models should integrate some microenvironmental cues while retaining the reproducibility and the capacity of cellular level imaging. A basic premise is the introduction of the third dimension for cell and ECM communication network, which dramatically affects integrin recognition, cell contraction and associated intracellular signaling (**Figure 1.2**). These three-dimensional (3D) cultures can bridge the gap between simplistic 2D cultures and extremely complex animal models[14].

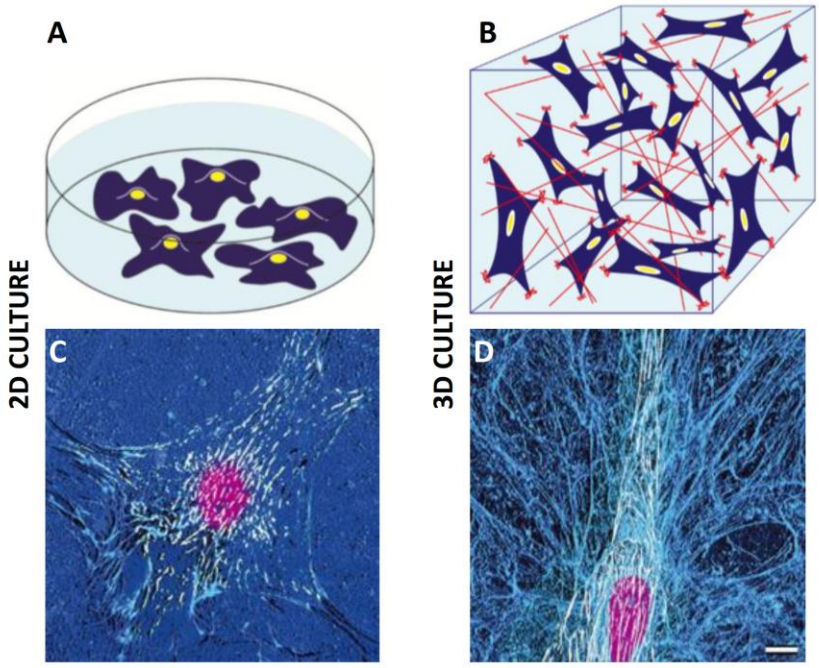

Figure 1.2. Cell morphology in 2D versus 3D microenvironments. (A) Cells expanded in 2D cultures are unnaturally polarized and they only establish partial contact with the adjacent cells and ECM. **(B)** When grown in 3D cultures, cells regain the 3D communication network that arises from cell-cell and cell-ECM interactions. Hence, they receive multiple environmental cues (mechanical, chemical and physical cues) that directly influence cellular identity and function. An example is illustrated by fibroblasts cultured on planar fibronectin, 2D **(C)** or in a mesenchymal cell-derived matrix, 3D **(D)**. The differences in overall cellular architecture are evidenced through the staining of fibronectin matrix (blue), α integrin-positive adhesion structures (white) and nuclei (magenta). In 2D cultures, fibroblasts adopt a spread-out and flat morphology, whereas in 3D they have a stellate morphology that resembles *in vivo* pattern. Scale bar of 10 µm. Adapted from Yamada et al.[7]

Knowledge from cell biology, materials science and bioengineering need to converge in order to successfully breakthrough in the development of 3D cultures. The integration of these disciplines resulted in the creation of tissue engineering (TE) field[15]. The main goal of TE is to give a comprehensive insight into the natural environment of cells and design a set of biomedical tools (e.g. biomaterials, biodevices and bioreactors) that could precisely reproduce it (biomimetics).

In cancer research, the first step in the application of biomimetic principles has been focused on the generation of multicellular spheroids. They re-establish tumour architecture pattern, particularly hollow cores that contain quiescent and hypoxic cells. Interestingly, experiments have demonstrated that they exhibit higher anticancer drug resistance as compared to conventional 2D cultures, better mimicking the *in vivo* situation[16]. However, these spheroids have important limitations, since they grow as independent cellular aggregates and show reduced interactions with an extracellular milieu[17].

Considering that microenvironment controls tumour progression, ECM analogues have been developed to embed cells in a 3D context and display some of the appropriate physical, chemical and mechanical cues. Pioneering work has been based on the use of biomaterials from

natural origin, principally collagen (main structural protein of the ECM) and Matrigel (reconstituted basement membrane (BM) isolated from Engelbreth–Holm–Swarm mouse sarcomas). In 1992, Mina J. Bissell group demonstrated that the phenotype of breast cancer cells was exclusively re-established in 3D cultures. This was the first demonstration of the ability of cancer cells to *in vitro* recapitulate the structural and functional differentiation characteristics of *in vivo* tumours[18]. In 1997, the same group reported the reversion of tumour phenotype after culturing cells in 3D cultures and treating them with integrin blocking antibodies. Results showed a significant role of integrins and, therefore, ECM receptors in directing polarity and cell phenotype[19] (**Figure 1.3**).

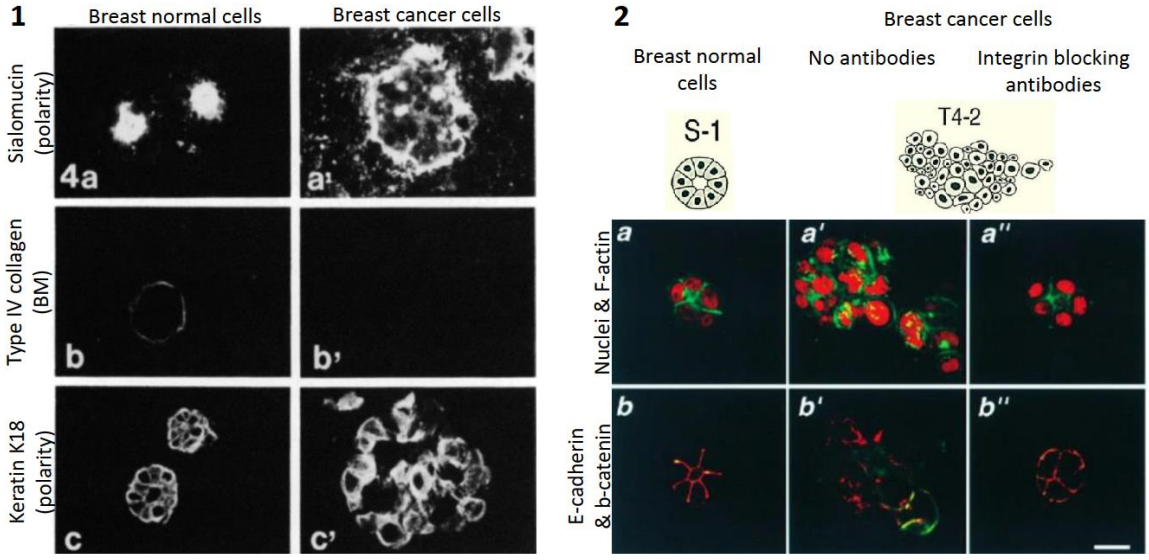

Figure 1.3. Tumor phenotype in 3D cultures. Tumour phenotype was exclusively re-established in 3D cultures. Immunofluorescence of normal breast acini **(1a-c)** and carcinoma colonies **(1a'-c')** in Matrigel scaffold. (1a) Apical accumulation of sialomucin in normal acini. (1a') Basal expression of sialomucin in carcinoma cultures. (1b) Type IV collagen staining around fully developed normal acini. (1b') No BM was present around carcinoma cells. (1c) Cortical accumulation of keratin K18 in normal acini. (1c') Cortical and apical accumulation of keratin k18 in carcinoma colonies. The coordinated loss of BM around cells and the lack of polarity are two distinguishable features of cancer cells as compared to normal cells. **(2)** β1-inhibitory antibody treatment of cancer cells leaded to reverted acini. **(2a–a'')** S-1 (2a) and T4- β1 reverted acini (2a'') showed basally localized nuclei (propidium iodide, red) and organized filamentous F-actin (FITC, green), while T4-2 colonies had pleomorphic nuclei and disorganized actin filaments (2a'). **(2b–b'')** In S-1 (2b) and T4- β1 reverted acini (2b''), E-cadherin (FITC, green) and β-catenins (Texas red) were co-localized at cell–cell junctions. Antibody-treated cancer cells showed the same morphology than normal cells, characterized by an organized cytoskeleton and co-localized cadherins and catenins expression at the cell-cell junctions. From Petersen *et al*[18] and Weaver *et al.*[19]

These experiments revealed that 3D cultures were capable of re-establishing the crosstalk between cancer cells and the surrounding stroma. However, this paradigm shift has been largely disregarded by both academia groups and pharmaceutical companies. Approximately 70-80% of cancer biologists still routinely use 2D cultures, which hamper the discovery and assessment of new therapeutic approaches[20].

1.1.3 TISSUE ENGINEERING IN CANCER RESEARCH

1.1.3.1 Scaffolds Design: Capturing Pathophysiology *in vitro*

The main challenge in TE is the design of biomaterials capable of recreating the *in vivo* microenvironment. Therefore, scaffolds are essentially inspired on the ECM in order to give to the cells the appropriate signals that guide their growth, proliferation, differentiation, invasion or apoptosis.

ECM is composed by two classes of macromolecules: fibrous proteins and proteoglycans. Fibrous proteins mainly comprise collagen, elastin, laminin and fibronectin. Collagen and elastin display a mechanical function by conferring strength and elasticity to the ECM respectively. Laminin and fibronectin act as adhesive molecules. They expose specific binding motifs that are recognized by other ECM macromolecules (collagen fibers and proteoglycans) and cellular adhesion receptors motifs (integrins-binding sequences). Therefore, they contribute to organize the matrix and mediate cellular attachment to it.

Secondly, proteoglycans consist of a protein core with covalently attached polysaccharide chains (glycosaminoglycans, GAGs), such as hyaluronic acid or heparin sulphate. The function of these macromolecules derives from the physicochemical characteristics of GAGs, which are characterized by a high density of negative charges that attract a cloud of cations (most notably Na^+) and cause a large amount of water stuck into the ECM. As a result, proteoglycans form a hydrated gel that exerts two functions. It provides swelling pressure to the tissue and enables it to withstand compressional forces. As a gel of variable pore size and charge density, it can regulate the traffic of soluble biomolecules and modulate the signaling activity[21].

Cells continuously sense and respond to extracellular signals through cell adhesion molecules (integrins, selectins, cadherins, immunoglobulin superfamily and proteoglycans). These motifs provide transient and stable communication channels among cell-cell and cell-ECM, creating a cytoplasmic and cytoskeletal-matrix fibers continuum respectively. Importantly, cells are responsible for secreting the whole range of proteins and polysaccharides that consecutively assemble into the organized ECM network. Cells also have the capacity to degrade the matrix by secreting proteolytic enzymes, which cause cell migration and tissue remodeling. Therefore, ECM emerges as a dynamic structure that has a unique composition in each tissue, working as a specific tissue signature to maintain the cellular identity and function.

ECM physical signaling

ECM is characterized by a highly porous nanostructure that provides anchorage to cells and controls diffusion of any soluble effector molecule. At microscopic level, a critical parameter during the design of TE scaffolds is their internal architecture, particularly pore size and interconnectivity. ECM has a pore size between 50 and 500 nm, 1,000 orders of magnitude

smaller than an average mammalian cell size (50-5,000 µm), which causes cells to sense a truly 3D milieu. In parallel, pores are flexible enough to ensure cell penetration, proliferation and migration through the formation of non-covalent interactions between matrix fibers[22]. At macroscopic level, tumors have a dense ECM and a poorly organized vasculature, which impose a physiological barrier for mass transport of oxygen, nutrients and waste products[23]. This inaccessibility cause hypoxia and quiescence in the cells buried within the core of the tumor. This characteristic can be *in vitro* reproduced through scaffold dimensions.

ECM chemical signaling

ECM exerts chemical signaling to cells through two mechanisms: (*i*) the binding of soluble signaling molecules and (*ii*) the exposure of ECM recognition sequences. First, ECM binds a wide variety of growth factors, cytokines and enzymes, modulating their diffusion and local concentrations. These soluble molecules can be secreted by the cell itself (autocrine signals), by other cells located in close vicinity (paracrine signals) or far apart, reaching the target through bloodstream network (endocrine signals). Regarding cancer biology, key soluble effector molecules have been identified. For instance, matrix-degrading enzymes cause the breakdown of the BM and the continuous remodeling of ECM components, especially members of the matrix metalloproteinase (MMP) family. The release of growth factors enhances vascular permeability and promotes new vessel formation. Moreover, they are able to induce inflammation and modify the repertoire of infiltrating T lymphocytes. Relevant examples are the vascular endothelial growth factor (VEGF), epithelial growth factor (EGF) and fibroblast growth factor (FGF)[21].

Secondly, ECM exposes specific adhesion receptors that are recognized by cellular adhesion proteins (integrins). As a result, ECM forms transient and stable interactions with cells, being dynamically integrated with their intracellular signaling pathways and participating in cell phenotype determination[24].

ECM mechanical signaling

ECM can have different composition, concentration and/or hierarchical organization of fibrous proteins and proteoglycans, resulting in different stiffness values. Cells sense these mechanical properties by continuously pushing and pulling on the ECM through cell-matrix adhesions (integrins). Cells respond to the resistance opposed by the microenvironment by balancing their internal tension, through Rho/ROCK (Rho-associated coiled-coil containing protein kinase) signaling pathway. In particular, Rho proteins modulate contraction of the actomyosin cytoskeleton and expression of ECM specific ligands. Therefore, mechanical signals from ECM alter cellular internal organization and ECM-cell interactions, inducing the activation or inhibition of genes involved in critical physiological processes as proliferation, migration and differentiation. This process of converting a mechanical stimulus in a cellular response is known as mechanotransduction[25,26] (**Figure 1.4**).

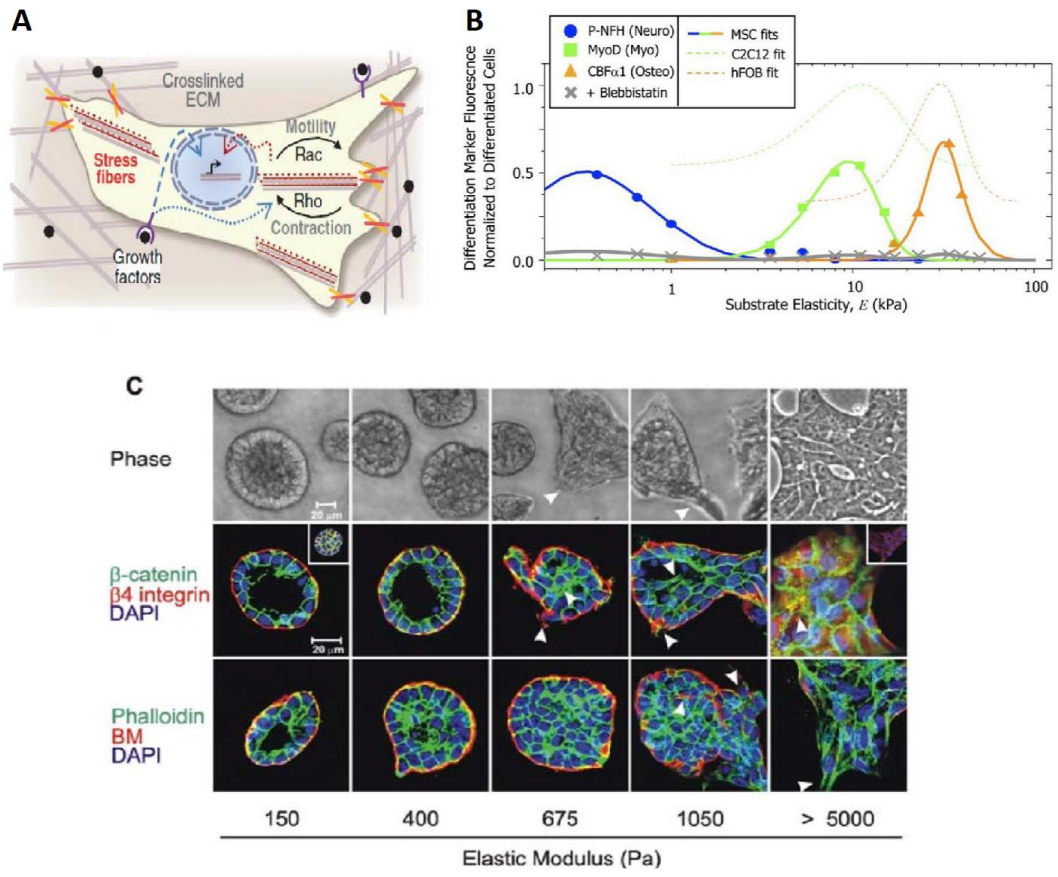

Figure 1.4. ECM mechanical signaling. ECM fibers composition, concentration and degree of crosslinking dictate matrix stiffness. This external resistance is balanced with the internal cellular tension by modulating cytoskeleton organization and ECM-cell adhesions. **(B)** Cell differentiation depends on matrix stiffness. The fluorescent intensity of differentiation markers was represented versus substrate compliance (kPa). Data revealed that maximal lineage specification was achieved at the stiffness value typical of each tissue. **(C)** Matrix stiffness regulates epithelial morphogenesis. Images of cancer cells colonies grown in 3D BM-crosslinked polyacrylamide (PA) gels. These cultures recapitulated the range of stiffness between normal (150 Pa) and malignant tissue (5000 Pa). Cancer cells colonies grown on a soft BM-PA gel showed cell-cell localized β-catenin, basally polarized β4 integrin and an assembled BM. Increasing matrix stiffness destabilized cell-cell junctions and perturbed tissue polarity (diffusive localization of β-catenin, β4 integrin and BM). Adapted from Discher *et al.*[26], Engler *et al.*[27] and Paszek *et al.*[28]

Most tumours are characterized by progressively become a stiffer tissue and, consequently, are frequently detected through physical palpation as a rigid mass. For instance, breast cancer tissue can be 10 times stiffer than healthy tissue[28]. This phenomenon is produced by an elevated deposition and remodelling of ECM components, mainly fibrilar collagen and hyaluronic acid. The link between cancer and matrix stiffness has been largely studied. Matrix stiffness perturbs epithelial architecture by increasing ROCK-generated cytoskeletal contractility and clustering integrins to promote focal adhesions (FA). Moreover, the FA kinase (FAK)-Rho signaling loop cause the hyperactivation of PI3 kinase (PI3K)[29] and mitogen-activated protein kinase (MAPK)[30] pathways, which enhance cell growth and drive a clinically relevant proliferation signature.

1.1.3.2 Natural Scaffolds: Using Nature Sources

TE scaffolds can be divided into two categories depending on their origin: synthetic or natural biomaterials. Natural biomaterials are ECM components directly extracted from plants, animals or human tissues. Up to date, collagen[31], reconstituted BM[32] and hyaluronic acid[33] constitute the gold standard for developing 3D cultures in cancer research.

Collagen is the major component of the ECM of all connective tissues, representing approximately 25% of the total dry weight of mammals. It provides structural support and establishes interactions with other matrix proteins and cellular receptors, participating in cell organization. Four different integrins ($\alpha_1\beta_1$, $\alpha_2\beta_1$, $\alpha_{10}\beta_1$ and $\alpha_{11}\beta_1$) can bind to collagen and 19 genetically distinct collagen types are described. All of them are characterized by having a triple helix structure, formed by repeating GXY sequences within each chain (X is a proline and Y a hydroxyproline). The most abundant collagen is Type I and it is composed of two α_1(I) and one α_2(I) chains to give a molecular organization of two $[\alpha_1(I)]_2\alpha_2(I)$. In tumor microenvironment, collagen has an ubiquitous nature due to its overexpression by stromal fibroblasts in a process known as desmoplastic reaction (DR)[34]. For instance, DR accounts for up to 90% of the tumor volume in pancreatic cancer.

The main advantages of natural biomaterials are their easy accessibility, biocompatibility and capacity to integrate a wide spectrum of the ECM signals that actively participate in tumor progression, mainly cell adhesion binding motifs. These matrices have produced important conceptual advances such as the expression of genes (pro-angiogenic factors, MMPs, epithelial-mesenchymal transition [EMT] markers, etc.) and the acquisition of drug resistance at similar levels than tumours[35–37]. Therefore, they are able to recreate the *in vivo* cellular response more precisely.

However, the simultaneous presence and the often unknown character of ECM signals make difficult to analyze the effect of specific factors. An example is the coupling between mechanical, physical and chemical properties. Characteristic tumor stiffness values can be easily recreated by increasing concentration or crosslinking density of these biomaterials. But, in parallel, they suffer modifications of fiber architecture, pore size and integrins presence, altering cell behavior independently of differences in mechanical properties[28]. Another drawback of natural biomaterials is that the same ECM component can be very variable in its composition, depending on the specie origin and industrial processing (extraction and purification steps). Consequently, the reproducibility of experiments is reduced[8].

1.1.3.3 Synthetic Scaffolds: Learning From Nature

A further step in cancer biology has involved the development of synthetic biomaterials as TE scaffolds. They are formed by non-instructive building blocks that provide both (*i*) a reproducible cellular microenvironment and (*ii*) the flexibility to individually tune a physical, mechanical or chemical feature. Therefore, they allow scientists to study the function and mechanism of specific factors during disease progression. Paradoxically, these advantages make this class of biomaterials far more challenging because they do not contain signaling motifs. Unless functionalization is performed (incorporation of bioactive sequences or molecules), scaffolds only serve to hold and guide cells in a 3D space until they produce their own physiological matrix environment[8,38]. Synthetic scaffolds can be mainly classified in microfiber polymers and nanofiber hydrogels.

The most popular polymeric scaffolds in cancer research are polyethylene glycol (PEG)[39], poly(lactide-co-glycolide) (PLG)[40], poly(lactic-co-glycolacid) (PLGA)[40] and polylactic acid (PLA)[41]. From the chemical perspective, these polymers can be covalently functionalized with integrin binding sites (arginine-glycine-aspartate, RGD sequences) or proteolytic degrading sites (MMPs target sequences). Moreover, they can be conjugated with specific soluble biomolecules (growth factors, angiogenic factors, cytokines, etc.), which are controllably released based on proteinase activity[42]. From the mechanical perspective, the stiffness of these synthetic biomaterials can be precisely tuned by changing concentration or cross-linking density without introducing an array of confusing cues (i.e. changes in cell ligand density). Up to date, only few studies based on varying the stiffness of synthetic PEG polymer scaffolds have been published and, therefore, more research is needed in this field[43]. Interestingly, results show that ECM stiffness *per se* can initiate tumour progression through modulation of integrin dynamics. From the physical perspective, polymeric scaffolds show a pore size between 50-500 µm, which is in the same order of magnitude than an average mammalian cell (10-100 µm). Consequently, cells do not experience a truly 3D microenvironment since scaffold pores should be significantly smaller than cells. Pore size is the main drawback of polymers[22].

The second class of synthetic scaffolds are nanofiber hydrogels. They contain biologically inspired sequences, being classified as peptide amphiphiles[44], β-hairpin peptides[45] and self-assembling peptides[46].They are characterized by having a pore size between 5-200 nm (1000 times smaller than mammalian cells). As a result, cells grow in a 3D milieu, mimicking the architecture of ECM (**Figure 1.5**).

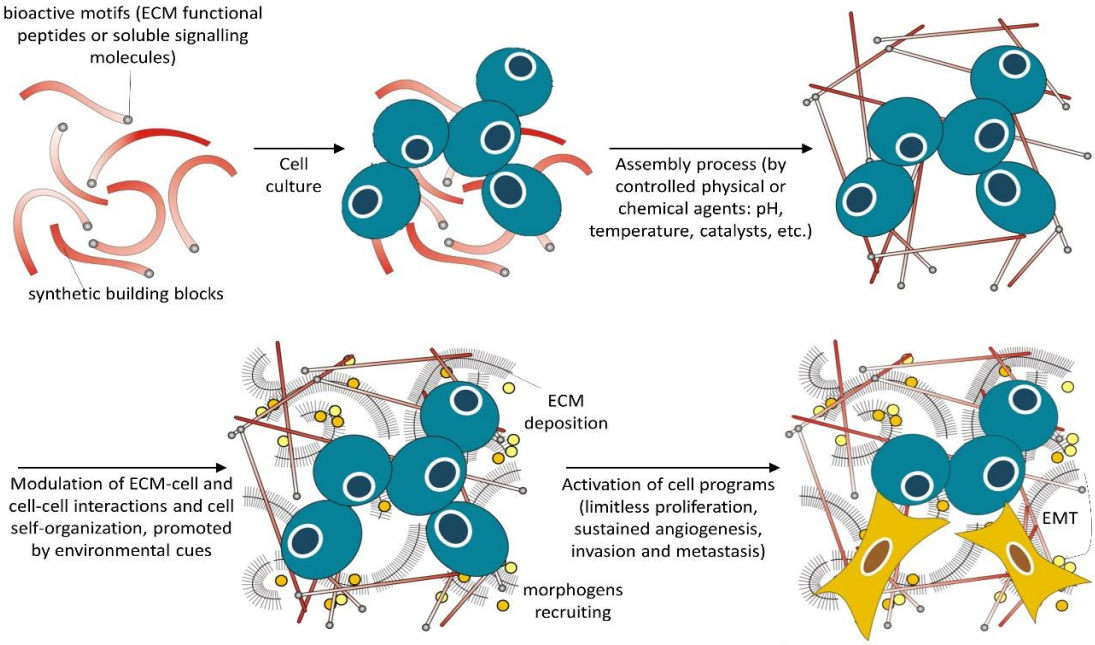

Figure 1.5. Applying biomimetic design principles to synthetic scaffolds. Synthetic scaffolds enable the deconstruction of the *in vivo* cellular microenvironment in order to understand the physical, mechanical and chemical signals that govern tumour progression at the molecular level**.** Nanofiber biomaterials consist of non-instructive building blocks that can be functionalized with epitopes, as bioactive sequences (e.g. adhesion cellular sites and proteases sensitive sites) and/or signalling molecules (e.g. growth factors). Synthetic scaffolds undergo an assembly process in response to controlled physical or chemical agents (pH, temperature, catalysts, etc.), rendering an ordered structure and embedding cells. Cells receive multiple environmental cues that arise from the 3D milieu, which can modulate cell-cell and cell-ECM interactions and initiate self-organization programs. For instance, cells can synthetize and deposit their own ECM together with the recruitment of morphogens. As consequence, synthetic scaffolds can activate cell programs, such as EMT in cancer pathophysiology.

Self-assembling peptides are the most used nanofiber scaffolds for TE applications. Molecular self-assembly is the spontaneous organization of molecules into well-defined arrangements because of non-covalent interactions occurring under thermodynamic equilibrium conditions. Nature commonly uses this mechanism to form highly organized and stable macromolecular entities, such as DNA double-helix annealing and BM assembly[46]. Following this principle, self-assembling peptides are composed of natural aminoacid sequences, which alternate hydrophilic and hydrophobic residues. Under the appropriate conditions, they spontaneously self-assemble to face the hydrophobic residues between them and the same for hydrophilic residues, forming a network of interweaving nanofibers. This process is driven by ionic side-chain interactions in addition to conventional β-sheet backbone hydrogen bonding. The non-covalent interactions between nanofibers enable cells to freely grow, migrate and establish intercellular contacts[47]. A promising self-assembling peptide is RAD16-I (commercially available as BD™ PuraMatrix™). It is a 16-aminoacid peptide, having the following sequence: AcN-$(RADA)_4$-$CONH_2$ (R arginine, A alanine and D aspartic acid). RAD16-I is inspired in zuotin, a yeast protein initially identified for its ability to bind left-handed Z-DNA. Through adjustment of the pH to neutrality or upon increase of the ionic strength to physiological solutions, RAD16-I self-assembles forming nanofibers of 10-20 nm diameter and 50-200 nm pore size[48,49] (**Figure 1.6**).

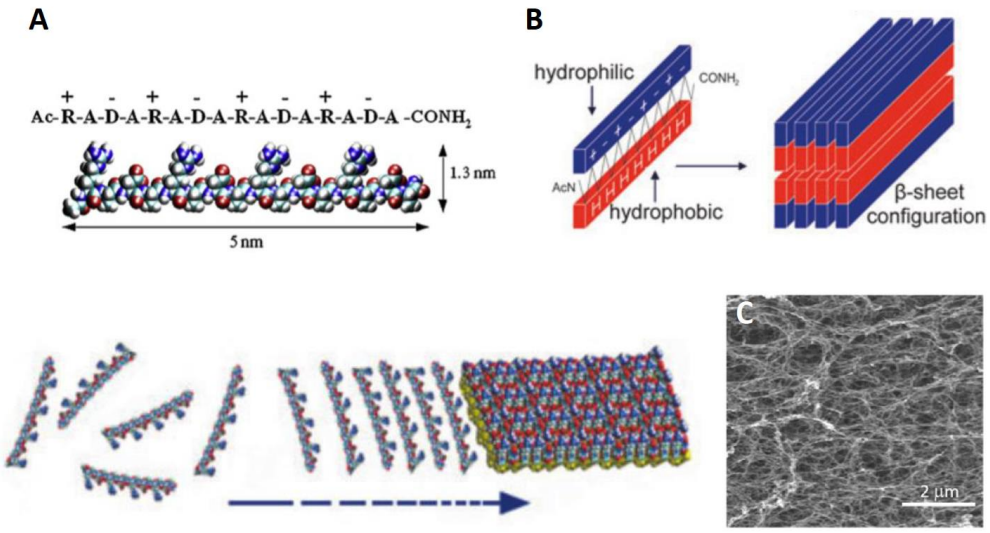

Figure 1.6. Self-assembling peptide RAD16-I. (A,B) Schematic model of self-assembling process. RAD16-I is an amphiphilic oligopeptide that presents alternatively repeating units of positively charged and negatively charged side groups. Under the appropriate conditions (strong ionic strength or neutral environments as physiological solutions), the peptide spontaneously self-organizes in anti-parallel arrangement to form a network of interweaving nanofibers of 10-20 nm diameter and 50-200 nm pore size. This process is driven by ionic side-chain interactions in addition to conventional β-sheet backbone hydrogen bonding. The non-covalent interactions between nanofibers enable cells to freely grow, migrate and established intercellular **(C)** Scanning electron microscopy of the nanofiber network. The molecular architecture of RAD16-I recreates natural ECM, in which cells experience a truly 3D milieu. Adapted from Alemany-Ribes *et al*.[50] and Genové *et al* [51].

Several experimental models show the potential of RAD16-I as TE scaffold. Particularly, it is proved to support growth and proliferation of a wide variety of cells as chondrocytes[47], neuronal cells[52], osteoblasts[53], endothelial cells[54] and hepatocytes[55]; as well as differentiation of progenitor cells to osteogenic[56], neural[57] and hepatic[58] lineage. Furthermore, it has been functionalized through solid-phase synthesis extension at the C-termini using short peptide sequences that act as recognition site for cellular adhesion, spreading and migration. Up to date, laminin-binding sequences (YIGSR, IKVAV, PDSGR) and collagen binding-sequences (PRGDSGYRGDS)[51,55,59] have been used to trigger different cell responses. However, the application of self-assembling peptide in cancer research remains poorly explored.

Each TE scaffold provides specific physical, chemical and mechanical cues, inducing a different cellular response. Hallmark experiments have largely demonstrated that culturing the same cells in different biomaterials results in changes in their morphology, proliferation rate, migratory potential and EMT gene expression[60]. For this reason, the selection of the scaffold is a key point when planning the experiments and it depends on multiple factors: (*i*) the application of the 3D model (comprehension of disease mechanism, development of drug screening processes, establishment of gene signatures to predict the prognosis of personalized cancer cases, etc.), (*ii*) the tissue of origin and tumor ethology and (*iii*) the concrete step of tumor progression to be recreated. As a result, data gathered from 3D culture models should be interpreted in the context of each experimental design.

1.1.3.4 Scaffolds Selection: Recreating Cancer Step By Step

As previously described, tumorigenisis is a multistage process characterized by limitless cellular proliferation, sustained angiogenesis and tissue invasion and metastasis. Considering its definition, tumor progression cannot be entirely recreated *in vitro* as it engages multiple cellular programs. Consequently, scaffolds are carefully designed depending on which step is modelled.

Limitless cellular proliferation

Significantly, 90% of cancers have an epithelial origin[61]. Epithelial tissues show some distinguishing microscopic features, such as cell polarity, specialized intercellular interactions and attachment to an underlying BM. This ordered architecture is necessary for the proper control of cellular proliferation and differentiation and is disrupted during the pathogenesis of epithelial tumors[7,62]. When cancer cells grow in 2D cultures, they acquire upper (dorsal) and lower (ventral) surfaces and, thus, experience an artificial epithelial polarity. Three-dimensionality can restore tumor morphology, independently of matrix composition and stiffness[63].

Seminal experiments reveal that integrin blocking antibodies can revert the malignant phenotype of cancer cells in 3D cultures[19,64]. Furthermore, it is reported that cells undergo minimal or no proliferation when cultured in non-instructive PEG hydrogel, compared to PEG functionalized with integrin binding sites (RGD sequences) or Matrigel[59]. Therefore, tumor architecture and function are orchestrated and maintained through ECM adhesion receptors. In particular, proliferation depends on the activation of integrin β1 family, which in turn phosphorylates FAK signaling pathway[65,66]. These findings are consistent with previous work involving animals. For instance, in transgenic mouse models for mammary or pancreatic cancer, knockdown of β1 integrin results in the inhibition of proliferation of mammary cancer cells and senescence of pancreatic beta cancer cells[67].

Sustained angiogenesis

Angiogenesis is the formation of new capillaries from pre-existing ones[68]. In cancer, this process is activated when the tumor demand for oxygen and nutrients surpasses the local supply, typically at a diameter between 1-2 mm. Tumor vasculature is required for cell growth and dissemination. Its architecture is characterized by a poor organization, due to the imbalance between pro- and anti-angiogenic factors and the stress generated by the uncontrolled proliferation rate that forces vessels to move apart[69]. As a result, tumor shows hypoxia, a low pH and a high interstitial fluid pressure, which provides a hostile and resistant microenvironment. Intensive research has been directed to the development of anti-angiogenic strategies in order to prevent tumor progression (i.e. thalidomine, Herceptin, AZD2171, etc.)[23].

Multiple studies demonstrate that the culture of cancer cells within scaffolds can neither promote nor support angiogenesis *per se*, strongly suggesting that stromal cells are an essential requirement in the formation of a capillary-like microvasculature[70]. 3D matrices constitute an advantageous framework to co-culture cancer cells with stromal cells. In fact, culturing cancer cells, endothelial cells and fibroblasts within collagen results in the recruitment and differentiation of endothelial cells to develop blood vessel-resembling structures. Cell-matrix interactions between endothelial cells and collagen induce the migration of endothelial cells towards the collagen-embedded layer of fibroblasts and cancer cells. Besides, cell-cell interactions cause the differentiation of endothelial cells into capillaries-like structures, through the delivery of pro-angiogenic factors in a spatiotemporal controlled manner[70,71]. Synthetic scaffolds like PEG and PLG are used for immobilization and subsequent release of chemical cues that may be involved in angiogenesis, making such systems powerful platforms to study tumor-dependent changes in angiogenic sprouting[72].

Finally, smart platforms located in the frontier between *in vitro* and *in vivo* conditions are introduced. An important case is the arterio-venous loop based on the microsurgical implantation of small caliber vessels in matrices of different composition. For instance, arterial explants from umbilical cords are embedded in Matrigel to study their interaction with cancer cells. These explants led to capillary-like structures autonomously, without stimulation with exogenous growth factors[17,73]. The dynamic observation of cancer cells that recruit, interact and stimulate the growth of new vessels can promote the understanding of tumor-driven angiogenesis.

Tissue invasion and metastasis

Metastasis is a poorly understood mechanism of tumor spreading[62]. During metastatic process, cells gain the capacity to degrade their BM and invade surrounding tissue. Subsequently, metastatic cells enter the lymphatic and circulatory systems in order to disseminate and undergo growth in distant parts of the body. This cascade of events is only possible if cells lose their epithelial phenotype and acquire a mesenchymal phenotype that switches on proteolysis and motility programs. This conversion is known as epithelial-mesenchymal transition (EMT) and involves changes in cellular architecture and function[74]. Due to its clinical relevance, a major effort has been directed to develop new models to capture specific steps of metastasis and, therefore, discover new insights of the molecular mechanism that drive metastasis.

One of the first questions to be addressed is how cells can migrate throughout the ECM. Experiments with natural scaffolds evidence that cancer cells overexpress ECM degrading enzymes (MMPs, hyaluronases, etc.) compared to normal cells[75,76]. For this reason, synthetic biomaterials like PEG are a neutral microenvironment to precisely tune structural cues, in this case MMP-sensitive motifs[39,77]. Results show that cells are able to tunnel through the matrix via proteolytic degradation executed by MMPs, resulting in its continuously remodeling. However, clinical studies demonstrate the incomplete therapeutic window covered by MMPs inhibitors in

cancer progression. 3D cultures are also used to identify other mechanisms responsible for the migratory capacity of cancer cells. Notably, synthetic scaffolds (PEG and RAD16-I)[43,60] and natural scaffolds (collagen)[78] can recreate micro-tunnels of the same size and topography as those produced by metastatic cells. These opened paths are used by MMPs-deficient cells to migrate using an amoeboid phenotype, displacing matrix fibers by actomyosin-based mechanical forces. Therefore, bioengineering tumor microenvironment can lead to the discovery of the synergism between proteolytic degradation and amoeboid movement for migration.

In a second stage, the molecular mechanisms that direct the circulation of cancer cells through the bloodstream are investigated using microfluidic platforms. Specifically, 3D cultures based on Matrigel[79] or collagen[80,81] scaffolds are subjected to continuous flow. These systems enable the analysis of fluidic forces (shear stress) as modulators of EMT process during tumorigenisis. Furthermore, methodologies are developed to produce endothelialized networks within 3D scaffolds in these microfluidic circuits[82,83]. Their main objective is to characterize the processes activated by cancer cells under shear stress conditions: adhesion with endothelial cells and degradation of the BM to undergo metastatic growth (extravasation).

Finally, colonization of cancer cells to a secondary metastatic site is evaluated by mimicking the host cellular niche. The location of metastasis is not random; each type of cancer tends to spread to a particular tissue or organ at a higher rate than expected by statistical chance. It is postulated that a non-permissive microenvironment, in which cancer cells are unable to properly adhere, triggers their dormancy[84]. For this reason, the modelling of the new microenvironment is a useful tool for understanding the mechanisms mediated by the ECM and neighboring cells that explain this specificity in metastasis location. For instance, the three most commonly diagnosed cancer types (prostate, lung and breast) tend to metastasize in the bone. Consequently, research is directed to the design of biomimetic organic collagen[85] and inorganic hydroxyapatite (HA)[85] that form bone. Results show that cancer cells mineralize in an active and regulated process similar to osteoblasts. Therefore, cells possess osteomimetic capabilities through the expression of bone marker proteins that allow them to adapt and flourish within the bone microenvironment (**Figure 1.7** and **Table 1.1**).

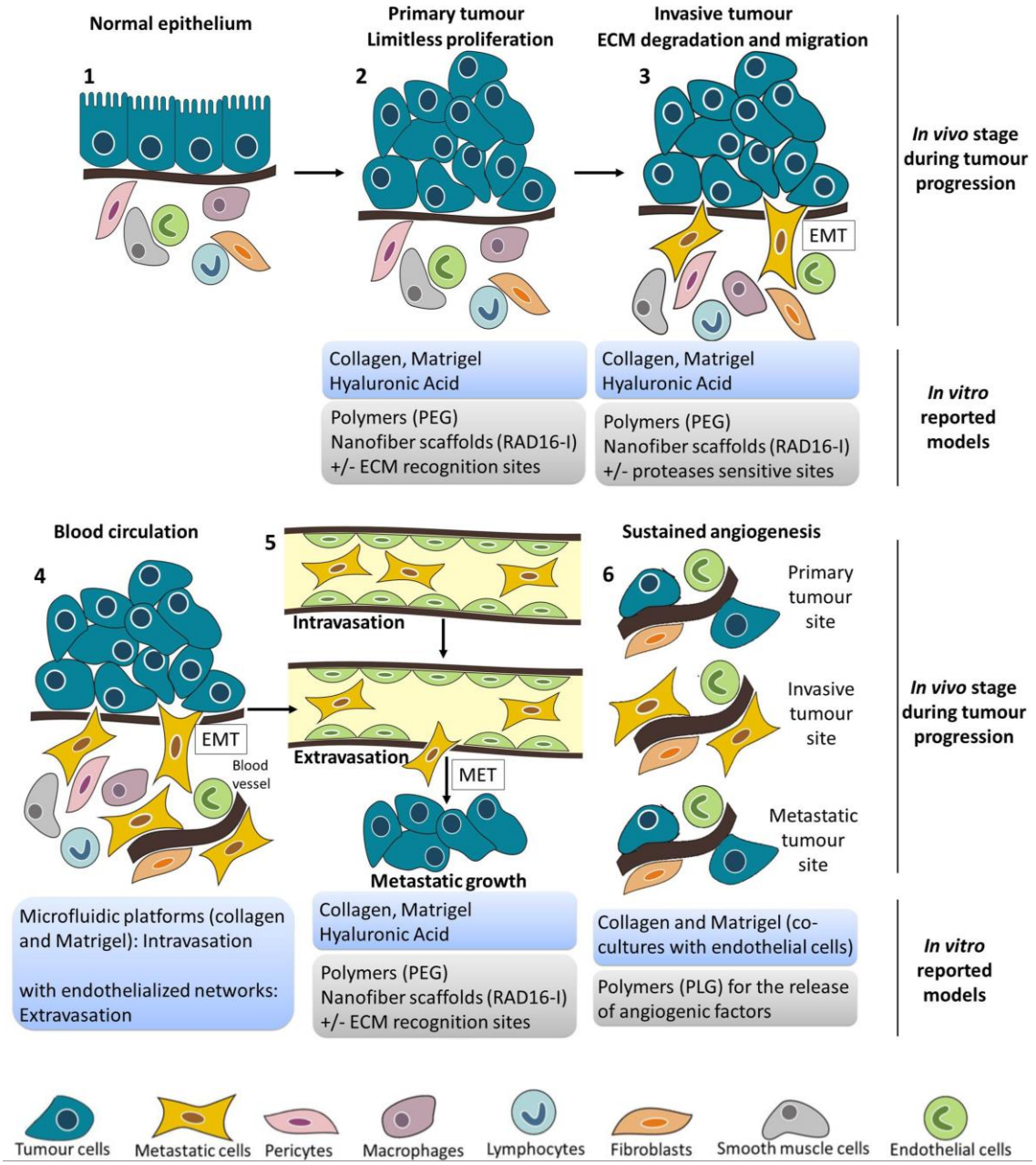

Figure 1.7. Tissue engineering scaffolds depend on the specific tumour step. Design parameters for 3D biomaterials depend on the tumour stage and the corresponding cellular programs that are recreated**.** Tumorigenisis is a multistage process defined by particular genetic and epigenetic hallmarks: (**1**) Normal tissue. (**2**) Primary tumour with limitless cellular proliferation. (**3**) Invasive tumour characterized by ECM degradation and migration (epithelial to mesenchymal transition, EMT). (**4**) Blood circulation that comprises (**5**) intravasation into lymph and blood vessels to allow cell passive transport to distant organs; extravasation to degrade the BM of lymph and blood vessels to colonize a secondary site and metastatic growth through mesenchymal to epithelial transition (MET). (**6**) Sustained angiogenesis takes places within primary, invasive and metastatic tumour site. The figure illustrates the most actual and relevant biomaterials (from both natural and synthetic origin) used to model each tumour stage.

TUMOR STAGE	3D CULTURES	
	NATURAL SCAFFOLDS	SYNTHETIC SCAFFOLDS
LIMITLESS PROLIFERATION	They provide a wide range of ECM receptors, basically adhesion and proteolytically remodeling complexes: **Matrigel**[19,32,64]**, collagen**[86] **and hyaluronic acid**[33,87]. They enable to modulate stiffness by increasing concentration or cross-linking density. In parallel, they suffer changes in pore size, fiber architecture and adhesion sites: **collagen**[28,30] and **hyaluronic acid**[88].	They are blank environments to systematically explore the role of ECM receptors: **PEG versus PEG-RGD sites and -MMP sensitive sites**[59,77]. They can independently tune stiffness, without introducing an array of confusing ECM signals: **PEG**[77] and **RAD16-I**[89].
SUSTAINED ANGIOGENESIS	Culturing cancer cells within 3D matrices is representative of pre-vascularized stages of tumor progression. The interaction between **cancer cells**, **endothelial cells** and **fibroblasts** within a 3D **collagen** environment is required for micro-vasculature formation[70]. Alternatively, **arterials explants** can be implanted into 3D matrices of different origin (collagen, Matrigel) containing cancer cells[17,73].	They enable the immobilization and subsequent release of angiogenic factors, in a controlled spatial and temporal manner: **PLG**[40,72].
ECM DEGRADATION AND MIGRATION	They provide suitable platforms to perform invasion assays and study the expression of ECM degrading enzymes: **Matrigel**[76], **collagen**[75,76] and **hyaluronic acid**[33]. They can recreate micro-tunnels for proteolytically inactive cells and study alternative mechanisms to ECM remodeling: **collagen**[78]. They can determine stiffness contribution on cancer invasive phenotype, in parallel to physical modifications of the matrix: **collagen**[28,30] and **hyaluronic acid**[88].	They are blank environments to systematically explore the role of ECM degrading enzymes: **PEG versus PEG-MMP sensitive sites**[59,77]. They enable to investigate the existence of migration mechanisms alternative to ECM remodeling: **PEG**[43] and **RAD16-I**[60]. The isolated impact of stiffness on migration can be studied: **PEG**[43] and **RAD16-I**[89].
BLOOD CIRCULATION	They are used in microfluidic platforms. Microchannels coated with stromal beds of **Matrigel**[79,80] and **collagen**[80,81] to evaluate hydrodynamic forces impact on EMT. **Endothelialized networks**[82,83] within fluidic circuits to characterize adhesions between cancer and endothelial cells and BM degradation	They can enable analyzing what chemical cues participate in the control of cancer cells circulation through the bloodstream. They can let to determine what adhesion complexes are needed to activate extravasation.
METASTATIC GROWTH	The biomaterial used depends on the metastatic growth site. In general, the 3D matrix should contain bioactive motifs through which cells are able to adhere or they enter into a dormancy state[84].	They are blank environments to systematically explore the role of adhesion sites: **PEG versus PEG-RGD sites**[59,77].

Table 1.1. The most representative 3D scaffolds used to model the different stages of tumor progression.

1.1.3.5 Cells Selection: Maintaining Tumor Identity

Apart from the continuous research in 3D scaffolds, a major challenge in cancer biology is the optimization of cell source in order to provide an accurate tissue engineering toolbox for identification and characterization of new therapeutic approaches. *In vitro* models are based on immortal cancer-derived cell lines. They constitute the most common means of studying cancer pathophysiology due to their accessibility, ease of culture and homogeneity. However, genomic studies demonstrate that cell lines only reflect a limited part of the gene expression profile that characterize the tumor *in vivo*, emerging as unreliable predictive preclinical models[90,91]. There are multiple reasons that explain this misrepresentation.

First, cell lines have been grown for several years or decades in 2D cultures, imposing a strong selective pressure on them and making adaptation only possible by changes at DNA level. As they are distributed in many laboratories, the same cell line might have undergone various selection steps due to differences in feeding and passage techniques[91]. Second, stroma is an active participant in tumor progression[5,6]. Finally, analyses reveal a high degree of genomic heterogeneity across cancer patients population, accounting for the variable clinical-response to treatment. A unique cell line does not capture this complexity[90].

The scientific community has more reliable cellular approaches, including mainly clinical biopsies or the parallel analysis of large panels of cell lines. Biopsies are obtained at the time of surgical resection and cells are freshly harvested and cultured in 2D or 3D conditions. The complex mixture of cells that are part of the tumor milieu can be preserved, recreating the crosstalk between stromal and cancer cells more precisely. This new methodology is the first step to personalized medicine, making possible the evaluation of drug sensitivity and resistance on a patient-by-patient basis. However, this platform is not representative of a tumor class since it only incorporates the genetic information of an individual patient[92,93].

The second strategy is focused on the establishment of cellular platforms in which each type of tumor is represented by a large number of cell lines. The most popular are National Cancer Institute 60 (NCI60) and Center for Molecular Therapeutics 1000 (CMT1000) platforms. For instance, these Centers have 6 and 51 cell lines for studying breast cancer respectively. This cell collection captures the genomic diversity of human cancers, correlating underlying genotypes with drug response. The obtained data can create molecular signatures that are clinically useful for both predicting drug sensitivity and elucidating mechanisms of drug action. The major limitation is the logistical challenge associated with the culture of large cancer cell lines panels, which considerably limits the throughput of the platform with respect to the number of compounds that can be realistically tested in a given period of time[90].

1.2 HYPOTHESIS AND GENERAL AIMS

This project was based on exploring different three-dimensional (3D) cell models for cancer research. Our working hypothesis was that 3D cultures could fulfill the need of reliable *in vitro* approaches to better comprehend the molecular mechanisms that rule both disease progression and therapies action.

Biomaterials characterized by different composition and stiffness values were used to developed 3D models and results were compared with conventional monolayers. The general aim was to deconstruct the complex tumor milieu and analyze the contribution of different microenvironmental cues in cancer biology. In particular, the following objectives were pursued:

(1) To analyze the role of environmental signals in the activation of epithelial to mesenchymal transition, a cell program required for initiating invasion tumor stage (Chapter 3).

(2) To design and develop 3D cell models for assessing both mode of action and efficacy of cancer treatment approaches as photodynamic therapy (Chapter 4).

(3) To study the molecular mechanisms that cancer cells engage in order to escape from drugs action and become resistant (Chapter 5).

1.3 CONTENT OF DISSERTATION

The first chapter was primarily focused on the cellular and molecular mechanisms that underlie early steps of epithelial to mesenchymal transition (EMT) and activate tumor invasion. 3D cells models could recapitulate the transition from a 2D to a 3D microenvironment that experience cancer cells when escape from epithelial layer and invade mesenchymal connective tissue. Moreover, these models allowed us to modify the chemical and mechanical properties of cellular microenvironment and analyze their potentiality to induce EMT. For this reason, self-assembling peptide RAD16-I and natural collagen type I were used as scaffolds at two working concentrations to culture pancreatic cancer cells. The effect of different surrounding compositions and stiffness values was evaluated in terms of (*i*) cell phenotype and (*ii*) cell-cell adhesions expression and regulation (E-cadherin, EMT marker) and was compared to conventional monolayer cultures.

The second chapter was based on developing different 3D cell models for predicting the outcome of cancer photodynamic therapy (PDT). Biomimetic approaches were designed and characterized to progressively incorporate increasing levels of biological complexity. In a first stage, the self-assembling peptide RAD16-I was used to mimic tumor architecture in terms of 3D cell-cell and cell-ECM communication networks together with a core of cells under hypoxic conditions. In a second stage, collagen was used to incorporate extracellular matrix (ECM)-binding motifs such as integrins- and metalloproteinases-recognition sequences. Finally, co-cultures between cancer cells and fibroblasts were performed to enable paracrine signaling between both cell types. Results gave insight into the influence of these micoenvironmental cues in PDT mechanism and efficacy. Part of the experimental procedures were performed with Dr. María García Díaz and Ester Boix Garriga (group of Dr. Santiago Nonell from IQS School of Engineering) and Dr. Pilar Acedo Núñez (group of Dr. Ángeles Villanueva from Universidad Autónoma de Madrid).

Finally, the third chapter explored the contribution of extracellular milieu to mechanisms of drug resistance. In particular, the effect of targeted cancer drugs as receptor tyrosine kinases inhibitors (TKIs) was assessed in different 3D cell models of pancreatic cancer cells and fibroblasts stromal cells. The expression pattern of specific blocked receptors was analyzed before and after drug treatment and compared to conventional monolayer cultures. Data reflected the diversity of strategies that survival cells developed to escape from drug action. Cells showed plasticity to adapt to changing pressures and dependence on the surrounding microenvironment. TKIs were synthetized by group of Dr. Ignacio Borrell from IQS School of Engineering.

1.4 REFERENCES

1. World Cancer Research Fund International (WCRF). Cancer statistics worlwide. http://www.wcrf.org/cancer_statistics/world_cancer (2012).

2. World Health Organization (WHO). Cancer. *http://www.who.int/mediacentre/factsheets/fs297/en/* (2012).

3. Hanahan, D. & Weinberg, R. A. Hallmarks of cancer: The next generation. *Cell* **144,** 646–674 (2011).

4. Bissell, M. J. & Radisky, D. Putting tumours in context. *Nat. Rev. Cancer* **1,** 46–54 (2001).

5. Mueller, M. M. & Fusenig, N. E. Friends or foes - Bipolar effects of the tumour stroma in cancer. *Nat. Rev. Cancer* **4,** 839–849 (2004).

6. Bhowmick, N. A., Neilson, E. G. & Moses, H. L. Stromal fibroblasts in cancer initiation and progression. *Nat. Rev. Cancer* **432,** 332–337 (2004).

7. Yamada, K. M. & Cukierman, E. Modeling tissue morphogenesis and cancer in 3D. *Cell* **130,** 601–610 (2007).

8. Griffith, L. G. & Swartz, M. A. Capturing complex 3D tissue physiology in vitro. *Nat. Rev. Mol. Cell Biol.* **7,** 211–224 (2006).

9. Illmensee, K. & Mintz, B. Totipotency and normal differentiation of single teratocarcinoma cells cloned by injection into blastocysts. *Proc. Natl Acad. Sci. USA* **73,** 549–553 (1976).

10. Dolberg, D. S. & Bissell, M. J. Inability of Rous sarcoma virus to cause sarcomas in the avian embryo. *Nature* **309,** 552–556 (1984).

11. Smalley, K. S. M., Lioni, M. & Herlyn, M. Life ins't flat: Taking cancer biology to the next dimension. *Vitr. Cell. Dev. Biol. - Anim.* **42,** 242–247 (2006).

12. Gurski, L. A., Petrelli, N. J., Jia, X. & Farach-Carson, M. C. 3D matrices for anti-cancer drug testing and development. *Oncol. Issues* **25**, 20–25 (2010).

13. Burdett, E., Kasper, F. K., Mikos, A. G. & Ludwig, J. A. Engineering tumors: A tissue engineering perspective in cancer biology. *Tissue Eng. Part B. Rev.* **16,** 351–359 (2010).

14. Pampaloni, F., Reynaud, E. G. & Stelzer, E. H. K. The third dimension bridges the gap between cell culture and live tissue. *Nat. Rev. Mol. Cell Biol.* **8,** 839–845 (2007).

15. Langer, R. & Vacanti, J. P. Tissue Engineering. *Science* **260,** 920–926 (1993).

16. Sutherland, R. M., Sordat, B., Bamat, J., Gabbert, H. & Bourrat, B. Oxygenation and differentiation in multicellular spheroids of human colon carcinoma. *Cancer Res.* **46,** 5320–5329 (1986).

17. Hutmacher, D. W. *et al.* Translating tissue engineering technology platforms into cancer research. *J. Cell. Mol. Med.* **13,** 1417–1427 (2009).

18. Petersen, O. W., Rønnov-Jessen, L., Howlett, A. R. & Bissell, M. J. Interaction with basement membrane serves to rapidly distinguish growth and differentiation pattern of normal and malignant human breast epithelial cells. *Proc. Natl. Acad. Sci. U. S. A.* **89,** 9064–9068 (1992).

19. Weaver, V. M. *et al.* Reversion of the malignant phenotype of human breast cells in three-dimensional culture and in vivo by integrin blocking antibodies. *J. Cell Biol.* **137,** 231–245 (1997).

20. Hutmacher, D. W. Biomaterials offer cancer research the third dimension. *Nat. Mater.* **9,** 90–93 (2010).

21. Frantz, C., Stewart, K. M. & Weaver, V. M. The extracellular matrix at a glance. *J. Cell Sci.* **123,** 4195–4200 (2010).

22. Semino, C. E. Can we build artificial stem cell compartments? *J. Biomed. Biotechnol.* **2003,** 164–169 (2003).

23. Fukumura, D. & Jain, R. K. Tumor microvasculature and microenvironment: Targets for anti-angiogenesis and normalization. *Microvasc. Res.* **74,** 72–84 (2007).

24. Juliano, R. L. & Haskill, S. Signal transduction from the extracellular matrix. *J. Cell Biol.* **120,** 577–585 (1993).

25. Wozniak, M. A. & Chen, C. S. Mechanotransduction in development: A growing role for contractility. *Nat. Rev. Mol. Cell Biol.* **10,** 34–43 (2009).

26. Discher, D. E., Mooney, D. J. & Zandstra, P. W. Growth factors, matrices and forces combine and control stem cells. *Science* **324,** 1673–1677 (2009).

27. Engler, A. J., Sen, S., Sweeney, H. L. & Discher, D. E. Matrix elasticity directs stem cell lineage specification. *Cell* **126,** 677–689 (2006).

28. Paszek, M. J. *et al.* Tensional homeostasis and the malignant phenotype. *Cancer Cell* **8,** 241–254 (2005).

29. Levental, K. R. *et al.* Matrix crosslinking forces tumor progression by enhancing integrin signaling. *Cell* **139,** 891–906 (2009).

30. Provenzano, P. P., Inman, D. R., Eliceiri, K. W. & Keely, P. J. Matrix density-induced mechanoregulation of breast cell phenotype, signaling and gene expression through a FAK-ERK linkage. *Oncogene* **28,** 4326–4343 (2009).

31. Chen, L. *et al.* The enhancement of cancer stem cell properties of MCF-7 cells in 3D collagen scaffolds for modeling of cancer and anti-cancer drugs. *Biomaterials* **33,** 1437–1444 (2012).

32. Zschenker, O., Streichert, T., Hehlgans, S. & Cordes, N. Genome-wide gene expression analysis in cancer cells reveals 3D growth to affect ECM and processes associated with cell adhesion but not DNA repair. *PLoS One* **7,** e34279 (2012).

33. David, L. *et al.* Reticulated hyaluronan hydrogels: A model for examining cancer cell invasion in 3D. *Matrix Biol.* **23,** 183–193 (2004).

34. Carletti, E., Motta, A. & Migliaresi, C. Scaffolds for tissue engineering and 3D cell culture. *Methods Mol. Biol.* **695,** 17–39 (2011).

35. Gurski, L. A., Jha, A. K., Zhang, C., Jia, X. & Farach-Carson, M. C. Hyaluronic acid-based hydrogels as 3D matrices for in vitro evaluation of chemotherapeutic drugs using poorly adherent prostate cancer cells. *Biomaterials* **30,** 6076–6085 (2009).

36. Dangi-Garimella, S., Strouch, M. J., Grippo, P. J., Bentrem, D. J. & Munshi, H. G. Collagen regulation of let-7 in pancreatic cancer involves TGF-β1-mediated membrane type 1-matrix metalloproteinase expression. *Oncogene* **30,** 1002–1008 (2011).

37. Fallica, B., Maffei, J. S., Villa, S., Makin, G. & Zaman, M. Alteration of cellular behavior and response to PI3K pathway inhibition by culture in 3D collagen gels. *PLoS One* **7,** e48024 (2012).

38. Dutta, R. C. & Dutta, A. K. Cell-interactive 3D-scaffold; advances and applications. *Biotechnol. Adv.* **27,** 334–339 (2009).

39. Loessner, D. *et al.* Bioengineered 3D platform to explore cell-ECM interactions and drug resistance of epithelial ovarian cancer cells. *Biomaterials* **31,** 8494–8506 (2010).

40. Fischbach, C. *et al.* Engineering tumors with 3D scaffolds. *Nat. Methods* **4,** 6–11 (2007).

41. Sahoo, S. K., Panda, A. K. & Labhasetwar, V. Characterization of porous PLGA/PLA microparticles as a scaffold for three dimensional growth of breast cancer cells. *Biomacromolecules* **6,** 1132–1139 (2005).

42. Rizzi, S. C. *et al.* Recombinant protein-co-PEG networks as cell-adhesive and proteolytically degradable hydrogel matrixes. Part II: Biofunctional characteristics. *Biomacromolecules* **7,** 3019–3029 (2006).

43. Soman, P. *et al.* Cancer cell migration within 3D layer-by-layer microfabricated photocrosslinked PEG scaffolds with tunable stiffness. *Biomaterials* **33,** 7064–7070 (2012).

44. Hartgerink, J. D., Beniash, E. & Stupp, S. I. Self-assembly and mineralization of peptide-amphiphile nanofibers. *Science* **294,** 1684–1688 (2001).

45. Schneider, J. P. *et al.* Responsive hydrogels from the intramolecular folding and self-assembly of a designed peptide. *J. Am. Chem. Soc.* **124,** 15030–15037 (2002).

46. Zhang, S. & Altman, M. Peptide self-assembly in functional polymer science and engineering. *React. Funct. Polym.* **41,** 91–102 (1999).

47. Kisiday, J. *et al.* Self-assembling peptide hydrogel fosters chondrocyte extracellular matrix production and cell division. *Proc. Natl. Acad. Sci. U. S. A.* **99,** 9996–10001 (2002).

48. Zhang, S., Lockshin, C., Herbert, A., Winter, E. & Rich, A. Zuotin, a putative Z-DNA binding protein in Saccharomyces cerevisiae. *EMBO J.* **1,** 3787–3796 (1992).

49. Xu, X. *et al.* Recreating the tumor microenvironment in a bilayer, hyaluronic acid hydrogel construct for the growth of prostate cancer spheroids. *Biomaterials* **33,** 9049–9060 (2012).

50. Alemany-Ribes, M., García-Díaz, M., Busom, M., Nonell, S. & Semino, C. E. Toward a 3D cellular model for studying in vitro the outcome of photodynamic treatments: Accounting for the effects of tissue complexity. *Tissue Eng. Part A* **19,** 1665–1674 (2013).

51. Genové, E., Shen, C., Zhang, S. & Semino, C. E. The effect of functionalized self-assembling peptide scaffolds on human aortic endothelial cell function. *Biomaterials* **26,** 3341–3351 (2005).

52. Semino, C. E., Kasahara, J., Hayashi, Y. & Zhang, S. Entrapment of migrating hippocampal neural cells in three-dimensional peptide nanofiber scaffold. *Tissue Eng Part A* **10,** 643–655 (2004).

53. Bokhari, M. A., Akay, G., Zhang, S. & Birch, M. A. The enhancement of osteoblast growth and differentiation in vitro on a peptide hydrogel-polyHIPE polymer hybrid material. *Biomaterials* **26,** 5198–5208 (2005).

54. Hernández Vera, R. *et al.* Interstitial fluid flow intensity modulates endothelial sprouting in restricted Src-activated cell clusters during capillary morphogenesis. *Tissue Eng. Part A* **15,** 175–185 (2009).

55. Genové, E. *et al.* Functionalized self-assembling peptide hydrogel enhance maintenance of hepatocyte activity in vitro. *J. Cell. Mol. Med.* **13,** 3387–3397 (2009).

56. Borros, S., Garreta, E., Genove, E. & Semino, C. E. Osteogenic Differentiation of Mouse Embryonic Stem Cells. *Tissue Eng. Part A* **12,** 1–14 (2006).

57. Taraballi, F. *et al.* Glycine-spacers influence functional motifs exposure and self-assembling propensity of functionalized substrates tailored for neural stem cell cultures. *Front Neuroeng* **3,** 1-9 (2010).

58. Semino, C. E., Merok, J. R., Crane, G. G., Panagiotakos, G. & Zhang, S. Functional differentiation of hepatocyte-like spheroid structures from putative liver progenitor cells in three-dimensional peptide scaffolds. *Differentiation* **71,** 262–270 (2003).

59. Weiss, M. S. *et al.* The impact of adhesion peptides within hydrogels on the phenotype and signaling of normal and cancerous mammary epithelial cells. *Biomaterials* **33,** 3548–3559 (2012).

60. Mi, K. *et al.* Influence of a self-assembling peptide, RADA16, compared with collagen I and Matrigel on the malignant phenotype of human breast-cancer cells in 3D cultures and in vivo. *Macromol. Biosci.* **9,** 437–443 (2009).

61. McCaffrey, L. M. & Macara, I. G. Epithelial organization, cell polarity and tumorigenesis. *Trends Cell Biol.* **21,** 727–735 (2011).

62. Christofori, G. New signals from the invasive front. *Nature* **441,** 444–450 (2006).

63. Debnath, J. & Brugge, J. S. Modelling glandular epithelial cancers in three-dimensional cultures. *Nat. Rev. Cancer* **5,** 675–688 (2005).

64. Weigelt, B., Lo, A. T., Park, C. C., Gray, J. W. & Bissell, M. J. HER2 signaling pathway activation and response of breast cancer cells to HER2-targeting agents is dependent strongly on the 3D microenvironment. *Breast Cancer Res. Treat.* **122,** 35–43 (2010).

65. Shibue, T. & Weinberg, R. A. Integrin β1-focal adhesion kinase signaling directs the proliferation of metastatic cancer cells disseminated in the lungs. *Proc. Natl. Acad. Sci. U. S. A.* **106,** 10290–10295 (2009).

66. Park, C. C., Zhang, H. J., Yao, E. S., Park, C. J. & Bissell, M. J. β1 integrin inhibition dramatically enhances radiotherapy efficacy in human breast cancer xenografts. *Cancer Res.* **68,** 4398–4405 (2008).

67. White, D. E. *et al.* Targeted disruption of β1-integrin in a transgenic mouse model of human breast cancer reveals an essential role in mammary tumor induction. *Cancer Cell* **6,** 159–170 (2004).

68. Folkman, J. Tumor angiogenesis. *Research in cancer research* **43**, 175–203 (1985).

69. Minchinton, A. I. & Tannock, I. F. Drug penetration in solid tumours. *Nat. Rev. Cancer* **6,** 583–592 (2006).

70. Kimlin, L. C., Casagrande, G. & Virador, V. M. In vitro three-dimensional (3D) models in cancer research: An update. *Mol. Carcinog.* **52,** 167–182 (2013).

71. Chan, J. M. *et al.* Engineering of in vitro 3D capillary beds by self-directed angiogenic sprouting. *PLoS One* **7,** e50582 (2012).

72. Verbridge, S. S., Chandler, E. M. & Fischbach, C. Tissue-engineered three-dimensional tumor models to study tumor angiogenesis. *Tissue Eng. Part A* **16,** 2147–2152 (2010).

73. Seano, G. *et al.* Modeling human tumor angiogenesis in a three-dimensional culture system. *Blood* **121,** e129–e137 (2013).

74. Thiery, J. P. & Sleeman, J. P. Complex networks orchestrate epithelial-mesenchymal transitions. *Nat. Rev. Mol. Cell Biol.* **7,** 131–142 (2006).

75. Oyanagi, J., Ogawa, T., Sato, H., Higashi, S. & Miyazaki, K. Epithelial-mesenchymal transition stimulates human cancer cells to extend microtubule-based invasive protrusions and suppresses cell growth in collagen gel. *PLoS One* **7,** e53209 (2012).

76. Nguyen-Ngoc, K.-V. *et al.* ECM microenvironment regulates collective migration and local dissemination in normal and malignant mammary epithelium. *Proc. Natl. Acad. Sci. U. S. A.* **109,** E2595–E2604 (2012).

77. Gill, B. J. *et al.* A synthetic matrix with independently tunable biochemistry and mechanical properties to study epithelial morphogenesis and EMT in a lung adenocarcinoma model. *Cancer Res.* **72,** 6013–6023 (2012).

78. Kraning-Rush, C., Carey, S., Lampi, M. & Reinhart-King, C. Microfabricated collagen tracks facilitate single cell metastatic invasion in 3D. *Integr Biol* **5,** 606–616 (2013).

79. Rizvi, I. *et al.* Flow induces epithelial-mesenchymal transition, cellular heterogeneity and biomarker modulation in 3D ovarian cancer nodules. *Proc. Natl. Acad. Sci. U. S. A.* **110,** E1974–E1983 (2013).

80. Huang, C. P. *et al.* Engineering microscale cellular niches for three-dimensional multicellular co-cultures. *Lab Chip* **9,** 1740–1748 (2009).

81. Polacheck, W. J., Charest, J. L. & Kamm, R. D. Interstitial flow influences direction of tumor cell migration through competing mechanisms. *Proc. Natl. Acad. Sci. U. S. A.* **108,** 11115–11120 (2011).

82. Cross, V. L. *et al.* Dense type I collagen matrices that support cellular remodeling and microfabrication for studies of tumor angiogenesis and vasculogenesis in vitro. *Biomaterials* **31,** 8596–8607 (2010).

83. Jeon, J. S., Zervantonakis, I. K., Chung, S., Kamm, R. D. & Charest, J. L. In vitro model of tumor cell extravasation. *PLoS One* **8,** e56910 (2013).

84. Barkan, D., Green, J. E. & Chambers, A. F. Extracellular matrix: A gatekeeper in the transition from dormancy to metastatic growth. *Eur. J. Cancer* **46,** 1181–1188 (2010).

85. Cox, R. F., Jenkinson, A., Pohl, K., O'Brien, F. J. & Morgan, M. P. Osteomimicry of mammary adenocarcinoma cells in vitro; increased expression of bone matrix proteins and proliferation within a 3D collagen environment. *PLoS One* **7,** e41679 (2012).

86. Egeblad, M., Rasch, M. G. & Weaver, V. M. Dynamic interplay between the collagen scaffold and tumor evolution. *Curr. Opin. Cell Biol.* **22,** 697–706 (2010).

87. Pedron, S., Becka, E. & Harley, B. A. C. Regulation of glioma cell phenotype in 3D matrices by hyaluronic acid. *Biomaterials* **34,** 7408–7417 (2013).

88. Ananthanarayanana, B., Kima, Y. & Kumara, S. Elucidating the mechanobiology of malignant brain tumors using a brain matrix-mimetic hyaluronic acid hydrogel platform. *Biomaterials* **32,** 7913–7923 (2011).

89. Miroshnikova, Y. *et al.* Engineering strategies to recapitulate epithelial morphogenesis within synthetic three-dimensional extracellular matrix with tunable mechanical properties. *Phys. Biol.* **8,** 026013 (2011).

90. Sharma, S. V, Haber, D. A. & Settleman, J. Cell line-based platforms to evaluate the therapeutic efficacy of candidate anticancer agents. *Nat. Rev. Cancer* **10,** 241–253 (2010).

91. Birgersdotter, A., Sandberg, R. & Ernberg, I. Gene expression perturbation in vitro - A growing case for three-dimensional (3D) culture systems. *Semin. Cancer Biol.* **15,** 405–412 (2005).

92. Leeper, A. D. *et al.* Determining tamoxifen sensitivity using primary breast cancer tissue in collagen-based three-dimensional culture. *Biomaterials* **33,** 907–915 (2012).

93. Truong, H. H. *et al.* Automated microinjection of cell-polymer suspensions in 3D ECM scaffolds for high-throughput quantitative cancer invasion screens. *Biomaterials* **33,** 181–188 (2012).

Chapter 2

Materials and methods

2.1 2D CULTURE OF MAMMALIAN CELLS

Human pancreatic adenocarcinoma (PANC-1) cell line was purchased from American Type Culture Collection (ATTC, CRL-1469). Human cervical adenocarcinoma (HeLa) cell line was purchased from ATTC (CCL-2). Green Fluorescent Protein (GFP)-labelled HeLa cell line was purchased from Cell Biolabs (AKR-213). Primary human normal dermal fibroblasts (hNDF) were kindly provided by Dr. Jesús Otero from Hospital Central de Asturias (Spain). GFP-labelled human foreskin fibroblasts (HFF) were kindly provided by Dr. Ángel Raya from Institute for Bioengineering of Catalonia (IBEC, Spain).

Cells were grown on traditional plastic flasks (75cm^2 of area) with culture medium consisting of Dulbecco's Modified Eagle's medium high glucose (4.5g/L) (DMEM, E15-009; PAA) supplemented with 10% (v/v) fetal bovine serum (FBS, DE14-801F; Lonza), 1% (v/v) L-glutamine (M11-044; PAA) and 1% (v/v) penicillin-streptomycin (L11-010; PAA). Cultures were maintained at 37°C in a humidified incubator equilibrated with 5% carbon dioxide (CO_2). All experiments were performed at 70 to 80% cell confluence using passages between 5 and 20.

2.2 3D CULTURE OF MAMMALIAN CELLS

2.2.1 3D CULTURE TECHNIQUE IN RAD16-I BIOMATERIAL

Self-assembling peptide RAD16-I (BD™ PuraMatrix™, 354250; BD Biosciences) was commercially available at a concentration of 10.0 mg/mL. To prepare RAD16-I scaffolds, the stock solution was diluted to a concentration two-fold higher than the desired one in 10% sucrose. In the present thesis, the final working concentrations of RAD16-I scaffold were 5.0, 3.0 and 1.5 mg/mL. Therefore, for encapsulations at 5.0 mg/mL, the stock solution was directly used. For encapsulations at 3.0 mg/mL peptide, 6.0 mg/mL peptide was prepared by diluting 600 µL of stock solution with 400 µL of 25% sucrose. For encapsulations at 1.5 mg/mL peptide, 3.0 mg/mL peptide was prepared by diluting 300 µL of stock solution with 700 µL of 14% sucrose. All these data is summarized in **Table 2.1**.

RAD16-I (Final concentration)	RAD16-I (Stock concentration)	RAD16-I (Commercial concentration 10 mg/mL)	Sucrose concentration	Sucrose volume
5.0 mg/mL	10.0 mg/mL	1000 µL		0 µL
3.0 mg/mL	6.0 mg/mL	600 µL	25% (w/v)	400 µL
1.5 mg/mL	3.0 mg/mL	300 µL	14% (w/v)	700 µL

Table 2.1. Protocol for the preparation of RAD16-I scaffolds.

Then, 9 mm diameter cell culture inserts (PICM01250; Millipore) were placed inside 6-well culture plates and their membrane was wet with 500 µL of culture medium. In the particular case in which encapsulations are forced to attach to the insert, the membrane was not wet prior to the loading of cells and peptide mixture. Therefore, spontaneous contraction of the encapsulation was mechanically blocked. Mammalian cells were harvested by trypsinization from the 2D culture flasks and suspended in 10% (w/v) sucrose to get a final concentration of $2 \cdot 10^6$ cells/mL. For co-culturing experiments, the cell suspension of $2 \cdot 10^6$ cells/mL contained $1 \cdot 10^6$ cells/mL of each cell type (50:50). 10% sucrose is an isotonic and nonionic solution that mantains physiological osmotic pressure and avoids RAD16-I self-assembling process during the mixing step.

Equal volumes of cell suspension and liquid peptide solution were mixed to obtain a final suspension of $2 \cdot 10^6$ cells/mL in 5.0, 3.0 and 1.5 mg/mL of RAD16-I. The suspension was loaded into the inserts, using different volumes (80 or 40 µL) depending on the experiment. The peptide was left gelling for approximately 20 minutes. During this waiting time, the higher ionic strength and the neutral pH of the medium, which was in contact with cell suspension and RAD16-I through the insert membrane, induced the spontaneous self-assembling of the peptide. Finally, a total volume of 500 µL of culture medium was added into the insert in consecutive small portions, favoring the leaching of the sucrose. The remaining medium in the well, rich in sucrose, was aspirated and replaced with fresh medium. Change of medium was done every day by removing 500 µL from the well and adding 500 µL of fresh medium into the insert. A schematic representation of the protocol is shown in **Figure 2.1**

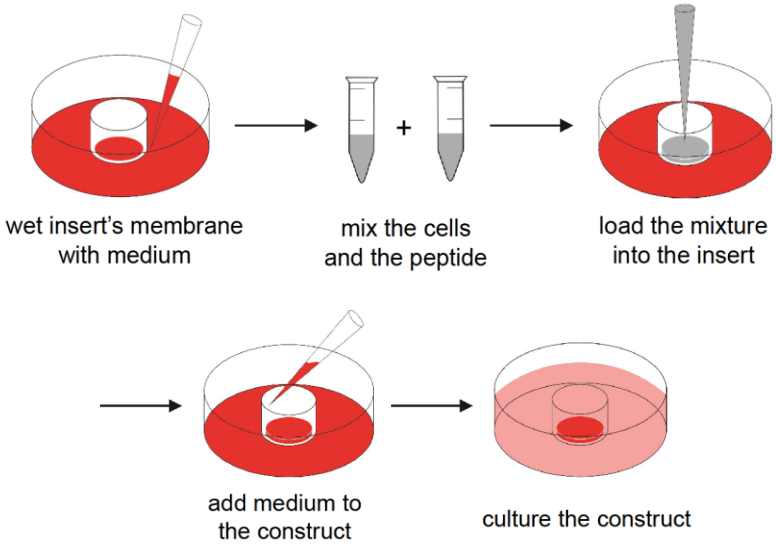

Figure 2.1. Schematic representation of the protocol for cell encapsulation in RAD16-I peptide. First step consists in wetting the membrane of the insert with culture medium. Then, cells are mixed with the liquid solution of self-assembling peptide. The mixture is loaded into the insert and medium diffuses into the suspension through the membrane, which induces the spontaneous self-assembling of RAD16-I. Washing steps are performed with culture medium in order to favor the leaching of the sucrose. Finally, the well and the insert are filled with medium.

2.2.2 3D CULTURE TECHNIQUE IN COLLAGEN BIOMATERIAL

Natural type I collagen (354249; BD Biosciences) was extracted from rat tail and commercially available at a concentration of 10.0 mg/mL. In the present thesis, the final working concentrations were 5.0, 3.0 and 1.5 mg/mL. To prepare 5.0 mg/mL collagen scaffolds, 1 µL of Phenol Red was mixed with 99 µL of phosphate buffered saline 10x (PBS), 800 µL of collagen type I 10.0 mg/mL and 100 µL of tissue culture water in order to obtain 1 mL of 8.0 mg/mL collagen solution. To prepare 3.0 mg/mL collagen scaffolds, 1 µL of Phenol Red was mixed with 99 µL of 10x PBS, 600 µL of collagen type I 10.0 mg/mL and 300 µL of tissue culture water in order to obtain 1 mL of 6.0 mg/mL collagen solution. To prepare 1.5 mg/mL of collagen scaffolds, 1 µL of Phenol Red was mixed with 99 µL of PBS 10x, 300 µL of collagen type I 10.0 mg/mL and 600 µL of tissue culture water in order to obtain 1 mL of 3.0 mg/mL collagen solution. All these data is summarized in **Table 2.2.**

Collagen (Final concentration)	Collagen (Stock concentration)	Collagen (Commercial concentration 10 mg/mL)	H_2O	PBS 10x	Phenol Red
5.0 mg/mL	8.0 mg/mL	800 µL	100 µL	99 µL	1 µL
3.0 mg/mL	6.0 mg/mL	600 µL	300 µL	99 µL	1 µL
1.5 mg/mL	3.0 mg/mL	300 µL	600 µL	99 µL	1 µL

Table 2.2. Protocol for the preparation of collagen scaffolds.

All solutions were brought to alkalinity to induce the gelation of collagen, using sodium hydroxide until the pH ranged from 8 to 9, which was checked with a pH test paper. Consequently, the color of the solution shifted from yellow to pink due to the presence of the Phenol Red pH indicator. This step was performed in ice to avoid collagen gelation before mixing it with cells, since the self-assembling process goes more slowly at colder temperatures.

Following collagen preparation, mammalian cells were harvested from the 2D culture flasks by trypsinization and suspended in PBS 1x to a final concentration of $2 \cdot 10^6$ cells/mL. For co-culturing experiments, the cell suspension of $2 \cdot 10^6$ cells/mL contained $1 \cdot 10^6$ cells/mL of each cell type (50:50). To obtain the required concentrations of collagen scaffolds, the following mixtures were performed: for 5.0 mg/mL, 50 µL of collagen 8.0 mg/ml and 30 µL of cell suspension; for 3.0 mg/mL, 40 µL of collagen 6.0 mg/ml and 40 µL of cell suspension; for 1.5 mg/mL, 40 µL of collagen 3.0 mg/ml and 40 µL of cell suspension. These volumes referred to the preparation of a single construct (80 µL). Constructs of 40 µL were also prepared, following the same volume-concentration ratios. Finally, 80 or 40 µL of the suspension were loaded into 48 well culture plates. Collagen was left gelling for approximately 30 minutes at 37°C. After gelation, 700 µL of medium were added on top of the construct. A change of medium was performed every day by removing 500 µL from the well and adding 500 µL of fresh medium.

2.3 3D CULTURE CHARACTERIZATION

2.3.1 CELL MORPHOLOGY ASSESSMENT

Cell morphology and organization within the 3D cultures were evaluated by fluorescence microscopy. In particular, nuclei and actin filaments were stained with 4',6-diamidino-2-phenylindole (DAPI, D1306; Molecular Probes) and phalloidin-tetramethylrhodamine B isothiocyanate (Phalloidin-TRITC, P1951; Sigma) dyes respectively. In particular, DAPI is a blue fluorescent probe that selectively binds to the minor groove of double stranded DNA, where its fluorescence is approximately 20-fold greater than in the unbound state. Phalloidin is attached to TRITC and binds polymeric F-actin and inhibits microfilament de-polymerization, revealing the distribution of actin filaments and enabling the visualization of the cytoskeleton.

Cells were cultured in the 3D scaffolds during 1 and 10 days. Then, 3D cultures were washed with PBS and fixed with 1 % (w/v) paraformaldehyde (PFA) for 1 hour. After the fixation protocol, they were incubated in 0.1 % (v/v) Triton x-100 in PBS for 30 minutes to permeabilize the cell membrane. Finally, they were incubated during 25 minutes with Phalloidin-TRITC (ext 540/em 570 nm) and 5 minutes with DAPI (ext 364/em 454 nm), both reagents at a final concentration of 0.1 µg/ml in PBS. After washing steps with PBS, samples were examined under a Zeiss Axiovert inverted microscope (Axiovert 200M; Carl Zeiss Inc.) with the Zeiss ApoTome system.

Cell morphology and organization was also analyzed by field emission gun–scanning electron microscopy (FEG-SEM). 3D cultures were washed with PBS, fixed with 5% (w/v) gluteraldehyde for 1h. Then, samples were submitted to a dehydration process, which included several immersions in ethanolic solutions during 10 minutes: once in 30% (v/v) ethanol, twice in 50% (v/v) ethanol, three times in 70% (v/v) ethanol, three times in 90% (v/v) ethanol, three times in 96% (v/v) and three times in 100% (v/v) ethanol. Samples were dried using a CO_2 critical point dryer (Polaron, CPD Jumbo E-3100), where ethanol was slowly exchanged by CO_2. Then, they were sputter-coated with a gold and platinum alloy using Emitech SC7620 (60 s, 18mA and chamber pressure 0.2 mbar) and examined with a FEG-SEM (JEOL JSM-7100F) at 13 kV.

2.3.2 3D VIABILITY ASSESSMENT

Cell viability was examined using LIVE/DEAD® Viability/Cytotoxicity Kit for mammalian cells (L3224; Invitrogen). In particular, calcein acetomethyl ester (calcein-AM) is transported into cells through their membrane. There, ubiquitous intracellular esterases removed the acetomethoxy group, leading to calcein that produces green fluorescence. On the other hand, ethidium homodimer-1 only enters cells with damaged membrane. There, it binds to nucleic acids and undergoes an enhancement of its fluorescence.

Cells were cultured in the 3D scaffolds during 1 and 10 days. Then, 3D cultures were washed with PBS and covered with calcein-AM (ex 494/em 517 nm) and ethidium homodimer-1 (ex 528/em 617 nm) for 15 minutes, both reagents at a final concentration of 2 µM in PBS. Then, constructs were washed with PBS in order to remove the excess of reagents and were examined under a Zeiss Axiovert inverted microscope (Axiovert 200M, Carl Zeiss Inc.) with the Zeiss ApoTome system.

2.3.3 MECHANICAL PROPERTIES ASSESSMENT

3D cultures were washed with PBS and fixed with 2% (w/v) PFA during 1 hour. A compression assay was performed in DMA Q800 (TA Instruments), using Dynamic Mechanical Assay (DMA) Multi-Frequency-Strain mode and a frequency sweep test. The conditions of the assay were: Amplitude= 1 µm, Preload force= 0.001 N and Frequency= 1 Hz. Construct diameter and thickness were measured for each sample. Results were obtained with TA Instrument Explorer software and analyzed with TA Universal analysis software.

2.4 GENE EXPRESSION BY REAL TIME RT-PCR

Real time reverse transcription polymerase chain reaction (Real Time RT-PCR) was performed in order to analyze gene expression in 2D and 3D cultures. The first step was RNA extraction, followed by complementary DNA (cDNA) synthesis and Real Time RT-PCR reactions.

2.4.1 RNA EXTRACTION AND PURIFICATION

2D and 3D cultures were washed with PBS. Then, they were lysed with RNA lysis buffer (12-6834-02; Peqlab) with immediate inactivation of endogenous and exogenous RNases. Constructs were disrupted by pipetting up and down with the micropipette or a pestle and stored at -80ºC. Then, RNA was isolated and purified with PeqGold Total RNA kit (12-6834-02, Peqlab), according to manufacturer's instructions. Briefly, the kit provided a quick method for total RNA isolation based on the reversible binding characteristics of RNA to PerfectBind silica filters in centrifugation columns.

The amount and purity of RNA was determined by measuring its absorbance at 230, 260, 280 and 320 nm with the spectrophotometer. In particular, RNA absorbs at 260 nm because of the double bonds of their nitrogenous bases. The quantification by this technique may be affected by scattering of light and impurities such as protein, phenol or other contaminants that also absorb near 260 nm. For this reason, some correction parameters are introduced. Absorbance at 320 nm corrects light scattering due to dust particles. Absorbance at 230 nm gives

information about contamination by chemicals: alcohol, phenol, guanidinium from the lysis buffer that can cause overestimation of RNA concentration. So, A260/A230 ratio could be calculated as indicated in **Equation 2.1**. To ensure a good RNA quantification, the ratio value should be in the range of 2-2.4.

$$A260/A230 = (A260 – A320) / (A230 – A320)$$

Equation 2.1. Relationship between nucleic acids and chemical impurities.

Absorbance at 280 nm gives information about protein contamination. For this reason, A260/A280 ratio was used to assess the purity of RNA (**Equation 2.2**). The ratio value should be in the range of 1.8-2.1.

$$A260/A280 = (A260 – A320) / (A280 – A320)$$

Equation 2.2. Relationship between nucleic acids and proteins.

The concentration of nucleic acid could be determined using Lambert-Beer's law, which predicts a linear change in absorbance with concentration (**Equation 2.3**).

$$A = \varepsilon \cdot l \cdot C$$

Equation 2.3. Lambert-Beer's law

Where A is absorbance, ε is the molar extinction coefficient, l is the light path traversed (1 cm with a standard cuvette) and C is the concentration of the absorbent substance. Although the extinction coefficient of nucleic acids depends on the particular sequence of nucleotides, some values could be estimated depending on nucleic acids type (**Table 2.3**).

Nucleic acids	Extinction coefficient ($cm^{-1} \cdot M^{-1}$)
Double stranded DNA	0.02
Single stranded DNA	0.03
RNA	0.025

Table 2.3. Extinction coefficient for different nucleic acids.

Consequently, the RNA amount was calculated as follows (**Equation 2.4**):

$$[RNA] / \mu g \cdot ml\text{-}1 = (A260 – A320) \times (1/0.025) \times \text{dilution factor}$$

Equation 2.4. RNA concentration.

2.4.2 cDNA SYNTHESIS

First, RNA was purified from genomic DNA with the Turbo DNA-free kit (AM1907; Applied Biosystems), according to manufacturer's instructions. Briefly, TURBO DNase Buffer and TURBO DNase were added to RNA sample and mixed gently. Then, samples were incubated at 37°C for 20–30 minutes. DNase Inactivation Reagent was added and incubated during 5 minutes at room temperature. Samples were centrifuged and transferred to a fresh tube.

cDNA was synthesized using a reverse transcriptase enzyme with the High Capacity cDNA Reverse Transcription Kit (4368814; Applied Biosystems), according to manufacturer's instructions. First, a master mix was prepared mixing MultiScribe™ Reverse Transcriptase, Reverse Transcriptase Buffer, dNTPs Mix and Primer Mix. Then, RNA was mixed with the corresponding volume of master mix. The reaction for cDNA synthesis was performed at 42°C and was then inactivated at 95°C. Primer Mix contained a specially optimized mix of oligo-dT and random primers that enable cDNA synthesis from all regions of RNA transcripts, even from 5' regions.

2.4.3 REAL TIME RT-PCR REACTIONS

Real Time RT-PCR reactions were performed with LightCycler® 480 Real-Time PCR System (Roche), using the iQ™ SYBR® Green Supermix (170-8882; Bio-Rad) as fluorescent reporter. SYBR® Green binds to double-stranded DNA and upon excitation emits fluorescence. Primers were designed using Primer Blast software from National Center for Biotechnology Information (NCBI). The following considerations were taken: a melting temperature around 60ºC, maximum of CG content of 60% (optimum between 40-50%), ending with cytosine or guanine bases, maximum of 3-4 dimmers and hairpins, 15-30 base pair of primer length and 200-80 base pair of PCR product length. Primers sequences are shown in **Table 2.4**:

Gene symbol	F/R	Primer sequence (5' to 3')	Length (bp)	Tm (ºC)
CDH1	F	AGCCAAAGACAGAGCGGAAC	20	60
	R	AAGCAGGCACTTGGGGATTC	20	60
SNAI1	F	TAGCGAGTGGTTCTTCTGCG	20	60
	R	AGGGCTGCTGGAAGGTAAAC	20	60
ZEB2	F	CCCAGGAGGAAAAACGTGGT	20	60
	R	CTGGACCATCTACAGAGGCTT	21	60
VEGF	F	TTGCTGCTCTACCTCCACCATGC	23	60
	R	GATGTCCACCAGGGTCTCGATTG	23	60
IGFBP3	F	CGGGTGTCTGATCCCAAGTTCC	22	60
	R	GTGTCTTCCATTTCTCTACGGCAGG	25	60
VEGFR2	F	CAAGTGGCTAAGGGCATGGA	20	60

	R	ATTTCAAAGGGAGGCGAGCA	20	60
FGFR2	F	CGCTGGGGAATATACGTGCT	20	60
	R	AGTCTGGCTTCTTGGTCGTG	20	60
IGFR1	F	AGCCTCCTGTGAAAGTGACG	20	60
	R	GTAGTAAGATGCCGGGCTCC	20	60

Table 2.4. Real Time RT-PCR primer sequences. Primers belong to human E-cadherin (CDH1), snail zing finger 1 (SNAI1), zinc finger E-box-binding 2 (ZEB2), vascular endothelial growth factor (VEGF), insulin-like growth factor-binding protein 3 (IGFBP3), VEGF receptor 2 (VEGFR2), fibroblast growth factor receptor 2 (FGFR2) and IGF receptor 1 (IGFR1).

Real-time RT-PCR was run with the following parameters: 1 cycle of 10 minutes at 95°C in order to activate the hot-start iTaq™ DNA polymerase, 40 cycles consisting in 15 seconds at 94°C for denaturation of the double stranded cDNA, 15 seconds at 60°C for primer annealing and 15 seconds at 72°C for extension. Finally, melting curve analyses and agarose electrophoresis were performed to test the specificity of PCR products. Relative gene fold variations were determined by the comparative CT method ($2^{-\Delta\Delta Ct}$)[1]. Expression of the target genes was normalized to housekeeping gene (ribosomal protein 27L, *RPL27*). The selection of a candidate housekeeping gene was critical when performing Real Time RT-PCR experiments.

2.4.4 HOUSEKEEPING GENES SELECTION

Housekeeping gene expression was used to standardize the amount of biological material between samples. Therefore, its expression pattern should remain unaffected by experimental conditions, being 2D versus 3D microenvironments. For this purpose, different housekeeping genes were selected: 18S ribosomal RNA (*18S*) and ribosomal proteins L22, L27, L30 (*RPL22, RPL27* and *RPL30*). Mammalian cells were grown in 2D and 3D cultures (RAD16-I and collagen scaffold). Then, RNA was extracted, cDNA was synthetized and Real Time RT-PCR reactions were performed.

It has been reported that 18S or 28S rRNA molecules do not represent good candidates for housekeeping genes, because mRNA and rRNA fractions are imbalanced. In particular, the total RNA fraction of a sample contains only a relatively small percentage of mRNA (10%), whereas rRNA molecules are predominant. In addition, certain biological factors and drugs may affect rRNA transcription. On the other hand, ribosomal proteins as S13, L27, L30, L22 showed an enhanced stability among a multitude of different experimental conditions[2,3]. In this particular study, the most stable HKGs under 2D versus 3D cultures conditions were *RPL27* and *RPL22* (**Figure 2.2**).

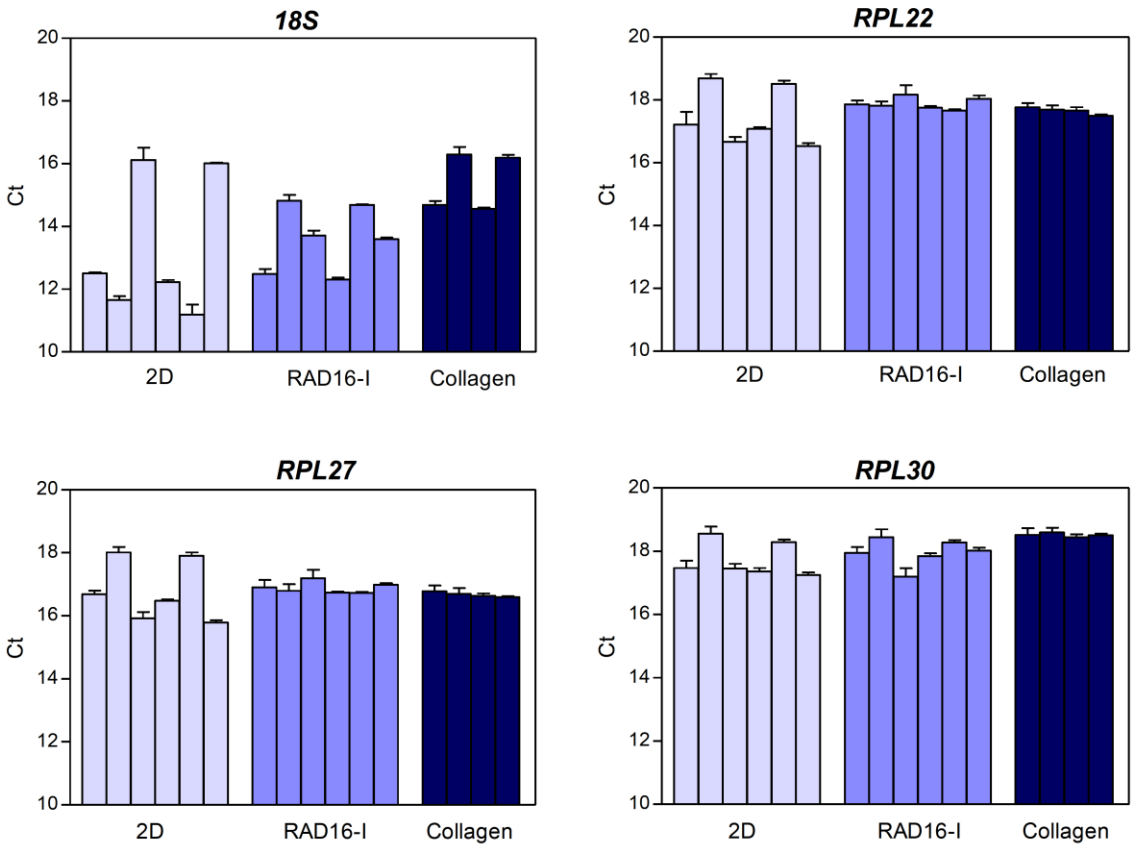

Figure 2.2. Selection of the optimal housekeeping gene for comparing 2D and 3D cultures. PANC-1 cells were cultured in different conditions (monolayers, RAD16-I scaffold and collagen scaffold). RNA was extracted and purified and cDNA synthesis was performed. Finally, Real Time RT-PCR reactions were run using 6 biological replicates for each condition. The obtained cycle threshold was compared for the candidate housekeeping genes (18S, RPL22, RPL27 and RPL30).

2.5 METHYLATION-SPECIFIC PCR

2.5.1 DNA EXTRACTION AND PURIFICATION

2D and 3D cultures were washed with PBS and lysed with DNA lysis buffer (56304; Qiagen), working with denaturing conditions (56ºC) and the presence of Proteinase K. Samples were disrupted by pipetting up and down with a micropipette or a pestle. Next, RNA was degraded using RNase A enzyme (19101; Qiagen). DNA was isolated and purified with the QIAamp DNA Micro Kit (56304; Qiagen), according to manufacturer's instructions. Briefly, samples were transferred to QIAamp MinElute Column, where DNA was adsorbed into the silica gel membrane. Consecutive washes were performed to wash out cellular debris and proteins, among other contaminants and DNA was eluted. The quantity and purity of DNA was determined by the absorbance at 230 nm, 260 nm, 280 nm and 320 nm wavelengths.

Bisulfite assay was based on the chemical modification of DNA sequence by converting all the unmethylated cytosines to uracils. The methylated cytosines were protected from this reaction (**Figure 2.3**).

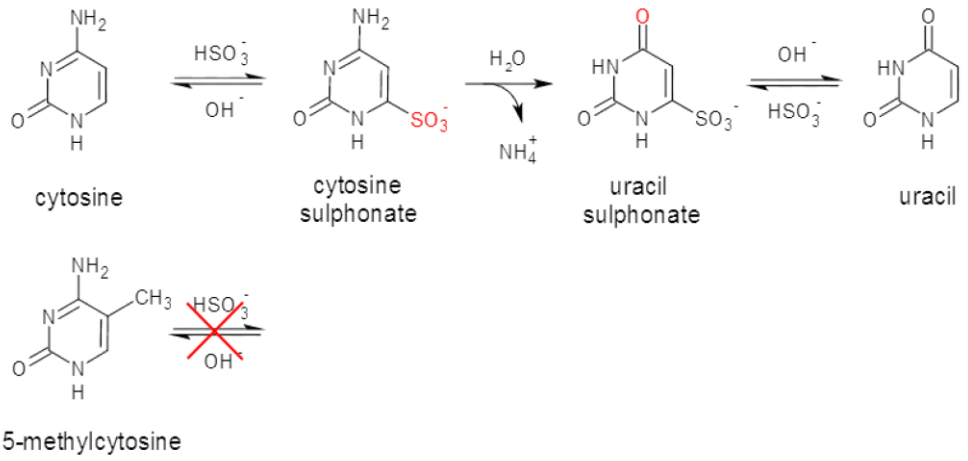

Figure 2.3. Schematic overview of bisulfite reaction. Genomic DNA is thermally denatured and bisulfite reagent is added. Unmethylated cytosines are sulphonated and deaminated, being converted to sulphonated uracils, which are subsequently desulphonated. Methylated cytosines are protected from this chemical conversion.

This treatment was performed with the *EpiTect® Bisulfite kit* (59104; Qiagen), according to manufacturer's instructions. Briefly, bisulfite reactions were prepared by adding the appropriate amount of DNA, bisulfite reagent, DNA protect Buffer and DNAse-free water. Reactions were performed with a thermal cycler and the following parameters: 5 minutes at 99ºC for denaturation, 25 minutes at 60ºC for incubation, 5 minutes at 99ºC for denaturation, 85 minutes at 60ºC for incubation, 5 minutes at 99ºC for denaturation and 175 minutes at 60ºC for incubation. During these steps, DNA suffered a thermal denaturation followed by a subsequent unmethylated cytosine sulfonation and deamination, converting unmethylated cytosines to uracils. Next, bisulfite reactions were cleaned-up form bisulfite salts and other chemicals by adsorption of DNA to EpiTect spin columns and consecutive washing steps with buffers. Membrane-bound DNA was desulfonated, removing desulfonation reagent through more washing steps. Finally, converted DNA was eluted from the spin column.

2.5.2 METHYLATION-SPECIFIC PCR

Methylation-specific PCR experiments were performed with Cristina Castells Sala as part of her PhD thesis.

DNA was amplified with a PCR reaction. The primers belong to the promoter region of the target gene (*CDH1* gene) and did not contain any CpG island. The parameters were the following: 1 cycle of 10 minutes at 95ºC in order to activate the hot-start DNA polymerase, 40

cycles consisting in 45 seconds at 94ºC for denaturation, 45 seconds at 53ºC for primer annealing and 90 seconds at 72ºC for extension. PCR reaction was performed using Platinium Taq Polymerase (10966018; Invitrogen). This polymerase has a nontemplate-dependent terminal transferase activity that adds a single adenosine to the 3' ends of PCR products, required for molecular cloning. Resulting PCR products were analyzed using 2% (w/v) agarose gels (**Table 2.5**).

Gene symbol	F/R	Primer sequence (5' to 3')	Lenght (bp)	Tm (ºC)
CDH1met	F	GTAATTTTAGGTTAGAGGGTTA	22	58
	R	CTCCAAAAACCCATAACTAAC	21	58

Table 2.5. Primer sequences for methylation-specific PCR.

2.5.3 DNA CLONING AND SEQUENCING

Molecular cloning of DNA sequences was performed with the TOPO TA Cloning Kit (K4500-01; Invitrogen), according to manufacturer's instructions. The kit provided a linearized vector with a single 3'-thymine overhanging and a Topoisomerase I enzyme covalently bound to it. On the other hand, the obtained DNA sequences had a single adenosine overhanging in 3' ends due to terminal transferase activity of the Platinium Taq Polymerse used during methylation-specific PCR. Therefore, ligation reaction was performed by simply mixing the PCR products with the vector.

Next, pCR II-TOPO plasmid was transformed into competent *E.coli* bacteria (DH5α-TOP10 *E.coli* Competent Cells, K4500-01; Invitrogen). For this purpose, the ligation probe was incubated with the competent bacteria during 30 minutes. During this time, DNA gets closer to bacteria membrane, which is positively charged because of the calcium method used for making them competent. Then, a heat shock was applied to permeabilize cell membrane and allow the entry of plasmid. Finally, bacteria were grown overnight on LB-Glucose (*0.2%(w/v)*)-Ampicillin (100 µg/mL) plate.

The third step in molecular cloning consisted in the selection of bacterial cells with internalized plasmids. The plasmid had two selections genes: one for ampicillin resistance and the other for β-galactosidose production. During the ligation step, DNA was inserted disrupting β-galactosidose enzyme in two peptides, LacZα and LacZΩ. They are not active by themselves, but together they reassemble into the functional enzyme. The LB plate contained ampicillin and 5-bromo-4-chloro-3-indolyl-β-D-galactopyranoside (X-gal). This reagent is a substrate for β-galactosidose, which is able to hydrolyze it and yield an insoluble blue compound. Therefore, positive cells were able to grow in ampicillin plate and showed a blue color.

Positive bacterial cells were analyzed through Colony PCR. Briefly, some cells were selected for each experimental condition (2D, RAD16-I scaffold and collagen scaffold after 1-

and 10-day culture). These clones were directly added to the PCR reaction using a pipette tip. The reaction contained the Platinum Taq Polymerase, dNTPs and primers for the plasmid (Sp6 Promoter as forward primer and T7 Promoter as reverse primer) (**Table 2.6**). PCR products were analyzed with 2% (w/v) agarose gel.

Gene symbol	F/R	Primer sequence (5' to 3')	Lenght (bp)	Tm (ºC)
Sp6 Promoter	F	GCCAAGCTATTTAGGTGACACTATAG	26	50
T7 Promoter	R	GAATTGTAATACGACTCACTATAGGG	26	50

Table 2.6. Primers sequence for PCR colony reaction.

Finally, a liquid bacterial culture was performed for the selected clones. Plasmids were isolated with the GenElute^{TM} Plamid Miniprep kit (PLN350; Sigma Aldrich). Briefly, bacterial cells were lysed and samples were added to a binding column. Consequently, plasmid DNA was adsorbed to the silica matrix. Consecutive washing steps were performed and DNA was eluted.

Desired plasmids were send to sequence (Macrogen). To analyze the sequences, BiQ Analyzer software (Max Plank Institute) was used. In particular, *CDH1* promoter region from NCBI database was aligned with the obtained DNA sequences.

2.6 PROTEIN EXPRESSION BY WESTERN BLOT

Western Blot was performed in order to analyze protein expression in 2D and 3D cultures. Samples were washed with PBS and lysed with protein lysis buffer, composed of radioimmunoprecipitation assay (RIPA) and a protease inhibitor cocktail (1836153; Roche). Constructs were disrupted by pipetting up and down with the micropipette or a pestle. In the case of obtaining not homogeneous samples, constructs were sonicated for 5 minutes. Then, they were stored at -20ºC.

Running gel was prepared based on 10% sodium dodecyl sulphate (SDS)-polyacrylamide gel (PAGE) solution and placed in the electrophoresis support to let it polymerize. Next, solution for stacking gel was prepared and placed on top of running gel. Electrophoresis buffer was prepared and the inner and outer electrophoresis cavities were filled with it. Total protein content from 2D and 3D samples was determined by bicinchoninic acid (BCA) Protein Assay (23227; Thermo Scientific), using bovine serum albumin (BSA) as calibration standards. Samples were aliquot containing 15 mg of protein each one. Then, they were mixed with protein loading buffer containing β-mercaptoethanol and heated at 95ºC during 10 minutes.

Samples were loaded into the wells of stacking gel. Constant voltage (150 V) was applied to the system, controlling running time through bromophenol front. Proteins of the gel were transferred onto polyvinylidene difluoride (PVDF) membrane for approximately 2 hours at 40 V and incubated in blocking buffer NaCl/Tris-Tween supplemented with 5% (w/v) skimmed milk for 2 hours. Then, membranes were incubated with primary antibody solution (E-cadherin, dilution 1:2500, 610181; BD Biosciences) for 2 hours at room temperature or overnight at 4ºC. After three washes of 10 minutes each in NaCl/Tris-Tween, membranes were incubated with anti-rabbit IgG horseradish peroxidase (HRP)-linked secondary antibody for 2 hours. Reactive bands were revealed using enhanced chemiluminescence reagents (luminol).

2.7 PHOTODYNAMIC THERAPY

2.7.1 PHOTOSENSITIZERS CONDITIONS

The cationic 5,10,15,20-tetrakis(N-methyl-4-pyridyl)-21H,23H-porphine was purchased from Sigma Aldrich (TMPyP, 323497). Zinc(II)-phthalocyanine was purchased from Sigma Aldrich (ZnPc, 341169). It was encapsulated in liposomes of 1-palmitoyl-2-oleoyl-*sn*-glycero-3-phosphocoline (POPC) and 1,2-dioleoyl-*sn*-glycer-3-[phosphor-*L*-serine] (OOPS), using a molar ratio of ZnPc: POPC: OOPS 1:90:10. Liposomes were developed by QLT Phototherapeutics, sponsored by Ciba Geigy (Novartis) and kindly provided by Professor Giulio Jori from Padua University (Italy). Photosensitizers were suspended in FBS-free culture medium at the final concentration indicated in **Table 2.7.**

Photosensitizers (PS)	[PS]/M	Incubation / hours	Light fluence /J·cm^{-2}	Irradiation wavelength/nm
TMPyP *proof of concept*	$5\cdot10^{-4}$-$1\cdot10^{-1}$	24	6 and 18	520-550
TMPyP *in vitro*	$1\cdot10^{-6}$	1	3.6	620-645
TMPyP *in vivo*	$3.5\cdot10^{-6}$	3	70	620-645
ZnPc *in vitro*	$5\cdot10^{-8}$	1	3.6	620-645
ZnPc *in vivo*	$9\cdot10^{-7}$	3	70	620-645

Table 2.7. Photosensitizers and light conditions used for photodynamic therapy

2.7.2 PHOTOSENSITIZERS UPTAKE

Cell internalization of photosensitizers (PSs) was determined by fluorescence spectroscopy and flow cytometry. For this purpose, cells were grown during 4-6 days in 3D

cultures and incubated in the dark with TMPyP and/or ZnPC at the corresponding concentrations (**Table 2.7**).

For fluorescence spectroscopy experiments, 2D and 3D cultures were washed with PBS and cells were lysed with 2% (w/v) sodium dodecyl sulphate in Milli-Q water. The resulting suspensions were centrifuged. The extent of PS uptake was assessed by measuring the fluorescence of the supernatants and normalizing them to their protein content with BCA assay. Appropriate controls were performed to ensure that signals were originated from PS molecules internalized by cells.

For flow cytometry experiments, 2D and 3D cultures were washed with PBS. Then, 2D and RAD16-I cultures were digested with trypsin (0.05 %/0.02 % trypsin-EDTA; Invitrogen) during 5 and 15 minutes respectively. On the other hand, collagen cultures were digested with collagenase (1 mg/mL; Sigma) during 15 minutes. All digested 3D cultures were pipetted up and down. Both enzymes were neutralized with the double volume of culture media. The resulting cellular suspensions were centrifuged and analyzed on a flow cytometer (BD FACSCanto II; BD Biosciences). In particular, TMPyP was measured using a 420-nm laser for excitation and a 650-nm filter for detection. ZnPc was measured using a 670-nm laser for excitation and 680-nm filter for detection.

2.7.3 PHOTOSENSITIZERS LOCATION

Cell location of PSs was determined by fluorescence microscopy. For 2D cultures, cells were grown on round coverslips (25 mm diameter) towards 80-85% confluence. For 3D cultures, cells were grown during 4-6 days in RAD16-I and collagen scaffolds. Both cultures were incubated in the dark with TMPyP and/or ZnPC at the corresponding concentrations. After some washing steps with PBS, cultures were incubated with Hoechst dye (33342; Molecular Probes) at a final concentration of 2.5 mg/mL during 30 minutes for nuclei staining. Finally, cultures were washed with PBS and examined under two-photon excitation microscopy (TCS-SP5; Leica). All images were uniformly adjusted for brightness and contrast.

2.7.4 PHOTOSENSITIZING REACTIONS

For 2D cell cultures, cells were seeded in 48-well plates and cultured toward 80%–85% confluence. For 3D cell cultures cells were grown during 4-6 days in RAD16-I and collagen scaffolds. To select the PS working concentration, both cultures were incubated in the dark with FBS-free culture media containing the concentration depicted in **Table 2.7**. Then, cultures were washed with PBS and cellular viability was assessed by MTT assay 24h after treatment. Dark cytotoxicity experiments yielded a survival cell fraction higher than 85%, demonstrating that

incubation with PSs at the working concentrations did not induce significant cell death without irradiation.

Photodynamic treatments were carried out after PS incubation in the dark during the incubation time depicted in **Table 2.7**. Cultures were washed with PBS and irradiated with the appropriate light fluences (from 6 to 70 J/cm^2) using a green or a red light LED source (520–550 nm; 620-645 nm for TMPyP and ZnPc respectively) at a fluence rate of 29 mW/cm^2. Cell viability was assessed by LIVE/DEAD® Viability/Cytotoxicity Kit (Invitrogen, previously explained), MTT assay and flow cytometry 24h after treatment. To decouple oxygen and drug gradients, additional photodynamic treatments were performed in an oxygen-saturated atmosphere during illumination by bubbling a stream of oxygen through the culture media of the 3D cultures.

For MTT assay, cell viability was examined incubating samples with 3-[4,5-dimethylthiazol-2-yl]-2,5-diphenyl tetrazolium bromide (MTT, M5655; Sigma). It is a water soluble tetrazolium salt, which yields a yellowish solution when prepared in PBS or culture medium. This dissolved MTT is converted into insoluble purple formazan crystals by cleavage of the tetrazolium ring by dehydrogenase enzymes. Therefore, this reaction only takes place when mitochondrial dehydrogenases are active, being used as a measure of viable cells. Formazan crystals can be solubilized using dimethyl sulfoxide (DMSO) and measured spectrophotometrically at 550 nm (**Figure 2.4**).

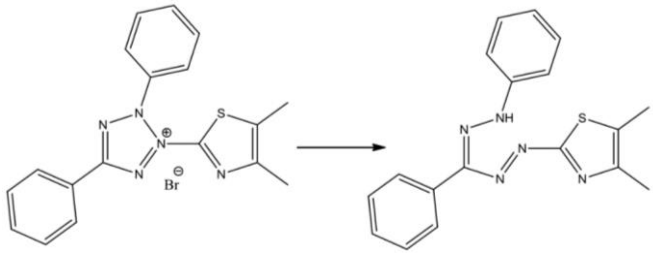

Figure 2.4. Reduction of MTT to formazan. This reaction is catalyzed by dehydrogenase enzymes and enables the assessment of cellular viability through spectrophotometry.

First, a MTT stock solution (10 mg/mL) was prepared with PBS, filtered through a 0.2 µm filter and stored at 2-8ºC. Then, MTT stock solution was dissolved with culture medium to a final concentration of 0.5 mg/mL. Then, it was incubated with 2D and 3D cultures during 3 hours at 37ºC. Following the incubation period, MTT solution was removed and formazan crystals solubilized with DMSO. Specifically, RAD16-I cultures were lysed by adding 300 µL of DMSO and pipetting up and down. In the case of collagen cultures, a mixture of 250 µL DMSO and 50 µL of collagenase was added. All solutions were let shaking for a minimum time of 15 minutes. Finally, their absorbance was read at 562 nm for triplicate. Three control wells of DMSO alone were included as blanks for absorbance readings. Cell viability was obtained from absorbance values, using **Equation 2.5.**

$$\text{Cell viability} = (Abs_{sample} - Abs_{blank})/(Abs_{control} - Abs_{blank})*100$$

Equation 2.5. Cell viability by MTT assay.

For flow cytometry experiments, cell viability was examined using Sytox Blue Dead Cell Stain (S34857; Molecular Probes). In particular, this dye cannot cross intact cell membrane and only enters to damaged cells, where binds to the double stranded DNA and increases its fluorescence. 2D and RAD16-I cultures were digested with trypsin and collagen cultures with collagenase, as previously explained. The resulting cellular suspensions were centrifuged. Then, collected cells were analyzed with a flow cytometer (BD FACSCanto II; BD Biosciences). In co-culture samples, cells were distinguished through fluorescence of GFP, analyzing the intrinsic viability of the two cell populations. The lasers and filters used are depicted in **Table 2.8**.

Fluorescent dye	Laser	Excitation wavelength/nm	Emission wavelength/nm	PMT name
TMPyP	405	420	650	V660
ZnPc	640	670	680	R660
Sytox Blue	405	444	480	V515
GFP	488	489	510	B530

Table 2.8. Excitation and emission wavelength for flow cytometry experiments. PMT is photomultiplier tube.

2.7.5 SINGLET OXYGEN MEASUREMENTS

Singlet oxygen ($^1O_2$) measurements were performed with Dr. María García Díaz as part of her PhD thesis.

For 2D cultures, cells were grown in 75 cm^2 flasks towards 80% confluence. They were incubated in the dark with the appropriate concentration and time incubation of PS (**Table 2.7.** Photosensitizers and light conditions used for photodynamic therapy). Cultures were washed with PBS, trypsinized and re-suspended in 1.5 mL of PBS or deuterium PBS (d-PBS) to a final concentration of $4 \cdot 10^6$ cells/mL. Cell suspensions were continuously stirred during the measurements.

For 3D cultures, cells were grown in RAD16-I and collagen scaffolds as previously described. They were incubated in the dark with the appropriate concentration and time incubation of PS (**Table 2.7.** Photosensitizers and light conditions used for photodynamic therapy). They were washed with PBS and carefully transferred to a 1-cm quartz cuvette. For deuterium oxide (D_2O)-based measurements, 3D cultures were incubated with d-PBS for 20 minutes before measurements to exchange the extracellular H_2O with D_2O. For control measurements, RAD16-I and collagen scaffolds without cells were obtained by inducing the self-assembling process of both peptides directly in a 0.4-cm quartz cuvette wall. Then, PSs were

incubated and the cuvette was washed several times with PBS or d-PBS until no signal measured in supernatant fluid.

Absorption spectra of PS in different culture models were recorded on a Cary 6000i UV-Vis-NIR spectrophotometer (Agilent Technologies). Fluorescence emission spectra were recorded in a Fluoromax-4 spectrofluorimeter (Horiba Jobin-Ybon). Fluorescence decays were recorded with a time-correlated single photon counting system (Fluotime 200, PicoQuant) equipped with a red sensitive photomultiplier. Excitation was achieved by means of a 405 nm picosecond diode laser working at 10 MHz repetition rate. The counting frequency was always below 1%. Fluorescence lifetimes were analyzed using PicoQuant FluoFit 4.0 data analysis software. $^1O_2$ phosphorescence was detected by means of a customized PicoQuant Fluotime 200 system.

In particular, phosphorescence of $^1O_2$ was determined through the following kinetic model: PS absorbs light energy that results in the development of PS excited states (PS*), from which energy transfer to nearby oxygen molecules can occur, ultimately yielding $^1O_2$ as illustrated in **Equation 2.6**:

$$PS + h\nu \rightarrow {}^1PS^*$$
$${}^1PS^* \rightarrow {}^3PS^*$$
$${}^3PS^* + O_2 \rightarrow PS + {}^1O_2$$

Equation 2.6. Mechanism of singlet oxygen photosensitization. Absorption of light by a photosensitizer PS promotes it to its singlet electronic excited state ($^1PS^*$). Radiationless processes change its spin from singlet to triplet ($^3PS^*$), which then transfers its energy to ambient dioxygen molecules yielding $^1O_2$.

$^1O_2$ molecules may diffuse away from the site of production and oxidize susceptible substrates before it decays, a process that is complete within a few microseconds in biological media. A small fraction (10^{-5}-10^{-7}) of $^1O_2$ molecules can undergo radiative decay emitting a photon in the near infrared (NIR). This extremely weak phosphorescence, centered at 1275 nm, provides the means for the most direct and unambiguous method for $^1O_2$ detection. The time-resolved measurement of this NIR emission is now a very well-established technique for monitoring $^1O_2$[4]. The production and decay of $^1O_2$ in a pulsed photosensitisation process obeys a biexponential kinetic model (**Equation 2.7**):

$$[{}^1O_2]_t = [{}^1O_2]_0 \cdot (\tau_\Delta/\tau_\Delta-\tau_T) \cdot (e^{-t/\tau\Delta} - e^{-t/\tau T})$$

Equation 2.7. Singlet oxygen kinetic model

Where τ_T is the lifetime of $^3PS^*$ and τ_Δ is the lifetime of $^1O_2$, and $[^1O_2]_0$ is the concentration of $^1O_2$ produced by the laser pulse.

On the other hand, for time-resolved phosphorescence measurements of PS, samples were irradiated at 532 nm and the signal obtained was fitted in **Equation 2.8.**

$$[^3PS]_t = K_1 \cdot e^{-t/\tau T}$$

Equation 2.8. Photosensitizer kinetic model

Where K_1 reflects the concentration of triplet excited states of PS.

2.8 RECEPTOR TYROSINE KINASES INHIBITORS

Three tyrosine kinase inhibitors and a placebo were kindly provided by Dr. José Ignacio Borrell from Grup d'Enginyeria Molecular (GEM) in IQS School of Engineering (Spain). Experiments were performed under blind conditions, without knowing the identity of the different molecules.

For 2D cultures, cells were grown toward 30%-50% confluence and drugs were incubated during 24 and 48 hours. For 3D cultures, the tyrosine kinase inhibitor that induced more cell death in 2D cultures was selected and experiments were performed after 24 hours of drug incubation. Cells were grown during 6 days within RAD16-I and collagen scaffolds in order to assure that cells were already adapted to the 3D culture system.

For 2D and 3D cultures, different drug concentrations were tested (0 µM, 1 µM, 5 µM, 10 µM, 50 µM and 100 µM). A stock solution of the different inhibitors was prepared by diluting them with DMSO. Control wells with a solution of 100 µL DMSO, which corresponded to the highest volume of solvent used, were added in order to demonstrate that the presence of DMSO did not induce significant cell death. To perform drug incubation, culture medium was removed and fresh culture medium supplemented with the inhibitor was added. Finally, cell viability was assessed by the LIVE/DEAD® Viability/Cytotoxicity Kit for mammalian cells (L3224, Invitrogen) and MTT assay.

2.9 STATISTICAL ANALYSIS

All data were expressed as mean values ± standard deviation (SD). Statistical differences were analyzed with GraphPad Prism 5. Unpaired Student's t test was used to test the significance level between two sets of measurements. The level of significance was $*p<0.05$, $**p<0.01$, $***p<0.001$.

2.10 REFERENCES

1. Livak, K. J. & Schmittgen, T. D. Analysis of relative gene expression data using real-time quantitative PCR and the 2-ΔΔCt method. *Methods* **25,** 402–408 (2001).

2. De Jonge, H. J. M. *et al.* Evidence based selection of housekeeping genes. *PLoS One* **9,** e898 (2007).

3. Mane, V. P., Heuer, M. A., Hillyer, P., Navarro, M. B. & Rabin, R. L. Systematic method for determining an ideal housekeeping gene for Real-Time PCR analysis. *J. Biomol. Tech.* **19,** 342–347 (2008).

4. Jimenez-Banzo, A., Ragas, X., Kapusta, P. & Nonell, S. Time-resolved methods in biophysics. Photon counting vs. analog time-resolved singlet oxygen phosphorescence detection. *Photochem. Photobiol. Sci.* **7,** 1003–1010 (2008).

Chapter 3

Development of 3D models to obtain mechanistic insights on epithelial to mesenchymal transition

3.1 BACKGROUND

3.1.1 TISSUE INVASION AND METASTASIS

Metastasis accounts for approximately 90% of all cancer deaths[1]. This process occurs when invading cancer cells penetrate basement membrane (BM) and endothelial walls from systemic vasculature, disseminate via circulation, exit the bloodstream and finally grow in distant organs and tissues (colonization)[2]. The fulfillment of this sequence depends on the reciprocal reprogramming of both cancer cells and surrounding tissue structures. Cells need to continuously reorganize their adhesion complexes and cytoskeletal dynamics in order to survive, proliferate and migrate under diverse structural milieu[3]. In parallel, cells can remodel extracellular matrix (ECM) to render highly linearized and oriented collagen fibrils that act as highways or activate the formation of new blood vessels[4,5].

Every step in the metastatic cascade requires the interactive engagement between cells and stroma, leading to plasticity and reciprocity[6]. Thus, metastasis might be envisaged as an evolutionary process in which genetically heterogeneous cells are driven to evolve by changing environmental pressures[7]. It is estimated that only 0.01% of the cancer cell population is able to undergo all the architectural and functional changes required to generate final metastasis[8]. The first requirement for cells is the acquisition of invasive capabilities. Cells need to leave their primary tumor site, comprising 90% of cases the epithelium[9].

Epithelial cells form layers kept together by specialized membrane structures (tight junctions, adherens junctions, desmosomes and gap junctions) that result in a lateral belt. Moreover, cells are polarized and show an asymmetric organization with two distinct cellular regions: the apical (top) and basolateral (bottom) regions. The apical surface forms a direct barrier against the external environment, protecting tissues and organs. Conversely, the basolateral surface is in contact with BM. It is a sheet of dense ECM of 100-300 nm of thickness that is mainly composed by a highly ordered and crosslinked type IV collagen and intercalated laminin complexes, providing structural support to the epithelium. Cells are tightly joined with BM through the localized expression of adhesion molecules such as cadherins and integrins.

This organization limits the movement of cells to the two-dimensional (2D) space of the epithelial plane. In order to escape from their epithelial neighbors, cells need to change their adhesion properties. Particularly, they downregulate cell-cell contacts and remodel cell-ECM contacts in order to define a front-back polarity with a leading edge enriched in integrins and matrix metalloproteinases (MMPs). To modify adhesion complexes repertoire, cells undergo a dramatic remodeling of the actin cytoskeleton and the disruption of the basal-apical polarity. Significantly, these new features define a mesenchymal phenotype, which allows cells to degrade BM and move through the three-dimensional (3D) space of ECM[10]. Therefore, the initial morphogenetic step in the metastatic cascade is the transition from an epithelial to a mesenchymal phenotype (**Figure 3.1**).

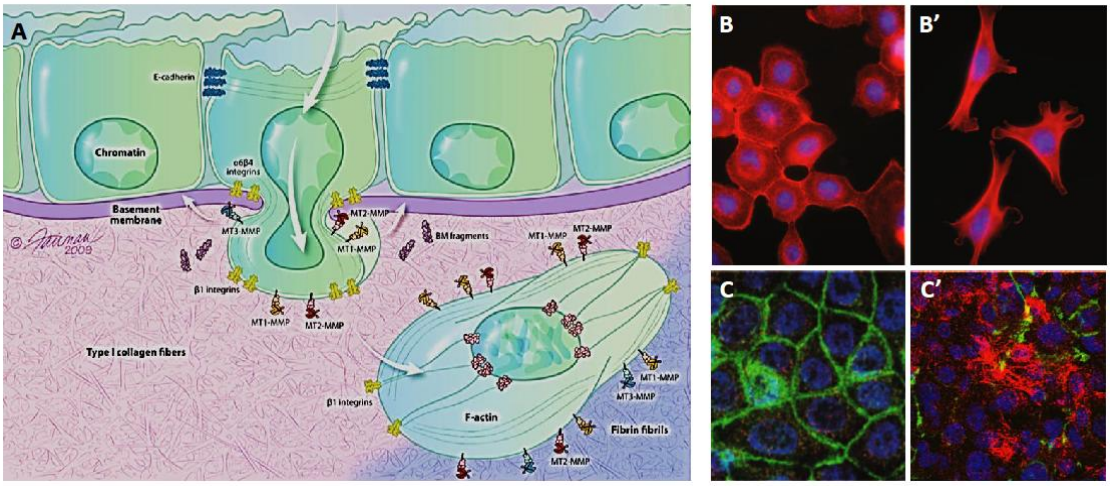

Figure 3.1. Transition from a 2D to a 3D microenvironment. (A) In a healthy stage, epithelial cells grow forming layers on top of BM and showing a 2D configuration. During tumor progression, cells gain the capacity to degrade BM via the action of MMPs and invade the 3D ECM. This 2D to 3D transition is possible through the downregulation of cell-cell adhesion molecules, disruption of polarity, remodeling of actin cytoskeleton and activation of proteases. Collectively, these changes in cell architecture and function result in the acquisition of a mesenchymal-like phenotype in a process known as epithelial to mesenchymal transition (EMT). **(B-C)** Confocal immunofluorescence images of EMT. **(B)** Murine mammary cells were treated with MMP-3 (**B'**) to induce EMT. Cells were stained with anti-phalloidin antibody (red) and DAPI (blue) to visualize actin microfilaments and nuclei respectively. **(C)** Murine mammary cells were treated with transforming growth factor-β (TGF-β) (**C'**) to induce EMT. Cells were stained with anti-E-cadherin (green) and anti-vimetin (red) antibody to visualize the proteins that form cell-cell adhesions of epithelial cells and intermediate filaments from the cytoskeleton of mesenchymal cells respectively. Adapted from Rowe *et al*.[11] and Thiery *et al*.[12]

3.1.2 EPITHELIAL TO MESENCHYMAL TRANSITION

Epithelial to mesenchymal transition (EMT) was reported by Frank Lillie in 1908, but the first detailed description was done in the late 1960s by Elisabeth Hay[13]. It is a highly conserved cellular program reminiscent of embryogenesis. It governs the formation of the three germ layers (ectoderm, mesoderm and endoderm) during gastrulation. In a later developmental stage, it participates in the formation of numerous tissues and organs, such as neural crest, heart, musculoskeletal system, craniofacial structures and the peripheral nervous system. In adults, cells access this fundamental program during wound healing and pathological conditions as tumor metastasis. The reversible process has been also characterized, MET (mesenchymal to epithelial transition). MET occurs during somitogenesis, kidney development and coelomic-cavity formation. In cancer disease, cells undergo MET during the establishment of secondary tumor sites in order to efficiently adhere to the microenvironment and begin to proliferate[14,15].

The term EMT encompasses a broad spectrum of cellular changes and does not necessarily refer to a complete lineage switch. Indeed, the precise changes that occur during EMT are determined by the integration of the signals that govern this process. In particular, EMT is triggered by an interplay of extracellular cues, including components of the ECM (collagen and hyaluronic acid) as well as soluble growth factors (members of the transforming growth factor

β [TGFβ], fibroblast growth factor [FGF], epithelial growth factor [EGF], hepatocyte growth factor [HGF], insulin-like growth factor [IGF] families). These signals induce changes in integrin and receptor tyrosine kinase expression that exert a stringent control of multiple intracellular regulatory circuits, such as transcription factors, members of small GTPase family (Ras, Rho and Rac) and Src tyrosine-kinase family[12,16]. Ultimately, these effectors orchestrate the disassembly of junctional complexes and the remodeling of cytoskeletal organization. Significantly, they all converge on the dissociation of epithelial cell-cell adhesion molecules, emerging epithelial-cadherin (E-cadherin) as the central complex[7]. Indeed, the expression pattern of E-cadherin is used for the diagnosis and prognosis of cancer.

3.1.2.1 E-Cadherin: A Central Player in EMT

Cells continuously sense and respond to extracellular signals through cell adhesion molecules (integrins, selectins, cadherins, immunoglobulin superfamily and proteoglycans). They provide transient and stable communication channels among cell-cell and cell-ECM, creating a cytoplasmic and cytoskeletal-matrix fibers continuum respectively. Therefore, adhesion molecules contribute to the formation and integrity of different tissues and also play an important role in cell signaling[17].

Cadherins form a type of cell-cell adhesions called adherens junctions (AJs). They are responsible for maintaining cell architecture and polarity along with limiting their movement and proliferation. Cadherins are a superfamily of transmembrane glycoproteins, whose extracellular domains mediate Ca^{2+} dependent adhesions via homophilic interactions with adjacent cells. Their conserved cytoplasmic domains form a protein complex with catenins that anchor them to actin cytoskeleton in order to transmit the adhesion signal. Hence, the clustering of cadherin-catenin complexes on adjacent cells leads to the localized actin remodeling that is required for AJs assembly[18,19].

E-cadherin (encoded by *CDH1* gene) is the prototypical member of type-1 classical cadherins. It was first discovered as a cell adhesion protein in early mouse embryo blastomeres[20]. Targeted knockout of *CDH1* gene in mice was reported to be lethal as embryos could not generate an epithelium, which is required for the development of multicellular organisms[21]. E-cadherin has five extracellular domain repeats, a single transmembrane domain and a cytoplasmic domain for binding catenin proteins, namely p120-catenin, β-catenin and α-catenin that is directly linked to the actin cytoskeleton[22]. E-cadherin regulation is an example of the tight and precise control of genes involved in EMT (**Figure 3.2**).

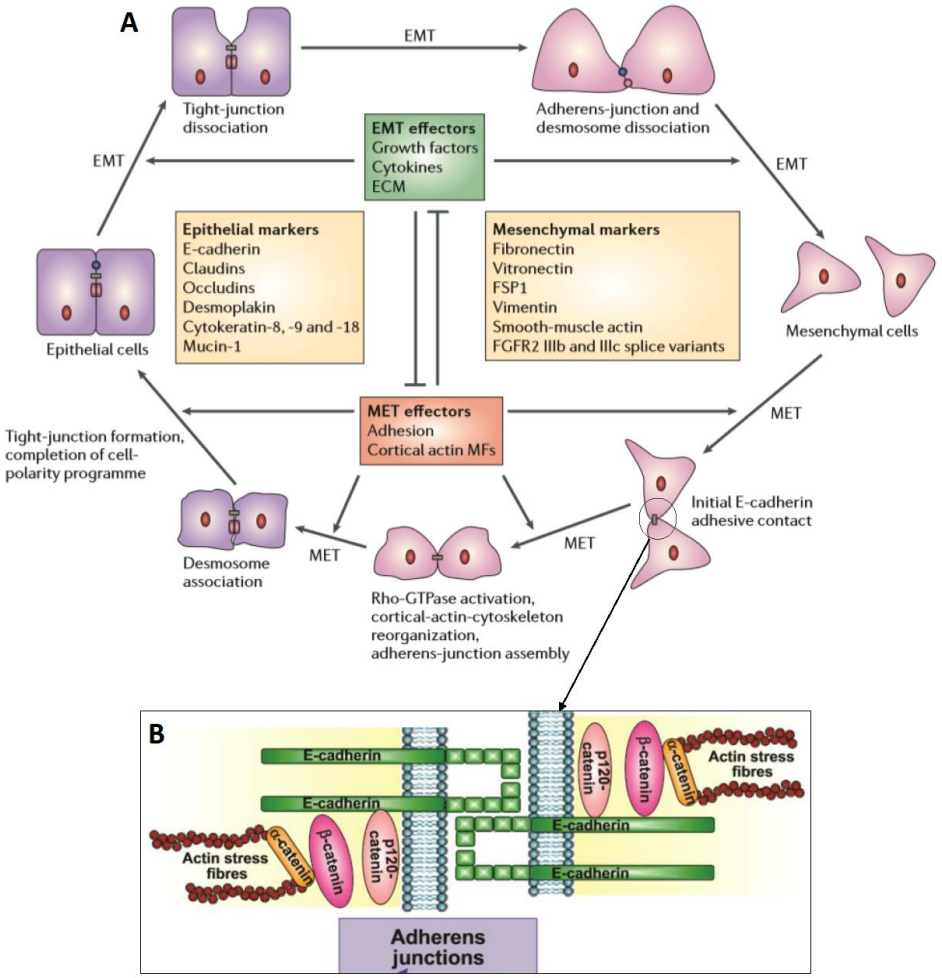

Figure 3.2. Cycle of epithelial plasticity during metastatic cascade. (A) During metastatic cascade, epithelial cells acquire some capabilities of mesenchymal cells to degrade BM, invade ECM, enter the lymphatic and circulatory systems (intravasation) and exit them (extravasation). On the other hand, the transition from mesenchymal to epithelial cells is activated when cells adhere to distant tissues and organs and proliferate, forming secondary tumor sites (colonization). Different effectors of EMT and MET have been identified, including numerous extracellular signals. During these transitions, cell-cell and cell-ECM adhesions are continuously remodeled. Significantly, E-cadherin plays a central role in the formation of the adherens junctions that maintain the integrity of epithelial layer and, therefore, emerge as the main marker of metastasis. **(B)** Schematic representation of E-cadherin-mediated cell–cell adherens junctions. E-cadherin is a single-pass transmembrane protein, whose extracellular domain mediates Ca^{2+} specific homophilic interactions with neighboring cells. The intracellular domain of E-cadherin associates with catenins and actin cytoskeleton. Adapted from Thiery *et al.*[12] and Canel *et al.*[22]

Genetic and epigenetic alterations are at the core of E-cadherin regulation. Genetic mechanisms include mutations and loss of heterozygosity of the wild type allele, which cause the uniform and irreversible loss of E-cadherin expression. This pattern occurs in a very low rate of cancer cases, basically in lobular breast[23] and diffusive gastric[24] carcinomas. They are characterized by invading very efficiently, but forming loosely dispersed structures (micro-metastases)[25]. Conversely, epigenetic alterations provide a dynamic mechanism for modulating E-cadherin expression, facilitating the phenotypic plasticity that drives metastatic progression.

3.1.3 EPIGENETICS IN CANCER PLASTICITY

Epigenetics is defined as the study of mitotically and/or meiotically heritable changes in gene function that cannot be explained by changes in DNA sequences[26]. Genomic regions can undergo transitions from an open, transcriptionally active conformation (eurochromatin) to a densely compacted, transcriptionally inactive conformation (heterochromatin) and vice versa. These transitions are vital to set the different expression patterns required during embryonic life, development or adult stage and rely on the control of histones and DNA. In particular, the epigenetic landscape includes a variety of covalent modifications that affect the methylation status of DNA and the post-translational status of histones, determining the structural configuration of chromatin[27].

Histones are the main protein moieties of chromatin. Their function is to package and order DNA structure. They can suffer a variety of post-transcriptional modifications of their N-terminal tails, including deacetylation, methylation, phosphorylation, sumoylation, ubiquitination and ADP ribosylation. The most frequent mechanism for histone modification is deacetylation, which involves the removal of acetyl groups by histone deacetylases (HDAC) enzymes. The deacetylated histone state helps to maintain nucleosomes in a compacted and transcriptionally silent state[28].

DNA can be covalently modified by the addition of a methyl group in a cytosine base in a process known as DNA methylation. The reaction is catalyzed by DNA methyltransferase (DNMT) enzyme, which transfers the methyl group from S-adenosyl-l-methionine (SAM) to the fifth carbon of a cytosine (C) located 5' to a guanine (G) in a CpG dinucleotide, forming a 5-methyl cytosine. Most CpG islands are found in the proximal promoter regions in mammalian genome and are, generally, unmethylated in active genes. In cancer, the hypermethylation of some specific promoter regions is a well-categorized epigenetic alteration and is associated with the inappropriate transcriptional silencing of key tumor-suppressor genes[29]. This transcriptional repression can be explained due to the steric inhibition of transcription activator complexes together with the recruitment of protein complexes formed by methyl-CpG-binding proteins (MBPs) and HDACs. Therefore, there is a link between the 'histone code' and the 'DNA code' (**Figure 3.3**). It is the combined presence of a myriad of modifications in a spatial and temporal-dependent controlled manner that ultimately programs the appropriate genome expression profile for each cellular identity[27]. Moreover, these methylation covalent modifications can predispose DNA to mutational events. For instance, 5-methyl cytosine is itself mutagenic since it can undergo spontaneous hydrolytic deamination, causing cytosine to thymine transitions[29].

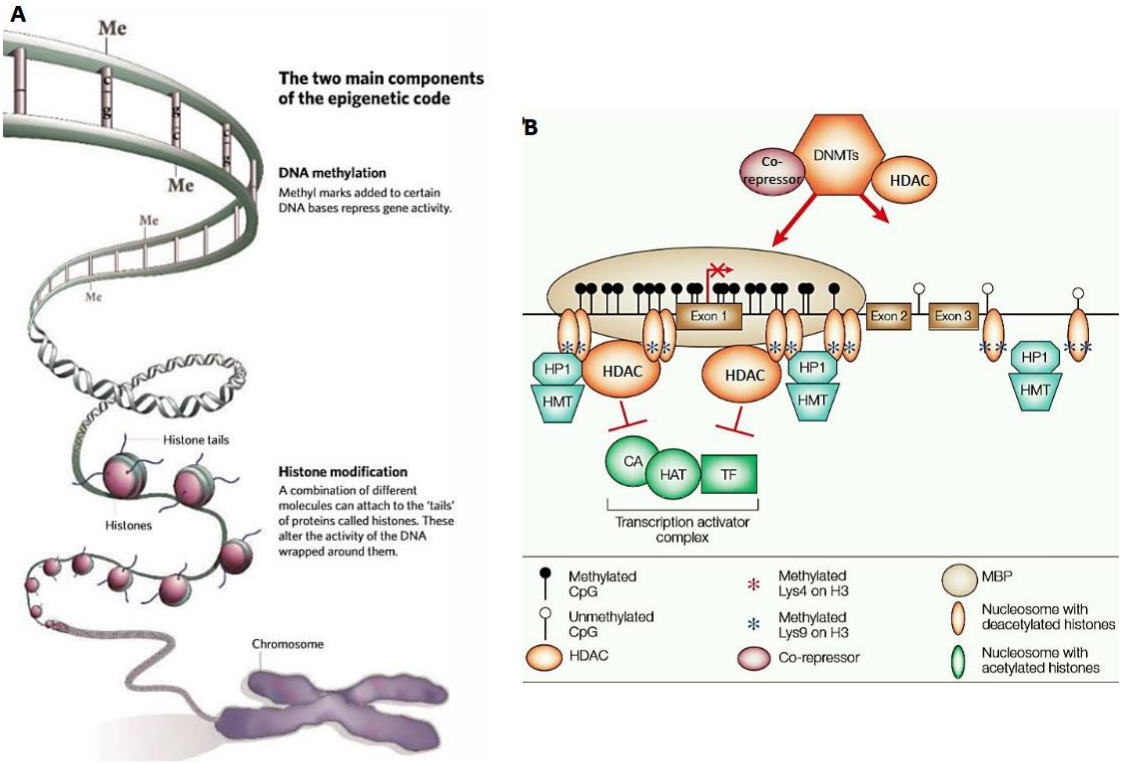

Figure 3.3. Epigenetic alterations confer plasticity to cancer cells. (**A**) The epigenetic landscape includes a variety of covalent modifications that affect the methylation status of DNA and the post-translational status of histones, determining the structural configuration of chromatin and, therefore, controlling the transcriptional outcome of the cell. These mechanisms play a central role during development and pathological states as cancer. (**B**) Experimental evidence links "DNA code" with "histone code". The image shows a schematic representation of a CpG-methylated promoter in a transcriptionally repressed state. In particular, most candidate CpG sites of the promoter are methylated and bound by methyl-cytosine-binding proteins (MBPs). These proteins are present in complexes that include histone deacetylases (HDACs). Consequently, histones are deacetylated and organized into regularly spaced and tightly compacted nucleosomes (heterochromatin). Transcription activator complexes, consisting of a transcription factor (TF), a co-activator protein (CA) and a protein with histone acetyltransferase (HAT) activity, cannot access to the promoter region by steric inhibition. Adapted from Qiu[30] and Jones *et al.*[29]

The epigenetic silencing of E-cadherin has emerged as the major regulatory mechanism during metastatic cascade. The E-cadherin gene is reported to be hypermethylated in a wide range of carcinomas, including lung, liver, stomach and bladder[31]. It has also been reported the presence of transcription repressor complexes formed by histones deacetylases (*HDAC1* and *HDAC2*) and factors from the snail (*SNAI1* and *SNAI2*), zinc finger E-box-binding homeobox (*ZEB1* and *ZEB2*) and basic helix-loop-helix (*bHLH:E47* and *TWIST*) families.

Complex signaling networks influence the expression of these repressors. Different growth factors (e.g. FGF, EGF, bone morphogenetic protein [BMP], platelet derived growth factor [PDGF]) can function in autocrine loops in cancer cells. In parallel, many signals derived from the ECM have been identified. Among these, laminin 5 has been described to be mechanistically dependent on active integrin α3. Angiogenic factors as VEGF and reactive oxygen species have been reported to be upregulated after a hypoxic situation. Finally, inflammatory components such as cyclooxygenase 2 (COX2) can act through nuclear factor κB (NFκB) and some interleukins[7] (**Figure 3.4**).

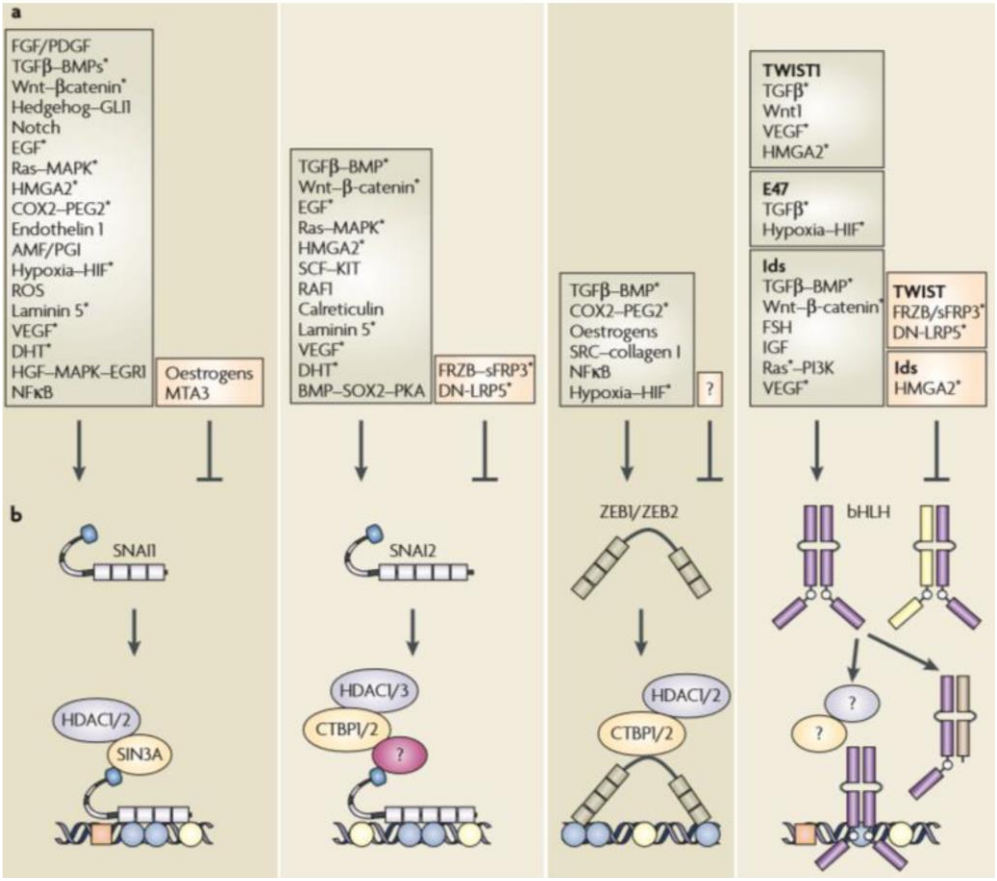

Figure 3.4. Epigenetic alterations implicated in E-cadherin regulation. (a) Snail, ZEB and bHLH factors act as transcriptional repressors of E-cadherin, modulating cell-cell adhesions configuration. Overview of the main signaling pathways implicated in the expression of Snail, bHLH and ZEB factors, including extracellular cues from the microenvironment. **(b)** Schematic representation of the link between these transcriptional repressors and histones modification machinery. Snail, bHLH and ZEB factors recruit histone deacetylates as HDAC1, HDAC2 and HDAC3 and, therefore, mediate post-transcriptional modifications of histones and chromatin structure. Some relevant growth factors and signaling pathways abbreviations: AMF (autocrine mobility factor), BMP (bone morphogenetic protein), COX (cyclooxygenase), DN-LRP5 (dominant negative low density lipoprotein receptor-related protein 5), EGF (epidermal growth factor), FGF (fibroblast growth factor), FRZB (frizzled-related protein), FSH (follicle stimulating hormone), HGF (hepatocyte growth factor), HMG (high mobility group), MAPK (mitogen activated protein kinase), MTA3 (metastasis-associated gene 3), PDGF (platelet derived growth factor), PEG2 (prostaglandin E2), PGI (phosphoglucose isomerase), PKA (protein kinase A), SCF (stem cell factor), sFRP3 (secreted frizzled-related protein 3), TGFβ (transforming growth factor β), VEGF (vascular endothelial growth factor). From Peinado *et al.*[7]

The characterization of E-cadherin regulation has provided important insights into the signaling pathways involved in metastasis. However, more research is needed to unravel this process at the molecular level, giving particular attention to microenvironment contribution. A major challenge to study E-cadherin expression underlies in *in vitro* capturing EMT process. A cancer model that can help to fulfil this objective is pancreatic cancer.

3.1.3.1 Pancreatic Cancer: A Model for Capturing EMT

Pancreatic cancer, also known as pancreatic ductal adenocarcinoma (PDAC), is one of the most aggressive types of cancer. PDAC is the fifth most common cause of cancer-related deaths, even though it represents less than 2% of cancer cases. In fact, the annual death rate equals the annual incidence of this disease. The bad prognosis for PDAC can be explained by its asymptotic nature in early stages, lack of sensitive diagnostic tools and high metastatic potential[32]. Less than 20% of patients show localized and potentially curable tumors[33].

A rational progression for this disease has been proposed: PDAC originates in the ductal epithelium, evolves to pre-malignant lesions (pancreatic intraepithelial neoplasms PanINs 1a/b, 2 and 3 grades) and finally originates invasive carcinoma. This process occurs parallel to the accumulation of genetic alterations involving early mutations in the *KRAS2* gene and overexpression of the *HER-2/neu* gene followed by later mutations in *p16*, *p53* and *DPC4* genes[33–36].

Recent publications have suggested that EMT and dissemination can precede primary tumor formation in PDAC[37]. Clinical observations have given rise to a new paradigm for metastasis. As previously explained, the classical model treats metastasis as the final step in a progressive Darwinian sequence in which cells invade and disseminate late in tumor evolution[38]. An alternative model considers metastasis as an inherent feature of the tumor, very early in its natural history[39]. Some studies of PDAC have suggested that EMT, bloodstream entry and seeding of distant organs can occur at a stage of tumor progression previously thought to be pre-invasive, based on standard histological examination[37]. More research is needed in this direction.

Research in PDAC has been focused on genome-centered models. However, the contribution of tumor microenvironment remains unclear, with special attention to invasion and metastatic steps. A schematic overview with the most relevant data concerning genetic and epigenetic alterations is presented in **Figure 3.5**. However, all these experiments have been performed in 2D cultures or histological sections of tumors without analyzing the specific role of microenvironmental cues. In the present thesis, the regulation of E-cadherin (main marker of EMT cell program) has been studied in different 3D tissue engineering scaffolds.

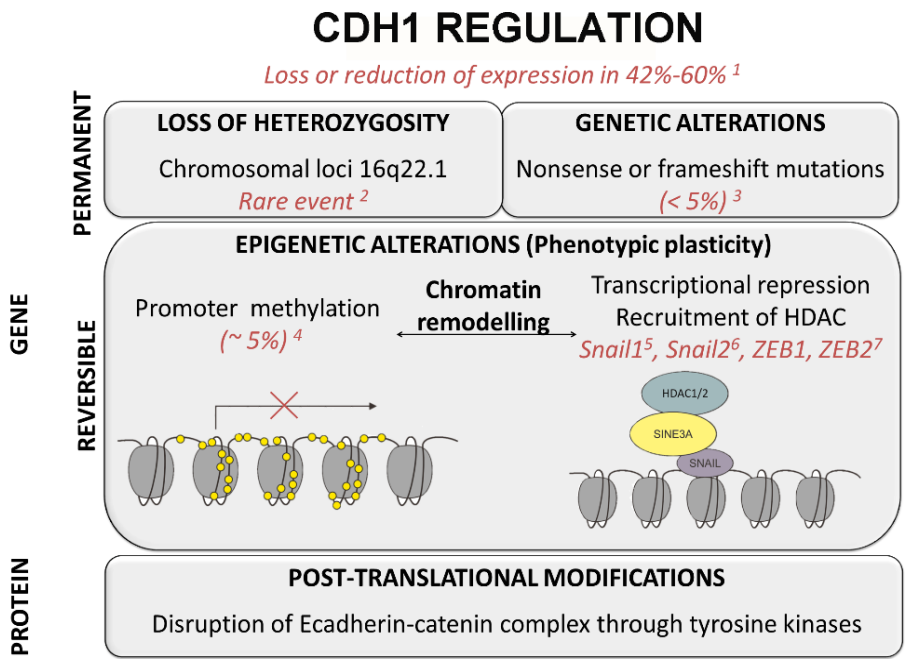

Figure 3.5. Schematic representation of E-cadherin regulation in pancreatic cancer. Loss or reduction of E-cadherin-mediated cell-cell adhesions is reported between 42-60% of the cases. It exists different levels of regulation at gene and/or protein level. Briefly, genetic alterations include mutations and loss of heterozygosity, leading to a permanent inactivation of the protein. In pancreatic cancer, both mechanism have been rarely described, correlating with the reversible definition of epithelial-mesenchymal transition. Epigenetic alterations include covalent modifications of DNA and histones, which ultimately affect chromatin structure. In pancreatic cancer, aberrant hypermethylation of the promoter region has been found in approximately 5% of cases. On the other hand, the most common signature on histones to silence genes is their deacetylation, which functions through the formation of protein complexes including HDAC and transcriptional repressors. In pancreatic cancer, Snail and ZEB factors have been reported to recruit HDAC1, HDAC2 and HDAC3 to regulate E-cadherin expression. At protein level, the main mechanism is based on the disruption of the functional complexes that form E-cadherin with β-catenin through tyrosine phosphorylation and desphosphorylation of β-catenin. The references cited in this figure are the following: 1.Hong *et al.* [39]; 2.Iacobuzio-Donahue *et al*. [40] and Thiery *et al*.[15]; 3. Aghdassi *et al*.[41] and Winter *et al.*[42]*; 4.* Aghdassi *et al*.[41] and Winter *et al.*[42], 5. Aghdassi *et al*.[41], von Burstin *et al*.[43], Shields *et al*.[44]; 6. von Burstin *et al*.[43] and 7. Aghdassi *et al*.[41], Imamichi *et al*.[45]

3.2 HYPOTHESIS AND SPECIFIC AIMS

The main motivation of this chapter was to study the contribution of tumor microenvironment during tissue invasion and metastasis in pancreatic cancer.

Our working hypothesis was that three-dimensional (3D) cultures could help to recapitulate the cell movement from a 2D to a 3D milieu that occurs during epithelial to mesenchymal transition (EMT) when cancer cells escape from their epithelial layer and invade mesenchymal connective tissue. These 3D cultures allowed us to change different chemical and mechanical properties of the scaffolds in order to evaluate the influence of these extracellular signals on EMT activation. In particular, EMT was monitored through E-cadherin expression patter, since this protein mediates epithelial cell-cell adhesions. The specific aims of this chapter were the following:

(1) To characterize pancreatic cancer cells plasticity through 3D cultures of different composition and stiffness.

(2) To study the microenvironmental control of E-cadherin dynamic expression and regulation in different 3D cancer models. E-cadherin is the main marker of EMT program during invasion and metastasis steps.

3.3 RESULTS AND DISCUSSION

3.3.1 MORPHOLOGICAL ASSESSMENT OF 3D CANCER MODELS

Different 3D models of a pancreatic ductal adenocarcinoma (PANC-1) cell line were developed in order to study the contribution of the microenvironment on cellular phenotype during tumor progression. Pancreatic cancer was selected as a study model due to its metastatic capacity, which is associated with the bad prognosis of this disease. Indeed, recent data suggests that epithelial to mesenchymal transition (EMT) and cellular dissemination leading to metastatic cascade could occur in parallel or prior to the formation of an identifiable primary tumor[37].

Cells were encapsulated in collagen type I and self-assembling RAD16-I peptide scaffolds at two different concentrations of 1.5 mg/mL and 5.0 mg/mL in order to evaluate the effect of composition and stiffness from the surrounding milieu. First, the macroscopic morphology of 3D cultures was characterized with a stereoscopic microscope (**Figure 3.6**):

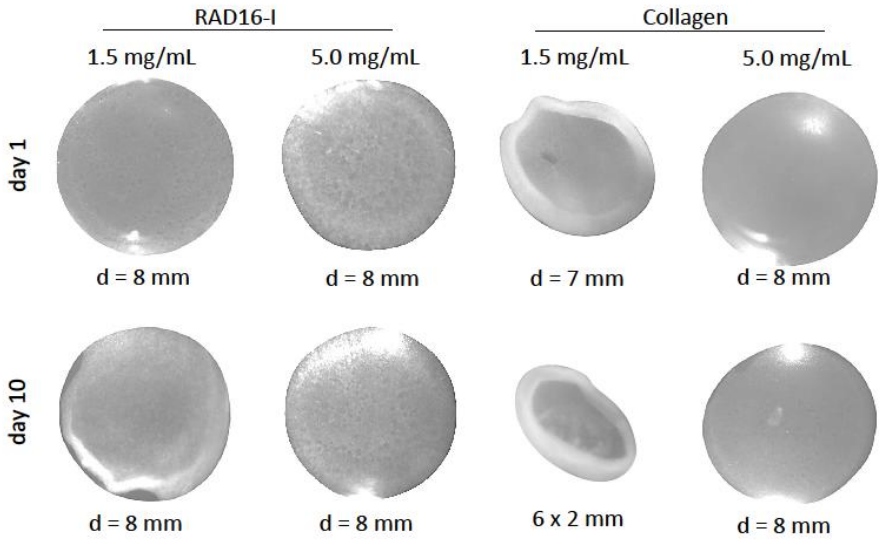

Figure 3.6. Morphologic assessment of 3D cultures at macroscopic level. Cells were encapsulated in RAD16-I and collagen scaffolds at two different concentrations (1.5 and 5.0 mg/mL). The resulting geometry was a disk of 8 mm of diameter and 500 µm of thickness. Collagen 1.5 mg/mL scaffolds suffered a spontaneous contraction process.

The geometry of the 3D cultures was a disk of approximately 8 mm diameter and 500 µm thickness. These dimensions were optimal for recreating tumor architecture. Many types of tumors are characterized by having a hypoxic and quiescent core. In these 3D cultures, the distance between surface exposed- and deeply buried-cells was around 250 µm, relevant dimensions for being subjected to mass transport limitations (the oxygen diffusion limit is approximately of 200 µm)[47].

Significantly, collagen scaffolds at a concentration of 1.5 mg/mL suffered a spontaneous asymmetric contraction process, showing an oval shape with average dimensions of 6 x 2 mm. Collagen contraction has been previously described in cancer biology as a self-organization process in which cells strongly interact with collagen fibrils through integrin signaling and form an extensive communication network capable of dragging the hydrogel[48]. Furthermore, cells could probably secrete metalloproteinases to degrade collagen making their microenvironment less stiff. Conversely, this morphological pattern was not observed when the concentration of the hydrogel was 5.0 mg/mL. Increasing the concentration of collagen is transduced in stiffening the matrix (studied in detailed below). Probably, cells could no longer overcome the surrounding resistance to drag the hydrogel with them. These results are consistent with recent publications, which state the dependence between matrix contraction and stiffness[49,50]. Indeed, stiffness has been shown to promote the remodeling of cell-matrix adhesions. Therefore, these findings reinforced the formation of a communication network between cells and collagen matrix through integrins (mainly $\alpha_2\beta_1$ in PANC-1 cells), as previously reported[51]. This morphological phenomenon could be further studied by incubating samples with integrin inhibitors.

Regarding RAD16-I scaffold, the contraction process was not observed at any concentration. This biomaterial does not provide specific recognition sites for integrins and, therefore, cells are were able to directly adhere to its nanofibers. Moreover, cells could not degrade RAD16-I matrix due to the lack of metalloproteinases-specific recognition sites.

3.3.2 MECHANICAL ASSESSMENT OF 3D CANCER MODELS

After macroscopic morphological assessment, the mechanical properties of 3D cultures were characterized by dynamic rheology (Dynamic-Mechanical Analysis, DMA). In particular, samples were deformed under an oscillating stress within a range of frequencies and the resultant sinusoidal strain was evaluated. The stress/strain ratio equals the complex viscoelastic modulus (G*), which can be defined as (**Equation 3.1**):

$$G^* = G' + iG''$$

Equation 3.1. Viscoelastic modulus equation

G' (storage modulus) represents the elastic component, measures the energy stored and is related to the stiffness of the sample. On the other hand, G'' (loss modulus) represents the viscous component, measures the energy converted to heat and is related to the ability of the sample to dissipate the energy through molecular motion[52]. In this case, the storage modulus of the 3D cultures was determined as a measure of matrix stiffness (**Figure 3.7**):

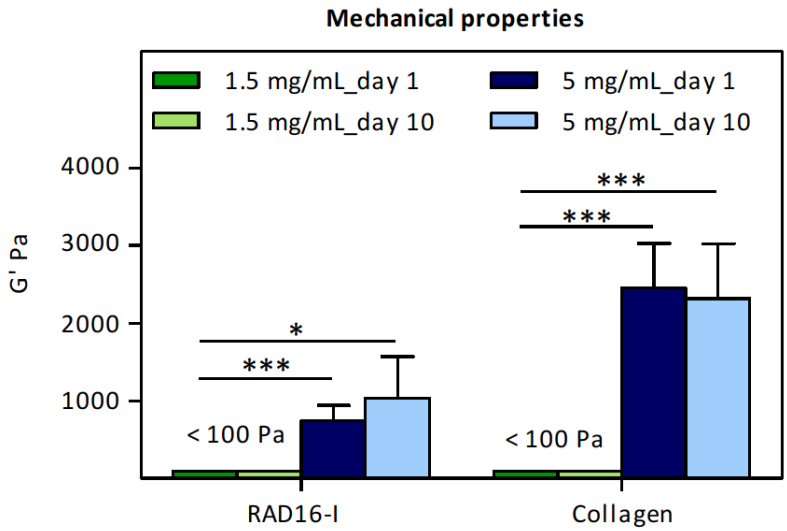

Figure 3.7. Mechanical assessment of 3D cultures. The storage elastic modulus (G') was determined by dynamic rheology and related to sample stiffness. Values represent the mean ± SD of six measurements from collagen and RAD16-I scaffolds, using concentrations of 1.5 and 5.0 mg/mL. *p<0.05 and ***p<0.001, (n=6).

The obtained mechanical properties were in agreement with the literature. Sieminski *et al.*[53] reported a storage modulus of approximately 100 Pa (1.5 mg/mL) and 1300 Pa (5.0 mg/mL) for RAD16-I biomaterial. Paszek *et al*.[54] obtained an average value of 170 Pa (1.0 mg/mL) and 1600 Pa (4.0 mg/mL) for collagen type I biomaterial.

The compliance of collagen and RAD16-I scaffolds at 1.5 mg/mL matched that of pancreatic normal tissue (ranging from 100-500 Pa)[55,56]. When the concentration raised to 5.0 mg/mL, collagen and RAD16-I scaffolds showed a storage modulus of approximately 3000 and 1500 Pa respectively, close to stiffness values for several types of tumours[54,57]. Therefore, results suggested that cells were able to sense the mechanical signaling that accompanies tumor progression due to the elevated deposition and remodeling of extracellular matrix (ECM) components.

For collagen scaffolds, global measures of stiffness values did not necessarily represent the real local value around cells due to the potential degradation of nanofibers by cells. Conversely, for RAD16-I scaffolds, cells could not degrade them due to the lack of metalloproteinases-recognition sequences, suggesting that stiffness was more stably maintained and probably global stiffness values did represent local ones over time. Therefore, we decided to continue working with the concentration of 5.0 mg/mL. The comparison between both concentrations could help to unravel the influence of tissue stiffness on E-cadherin regulation. The morphological effects are described in the next section.

3.3.3 CELL PHENOTYPE AND PLASTICITY IN 3D CANCER MODELS

Cell morphology and organization within the 3D cultures were characterized. In particular, nuclei and actin microfilaments of the cytoskeleton were stained with DAPI (blue) and Phalloidin-TRITC (red) dyes respectively.

The fluorescence microscope used to examine 3D cultures was equipped with the ApoTome system (Zeiss Company). This system created optical sections through the elimination of scattered light of out-of-focus planes. It was based on structured illumination, projecting a grid into the focal plane and moving it in a very precise manner. A mathematical algorithm calculated a resolved optical section from at least three single images with different grid positions[58] (**Figure 3.9**).

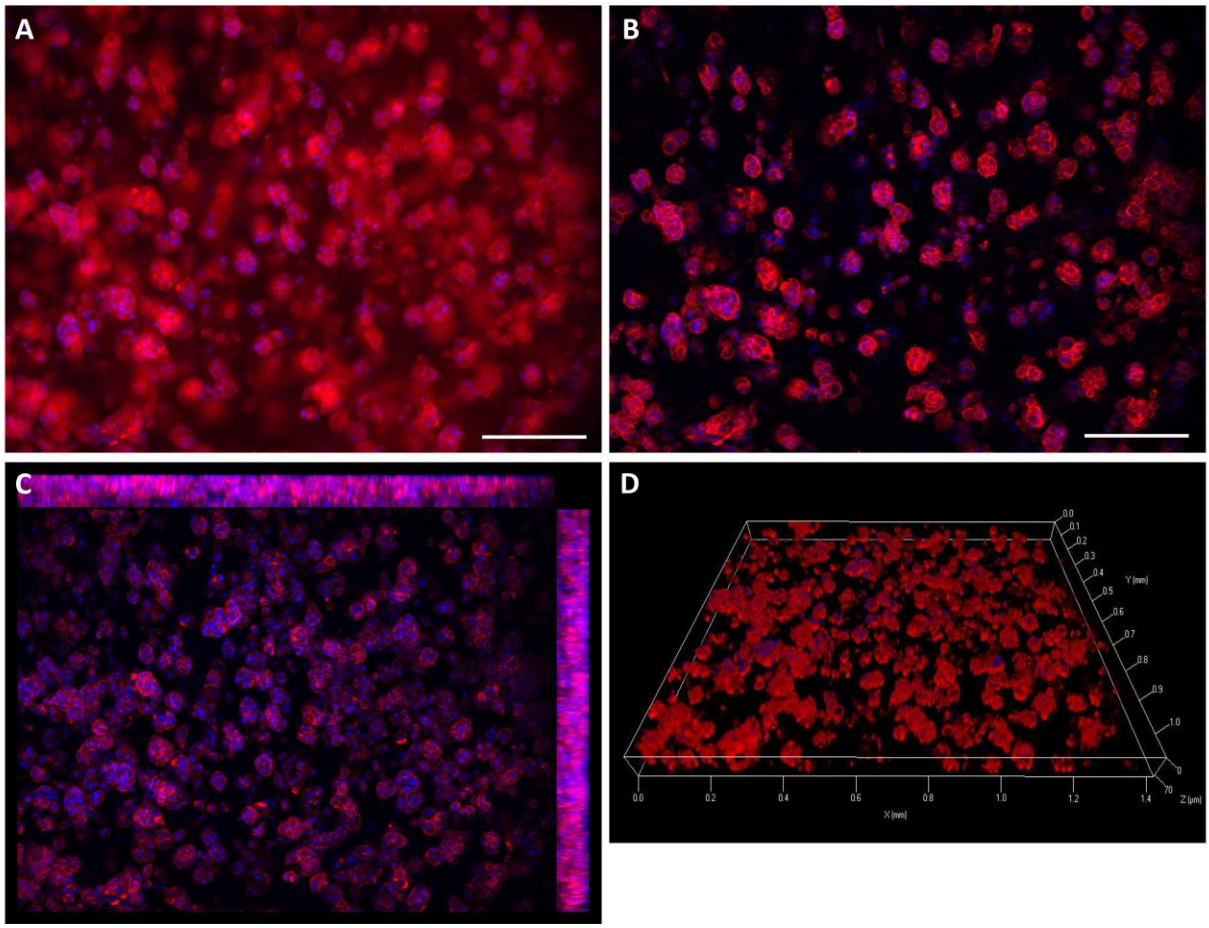

Figure 3.8. Optical sectioning and 3D reconstruction. Cell morphology and organization were evaluated through DAPI (blue) and Phalloidin-TRITC (red) staining. (A) Conventional fluorescence acquired without using the optical sectioning ApoTome system revealed the 3D distribution of cells. Fluorescence emission from both directions above and below the focal plane occurred and was captured. (B) One optical sectioning was acquired using the ApoTome system. Fluorescence emission from out-of-focus plane was eliminated through a mathematical algorithm based on structural illumination, such that only cells within a single optical section were shown. (C) Maximum Intensity Projection (MIP) of 10 optical sections. (D) 3D reconstruction in a volume render. The optical sections above were translated into a 3D volume render. Scale bar of 200 µm.

Optical sectioning was performed in all 3D cultures. These fluorescent images allowed us to analyze the influence of different microenvironmental cues (matrix composition and stiffness) on tumor phenotype (**Figure 3.9**).

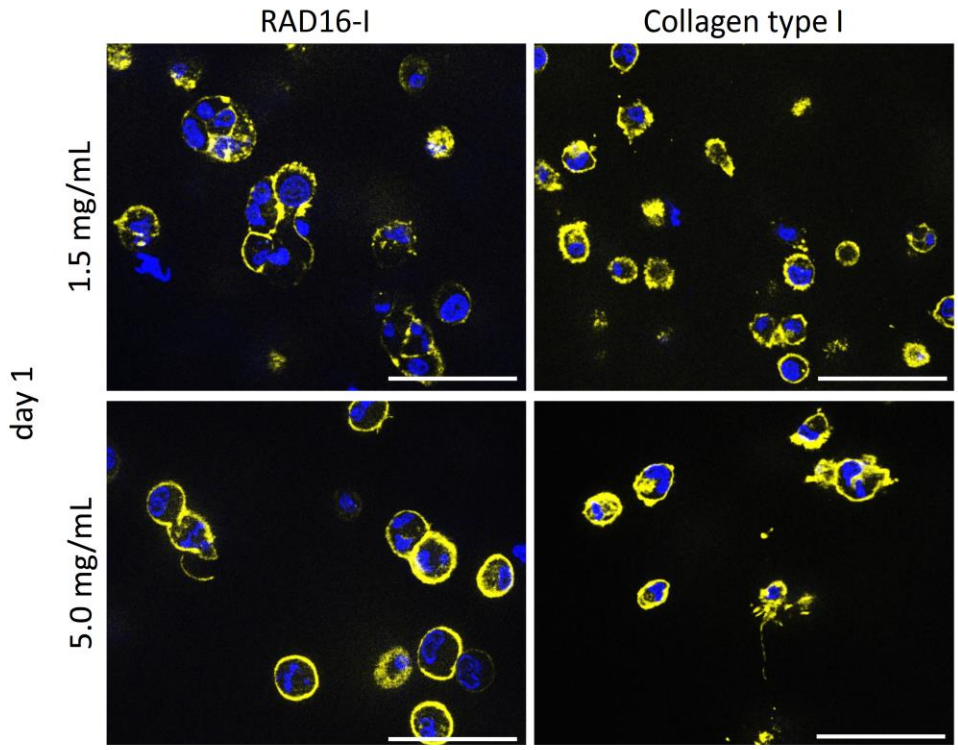

Figure 3.9. Cell morphology and organization in a 3D environment after 1 day of culture. The influence of different microenvironmental signals (matrix stiffness and composition) on cancer cell phenotype was analyzed. In particular, cells were grown within the synthetic self-assembling RAD16-I and the natural collagen type I hydrogels, using concentrations of 1.5 mg/mL and 5.0 mg/mL. After 1-day culture, samples were fixed and stained for actin microfilaments (phalloidin, pseudo-colored in yellow to increase contrast) and nuclei (DAPI, blue). Scale bar of 50 µm.

The first day after encapsulation, cells exhibited a round morphology shared by any of the culture conditions assayed in this work. They had prominent and irregular nuclei, distinguishing feature of the genomic instability and abnormal division patterns commonly observed in cancer cells. Moreover, their actin filaments were assembled into cortical thin bundles, following the particular cytoskeleton organization of epithelial cells. During the next culture days, they started to extend cellular processes characteristic of cells undergoing proliferation and cytoskeleton remodeling (**Figure 3.10**).

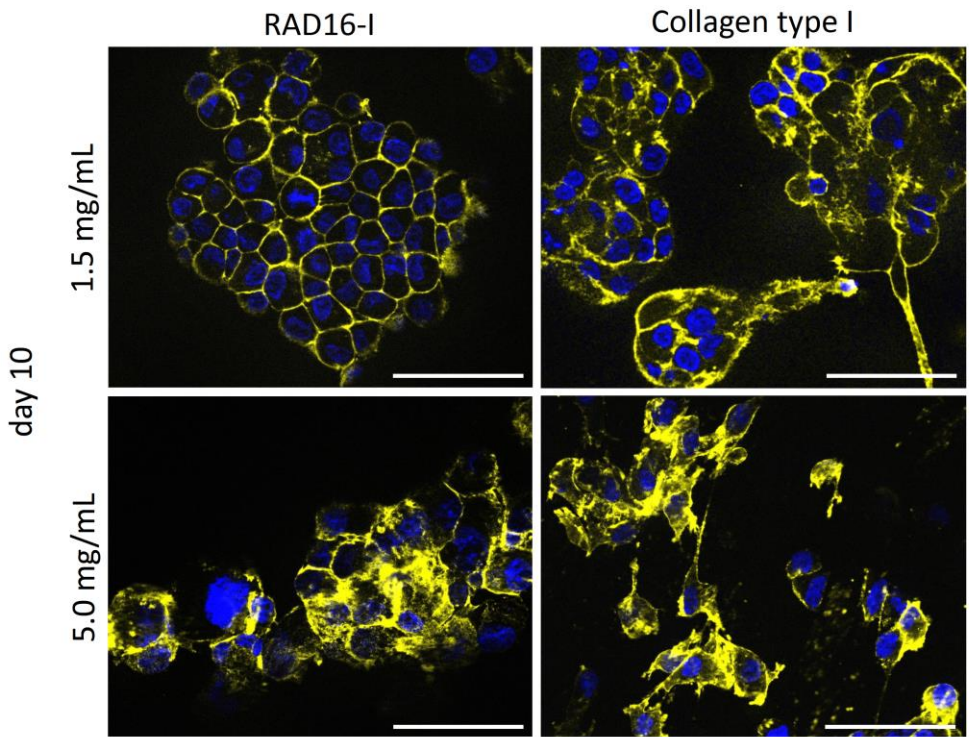

Figure 3.10. Cell morphology and organization in a 3D environment after 10 of day culture. Theinfluence of different microenvironmental signals (matrix stiffness and composition) on cancer cell phenotype was analyzed. In particular, cells were grown within the synthetic self-assembling RAD16-I and the natural collagen type I hydrogels, using concentrations of 1.5 mg/mL and 5.0 mg/mL. After 10-day culture, samples were fixed and stained for actin microfilaments (phalloidin, pseudo-colored in yellow) and nuclei (DAPI, blue). Scale bar of 50 µm.

After 10 days of culture, cells grew forming spheroid clusters. However, different cellular phenotypes could be observed depending on matrix composition and stiffness. These data demonstrated the remarkable plasticity of cancer cells.

Regarding collagen scaffold 1.5 mg/mL (<100 Pa), most of the cells maintained their actin filaments assembled in cortical thin bundles. However, stiff values (approximately 3000 Pa) promoted the remodeling of actin filaments that began to fill the intracellular space. These structures formed stress fibers, a distinctive feature of mesenchymal cells[59]. Furthermore, in both concentration conditions, cells adopted a more elongated and spindle-shape morphology relative to 2D and RAD16-I cultures. Significantly, collagen scaffold at 5.0 mg/mL induced the scattering of cancer cells, detaching them from clusters and causing the acquisition of protrusions on the cellular surface. Previous publications have described these protrusions as the cellular engines that enable migration since they focalize cell-matrix adhesions containing integrin clusters and proteolytic activity[60,61]. Therefore, culturing cancer cells in 3D collagen cultures compromised epithelial tissue organization and induced the development of a more mesenchymal-like phenotype as observed in morphological assessment. Remarkably, matrix stiffening exacerbated phenotypic transitions as EMT since cells showed increased invasive morphologies.

RAD16-I scaffolds do not have the intrinsic cell-matrix adhesion motifs essential for cell anchoring and signaling. In this case, fluorescent images from 1 to 10 days showed that cells grew and interacted with each other to form colonies. Therefore, cells were able to adapt to RAD16-I milieu (studied in more detail in section 3.3.5. CHARACTERIZATION OF E-CADHERIN EXPRESSION). Parallel to the collagen case, stiffening of RAD16-I scaffold (approximately 2000 Pa) induced similar actin cytoskeleton dynamics characterized by the assembling of actin filaments predominantly filling the intracellular space. However, cells did not spread to the same extent and did not form protrusions. Lack of protrusions was related to the incapacity of cells to degrade RAD16-I nanofibers and extend matrix remodeling processes. Images revealed that RAD16-I stiffness *per se* could recapitulate some cellular features of EMT as enhanced cell contractility (cytoskeletal dynamics). However, the acquisition of an elongated and spindle-shape morphology was not observed as in the collagen scaffold.

3.3.4 CELL VIABILITY OF 3D CANCER MODELS

Next, cell viability was analyzed through a qualitative assay based on the use of Calcein-AM (green) and Ethidium homodimer-1 (red) dyes that stained live and dead cells respectively. **Figure 3.11** shows the 3D reconstruction of the culture through different optical sections obtained in a pseudo-confocal microscope.

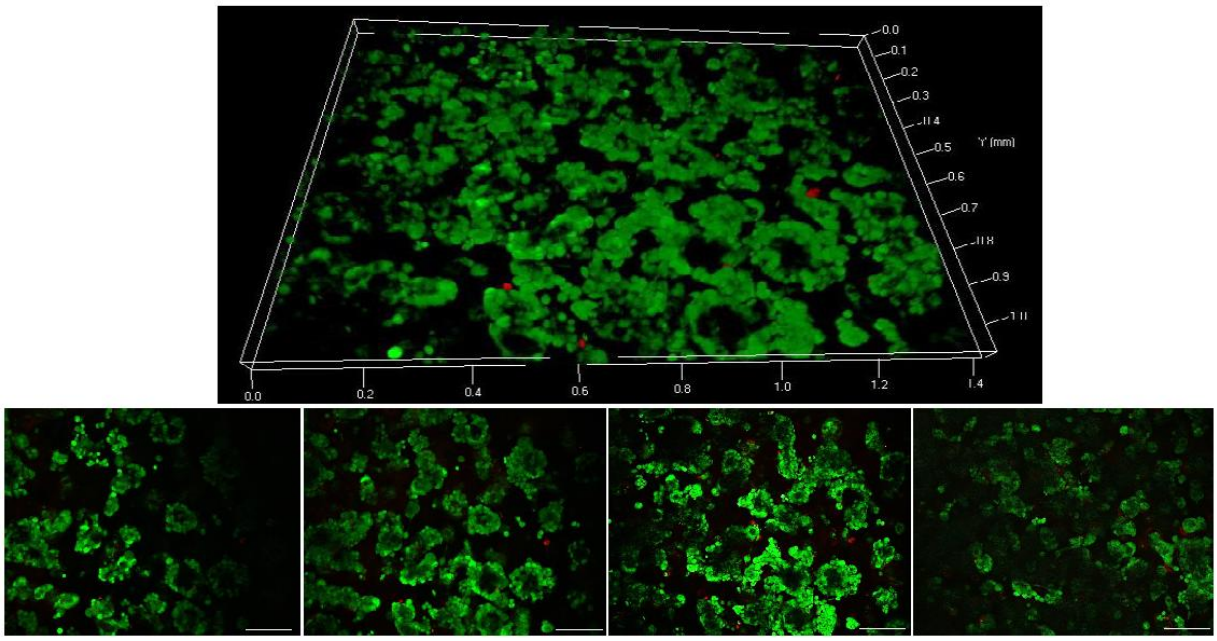

Figure 3.11. 3D reconstruction of the cellular viability in cancer models. The image corresponds to a 3D reconstruction from optical sections taken with a semi-confocal microscope. After 10-day culture, 3D cultures were stained with calcein dye for live cells (green) and ethidium homodimer-1 for dead cells (red). Scale bar of 50 µm.

Cell viability staining and further 3D reconstruction was performed for all the experimental conditions (RAD16-I and collagen scaffolds at concentrations of 1.5 and 5 mg/mL) (**Figure 3.12**):

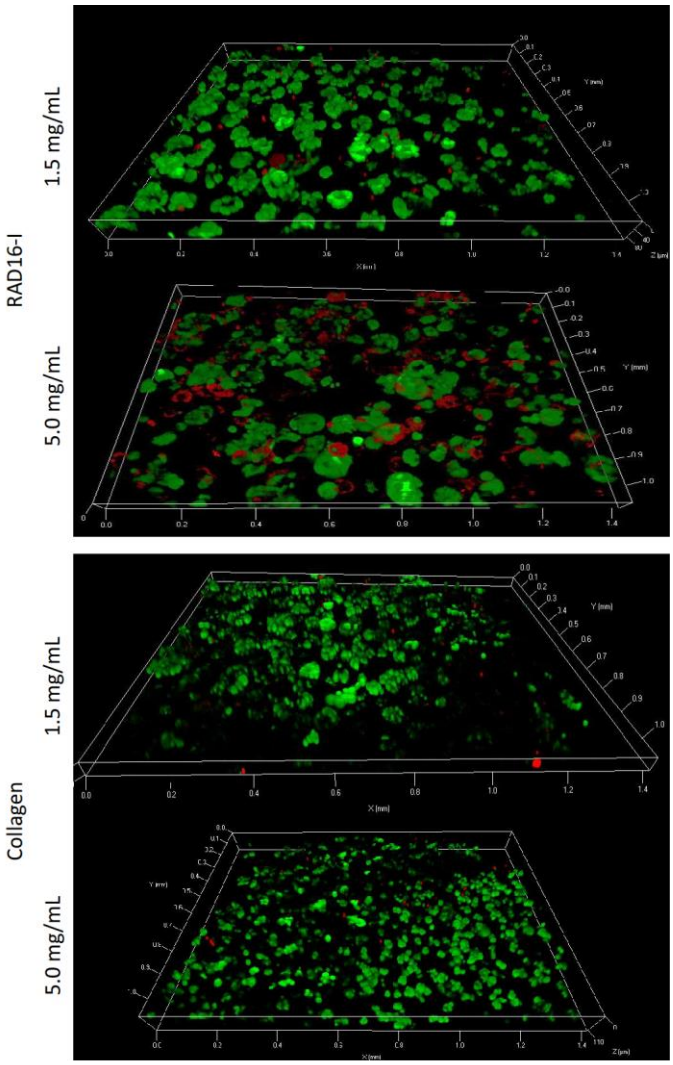

Figure 3.12. Cellular viability of the different 3D cancer models. PANC-1 cells were grown in RAD16-I and collagen scaffolds. After 10-day cultures, they were stained with calcein dye for live cells (green) and ethidium homodimer-1 for dead cells (red). The majority of cell population remained alive along the whole 3D culture period. Fluorescent images from optical sections were taken and stacked to perform a 3D reconstruction of the constructs.

In terms of cell viability, RAD16-I 5.0 mg/mL scaffolds showed the highest cellular death ratio. Two different hypotheses were formulated. First, RAD16-I stock solution could be acid for cells (concentration of 10 mg/mL delivered at pH=3). When liquid RAD16-I biomaterial came into contact with the culture medium, pH value was adjusted to physiological conditions (pH=7) in order to induce the self-assembling process of the peptide. Therefore, cells were exposed to acidic conditions only for a few minutes. Second, RAD16-I could provide a constrained microenvironment to cells as demonstrated by the measured stiffness values. Cells in these

scaffolds were not able to degrade and remodel the matrix. In any case, most of the cells were alive, revealing that all tissue engineering scaffolds and concentrations used for this work were suitable for 3D cultures.

In the case of collagen 5.0 mg/mL scaffold, cell colonies were smaller compared to the other culturing conditions. This data was in agreement with morphology fluorescence images, which revealed that cells detached from clusters and acquired a mesenchymal-like phenotype

3.3.5 CHARACTERIZATION OF E-CADHERIN EXPRESSION

Cells were moved from a 2D to a 3D microenvironment through their culture in RAD16-I and collagen scaffolds. This event could resemble the cellular mechanisms involved in invasion during tumor progression (EMT). During this step, cells downregulate the expression of cell-cell adhesions in order to escape from their epithelial neighbors and invade the 3D stromal ECM. The effect of microenvironment on triggering the EMT program was analyzed through the expression pattern of E-cadherin (*CDH1* gene), a key epithelial cell-cell adhesion molecule, using different 3D scaffolds (**Figure 3.13**).

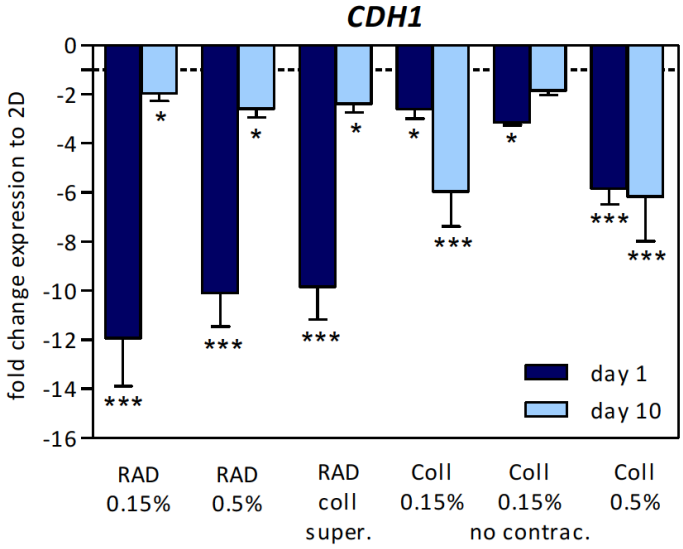

Figure 3.13. Effect of the microenvironment on E-cadherin (*CDH1* gene) expression. Cells were grown in 2D and 3D (RAD16-I and collagen type I) cultures during 1- and 10-day culture. The expression of E-cadherin was assessed by Real Time RT-PCR experiments, selecting conventional monolayer cultures as the calibrator. Results showed the role of microenvironmental signals on cell-cell adhesions. *$p < 0.05$ and ***$p < 0.001$, (N=2, n=6).

The first day after encapsulation, E-cadherin expression was significantly downregulated in RAD16-I scaffolds, between 10- and 12-fold relative to confluent 2D and collagen 1.5 mg/mL cultures. This expression pattern was observed in all RAD16-I culture conditions (1.5 and 5.0

mg/mL). A possible explanation for this phenomenon came from the lack of both anchoring and signaling motifs provided by the self-assembling peptide. Therefore, cells probably identified RAD16-I as a hostile and non-instructive milieu through which they were not able to establish communication channels.

Cells increased E-cadherin expression after 10 days of culture in RAD16-I scaffold. In particular, they showed similar levels to confluent monolayers (2-fold downregulation). This data suggested that cells could decorate RAD16-I scaffold through the synthesis of their own physiological ECM. These results could be in agreement with previous reports that demonstrated the capacity of cancer cells of secreting laminin[62,63] and fibronectin[64] when they fail to properly adhere to their surrounding milieu, partially replacing the role of stromal cells as fibroblasts. More research is needed to confirm this working hypothesis. For instance, immunofluorescence of fibronectin and Collagen I proteins together with Western Blot analysis of phosphorylated versus unphosphorylated focal adhesions could be performed at day 1 and 10 of RAD16-I cultures.

The next experiment consisted in daily transferring the supernatant from collagen cultures to RAD16-I cultures. Accordingly, RAD16-I cultures could receive all the soluble paracrine factors (e.g. growth factors, cytokines) that cancer cells released due to the evolving crosstalk with collagen. Importantly, no effect in E-cadherin expression was observed, reinforcing the critical role of integrins in tumor phenotype.

The first day after encapsulation, cells showed different E-cadherin expression levels depending on collagen experimental conditions. Cells grown in collagen 1.5 mg/mL scaffold downregulated E-cadherin between 2- and 3-fold relative to 2D cultures. This pattern probably responded to the different configuration that epithelial cells acquired in a 3D milieu relative to 2D. Indeed, these values were the same than the ones obtained for RAD16-I cultures at 10 days. Interestingly, cells grown in collagen 5.0 mg/mL downregulated E-cadherin expression 6- to 8-fold relative to 2D cultures. This data suggested a more pronounced disassembly of epithelial cell-cell adhesions, in agreement with fluorescence microscopy characterization. The differences observed between both concentrations responded to mechanical properties (stiffness value) and chemical properties (concentration of integrin adhesion sites). These cues have been reported to drive EMT through integrin clustering and cytoskeleton dynamics[54,65].

After 10 days of culture, cells grown in collagen at 1.5 mg/mL scaffold mimicked E-cadherin expression levels relative to collagen 5.0 mg/mL scaffold (between 6- and 8-fold change of 2D cultures). This pattern correlated with the spontaneous contraction of collagen 1.5 mg/mL. It has been reported that contraction induces the reorganization of matrix fibrils, enhancing the density of integrin-binding motifs[48]. Therefore, the increase in cell-matrix adhesion sites probably caused that collagen scaffolds at 1.5 mg/mL could partially mimic the internal structure of collagen at higher concentrations (5.0 mg/mL). At the microscopic level, cells did not adopt a mesenchymal-like phenotype as pronounced as in collagen 5.0 mg/mL (**Figure 3.10**). These differences between E-cadherin expression and morphological assessment could indicate that

E-cadherin is a good marker for the initial steps of EMT, but additional information is required in order to monitor more precisely the serial of events that occur during the progressive acquisition of a mesenchymal-like phenotype.

To confirm the relevance of integrin signaling, collagen contraction was mechanically blocked by attaching the construct to the culture plate. Cultures showed the same E-cadherin expression levels than collagen 1.5 mg/mL at day 1, being 2-fold downregulated relative to 2D cultures. Therefore, data revealed that the density of integrins was critical for EMT and invasion progression.

3.3.6 MECHANISMS OF E-CADHERIN REGULATION

Dynamic deregulation of cell adhesions can be explained through epigenetic alterations. Two main mechanisms emerge at the core of the pathological state: DNA methylation and histones deacetylation, which directly influence the chromatin structure[27].

First of all, the methylation state of *CDH1* promoter was analyzed in all experimental conditions (2D, RAD16-I and collagen cultures). To avoid miss-interpretations, the presence of mutations in *CDH1* promoter sequence was studied prior to any methylation-specific treatment. The obtained sequences were compared to the National Center for Biotechnology Information (NCBI) database (**Figure 3.14**).

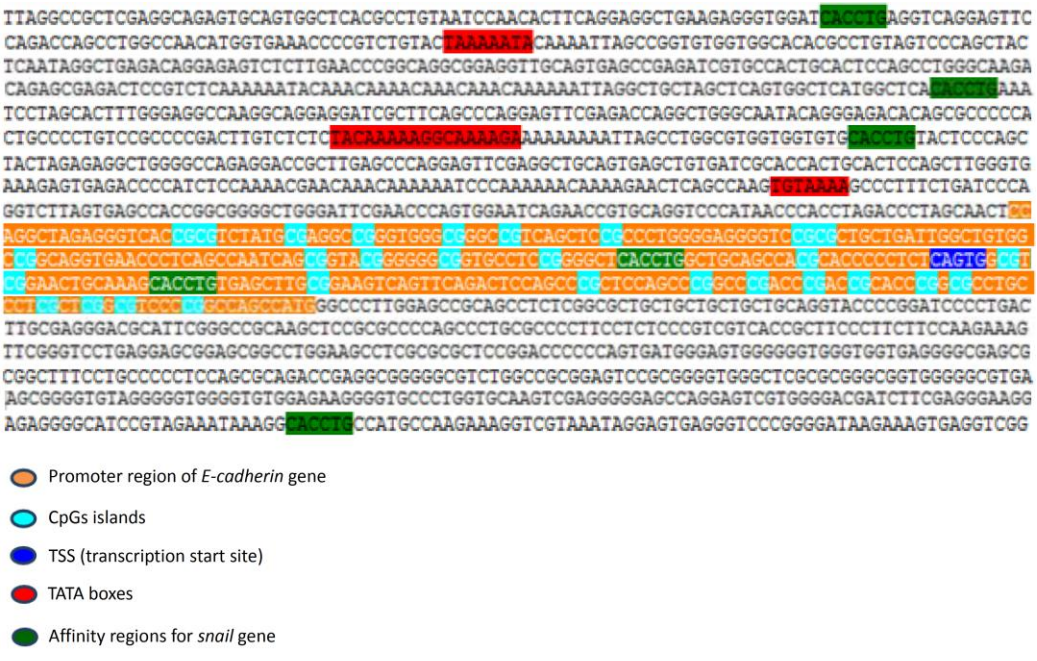

Figure 3.14. Schematic overview of *CDH1* promoter region. Relevant DNA sequences are highlighted in the promoter region: CpG islands, transcription start site (TSS), TATA boxes and affinity regions for *SNAI1* transcription regions.

All samples showed one single nucleotide polymorphism (SNP) at nucleotide -160 (*CDH1* -160C>A) of E-cadherin promoter region. This allelic variation was located around the transcription start site (TSS). Based on literature, this SNP only alters the transcriptional activity of the promoter and correlates with the susceptibility of developing cancer. For this reason, it is identified as a predisposition locus[66,67]. All samples showed this SNP and, thus, differences in E-cadherin expression among microenvironmental conditions were not caused by genetic alterations within the promoter region. Next, epigenetic alterations were analyzed.

The methylation of CpG islands in E-cadherin promoter was investigated. Briefly, DNA was extracted and submitted to bisulfite treatment in order to distinguish methylated from non-methylated cytosines. Samples were PCR-amplified and cloned for sequencing (**Figure 3.15**).

Figure 3.15. Regulation of E-cadherin expression through DNA methylation patterns. Schematic representation of the methylation state of cytosines in CpG islands located in *CDH1* promoter region. The blue color indicates the non-methylated CpGs; the yellow, the methylated CpGs and the grey, the not presented CpGs (*N*=2, *n*=5-6). Methylation experiments were performed with Cristina Castells-Sala (group of Dr. Carlos E. Semino from IQS School of Engineering).

Bisulfite sequencing experiments revealed that any significant hypermethylation of E-cadherin promoter did not occur during different culture conditions. Therefore, results suggested that covalent modification of DNA sequence did not emerge as a regulatory mechanism for E-cadherin expression in pancreatic cancer, confirming previous publications[42].

The second epigenetic mechanism involved in cancer disease is the covalent modification of histones, being their deacetylation the most common signature for dynamic gene silencing. Histones deacetylases (HDAC) are the enzymes responsible for catalyzing this chemical reaction. They usually form protein complexes with transcriptional repressors. In the case of E-cadherin, these repressors are members of the snail, zinc finger E-box-binding homeobox (ZEB) and basic helix-loop-helix (bHLH) families. Therefore, the epigenetic modification of histones was studied through the expression of transcriptional repressors. In particular, the expression of *SNAI1*[42,44,45] and *ZEB2*[42,46] genes is reported to be upregulated in pancreatic cancer (**Figure 3.16**).

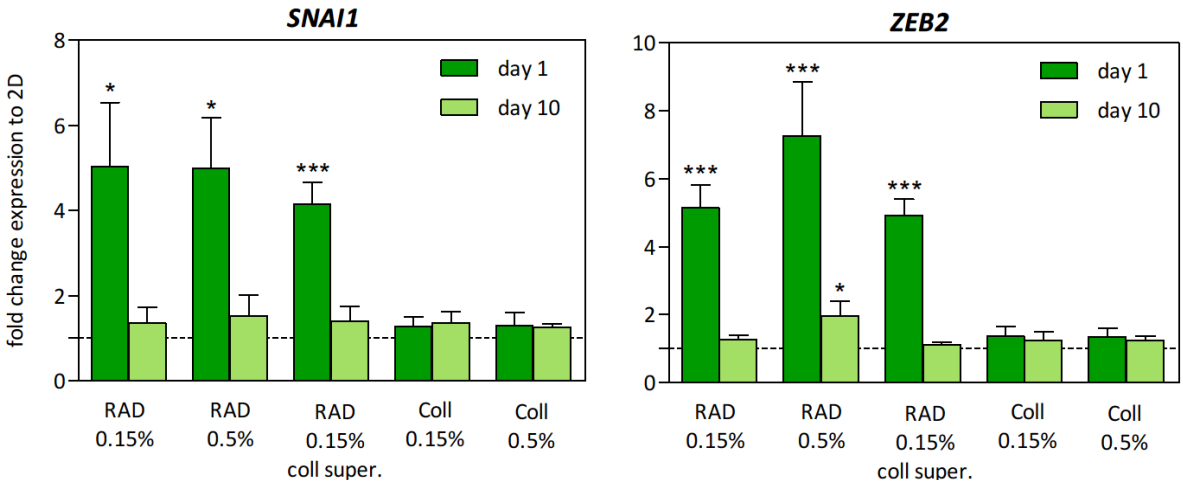

Figure 3.16. Effect of the microenvironment on E-cadherin transcriptional repressors: *SNAI1* and *ZEB2* genes. Cells were grown in 2D and 3D (RAD16-I and collagen type I) cultures during 1- and 10-day culture. The expression of *SNAI1* and *ZEB2* genes was assessed by Real Time RT-PCR, using conventional monolayer cultures as a calibrator. Results showed the role of microenvironmental signals on the regulation of cell-cell adhesions. *p<0.05 and ***p<0.001, (N=2, n=6).

After 1 day of culture, *SNAI1* and *ZEB2* genes were significantly upregulated in RAD16-I cultures, showing approximately 5-fold change relative to 2D cultures. These results correlated with E-cadherin downregulation. It has been largely demonstrated that snail1 and ZEB2 recruit HDAC1/2 proteins[7]. Therefore, this data suggested the existence of a link between the epigenetic modification of histones and the disassembly of cell-cell adhesions, being induced by tumor microenvironment. After 10 days of culture, both transcriptional repressors were expressed at similar levels than 2D cultures, in agreement with E-cadherin results in RAD16-I scaffold.

Regarding collagen cultures, *SNAI1* and *ZEB2* genes were not upregulated despite E-cadherin downregulation after 1- and 10-days of culture. Different hypotheses can explain the obtained pattern and experiments are under development to continue investigating the role of tumor microenvironment in E-cadherin expression.

3.3.7 FUTURE DIRECTIONS

First, *SNAI1* and *ZEB2* could be upregulated in different time points than E-cadherin downregulation. For this reason, future research includes Real Time RT-PCR assays between 1 and 10 days of culture (e.g. 3, 5 and 7 days). Secondly, other transcriptional repressors could be involved in cell-cell adhesion disruption (slug, ZEB1, bHLH) in collagen scaffolds. Collagen provides integrin-recognition sequences and, therefore, E-cadherin regulatory mechanisms can differ from RAD16-I scaffold. To elucidate in more detail the role of integrin signaling, next step can consist in the functionalization of RAD16-I scaffold, for instance with RGD sequences.

On the other hand, the level of protein expression of E-cadherin and transcriptional repressors (snai1 and ZEB2) can be studied. Preliminary Western Blot experiments were performed in order to detect the presence of E-cadherin protein. However, results were not normalized to cell protein content and, thus, were not quantified (**Figure 3.17**). More research is needed in this direction.

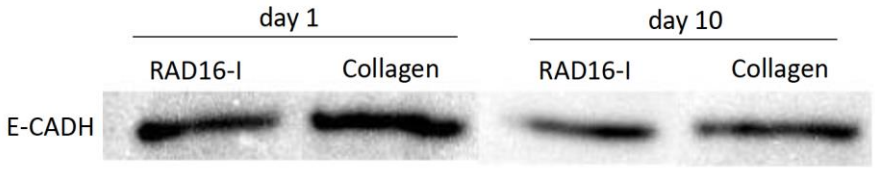

Figure 3.17. E-cadherin protein levels in different microenvironments. Cells were grown in RAD16-I and collagen scaffolds during 1 and 10 days of culture. The expression of E-cadherin protein was analyzed through Western Blot without normalizing samples with protein content. The main objective of the experiment was the detection of E-cadherin at protein level.

3.4 CONCLUDING REMARKS

Cancer is caused by the accumulation of multiple and consecutive genetic alterations together with the evolving crosstalk with the surrounding microenvironment[68]. The influence of microenvironment has been largely disregarded by cancer biologists. They routinely use two-dimensional (2D) cultures for studying the mechanisms involved in this disease, being genome-centered models. The development of three-dimensional (3D) cultures that integrate multiple physical, mechanical and chemical cues from the extracellular matrix (ECM) is crucial to get closer to the real scenario and continue advancing in research. 3D cultures are particularly useful for recapitulating the 2D to 3D transition experienced by cancer cells during invasion. This tumor stage is only possible if cells lose their epithelial phenotype, which results in the disruption of intercellular adhesions (E-cadherin) and the dramatic remodeling of actin cytoskeleton. Consequently, cells acquire a mesenchymal phenotype that switches on motility programs in a process known as epithelial to mesenchymal transition (EMT)[15]. Different 3D cancer models were developed to study the contribution of tumor microenvironment on triggering EMT cell program. Tissue engineering scaffolds based on self-assembling peptide RAD16-I and natural collagen type I biomaterials were used to provide cells with different compositions and stiffness.

Cells showed different phenotypes depending on the experimental culture conditions, demonstrating their plasticity. This property enabled cells to adapt to the evolving microenvironment. RAD16-I scaffolds provided a 3D and non-instructive milieu since they did not contain any cell-ECM recognition sequence. Cells were able to extend processes in these scaffolds: they grew in spheroids clusters and interacted with each other as demonstrated by E-cadherin upregulation from 1- to 10-day culture. Therefore, results suggested that cancer cells could activate mechanisms in order to adapt to a microenvironment in which they fail to properly adhere. Perhaps they could synthetize some ECM components in agreement with previous reports[69]. However, more research is needed in this direction. On the other hand, stiffening of RAD16-I scaffold caused the remodeling of actin cytoskeleton. Cells could balance the exogenous mechanical properties with their endogenous cytoskeleton contractility, compromising epithelial morphology. However, cells did not show distinguishing features of a mesenchymal-like phenotype, such as a spindle-shape morphology or protrusions probably because they could not degrade RAD16-I nanofibers. Therefore, RAD16-I could not completely recapitulate the EMT program due to the lack of ECM-binding motifs as integrin- and metalloproteinases-recognition sequences, revealing their key role in metastatic cascade.

Collagen scaffolds helped us to go a step further, revealing that the presence and concentration of ECM binding motifs was critical. Collagen at 5.0 mg/mL cultures could recapitulate the disruption of epithelial morphology, the disassembly of cell-cell adhesions and the acquisition of protrusions to migrate as individual cells. During disease progression, EMT is accompanied by the desmoplastic reaction (upregulation of type I collagen). Therefore, data suggested that collagen at 5.0 mg/mL scaffolds could mimic tumor microenvironment in terms of physical (3D architecture), mechanical (elastic modulus of 3000 Pa) and chemical (presence

of integrins sites) cues. In fact, these parameters are interconnected since the stiffening of the matrix is achieved by increasing its concentration and, in parallel, enhancing integrin-binding sites density. Collagen 1.5 mg/mL scaffolds could recapitulate these morphological features of EMT when scaffolds suffered a spontaneous contraction process. Thus, recreating only some variables was not sufficient to induce EMT, as demonstrated by RAD16-I (3D milieu) and collagen 1.5 mg/mL (integrins) scaffolds.

The role of tumor microenvironment was also investigated in the mechanisms that regulate E-cadherin expression. At the genetic level, the presence of a single nucleotide polymorphism (SNP) was detected at nucleotide -160C>A relative to the transcriptional start site. Previous research correlates this SNP with lower transcriptional activity of gene promoter[66,67]. All samples (100% of cases) showed this allelic variation. Results suggested that the differences observed in E-cadherin expression among different microenvironmental conditions were not caused by genetic mechanisms within the promoter region.

Regarding epigenetic alterations, no significant hypermethylation of *CDH1* promoter region was reported. Therefore, DNA covalent modifications did not emerge as a primary E-cadherin regulatory mechanism in pancreatic cancer cells (PANC-1). Methylation experiments in 3D cultures were previously reported in breast[25] and squamous[70] cancer, but this was the first study relative to pancreatic cancer.

On the other hand, the upregulation of transcriptional repressors as *SNAI1* and *ZEB2* was described in RAD16-I cultures, being irreversibly correlated with E-cadherin expression levels. This pattern was not detected in collagen cultures, so further research is needed to elucidate the mechanisms involved in E-cadherin regulation in this milieu. Different tumor microenvironments could work in distinct ways to regulate epigenetic modifications. In particular, more time points for Real Time RT-PCR experiments and different transcriptional repressors (slug, ZEB1, bHLH) could be analyzed. All these transcription repressors form protein complexes with histones deacetylases (HDAC) enzymes, which are required for covalently modify histones.

It has been described that DNA and histones covalent modifications can act as a gradient of epigenetic gene silencing during cancer progression, dictating the grade of reversibility in E-cadherin expression[71]. Therefore, the detection of *SNAI1* and *ZEB2* transcriptional repressors along with the absence of significant hypermethylation of gene promoter probably suggested that E-cadherin remained in a transient silenced state in pancreatic cancer. These findings could correlate with the high metastatic capacity that characterizes pancreatic cancer, which easily disseminates and establishes secondary tumor sites. However, further experiments with 3D cultures are needed to better describe this epigenetic landscape.

3.5 REFERENCES

1. Christofori, G. New signals from the invasive front. *Nature* **441,** 444–450 (2006).

2. Yilmaz, M. & Christofori, G. EMT, the cytoskeleton, and cancer cell invasion. *Cancer Metastasis Rev.* **28,** 15–33 (2009).

3. Stevenson, R. P., Veltman, D. & Machesky, L. M. Actin-bundling proteins in cancer progression at a glance. *J. Cell Sci.* **125,** 1073–1079 (2012).

4. Sabeh, F., Shimizu-hirota, R. & Weiss, S. J. Protease-dependent versus -independent cancer cell invasion programs: Three-dimensional amoeboid movement revisited. *J. Cell Biol.* **185,** 11–19 (2009).

5. Ng, M. R. & Brugge, J. S. A stiff blow from the stroma: Collagen crosslinking drives tumor progression. *Cancer Cell* **16,** 455–457 (2009).

6. Friedl, P. & Alexander, S. Cancer invasion and the microenvironment: Plasticity and reciprocity. *Cell* **147,** 992–1009 (2011).

7. Peinado, H., Olmeda, D. & Cano, A. Snail, Zeb and bHLH factors in tumour progression: An alliance against the epithelial phenotype? *Nat. Rev. Cancer* **7,** 415–428 (2007).

8. Gupta, P. B., Mani, S., Yang, J., Hartwell, K. & Weinberg, R. A. The evolving portrait of cancer metastasis. *Cold Spring Harb. Symp. Quant. Biol.* **70,** 291–297 (2005).

9. McCaffrey, L. M. & Macara, I. G. Epithelial organization, cell polarity and tumorigenesis. *Trends Cell Biol.* **21,** 727–735 (2011).

10. Berx, G., Raspé, E., Christofori, G., Thiery, J. P. & Sleeman, J. P. Pre-EMTing metastasis? Recapitulation of morphogenetic processes in cancer. *Clin Exp Metastasis* **24,** 587–597 (2007).

11. Rowe, R. G. & Weiss, S. J. Navigating ECM barriers at the invasive front: The cancer cell-stroma interface. *Annu. Rev. Cell Dev. Biol.* **25,** 567–595 (2009).

12. Thiery, J. P. & Sleeman, J. P. Complex networks orchestrate epithelial-mesenchymal transitions. *Nat. Rev. Mol. Cell Biol.* **7,** 131–142 (2006).

13. Hay, E. D. Organization and fine structure of epithelium and mesenchyme in the developing chick embryo. Epithelial-mesenchymal interactions. *Williams Wilkins, Balt.* **2,** 31–35 (1968).

14. Thiery, J. P., Acloque, H., Huang, R. Y. J. & Nieto, M. A. Epithelial-mesenchymal transitions in development and disease. *Cell* **139,** 871–890 (2009).

15. Thiery, J. P. Epithelial-mesenchymal transitions in tumour progression. *Nat. Rev. Cancer* **2,** 442–454 (2002).

16. Guo, W. & Giancotti, F. G. Integrin signalling during tumour progression. *Nat. Rev. Mol.* **5,** 816–826 (2004).

17. Alberts, B. *et al. Molecular biology of the cell*. *Mol. Biol. Cell* **London: Ga,** (2007).

18. Daniel, J. M. & Reynolds, A. B. Tyrosine phosphorylation and cadherin/catenin function. *BioEssays* **19,** 883–891 (1997).

19. Conacci-Sorrell, M., Zhurinsky, J. & Ben-Ze'ev, A. The cadherin-catenin adhesion system in signaling and cancer. *J. Clin. Invest.* **109,** 987–991 (2002).

20. Hyafil, F., Babinet, C. & Jacob, F. Cell-cell interactions in early embryogenesis: A molecular approach to the role of calcium. *Cell* **26,** 447–454 (1981).

21. Riethmacher, D., Brinkmann, V. & Birchmeier, C. A targeted mutation in the mouse E-cadherin gene results in defective preimplantation development. *Proc. Natl Acad. Sci. USA* **92,** 855–859 (1995).

22. Canel, M., Serrels, A., Frame, M. C. & Brunton, V. G. E-cadherin-integrin crosstalk in cancer invasion and metastasis. *J. Cell Sci.* **126,** 393–401 (2013).

23. Kanai, Y., Oda, T., Tsuda, H., Ochiai, A. & Hirohashi, S. Point mutation of the E-cadherin gene in invasive lobular carcinoma of the breast. *Cancer Sci.* **85,** 1035–1039 (1994).

24. Oda, T. *et al.* E-cadherin gene mutations in human gastric carcinoma cell lines. *Proc. Natl Acad. Sci. USA* **91,** 1858–1862 (1994).

25. Graff, J. R., Gabrielson, E., Fujii, H., Baylin, S. B. & Herman, J. G. Methylation patterns of the E-cadherin 5' CpG island are unstable and reflect the dynamic, heterogeneous loss of E-cadherin expression during metastatic progression. *J. Biol. Chem.* **275,** 2727–2732 (2000).

26. Russo, V. E. A., Martienssen, R. A. & Riggs, A. D. Epigenetic mechanisms of gene regulation. *Cold Spring Harb. Lab. Press. Cold Spring Harb. NY.* (1996).

27. Guil, S. & Esteller, M. DNA methylomes, histone codes and miRNAs: Tying it all together. *Int. J. Biochem. Cell Biol.* **41,** 87–95 (2009).

28. Glozak, M. A. & Seto, E. Histone deacetylases and cancer. *Oncogene* **26,** 5420–5432 (2007).

29. Jones, P. A. & Baylin, S. B. The fundamental role of epigenetic events in cancer. *Nat. Rev.* **3,** 415–428 (2002).

30. Qiu, J. Unfinished symphony. *Nat. news Featur.* **441,** 143–145 (2006).

31. Yoshiura, K. *et al.* Silencing of the E-cadherin invasion-supressor gene by CpG methylation in human carcinomas. *Proc. Natl. Acad. Sci. U. S. A.* **92,** 7416–7419 (1995).

32. Hernández-Muñoz, I., Skoudy, A., Real, F. X. & Navarro, P. Pancreatic ductal adenocarcinoma: Cellular origin, signaling pathways and stroma contribution. *Pancreatology* **8,** 462–469 (2008).

33. Hidalgo, M. Pancreatic cancer. *N. Engl. J. Med.* **362,** 1605–1617 (2010).

34. Neesse, A. *et al.* Stromal biology and therapy in pancreatic cancer. *Gut* **60,** 861–868 (2011).

35. Hruban, R. H., Goggins, M., Parsons, J. & Kern, S. E. Progression model for pancreatic cancer progression. *Clin Cancer Res.* **6,** 2969–2972 (2000).

36. Jones, S. *et al.* Core signaling pathways in human pancreatic cancers revealed by global genomic analyses. *Science (80-.).* **321,** 1801–1806 (2008).

37. Rhim, A. D. *et al.* EMT and dissemination precede pancreatic tumor formation. *Cell* **148,** 349–361 (2012).

38. Cairns, J. Mutation selection and the natural history of cancer. *Nature* **255,** 197–200 (1975).

39. Klein, C. A. Parallel progression of primary tumours and metastases. *Nat. Rev. Cancer* **9,** 302–312 (2009).

40. Hong, S. *et al.* Loss of E-cadherin expression and outcome among patients with resectable pancreatic adenocarcinomas. *Mod. Pathol.* **24,** 1237–1247 (2011).

41. Iacobuzio-Donahue, C., Fu, B. & Yachida, S. DPC4 gene status of the primary carcinoma correlates with patterns of failure in patients with pancreatic cancer. *J Clin Oncol* **27,** 1806–1813 (2009).

42. Aghdassi, A. *et al.* Recruitment of histone deacetylases HDAC1 and HDAC2 by the transcriptional repressor ZEB1 downregulates E-cadherin expression in pancreatic cancer. *Gut* **61,** 439–448 (2012).

43. Winter, J. M. *et al.* Absence of E-Cadherin expression distinguishes noncohesive from cohesive pancreatic cancer cohesive pancreatic cancer. *Clin Cancer Res.* **14,** 412–418 (2008).

44. Von Burstin, J., Eser, S. & Paul, M. E-cadherin regulates metastasis of pancreatic cancer in vivo and is suppressed by a SNAIL/HDAC1/HDAC2 repressor complex. *Gastroenterology* **137,** 361–371 (2009).

45. Shields, M. A., Dangi-Garimella, S., Krantz, S. B., Bentrem, D. J. & Munshi, H. G. Pancreatic cancer cells respond to type I collagen by inducing snail expression to promote membrane type 1 matrix metalloproteinase-dependent collagen invasion. *J. Biol. Chem.* **286,** 10495–10504 (2011).

46. Imamichi, Y., Ko, A., Gress, T. & Menke, A. Collagen type I-induced Smad-interacting protein 1 expression downregulates E-cadherin in pancreatic cancer. *Oncogene* **26,** 2381–2385 (2007).

47. Griffith, L. G. & Swartz, M. A. Capturing complex 3D tissue physiology in vitro. *Nat. Rev. Mol. Cell Biol.* **7,** 211–224 (2006).

48. Jokinen, J. *et al.* Integrin-mediated cell adhesion to type I collagen fibrils. *J. Biol. Chem.* **279,** 31956–31963 (2004).

49. Dikovsky, D., Bianco-Peled, H. & Seliktar, D. Defining the role of matrix compliance and proteolysis in three-dimensional cell spreading and remodeling. *Biophys. J* **94,** 2914–2925 (2008).

50. Ehrbar, M. *et al.* Elucidating the role of matrix stiffness in 3D cell migration and remodeling. *Biophys. J.* **100,** 284–293 (2011).

51. Grzesiak, J. J. & Bouvet, M. The α2β1 integrin mediates the malignant phenotype on type I collagen in pancreatic cancer cell lines. *Br. J. Cancer* **94,** 1311–1319 (2006).

52. TA Insruments. *DMA Q800 Specifications*. 1–22 (2014).

53. Sieminski, A. L., Was, A. S., Kim, G., Gong, H. & Kamm, R. D. The stiffness of three-dimensional ionic self-assembling peptide gels affects the extent of capillary-like network formation. *Cell Biochem. Biophys.* **49,** 73–83 (2007).

54. Paszek, M. J. *et al.* Tensional homeostasis and the malignant phenotype. *Cancer Cell* **8,** 241–254 (2005).

55. Levental, I., Georges, P. C. & Janmey, P. A. Soft biological materials and their impact on cell function. *Soft Matter* **3,** 299–306 (2007).

56. Walter, N., Busch, T., Seufferlein, T. & Spatz, J. P. Elastic moduli of living epithelial pancreatic cancer cells and their skeletonized keratin intermediate filament network. *Biointerphases* **6,** 79–85 (2011).

57. Haage, A. & Schneider, I. C. Cellular contractility and extracellular matrix stiffness regulate matrix metalloproteinase activity in pancreatic cancer cells. *FASEB J.* **28,** 3589–3599 (2014).

58. ApoTome. Optical Sectioning Using Structured Illumination. *http://www.zeiss.com/microscopy/en_de/home.html* (2014).

59. Haynes, J., Srivastava, J., Madson, N., Wittmann, T. & Barber, D. L. Dynamic actin remodeling during epithelial-mesenchymal transition depends on increased moesin expression. *Mol. Biol. Cell* **22,** 4750–4764 (2011).

60. Wolf, K. *et al.* Multi-step pericellular proteolysis controls the transition from individual to collective cancer cell invasion. *Nat. Cell Biol.* **9,** 893–904 (2007).

61. Friedl Peter & Wolf Katarina. Tumour-cell invasion and migration: Diversity and escape mechanisms. *Nat. Rev. Cancer* **3,** 362–374 (2003).

62. Zahir, N. *et al.* Autocrine laminin-5 ligates alpha6beta4 integrin and activates RAC and NFkappaB to mediate anchorage-independent survival of mammary tumors. *J. Cell Biol.* **163,** 1397–407 (2003).

63. Davis, T. L., Cress, A. E., Dalkin, B. L. & Nagle., R. B. Unique expression pattern of the alpha6beta4 integrin and laminin-5 in human prostate carcinoma. *Prostate* **46,** 240–248 (2001).

64. Ioachim, E. *et al.* Immunohistochemical expression of extracellular matrix components tenascin, fibronectin, collagen type IV and laminin in breast cancer: Their prognostic value and role in tumour invasion and progression. *Eur. J. Cancer* **38,** 2362–2370 (2002).

65. Provenzano, P. P., Inman, D. R., Eliceiri, K. W. & Keely, P. J. Matrix density-induced mechanoregulation of breast cell phenotype, signaling and gene expression through a FAK-ERK linkage. *Oncogene* **28,** 4326–4343 (2009).

66. Pittman, A. M. *et al.* The CDH1-160C>A polymorphism is a risk factor for colorectal cancer. *Int. J. Cancer* **125,** 1622–1625 (2009).

67. Wang, L., Wang, G., Lu, C., Feng, B. & Kang, J. Contribution of the -160C/A polymorphism in the E-cadherin promoter to cancer risk: A meta-analysis of 47 case-control studies. *PLoS One* **7,** e40219 (2012).

68. Mueller, M. M. & Fusenig, N. E. Friends or foes - Bipolar effects of the tumour stroma in cancer. *Nat. Rev. Cancer* **4,** 839–849 (2004).

69. Barkan, D., Green, J. E. & Chambers, A. F. Extracellular matrix: A gatekeeper in the transition from dormancy to metastatic growth. *Eur. J. Cancer* **46,** 1181–1188 (2010).

70. Desrochers, T. M. *et al.* The 3D tissue microenvironment modulates DNA methylation and E-cadherin expression in squamous cell carcinoma. *Epigenetics* **7,** 34–46 (2012).

71. Issa, J. & Kantarjian, H. Targeting DNA methylation. *Clin Cancer Res.* **15,** 3938–3946 (2009).

CHAPTER 4

DEVELOPMENT OF 3D MODELS TO STUDY PHOTODYNAMIC THERAPY OUTCOME

4.1 BACKGROUND

4.1.1 PHOTODYNAMIC THERAPY

Photodynamic therapy (PDT) is a clinically approved procedure for the treatment of diseases characterized by uncontrolled cell proliferation, principally cancer[1]. Up to date, it shows successful results in a variety of cancer types including skin, bladder, lung, breast, esophagus and cervix[2]. PDT is also used in other fields of medicine with a particular interest in ophthalmology (macular degeneration and choroidal neovascularization)[3,4], dermatology (acne, actinic keratosis and psoriasis)[5] and antimicrobial therapies (antibiotic-resistant localized infections)[6].

PDT involves the interaction of three independent and individually non-toxic factors: a photoactive dye called photosensitizer (PS), visible light and molecular oxygen. The principle of this therapy relies on the administration of the PS, followed by the irradiation of the diseased area with light of appropriate wavelength. In the presence of molecular oxygen, highly cytotoxic reactive oxygen species (ROS) are generated, leading to the selective destruction of cancer cells.

Mechanistically, PS absorbs a photon when it is irradiated with light of the appropriate wavelength and an electron is promoted from the ground state (S_0) to an electronically excited state (S_1*). This short-lived specie can release its energy through light emission (fluorescence), internal conversion to heat or intersystem crossing to form a more stable triplet state (T_1*). The relative long lifetime of the triplet state allows the interaction of the excited PS with the surrounding molecules, performing two classes of reactions defined as Type I and Type II mechanisms. In the Type I mechanism, PS reacts directly with an organic molecule from the cellular microenvironment, transferring a hydrogen atom or an electron to form radical species. These free radicals further react with molecular oxygen and lead to ROS such as superoxide anion (O_2^{-}), hydrogen peroxide (H_2O_2) or hydroxyl radicals ($HO^{\cdot}$). Alternatively, the Type II mechanism is initiated by the energy transfer between the triplet excited state of the PS and nearby oxygen molecules, generating the singlet excited state of oxygen that is referred as singlet oxygen ($^1O_2$). The majority of PSs operate via a Type II mechanism. During this process, PS is regenerated and acts in a catalytically manner. As consequence, many cycles of $^1O_2$ production can occur for each PS molecule[7] (**Figure 4.1**).

Singlet oxygen is the major cytotoxic agent involved in PDT and its presence induces tumor regression by three mechanisms: direct killing of cancer cells, damage to microvasculature and triggering of a local immune response[8].

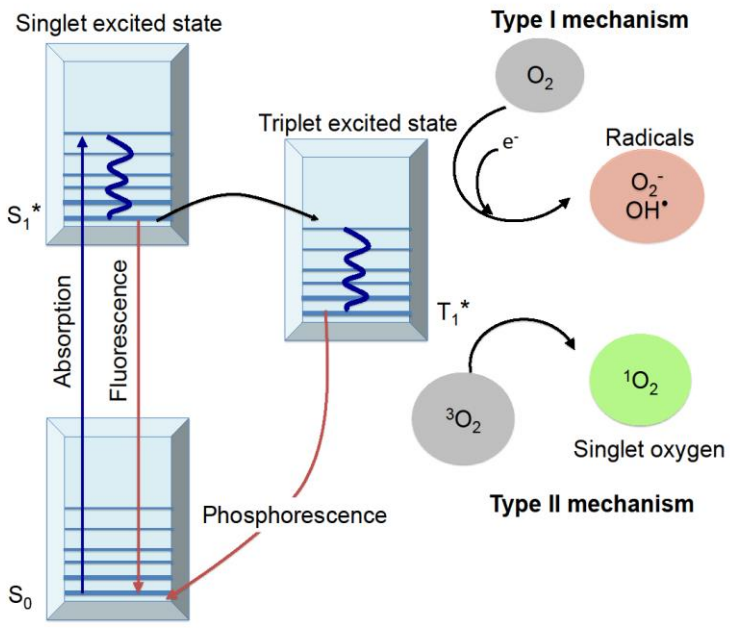

Figure 4.1. Principle of photodynamic therapy (PDT). Schematic overview of the Jablonski diagram of photosensitizer (PS) excited states and their interaction with molecular oxygen. During PDT, PS is administrated and the diseased area is irradiated with light of appropriate wavelength. Consequently, PS absorbs a photon, promoting an electron from the ground state (S_0) to an electronically excited state (S_1*). PS excited state can release its energy by undergoing intersystem crossing to form a more stable triplet state (T_1*). This triplet state can undergo electron transfer to organic molecules of the surrounding milieu generating superoxide, hydrogen peroxide and hydroxyl radicals (Type I reaction) or can undergo energy transfer to molecular oxygen producing highly cytotoxic singlet oxygen (Type II reaction). All these highly cytotoxic reactive oxygen species trigger the selective destruction of cancer cells.

PDT causes an acute cellular stress response that leads to the activation of multiple signaling pathways and ultimately evokes to any of the three main death mechanisms: apoptosis, necrosis or autophagy-associated cell death. The type and extent of photodamage mainly depend on PS subcellular localization since $^1O_2$ lifetime is very short (<0.04 µs) and limits its radius of action (10-55 nm)[9]. PSs can associate with plasma membrane or intracellular membranes of the endoplasmic reticulum, mitochondria, lysosomes and/or Golgi apparatus. In these locations, PDT triggers the photo-oxidation of unsaturated lipids, which damages membranes, allows leakage of cellular contents and/or inactivates transport systems. As a result, affected cells produce a variety of cytokines and stress proteins that act over neighboring cells[10].

Tumors require the formation of new blood capillaries from pre-existing ones (angiogenesis)[11]. These capillaries display two main functions: (*i*) supply of nutrients and oxygen to fulfill the metabolic requirements of proliferating cancer cells and (*ii*) establishment of a transport network to enable the colonization of metastatic cancer cells. This process is driven by the tight release both spatially and temporally of pro-angiogenic factors. They are responsible for stimulating endothelial cells to migrate, proliferate and differentiate in a new lumen-containing vessel. Subsequently, endothelial cells generate a new basement membrane and secrete more growth factors for the recruitment of supporting cells that ensure the stability of the new vessel (i.e. pericytes)[12]. Endothelial cells are highly sensitive to PDT effects and,

therefore, this therapy has the potential to damage or destroy tumor blood vessels[1]. Indeed, the combination of PDT with drugs capable of inhibiting pro-angiogenic factors, such as vascular endothelial growth factor (VEGF) and angiopoietin 2 (Ang2), has been successfully applied in clinic. Good results account for the simultaneous damage of the vasculature network together with the inhibition of neo-angiogenesis processes[13,14].

Another important aspect of PDT is its capacity to stimulate the immune system in order to recognize and destroy any remaining cancer cell, from either primary tumor or distant metastasis. This response is caused by the emission of alarm/danger signals, also called damage-associated molecular patterns (DAMPs). DAMPs are retained in cells under normal conditions, but exposed on their surface or released in response to damage or stress. Some examples include endoplasmic reticulum chaperon CRT, heat-shock protein HSP90 and nuclear protein HMGB1[15]. PDT induces the presence of these alarm signals by triggering an acute inflammatory response. DAMPs are recognized by dendritic cells and neutrophils, which mature and home to the regional lymph nodes. There they present antigens to the T lymphocytes that migrate to the tumor in order to kill cancer cells. Therefore, PDT mediates the formation of T-cell adaptive immunity and induces an immunogenic cell death[8] (**Figure 4.2**).

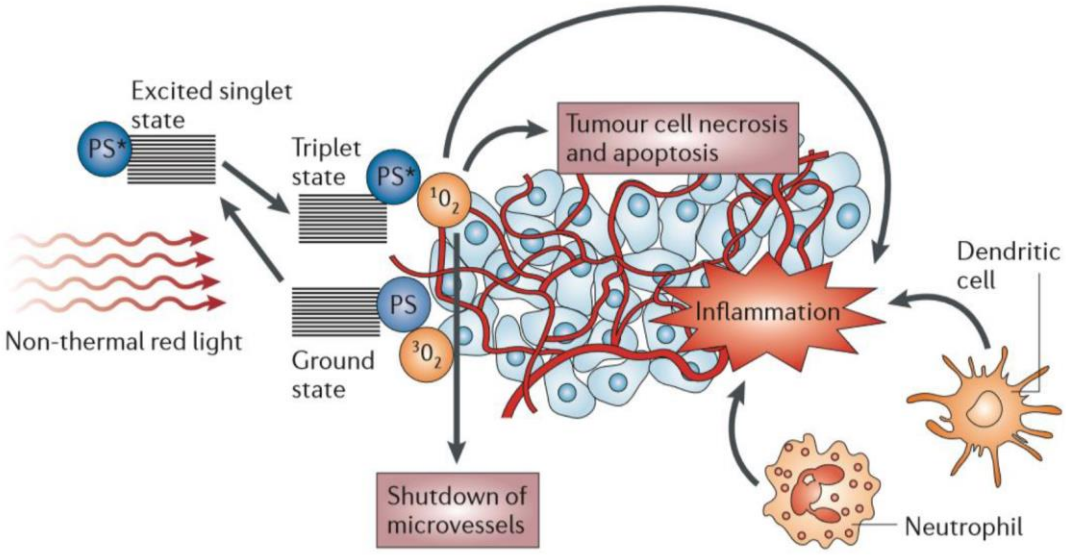

Figure 4.2. Mechanism of action of photodynamic therapy in cancer. Singlet oxygen can directly kill cancer cells by the induction of necrosis, apoptosis or autophagy after an acute stress response. Simultaneously, it can cause the destruction of the vasculature network in tumor microenvironment and the stimulation of the immune system. In particular, cancer dead cells express a spatiotemporally defined combination of damage-associated molecular patterns (DAMPs). These endogenous signals are recognized by dendritic cells and neutrophils, which are home to the regional lymph nodes and present antigens to the T lymphocytes. Therefore, DAMPs mediated the formation of T-cell adaptive immunity. From Castano *et al*.[8]

4.1.1.1 Practical Considerations of Photodynamic Therapy

The use of PDT as cancer therapy is particularly attractive because of its dual selectivity. First, PS is preferentially accumulated in the tumor rather than the healthy tissue. Second, its activation can be confined by restricting the illumination to a specific area. The exact mechanisms that account for PS preferential location are not fully understood, but reveal the important contribution of the abnormal tumor physiology: poor lymphatic drainage, leaky and permeable vasculature, low pH and high number of receptors for low-density lipoprotein that mediated drug intracellular transport[1].

Furthermore, PDT does not induce significant levels of resistance in cancer cells. Only two mechanisms are described based on the variation of cellular antioxidant levels and the expression of enzymes capable of detoxifying ROS[1]. Finally, PDT is immunostimulatory, being located at the opposite end of immunosuppressive chemotherapy and radiotherapy. Both therapies are toxic to bone marrow, which is the source of cells from the immune system[8].

Paradoxically, the advantage of selectivity turns into an intrinsic limitation when treating metastatic lesions due to the impossibility of irradiating the whole body with appropriate doses[1]. Another disadvantage of PDT comes from its low therapeutic efficacy that can be explained through the non-homogeneous oxygen distribution (hypoxia in the core of the tumor) together with oxygen depletion during the photodynamic reaction[7]. Pain and a persistent skin photosensitivity are also described.

4.1.1.2 Approved Photosensitizers and Perspectives

Nowadays, only four PS agents are approved for PDT: (*i*) porfimer sodium, an hematoporphyrin derivate commercially available as Photofrin® and PhotoBarr®; (*ii*) temoporfin or 5,10,15,20-tetra(m-hydroxyphenyl)chlorin (m-THPC) as Foscan®; (*iii*) 5-aminolevulinic acid (ALA) and its methyl ester (M-ALA) as Levulan® and Metvix® respectively; and (*iv*) verteporfin or benzoporphyrin derivative monoacid ring A (BPD-MA) as Visudyne®[16,17]. However, none of them fulfils all the demands required for standardized applications in oncology. They present low selectivity between tumour and healthy tissue and a low therapeutic efficacy. Furthermore, porfimer sodium and temoporfin induce a pronounced and lengthy skin photosensitivity[1,16].

Based on these considerations, concerted efforts are made towards the development of new PSs with the overall aim of improving therapeutic outcomes for patients. Current examples include members of porphyrins, chlorins, bacteriochlorins, purpurins, phthalocyanines, naphthalocyanines, texaphyrins and porphycenes families[17]. In the present thesis, two PSs are used: zinc phthalocyanine (ZnPc) and cationic porphyrin 5,10,15,20-tetrakis(N-methyl-4-pyridilium)-21H, 23H-porphine (TMPyP).

ZnPc is a promising PS because of its high optical absorption coefficient in the 600- to 800-nm therapeutic window (optimal tissue penetration). Moreover, the incorporation of a diamagnetic metal (Zn) into the phthalocyanine macrocycle causes a long-life triplet state, resulting in efficient photosensitization reactions. However, ZnPc is extremely hydrophobic and prone to self-aggregate in aqueous solutions. This property makes necessary the use of specific carriers for its delivery into biological systems[18]. ZnPc is usually formulated in liposomes composed of palmitoyl-oleoyl-phosphatidylcholine (POPC) and di-oleoyl-phosphatidylserine (OOPS) in a ratio of ZnPc:OPOC:OOPS at 1:90:10 (w/w/w). It is developed by QLT Phototherapeutics and sponsored by Ciba Geigy (Novartis). Significantly, ZnPc is the first phthalocyanine reaching clinical trials (Phase I/II, Switzerland) for PDT[19].

TMPyP shows different absorption peaks like all porphyrins. Its maximum is located in Soret band (424 nm), but has an additional peak at 630 nm wavelength. It is hydrophilic and has an elevate quantum yield for singlet oxygen production, making it very interesting for singlet oxygen investigations[20,21] (**Figure 4.3**).

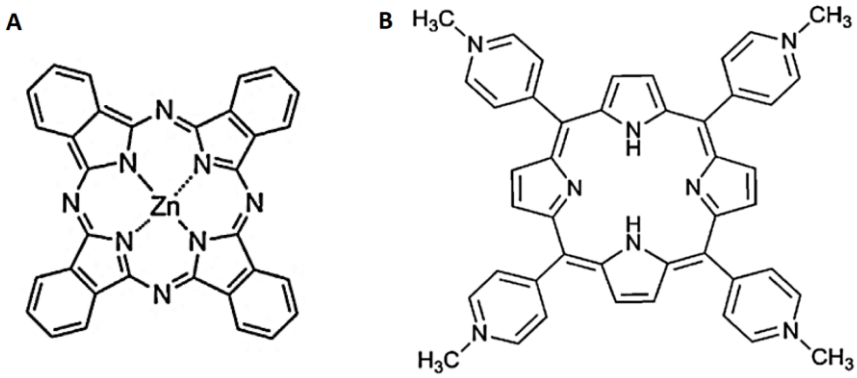

Figure 4.3. Chemical structure of ZnPc and TMPyP photosensitizers. (**A**) ZnPc is a phthalocyanine that has a high optical absorption coefficient in 600-800 nm. It is hydrophobic, making necessary the use of carriers like liposomes for its cellular delivery. (**B**) TMPyP is a cationic porphyrin that has different absorption peaks, having its maximum in Soret band (424 nm). It is very hydrophilic and can be directly delivered.

Therefore, a major challenge in PDT is the development of new PSs. However, drug discovery is an inefficient process. It is estimated that only 8% of candidates that enter Phase I trials receive final approval from American Food and Drug Administration (FDA)[22]. This high failure rate is in part related with the continued use of cellular systems that alter or miss many important tissue-related functions, impairing their predictive power. A current demand for both academia groups and pharmaceutical industry is to set up models that reproduce the phenotype of the target tissue more precisely in order to obtain reliable biomedical data that correlates with *in vivo* tests.

4.1.2 TISSUE ENGINEERING AND PHOTODYNAMIC THERAPY

In drug development processes, early biological-activity assessment has traditionally depended on two-dimensional (2D) cultures and animal models[23]. 2D cultures have provided valuable information on cellular responses after drug treatments. However, it is commonly accepted that the flat and hard plastic substrates are not representative of the cellular microenvironment. At the opposite end of experimental platforms, animal models can display the integrated responses that result from complex interactions between tissues and organs. Inconveniently, they fail to capture important facets of human responses, are very costly, time-consuming and ethically controversial[24].

There is a high demand for models that capture the complexity of human tissues while retaining the ability for high-throughput screening and cellular level imaging. As a result, three-dimensional (3D) cultures are under development. They provide the third dimension that is essential to (*i*) reproduce the molecular gradients that exist in tissues for any soluble component such as oxygen and drugs and (*ii*) integrate multiple cues that arise from extracellular matrix (ECM) and neighboring cells[24].

3D cultures can help to bridge the gap between 2D cultures and animal models. They can be used to study the molecular mechanisms underlying human diseases and/or predict drugs outcome (**Figure 4.4**).

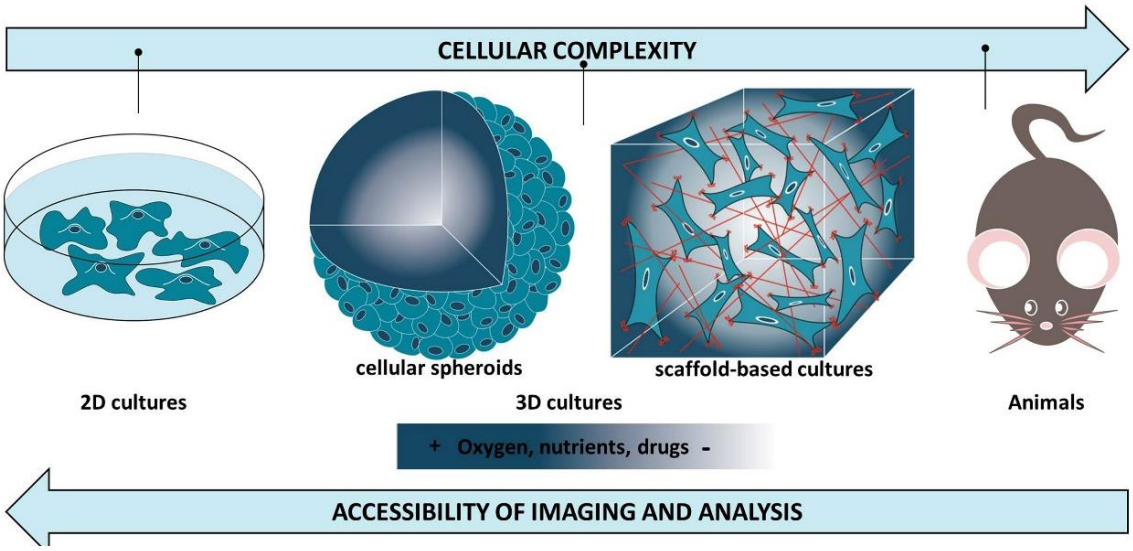

Figure 4.4. Rethinking drug screening processes. 3D cultures can recreate the complex cellular microenvironment more precisely than traditional 2D cultures due to the incorporation of the third dimension for cell growth. Consequently, multiple cues that arise from ECM-cell and cell-cell interactions are integrated in 3D cultures. Moreover, molecular gradients for soluble molecules (i.e. oxygen and drugs) are captured. At the opposite end of the experimental continuum, animals do not capture important facets of human behavior and they are not feasible for high-throughput applications since they are costly, time-consuming and ethically controversial.

In drug discovery field, the most commonly used 3D cultures are spheroids and scaffold-based cultures[22]. They provide tissue-specific information at different and complementary levels of complexity. However, their optimization and exploitation in PDT pre-clinical research remains largely unexplored.

4.1.2.1 Cellular Spheroids for Photodynamic Therapy

Spheroids are compact cellular clusters based on the natural tendency of many cell types to aggregate. They contain both surface exposed and deeply buried cells. Therefore, they establish zones of proliferating cells in the outside and quiescent cells in the inside due to nutrient and oxygen gradients. These systems capture many aspects of the pathophysiology milieu in human tumor tissues[25]. Sutherland and collaborators[26,27] were pioneers in using spheroids in cancer research. They characterized their morphology through growth rate and oxygenation studies.

In PDT field, the group of De Witte[28–31] used spheroids to mimic bladder carcinoma and evaluate PDT outcome compared with classical 2D cultures. Cells were grown until aggregates reached 450-500 µm in diameter, mimicking mass transport limitations occurring *in vivo* (diffusion limit for oxygen and drugs states in 150-250 µm)[24,32]. 3D cultures showed a heterogeneous distribution of PS with high concentrations at the periphery that decreased rapidly in the inner spheroidal regions. As a consequence of poor drug penetration and oxygen depletion, spheroids showed a dramatically low phototoxicity[28]. Finally, they studied the cellular mechanisms underlying PDT with a special focus on PS location. They demonstrated that drug accumulation inversely correlated with the expression of intercellular adhesion proteins (E-cadherin)[29–31].

Spheroids have led to major conceptual advances in understanding discrepancies in PDT mechanisms and efficacy between 2D cultures and *in vivo* experiments. However, they are limited by slow spontaneous aggregation and uncontrolled final size and shape, which importantly difficult a precise control of oxygen and compounds gradients[25,33].

4.1.2.2 Scaffold-Based Cultures for Photodynamic Therapy

Scaffold-based cultures are considered a good alternative to spheroids, offering two important advantages. First, scaffolds can be designed to specifically incorporate environmental signals depending on the tumor tissue and stage. Secondly, scaffold architecture and dimensions can be precisely defined to control the spatial distribution of drug and oxygen[24]. As previously mentioned, Bissell and collaborators[34,35] were pioneers in using scaffold-based models in cancer research.

In PDT field, the group of Hasan[32,36,37] developed a 3D cervical cancer model to mimic the avascular metastatic tumors that coat surfaces of the peritoneal cavity. Briefly, cells were cultured on the surface of Matrigel™ and grown until achieving a population of nodules larger than 200 μm in diameter. They used this model as a platform to screen drug candidates capable of breaking the protective microenvironment created by hypoxia. For this purpose, they developed two different strategies. First, they proposed the use of PSs that could impart cytotoxicity across Type I and II photodamage mechanisms and, thus, were able to treat hypoxic-resistant cells through Type I reaction[32]. The second strategy was based on the synergic effect of combining PDT with chemotherapeutic drugs[37]. During other studies, they co-cultured cancer and stromal cells (fibroblasts and endothelial cells) in Matrigel to study the contribution of cell-cell interactions in treatment response[36,38].

A further step towards the development of 3D models for PDT research can be the use of synthetic scaffolds in order to flexibly tune different ECM properties and analyze their intrinsic role in treatment response. Secondly, the contribution of stromal cells in PDT can be extensively studied. It has been largely demonstrated that the crosstalk between cancer and stromal cells drives tumor progression[39]. For instance, fibroblasts are responsible for the synthesis, deposition and modelling of much of the ECM components. Moreover, they are a source of paracrine growth factors that induce cancer cell growth[40,41]. Therefore, these cells act as active participants in disease progression rather than passive bystanders.

4.2 HYPOTHESIS AND SPECIFIC AIMS

The main motivation of this chapter was to study the contribution of tumor microenvironment in photodynamic therapy (PDT) response.

Our working hypothesis was that three-dimensional (3D) cultures could help us to evaluate the role of specific extracellular signals in the mechanism and efficacy of this cancer therapy. For this reason, these cultures were designed to sequentially incorporate increasing levels of biological complexity. The specific aims of this chapter were the following:

(1) To develop a 3D cell model that allowed us to analyze the influence of 3D architecture in PDT outcome.

(2) To develop a 3D cell model that allowed us to analyze the influence of extracellular matrix (ECM) signaling motifs in PDT outcome.

(3) To develop a 3D cell model that allowed us to analyze the influence of the crosstalk between cancer and stromal cells (fibroblasts) in PDT outcome.

4.3 RESULTS AND DISCUSSION

4.3.1 DEVELOPMENT OF 3D CELL MODELS FOR DRUG TESTING

Different three-dimensional (3D) cell models with increasing levels of biological complexity were developed. The main purpose was to analyze how cells respond to changes in microenvironmental signaling and isolate the effects of specific extracellular matrix (ECM) properties and stromal cells on therapy testing.

The first model was based on culturing human normal dermal fibroblasts (hNDF) in the self-assembling peptide RAD16-I. This hydrogel provided a non-instructive and defined milieu to cells, allowing us to study the influence of 3D architecture in photodynamic therapy (PDT) outcome. Fibroblasts were selected as cell source since one of the main therapeutic targets for PDT are skin afflictions, such as non-melanoma skin cancer, actinic keratosis, keloid disease, psoriasis, acne or rosacea[42,43]. Moreover, they are the major constituents of tumor stroma, being a 3D model that can be further used to examine the effects of co-cultures with cancer cells[41].

Cell morphology and organization in the 3D cultures were characterized. In particular, nuclei and actin microfilaments of the cytoskeleton were stained with DAPI (blue) and Phalloidin-TRITC (yellow, pseudo-color) dyes respectively (**Figure 4.5**).

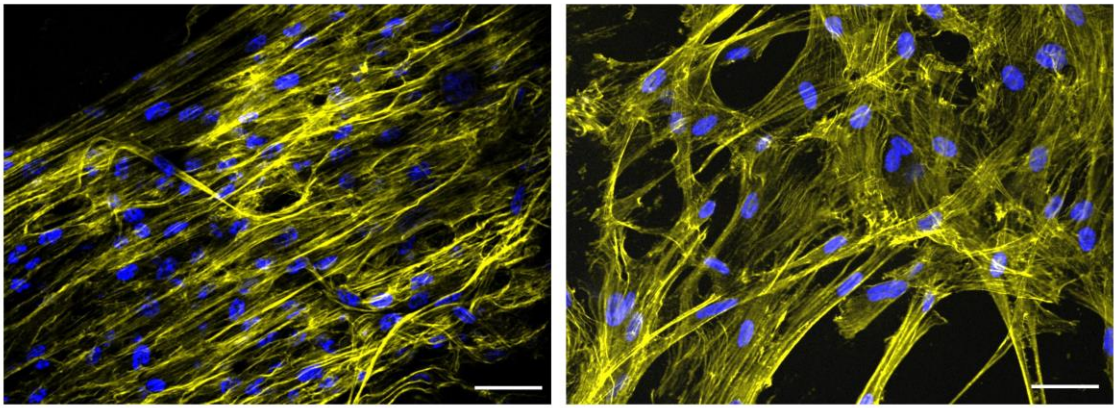

Figure 4.5. Fibroblasts morphology and organization in a 3D environment. Fibroblasts were grown in the synthetic self-assembling RAD16-I. After 5-day culture, samples were fixed and stained for actin microfilaments (phalloidin, pseudo-colored in yellow) and nuclei (DAPI, blue). These fluorescent images correspond to different optical sections of the same 3D culture, revealing a dense and intricate cellular network. Scale bar of 50 µm.

Fibroblasts embedded in the 3D milieu spread and adopted an in *vivo*-like lengthened shape. Furthermore, they established many intercellular contacts. At the edge of the construct, they oriented in the same direction (first image) suggesting a self-organization process. This cellular elongation and network formation was developed due to the permissive

microenvironment provided by RAD16-I hydrogel, which is characterized by having non-covalent interaction between its nanofibers.

Further morphological evaluation was performed through field emission gun scanning electron microscopy (FEG-SEM). Optical sections of different structural parts of the 3D cultures were taken (internal core, surface and edge) as revealed in **Figure 4.6**

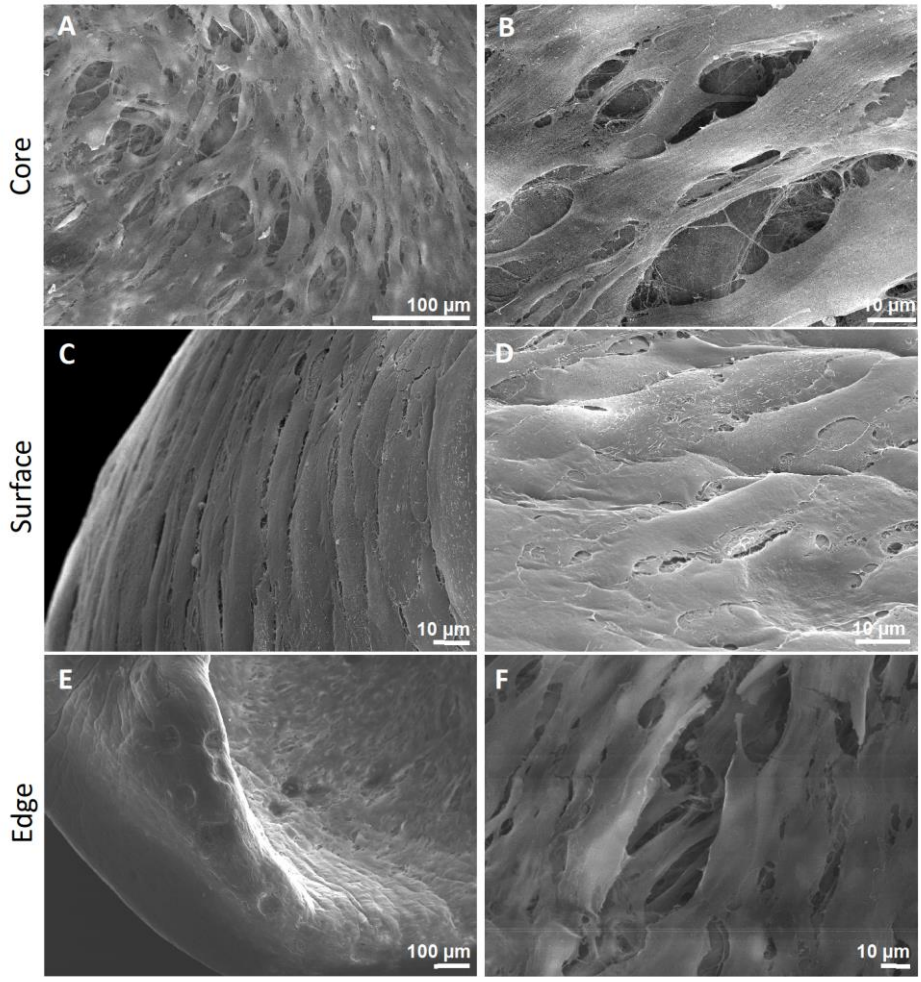

Figure 4.6. FEG-SEM analysis of 3D cultures. Optical sections of different locations in the same 3D culture are shown: internal core (**A-B**), surface (**C-D**) and edge (**E-F**). FEG-SEM images revealed cell morphology and organization complementary to immunofluorescence microscopy. Scale bar is indicated in the images.

FEG-SEM images also showed a continuous and intricate cellular network along different regions of the 3D culture. A cohesive layer of elongated and highly oriented cells was observed at both the surface and the edge, being in agreement with fluorescence microscopy. Close-up of FEG-SEM images showed the development of membrane protrusions (i.e. filopodia) and fenestrations (image B, D and F) between cell-cell and cell-matrix that were responsible for the establishment of a communication continuum.

Cell viability was analyzed through a qualitative assay based on the use of Calcein-AM (green) and Ethidium homodimer-1 (red) dyes that stained live and dead cells respectively. **Figure 4.7** shows different optical sections and their corresponding 3D reconstruction obtained in a pseudo-confocal microscope:

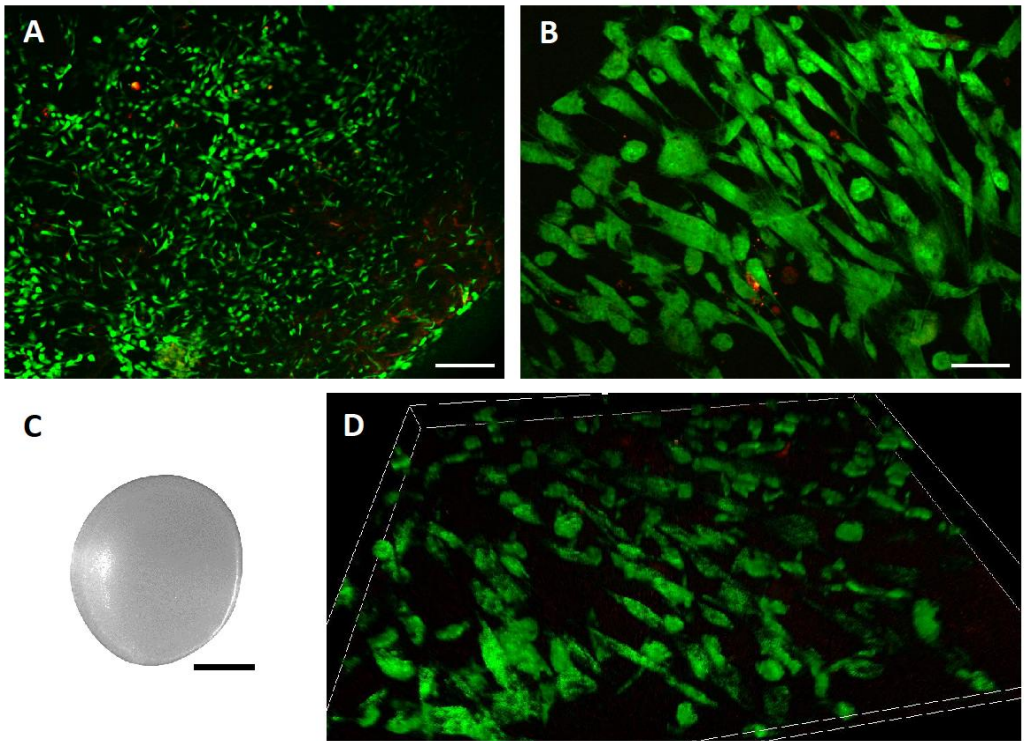

Figure 4.7. Cell viability of 3D cultures. (**A-B**) Individual optical sections were taken at different magnitudes. (**C**) At macroscopic level, the morphologic assessment of 3D cultures was performed through a stereoscopic microscope. (**D**) Next, the 3D reconstruction of viability images was performed. Scales bars of (A) 200 µm, (B) 50 µm and (C) 2mm.

Fibroblasts remained alive during all culture period. The resulting geometry of the 3D model was a disk of approximately 5 mm diameter by 0.5 mm thickness, relevant dimensions for being subjected to oxygen and drug limitations since oxygen diffusion limit is approximately 200 µm[24]. Next, photosensitizer (PS) and oxygen gradients were precisely characterized in this 3D culture and correlated with the architecture of the scaffold.

4.3.2 DRUG AND OXYGEN GRADIENTS IN 3D CELL MODELS

4.3.2.1 Efficiency of Drug Uptake

2D cultures are characterized by uniformly rich nutrition and oxygenation, while tissues experience mass transfer effects for any soluble agent. Indeed, this situation is worsened in tissues originated from abnormal cellular proliferation (PDT main therapeutic targets) as they have a primitive vascular network that causes an inefficient delivery of oxygen and drugs. Thus, 3D cultures were designed to mimic these diffusion limitations occurring *in vivo*.

TMPyP was the selected PS since it is water soluble and both fluorescent and phosphorescent, essential characteristics to study mass transport phenomena. The extent of TMPyP uptake was analyzed through fluorescence spectroscopy of cellular lysates at different incubation times ranging from 30 minutes to 48 hours. Experiments were performed with two different concentrations of TMPyP (**Figure 4.8**).

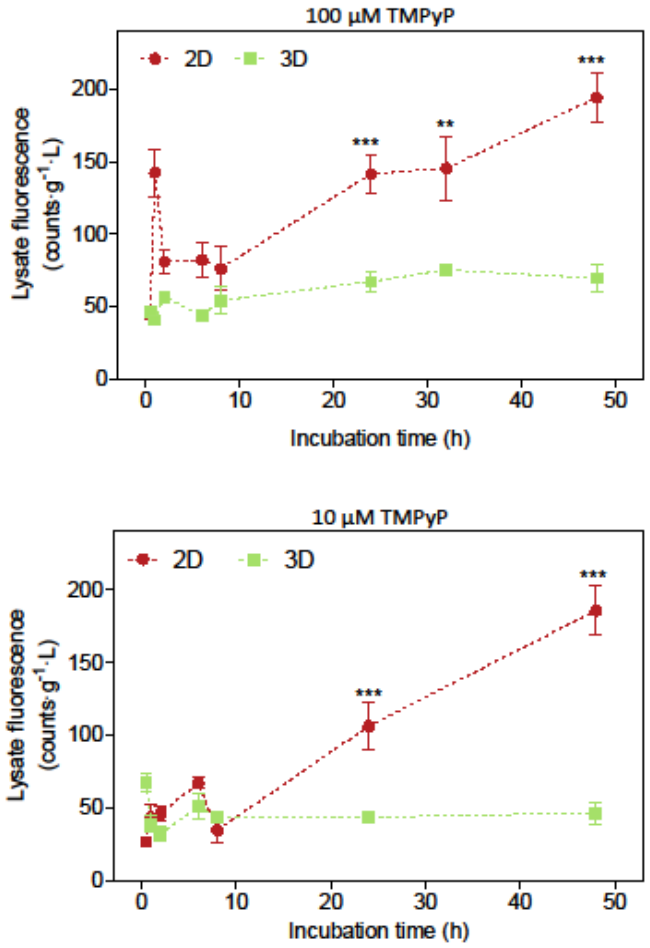

Figure 4.8. Photosensitizer uptake profile through fluorescence spectroscopy. 2D and 3D cultures were incubated with 10 and 100 µM of TMPyP at different times. The extent of TMPyP uptake was determined through fluorescence emission normalized with protein content. Error bars are standard deviation. $^{**}p<0.01$ and $^{***}p<0.001$. (N=2, n=6)

Both concentrations showed the same kinetics profile of TMPyP cellular uptake. It was characterized by a significantly lower drug uptake in cells growing in 3D cultures relative to 2D ones. As a result, a question was raised: Do cells internalized less drug or fewer cells participated in the process? To address this issue, 3D cultures were incubated with TMPyP, digested to obtain intact cells and then flow cytometry was performed. This assay allowed us to assess the drug content in each individual cell (**Figure 4.9**).

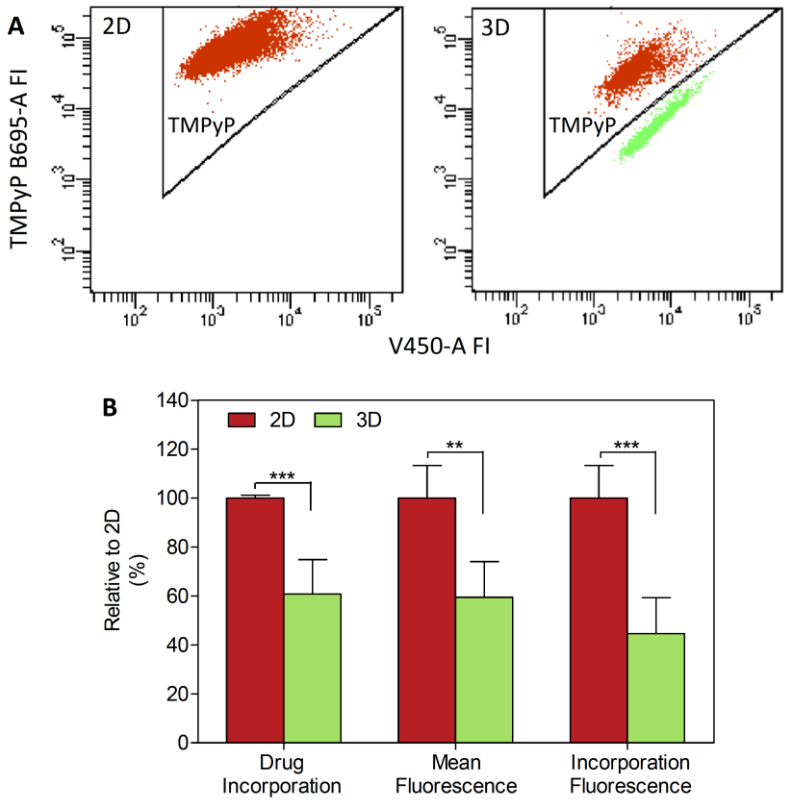

Figure 4.9. Photosensitizer uptake profile through flow cytometry. (**A**) The individual cellular content of TMPyP PS was evaluated by flow cytometry: TMPyP-positive cells (red) and -negative cells (green). (**B**) Data from flow cytometry was quantified. Drug incorporation and mean fluorescence in 3D cultures were analyzed and plotted as percentages relative to 2D cultures. Total TMPyP uptake was also expressed as percentage number of positive cells multiplied by their mean fluorescence. Error bars correspond to standard deviation. $^{**}p<0.01$ and $^{***}p<0.001$. (N=3, n=9).

Interestingly, only 60% of fibroblasts incorporated TMPyP molecules in 3D cultures versus 100% in 2D cultures. Moreover, the amount of TMPyP in those cells was 40% lower. Therefore, the decrease in drug uptake was related to the sum of two effects: fewer cells internalized drug and from these less amount of drug was detected.

Then, the subcellular location of the PS in 2D and 3D cultures was studied by confocal fluorescence microscopy. In particular, TMPyP showed intrinsic fluorescence at 650 nm (green, pseudo-colored) and cell nuclei were stained with Hoechst dye (blue) (**Figure 4.10**).

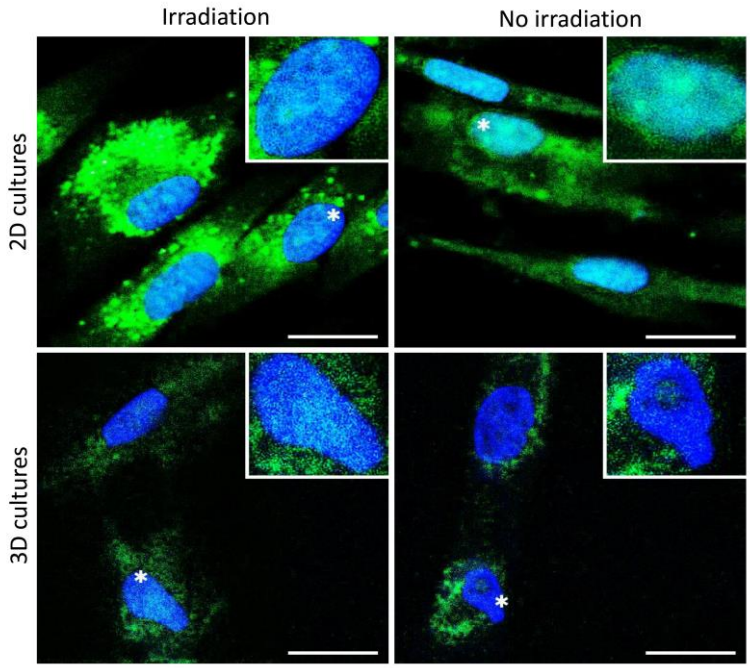

Figure 4.10. Confocal microscopy of TMPyP location in 3D cultures. Images were registered after TMPyP incubation, both before and after irradiation. They correspond to the overlay of TMPyP fluorescence signal (green, pseudo-colored) and nuclei staining (blue). All experiments were performed with 100 mM TMPyP. Scale bars of 20 µm.

In both cultures, TMPyP initially localized in cytoplasmic vacuoles and re-localized in the nucleus after irradiation. This behavior was consistent with literature reports[44] and was further confirmed by time-resolved fluorescence measurements (see below section 4.3.4 MECHANISITC INSIGHTS INTO PHOTODYNAMIC THERAPY). On the other hand, the fluorescence signal intensity was lower in 3D, in agreement with flow cytometry and cell uptake results. Next, oxygen availability was studied.

4.3.2.2 Efficiency of Oxygen Diffusion

The cellular response to PDT is also governed by oxygen diffusion. Oxygen level within the 3D culture was characterized by the expression of two hypoxia-responsive genes through real-time RT-PCR. Specifically, vascular endothelial growth factor-A (*VEGF-A*) and insulin-like growth factor-binding protein 3 (*IGFBP3*) were selected (**Figure 4.11**).

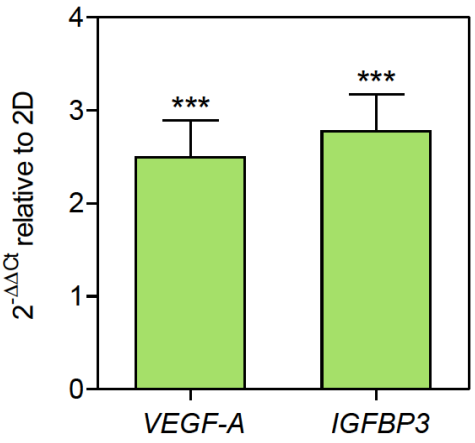

Figure 4.11. Oxygen availability in 3D cultures. Expression levels of two oxygen-responsive genes was determined through real-time RT-PCR. Quantification is reported as fold increase (ΔΔCt) relative to 2D cultures. Error bars are standard deviation. ***p<0.001, (N=2, n=6).

Cells grown in 3D cultures upregulated the expression of both hypoxia markers. The mRNA fold induction increased by a factor of 2–4 relative to 2D cultures, reaching similar levels than tissues exposed to systemic hypoxia[45]. The situation would be aggravated during PDT treatments due to oxygen consumption.

Therefore, 3D cultures could recreate mass transport limitations occurring *in vivo*, distancing from the artificial situation of rich oxygenation and nutrition present in 2D cultures. Hypoxic and TMPyP-free cells were probably buried in the inner part of the scaffold. Finally, photosensitization experiments were performed to determine the effect of limited oxygen and TMPyP diffusion on PDT response.

4.3.3 CELL RESPONSE TO PHOTODYNAMIC THERAPY

Photosensitization experiments were performed in 2D and 3D cultures under the same conditions of drug incubation and light irradiation. Oxygen and TMPyP mass transport effects were further decoupled by circulating an oxygen stream during irradiation. Cell viability was assessed by MTT assay 24h after PDT treatment. None experimental condition was cytotoxic without irradiation, yielding a survival cell fraction higher than 85%. (**Figure 4.12**).

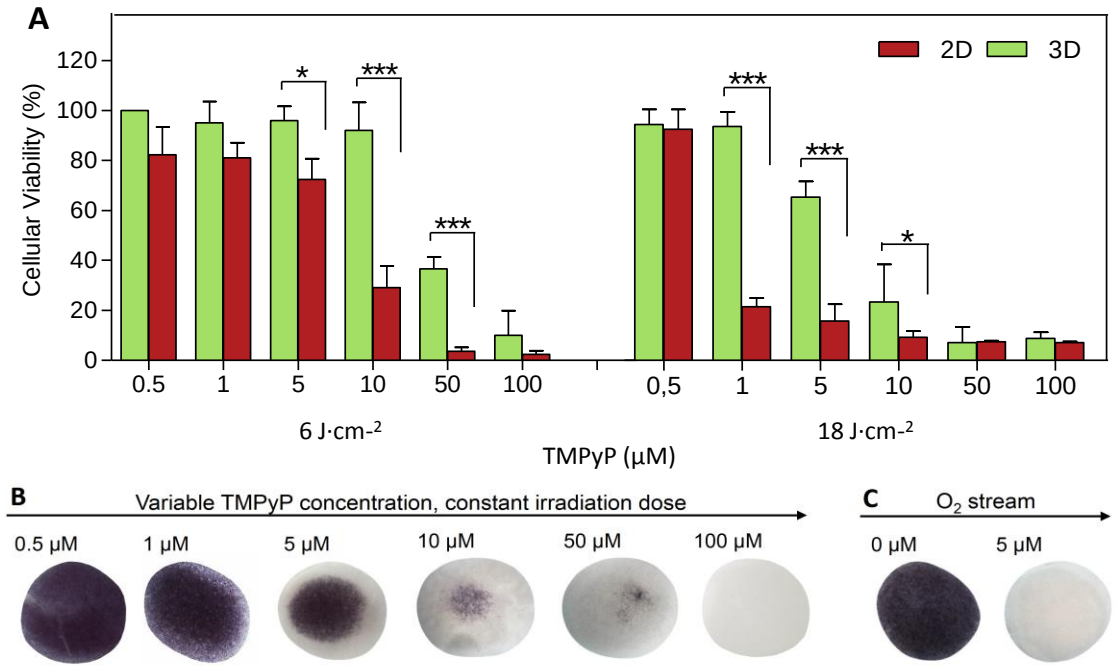

Figure 4.12. Effect of photodynamic therapy in 3D cultures. (**A**) Cells were subjected to PDT, working with different TMPyP concentrations and light doses. The resulting cellular viability was assessed by MTT assay and compared between both culture models to study the effect of drug and oxygen gradient (*N*= 3, *n* =9). (**B**) MTT assay showed the survival pattern in 3D cultures. (**C**) Oxygen gradient was decoupled from drug gradient by circulating an oxygen stream. Error bars are standard deviation. **p*< 0.05, ***p* <0.01, ****p* <0.001.

Cells responded differently to PDT depending on their microenvironment. 3D cultures were more resistant to photosensitizing reactions, being consistent with previous reports[28,37]. They exhibited a radial survival pattern in which the core of the culture maintained a larger percentage of living cells. Oxygen and TMPyP mass transport effects were further decoupled by circulating an oxygen stream during irradiation. Complete cell death was observed under conditions in which cell viability had been 80% in the absence of gas flow. This data indicated that the high cellular survival observed under static conditions was due to low oxygen concentration in the core of the culture, which limited cytotoxic action of therapy.

Therefore, total death was only observed using a 20-fold higher TMPyP concentration or maintaining a continuous flow of oxygen during PDT treatments, despite the demonstrated presence of free-drug and/or hypoxic cells that could not undergo photosensitization. This apparent paradox encouraged us to formulate the hypothesis of a death-signaling cascade that could be triggered to break the protective microenvironment created by oxygen and drug limitations, inducing neighboring cell death[46]. These results needed further in-depth studies to determine the nature of these phenomena. Whenever this protective barrier was not exceeded, 3D cultures yielded a heterogeneous population of cells in which a niche more resistant to PDT was localized in the core of the construct. Thus, this 3D cell model aptly reproduced one of the most important factors compromising the efficacy of PDT in clinical practice: mass transfer limitations. Moreover, it enabled us to address mechanistic studies concerning mode of action of PDT due to its capacity of cellular imaging.

4.3.4 MECHANISITC INSIGHTS INTO PHOTODYNAMIC THERAPY

Spectroscopic and photophysic measurements were performed to elucidate whether mass transfer limitations affected the intrinsic mechanism of action of PDT. First of all, normalized steady-state and time-resolved fluorescence emission spectra of TMPyP provided direct evidence about drug microenvironment and accessibility to oxygen. Secondly, time-resolved phosphorescence of singlet oxygen ($^1O_2$) centered at 1275 nm monitored the production and fate of this reactive oxygen species (ROS) within the cell, offering a powerful tool for studying oxygen-cell interactions[47] (**Figure 4.13**).

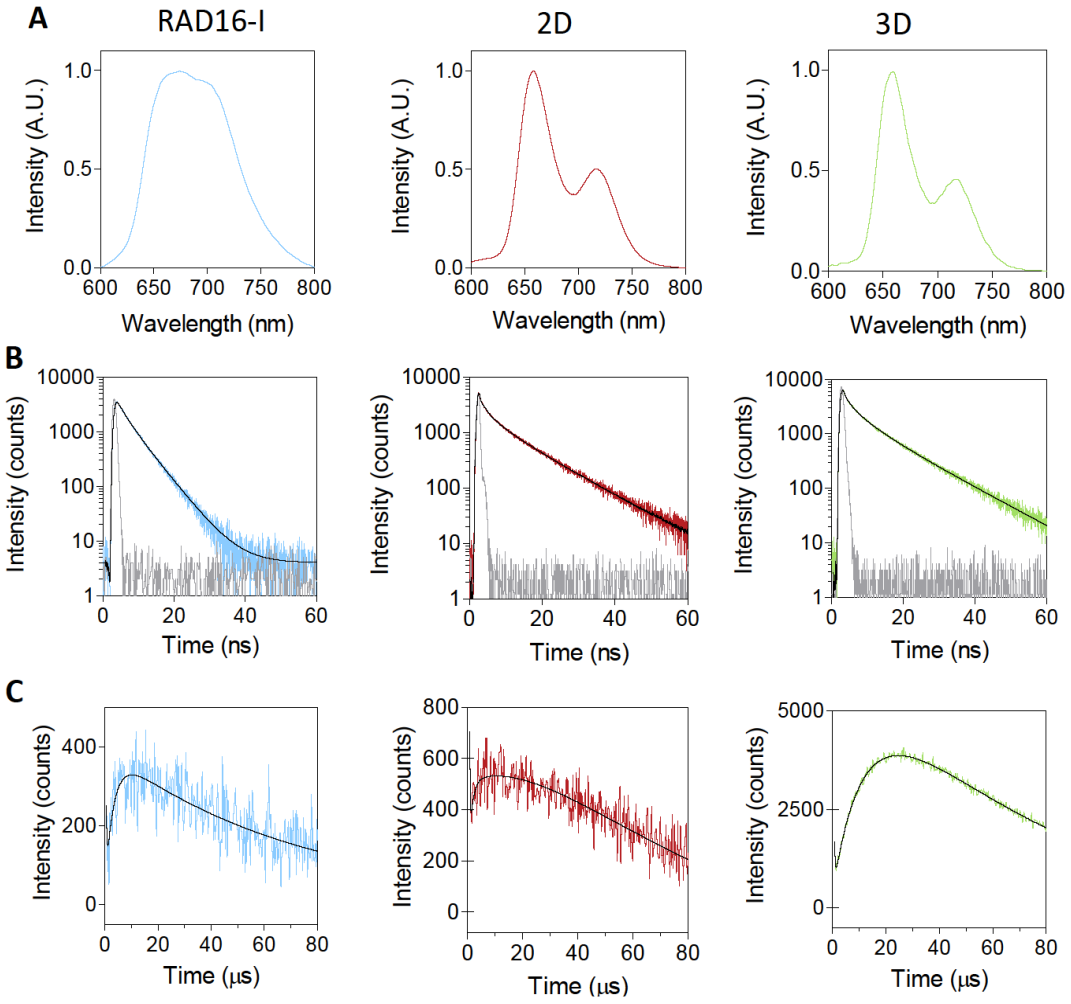

Figure 4.13. TMPyP and singlet oxygen measurements. (**A**) Normalized steady-state and (**B**) time-resolved fluorescence emission spectra of TMPyP (*N*= 5, *n* =10). (**C**) Time-resolved singlet oxygen phosphorescence at 1275 nm (*N*= 5, *n* =10). Data was obtained working with three different conditions: RAD16-I scaffold without cells, 2D cultures and 3D cultures. Spectroscopic and photophysic experiments performed with Dr.María García (group of Dr. Santi Nonell from IQS School of Engineering). This figure is also shown in her thesis.

The fluorescence emission spectra of TMPyP in 2D and 3D cultures showed two well-resolved bands in contrast to the structure-less broad band typically observed in water and RAD16-I self-assembling hydrogel. These results indicated that TMPyP was internalized by cells in both types of culture and was hardly retained by the nanofibers. The fact that the lifetime was slightly longer in RAD16-I scaffold than the typical value obtained in buffered solution (4.6 ns) would indicate that TMPyP was partially attracted by the negative charges of RAD16-I peptide sequence, restraining the rotation and vibration of the molecules. Secondly, TMPyP showed a multiexponential decay kinetics in 2D and 3D cultures (lifetime 1.5, 5.7 and 12 ns) as opposed to the monoexponential decay in RAD16-I aqueous-like environments (lifetime 5 ns). These results further confirmed drug internalization in multiple subcellular sites, mainly nuclear DNA[48,49] and lysosomes[50] consistently with literature data and microscope results.

Regarding ROS, time-resolved phosphorescence at 1245 nm unambiguously demonstrated the production of cytotoxic $^1O_2$ upon excitation of TMPyP in 2D and 3D cultures. This was the first experimental observation of $^1O_2$ phosphorescence in a 3D culture. As in the case of TMPyP, a biexponential behavior was found in both types of culture in contrast to the monoexponential decay obtained for RAD16-I scaffold.

Next, TMPyP triplet and $^1O_2$ lifetimes were quantified through time-resolved phosphorescence. In addition to water, spectroscopic measurements were performed in the presence of deuterated solvents (D_2O) and bovine serum albumin (BSA). D_2O has the capacity to increase $^1O_2$ lifetime. On the other hand, BSA is an efficient extracellular $^1O_2$ quencher since it cannot penetrate cell membranes. A summary of lifetimes is given in **Figure 4.14**.

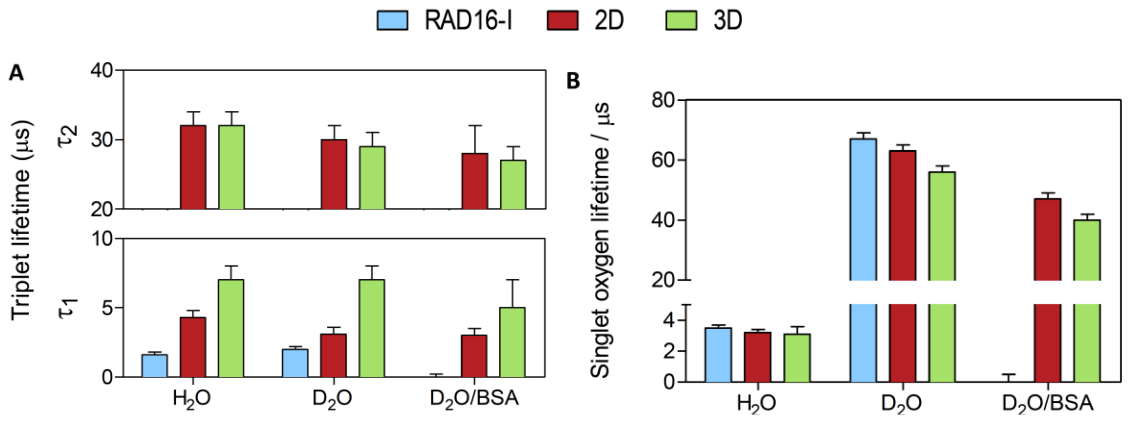

Figure 4.14. Triplet state kinetics from phosphorescence measurements. (**A**) TMPyP triplet state and (**B**) singlet oxygen lifetimes were registered in H_2O, D_2O and D_2O with 0.77 mM BSA in three different experimental conditions: RAD16-I scaffold without cells, 2D cultures and 3D cultures (*N*= 5, *n* =10). Error bars are standard deviation. Spectroscopic and photophysic experiments performed with Dr.María García (group of Dr. Santi Nonell from IQS School of Engineering). This figure is also shown in her thesis.

TMPyP triplet state showed two lifetimes (τ_1 and τ_2). Based on literature data, the longer lifetime was assigned to molecules bound to nuclear DNA[50], being indicative of poor oxygen accessibility to TMPyP. The shorter lifetime was assigned to molecules in the lysosomes. Interestingly, lysosomal population had a longer lifetime in 3D cultures than in 2D ones, suggesting that TMPyP was less accessible to oxygen and produced ROS with lower efficiency. These findings were consistent with the different cellular response to PDT observed between both culture types and the enhancing effect of the oxygen stream on cell death.

On the other hand, the kinetics of $^1O_2$ decay reflected the localization, mobility and reactivity of this ROS. Advantage was taken of the well-known deuterium isotope effect on $^1O_2$ lifetime (t_Δ) to reveal differences in its kinetics between both culture types. The higher t_Δ value was obtained for RAD16-I scaffold, which ruled out any significant quenching effect by the nanofiber peptide. t_Δ in 3D cultures was lower than in 2D ones, being assigned to $^1O_2$ quenching effect by the secreted ECM proteins. These results were confirmed by externally adding proteins as BSA. In the presence of this extracellular quencher, $^1O_2$ lifetime decreased further down. Taken together, these results indicated that major differences between 2D and 3D cultures came from dynamic mass transfer effects rather than intrinsic PDT mechanism of action.

4.3.5 INCREASING BIOLOGICAL COMPLEXITY TO 3D CELL MODELS

The non-instructive and defined milieu of RAD16-I scaffold demonstrated that 3D architecture compromised PDT efficacy due to the establishment of molecular gradients without altering therapy mechanism. The second step consisted in increasing the level of complexity of 3D cultures in order to analyze the role of other extracellular signals in drug screening processes. In particular, different chemical cues were sequentially investigated: (*i*) ECM binding sequences through collagen scaffolds (i.e. integrin recognition sites and proteolytic degrading sites) and (*ii*) paracrine factors through co-cultures between fibroblasts and cancer cells. The selected cancer cells were human cervical adenocarcinoma cells (HeLa) because they have been extensively used for pre-clinical research in PDT[18,20,21,51].

Therefore, six different cell models were developed: (*i*) fibroblasts in RAD16-I scaffolds, (*ii*) fibroblasts in collagen scaffolds, (*iii*) cancer cells in RAD16-I scaffolds, (*iv*) cancer cells in collagen scaffolds, (*v*) co-cultures of cancer cells and fibroblasts in RAD16-I scaffolds and (*vi*) co-cultures of cancer cells and fibroblasts in collagen scaffolds (**Table 4.1**). Data gathered from these experiments could help us to optimize a suitable model for drug screening processes in PDT, balancing between cell complexity and analysis simplicity.

	Fibroblasts	Cancer cells
RAD16-I	X	
RAD16-I		X
RAD16-I	X	X
Collagen	X	
Collagen		X
Collagen	X	X

Table 4.1. 3D cell models with increasing levels of biological complexity.

Individual cell models of cancer cells and fibroblasts were previously described and characterized (section 3.3.3 CELL PHENOTYPE AND PLASTICITY IN 3D CANCER MODELS and section 4.3.1 DEVELOPMENT OF 3D CELL MODELS FOR DRUG TESTING). They allowed us to study the influence of environmental cues on cell phenotype. In this particular section, research was focused on the morphological assessment of co-cultures. Nuclei and actin microfilaments of the cytoskeleton were stained with DAPI (blue) and Phalloidin-TRITC (yellow pseudo-color) dyes respectively. Cell populations were distinguished through Green Fluorescent Protein (GFP, red pseudo-colored) (**Figure 4.15**).

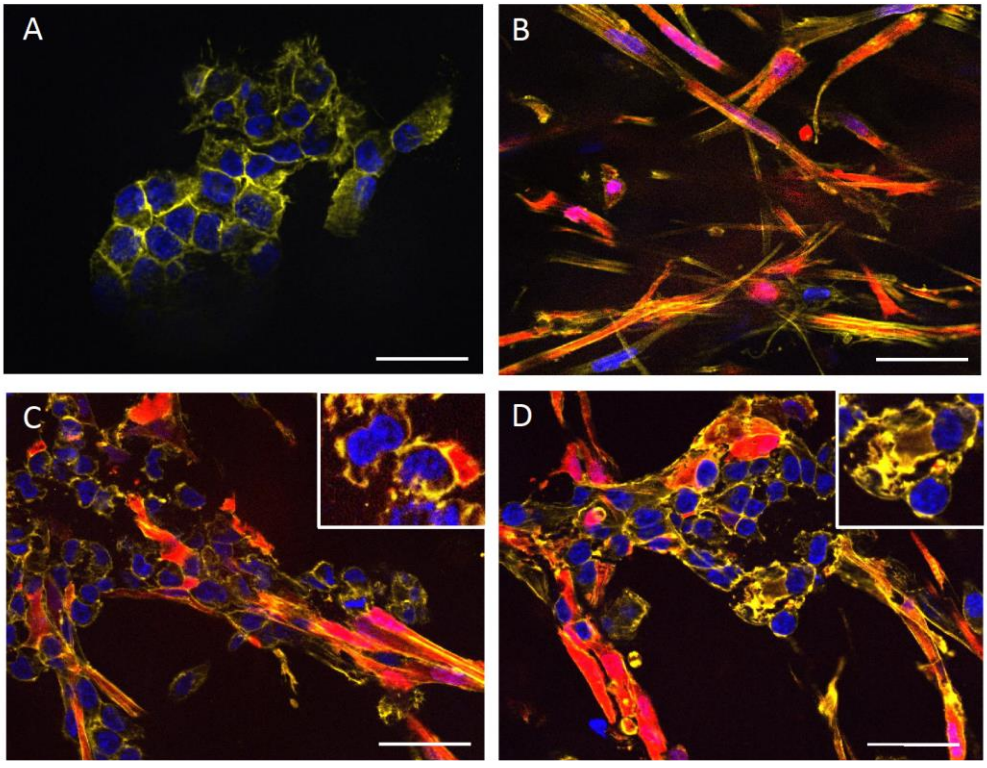

Figure 4.15. Morphological assessment of fibroblast and cancer cells co-cultures in RAD16-I scaffold. (**A**) Cancer cells, (**B**) fibroblasts labelled with green fluorescent protein (GFP, pseudo-colored in red) and (**C-D**) co-cultures of cancer cells and fibroblasts. After 5-day culture, samples were stained for actin microfilaments (phalloidin, pseudo-colored in yellow) and nuclei (DAPI, blue). Scale bar of 50 µm.

In 2D cultures, cancer cells exhibited epithelial features: polygonal shape, actin filaments assembled in cortical thin bundles and growth pattern of spheroid clusters. The culture in a 3D microenvironment promoted some of the morphological changes that accompanied epithelial-mesenchymal transition (EMT). In particular, cancer cells showed a more spindle-shape phenotype and stress fibers were located intercrossing the cell extent. All these changes were more pronounced in collagen scaffold (images not shown, see section 3.3.3 CELL PHENOTYPE AND PLASTICITY IN 3D CANCER MODELS) than RAD16-I scaffold.

Fibroblasts were labelled with green fluorescent protein (GFP) in order to distinguish different cell populations during co-culture experiments. They elongated and showed a characteristic spindle-shape phenotype. Moreover, they created a continuous cellular network that promoted cell-cell and cell-ECM interactions (section 4.3.1 DEVELOPMENT OF 3D CELL MODELS FOR DRUG TESTING).

Finally, co-cultures were examined. The presence of fibroblasts induced the scattering of cancer cells, detaching them from clusters. Indeed, cancer cells seemed to move along fibroblasts network[52]. Therefore, the crosstalk between both cell populations could enhance the perturbation of epithelial pattern and the recapitulation of some morphogenetic steps of EMT program. Conversely, fibroblasts did not suffer any phenotypic changes after culturing them with cancer cells. Significant morphological differences in co-cultures between collagen and RAD16-I scaffolds were not observed (data not shown).

PDT experiments were performed in these different cell models and key parameters as drug uptake and therapy cytotoxicity were evaluated. Obtained results were correlated with the different environmental signals that cells received as observed during morphological assessment.

4.3.6 PHOTODYNAMIC THERAPY TO DIFFERENT 3D CELL MODELS

4.3.6.1 Photosensitizer Uptake and PDT Cytotoxicity: Influence of ECM Binding Motifs

All experiments were performed with two synergic PSs: the liposomal Zinc(II)-phthalocyanine (ZnPc) and the cationic 5,10,15,20-tetrakis(N-methyl-4-pyridilium)-21H, 23H-porphine (TMPyP). This specific PDT treatment was previously studied in 2D cultures of established cancer cell lines (human and murine)[53] and mice models (C57BL/6 mice)[54]. Therefore, data obtained from 3D cultures could be compared to traditional models in order to optimize a 3D platform for drug screening processes.

First, the extent of PSs uptake was examined in RAD16-I and collagen cultures. Samples were incubated with TMPyP and/or ZnPc and flow cytometry was performed (**Figure 4.16**).

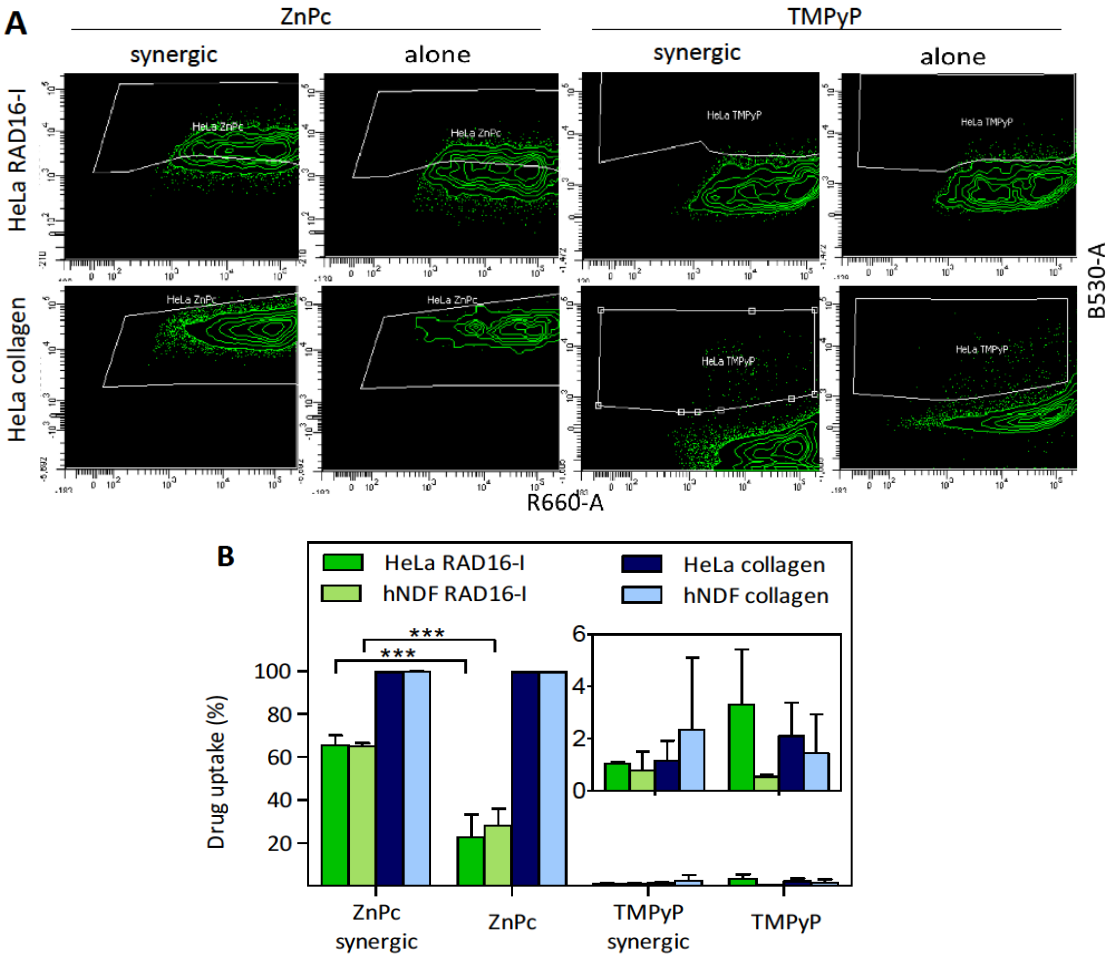

Figure 4.16. Photosensitizer uptake profile in RAD16-I and collagen cultures. Individual cellular content of TMPyP and ZnPc PSs was evaluated by (A) flow cytometry and (B) quantified in different 3D cell models (*N*=2, *n*=6). Error bars are standard deviation. ***$p<0.001$. Uptake experiments were performed with Dr.Pilar Acedo (group of Dr. Ángeles Villanueva from Universidad Autónoma de Madrid). This figure is also shown in her thesis.

Interestingly, less than 6% of cell population was capable of internalizing TMPyP molecules. These results belonged to all experimental cases, independently of cell type, scaffold or drug formulation. This low percentage differed from previous results related to TMPyP (section 4.3.2.1 Efficiency of Drug Uptake) because the initial drug concentration was not 100 µM. Instead, it was $3 \cdot 10^{-3}$ µM, conditions used for synergic experiments in 2D cultures and mice models[54]. On the other hand, ZnPc penetrated 3D cultures more efficiently. In collagen, this drug reached all the target cellular population. In RAD16-I, 60% of cells internalized synergic ZnPc whereas only 20-30% internalized individual ZnPc. There were no significant differences in uptake results between cultures of cancer cells and fibroblasts.

3D cultures evidenced the difference in cellular internalization between TMPyP (free drug) and ZnPc (liposomal drug), demonstrating the efficacy of nanocarriers to increase local drug concentration. The major advantage of liposomes could come from the activation of

receptor-mediated endocytosis as an active target transport, in contrast to the passive membrane diffusion that free drugs experiment. In particular, ZnPc is encapsulated in POPC/OOPS liposomes, which provide a vehicle for the direct transfer of PSs to lipoprotein receptors according to literature[55,56]. This approach could also allow PSs to bypass the activity of drug resistance transporters that actively pump drugs out of the cells by means of being protected within an endosome[57,58].

RAD16-I and collagen scaffolds showed the same 3D architecture, guarantying the establishment of similar molecular gradients. This property is essential when working with free drugs whose mechanism of transport is passive diffusion. However, RAD16-I and collagen scaffolds did not have the same molecular composition. RAD16-I scaffold provided a non-instructive microenvironment for cells while collagen scaffold had a wide range of ECM binding motifs (mainly integrin-recognition sites) that mediated crucial transduction cascades for tumor progression. Results suggested that collagen upregulated the expression of lipoprotein receptors, causing an increase in PSs intracellular concentration. This regulation was reflected when working with nanocarriers as vehicle drugs, since they promoted a receptor-mediated endocytosis. More research would be necessary to corroborate this working hypothesis. For instance, the functionalization of RAD16-I with integrin recognition sites could be performed.

Finally, the synergistic potential of TMPyP and ZnPc-combined therapy was reflected through increased uptake in RAD16-I, compared with the individual ZnPc. POPC/OOPS liposomes were negatively charged and we hypothesized that could develop electrostatic repulsion with the negative nanofibers of RAD16-I and collagen biomaterials. Then, cationic TMPyP molecules could bind to the liposomal formulation, blocking their unspecific repulsion with nanofibers and enhancing their transport. Indeed, previous spectroscopic mechanistic measurements indicated the attraction between TMPyP molecules and RAD16-I scaffold (see section 4.3.4 MECHANISITC INSIGHTS INTO PHOTODYNAMIC THERAPY).

TMPyP- and ZnPc-mediated photosensitization experiments were performed to determine the effects of 3D models on PDT response. In particular, results gave insight on the influence of ECM binding motifs on therapy efficacy. Conditions of drug incubation and light irradiation were the same than 2D cultures (termed *in vitro* conditions)[53] and mice (termed *in vivo* conditions)[54]. Cellular viability was assessed by flow cytometry and MTT assay 24 hours after treatment (**Figure 4.17**).

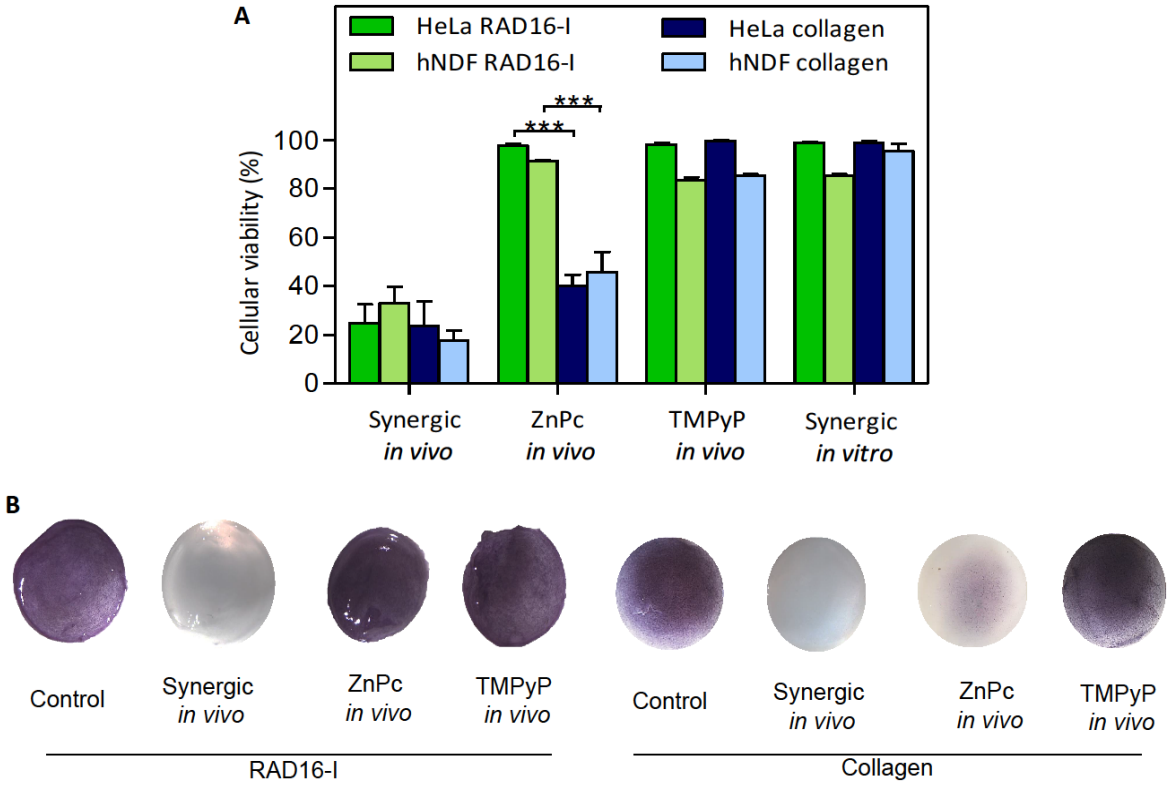

Figure 4.17. Effect of photodynamic therapy in RAD16-I and collagen scaffolds. (**A**) Cellular viability was assessed by MTT assay and flow cytometry. Conditions of drug incubation and light irradiation were the same than 2D cultures (termed in vitro conditions) and mice (termed in vivo conditions) (*N*=2, *n*=6). (**B**) MTT assay showed the survival pattern in 3D cultures. Error bars are standard deviation. ***p<0.001. Cellular viability experiments were performed with Dr.Pilar Acedo (group of Dr. Ángeles Villanueva from Universidad Autónoma de Madrid). This figure is also shown in her thesis.

The PSs concentration and light irradiation used in 2D cultures (*in vitro* termed conditions) did not induce significant cell death in neither collagen nor RAD16-I scaffolds. Conversely, experimental conditions optimized for mice (*in vivo* termed conditions) showed percentages of approximately 75% of cell death. Therefore, data suggested that 3D cultures could bridge the gap between 2D cultures and animal models in drug screening.

Results obtained for *in vivo* photosensitization experiments were deeply studied. As expected, TMPyP did not induce cell death individually. Uptake experiments revealed that this drug was not internalized by target cells. Then, the effect of individual ZnPc was analyzed. Cell death was not observed in RAD16-I scaffold, in contrast to collagen scaffold that showed percentages of approximately 60% of cell death. The increased efficiency of ZnPc-photosensitization experiments detected in collagen scaffold correlated with uptake experiments, in which all cell population internalized the drug. The difference between RAD16-I and collagen scaffolds could be explained through the regulation of lipoprotein-receptor expression that could modulate the cellular uptake of PSs. Finally, the effect of the synergic was assessed. The combination of drugs significantly potentiated their individual effect in both scaffolds, obtaining a cellular death of approximately 75%. Two main hypotheses could explain

this data: the different location of PSs within the 3D culture and/or the enhanced internalization of ZnPc in the synergic formulation. As demonstrated in uptake experiments, TMPyP could not enter the cell, generating $^1O_2$ in the extracellular milieu whereas ZnPc effect was intracellular. Therefore, the combination of both PSs could damage the target cells together with the protective microenvironment. Second, TMPyP molecules could enhance the receptor-mediated endocytosis of liposomal ZnPc by blocking its repulsion with the nanofibers from both scaffolds.

Importantly, both scaffolds predicted a similar cell response to PDT when drugs intracellular concentration was higher than a certain threshold value. PDT is based on the generation of ROS that cause an acute stress response through the photo-oxidation of proteins and unsaturated lipids. Therefore, this therapy triggers an unspecific cell damage without affecting specific signaling cascades modulated by the microenvironment. Difference in molecular composition between RAD16-I and collagen type I was only evident for uptake experiments when drug was vehicle with nanocarriers for active transport.

4.3.6.2 PDT Uptake and Cytotoxicity: Influence of Co-cultures Crosstalk

Next step consisted in studying the influence of the crosstalk between cancer cells and fibroblasts on PDT response. In particular, results gave insight on the contribution of paracrine signaling on therapy efficacy. Conditions of drug incubation and light irradiation were the same than 2D cultures (termed *in vitro* conditions)[53] and mice (termed *in vivo* conditions)[54]. Cellular viability was assessed by flow cytometry and MTT assay 24 hours after treatment in terms of drugs uptake and cytotoxicity (**Figure 4.18**).

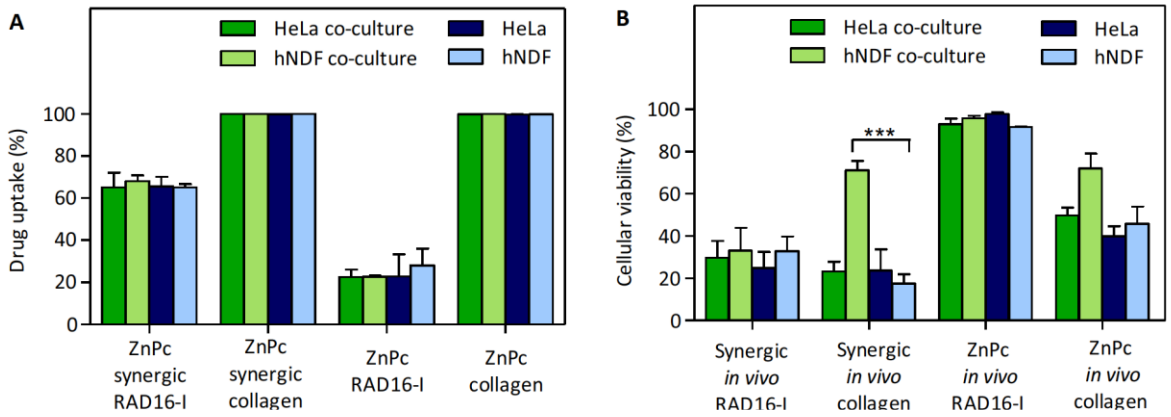

Figure 4.18. Photosensitizer uptake and PDT cytotoxicity in co-cultures. (**A**) The content of TMPyP and ZnPc in co-cultures was evaluated by flow cytometry and compared to individual cell cultures (N=2, n=6). (**B**) Co-cultures were subjected to PDT with the conditions shown in Table 2.7. and cellular viability was assessed by flow cytometry and MTT. Obtained results were compared to individual cell cultures (N=2, n=6). Error bars are standard deviation. ***p<0.001. Uptake and cellular viability experiments were performed with Dr.Pilar Acedo (group of Dr. Ángeles Villanueva from Universidad Autónoma de Madrid). This figure is also shown in her thesis.

Co-cultures did not affect drug uptake (data related to TMPyP is not shown). Regarding cytotoxic experiments, the only difference in therapy efficacy was observed when fibroblasts were co-cultured with cancer cells in collagen scaffolds, being more resistant than individual ones. These findings reinforced the contribution of ECM binding motifs on the modulation of tumor signaling cascades, which could induce a more aggressive cell phenotype. Consequently, cancer cells could have greater capacity to stimulate the transformation of fibroblasts into cancer-associated fibroblasts through paracrine signaling. These results gave insight on the importance of targeting the microenvironment during cancer treatments.

Co-culture models were performed using normal fibroblasts instead of cancer-associated fibroblasts (CAFs) or interface zone fibroblast (INFs). Under the same experimental conditions, CAFs and INFs have a greater capacity than NFs to interact with cancer cells, reciprocally modulating their behavior[60].

4.4 CONCLUDING REMARKS

Photodynamic therapy (PDT) is a clinically approved procedure for the treatment of diseases characterized by uncontrolled cell proliferation, mainly cancer. It causes a selective cytotoxic activity towards cancer cells by the combined effect of three components: a photosensitizer (PS), light and oxygen. PDT overcomes two relevant drawbacks of conventional chemotherapy and radiotherapy by inducing low levels of cellular resistance and stimulating host immune response. However, PSs show low selectivity and efficacy, requiring the design and synthesis of new agents[1]. Drug screening processes have traditionally depended on two-dimensional (2D) cultures, which do not properly recreate the target tissue and impair biomedical data[22].

The main objective of the present chapter was the development and characterization of three-dimensional (3D) models with increasing levels of biological complexity in order to analyze the contribution of specific environmental signals on PDT-mediated cell response. In particular, 3D cultures were based on cervical cancer cells and fibroblasts grown within the synthetic self-assembling peptide RAD16-I and the natural collagen type I.

Cellular phenotype in 3D cultures was carefully studied. In comparison to 2D cultures, cervival cancer cells grown in collagen and RAD16-I scaffolds exhibited a more spindle-shape morphology and cytoskeleton filaments intercrossed cell extent rather than being aligned along cell membrane. All these distinguishing features conferred a more mesenchymal-like phenotype. On the other hand, fibroblasts had an *in vivo*-lengthen morphology and created an intricate cell network that promoted cell-cell and cell-extracellular matrix (ECM) interactions in the 3D context provided by RAD16-I and collagen scaffolds. Finally, co-cultures between cervical cancer cells and fibroblasts caused the scattering of cancer cells, detaching them from clusters and promoting their presence along fibroblast network. Therefore, co-cultures exacerbated the epithelial to mesenchymal transition of cancer cells.

First, the influence of 3D architecture was studied through synthetic scaffolds (RAD16-I) that provided a non-instructive and defined milieu. Results demonstrated that oxygen and drugs were not able to diffuse along all the 3D culture, establishing molecular gradients and developing a protective microenvironment. Total cell death was only observed using a 20-fold higher photosensitizer (PS) concentration or maintaining a continuous flow of oxygen relative to 2D cultures. Therefore, 3D cultures could reproduce the existence of a heterogeneous cell population with resistant cancer cells located within the core of the culture, which explained PDT inefficacy in clinical practice. At mechanistic level, the production and decay of cytotoxic singlet oxygen was observed in a 3D culture for the first time. Significantly, the mechanism of action of the therapy was maintained between 2D and 3D cultures, revealing that mass transfer effects accounted for major differences in PDT outcome. All data suggested that introduction of three-dimensionality in drug screening processes was required for obtaining valuable biomedical data.

Next step consisted in analyzing the contribution of ECM binding motifs on PDT response through natural scaffolds (collagen) compared to synthetic ones (RAD16-I). Collagen is the major component of tumor microenvironment and has a wide range of integrin- and metalloproteinases- recognition sequences that can drive disease progression through the regulation of signaling pathways. For instance, integrins act as communication channels between extracellular matrix (ECM) and cellular cytoplasm, transducing mechanical and chemical cues. Results suggested that ECM signaling could mainly affect drug uptake processes when they were regulated by active transport mechanisms such as liposomes-mediated endocytosis. Consequently, cellular viability experiments were simultaneously affected in these cases. However, when the predicted uptake values were similar, the obtained PDT cytotoxic activity was the same between RAD16-I and collagen scaffolds. This finding could be explained because PDT is based on an acute and general stress cellular effect and it is not directed to specific signaling pathways. Indeed, data indicated that the introduction of ECM binding motifs was required for mimicking cell processes that depended on signaling cascades regulated by tumor microenvironment such as active transport mechanisms.

Finally, the crosstalk between different cell populations (cancer cells and fibroblasts) was evaluated. Results suggested that cancer cells induced the transformation of fibroblasts through paracrine signaling, making them more resistant to PDT. This effect was exclusively observed in collagen scaffolds, reinforcing the role of ECM adhesion motifs in tumor cascades. However, co-culture models were performed using normal fibroblasts instead of cancer-associated fibroblasts (CAFs) or interface zone fibroblast (INFs). Publications have reported that CAFs and INFs have a greater capacity to interact with cancer cells, reciprocally modulating their phenotype[60]. Therefore, more research should be focused in this direction.

4.5 REFERENCES

1. Agostinis, P. *et al.* Photodynamic therapy of cancer: An update. *CA. Cancer J. Clin.* **61,** 250–281 (2011).

2. Triesscheijn, M., Baas, P., Schellens, J. H. & Stewart, F. A. Photodynamic therapy in oncology. *Oncologist* **11,** 1034–1044 (2006).

3. Agosta, E. *et al.* Pharmacogenetics of antiangiogenic and antineovascular therapies of age-related macular degeneration. *Pharmacogenomics* **13,** 1037–1053 (2012).

4. Elizalde, J., Vasquez, L., Iyo, F. & Abengoechea, S. Photodynamic therapy in the management of circumscribed choroidal hemangioma. *Can J Ophthalmol* **47,** 16–20 (2012).

5. Babilas, P., Schreml, S., Landthaler, M. & Szeimies, R. M. Photodynamic therapy in dermatology: State-of-the-art. *Photodermatol. Photoimmunol. Photomed.* **26,** 118–132 (2010).

6. Dai, T., Huang, Y. Y. & Hamblin, M. R. Photodynamic therapy for localized infections-state of the art. *Photodiagnosis Photodyn. Ther.* **6,** 170–188 (2009).

7. Palumbo, G. Photodynamic therapy and cancer: A brief sightseeing tour. *Expert Opin. Drug Deliv.* **4,** 131–148 (2007).

8. Castano, A. P., Mroz, P. & Hamblin, M. R. Photodynamic therapy and anti-tumour immunity. *Nat. Rev. Cancer* **6,** 535–545 (2006).

9. Dysart, J. S. & Patterson, M. S. Characterization of Photofrin photobleaching for singlet oxygen dose estimation during photodynamic therapy of MLL cells in vitro. *Phys Med Biol.* **50,** 2597–2616 (2005).

10. Castano, A. P., Demidova, T. N. & Hamblin, M. R. Mechanisms in photodynamic therapy: part two—cellular signaling, cell metabolism and modes of cell death. *Photodiagnosis Photodyn. Ther.* **2,** 1–23 (2005).

11. Folkman, J. Tumor angiogenesis. *Advances in cancer research* **43**, 175–203 (1985).

12. Cross, M. J. & Claesson-Welsh, L. FGF and VEGF function in angiogenesis: Signalling pathways, biological responses and therapeutic inhibition. *Trends Pharmacol. Sci.* **22,** 201–207 (2001).

13. Postiglione, I., Chiaviello, A. & Palumbo, G. Enhancing photodynamic therapy efficacy by combination therapy: Dated, current and oncoming strategies. *Cancers (Basel)* **3,** 2597–2629 (2011).

14. Makowski, M. *et al.* Inhibition of cyclooxygenase-2 indirectly potentiates antitumor effects of photodynamic therapy in mice. *Clin Cancer Res.* **9,** 5417–5422 (2003).

15. Galluzzi, L., Kepp, O. & Kroemer, G. Enlightening the impact of immunogenic cell death in photodynamic cancer therapy. *EMBO J.* **31,** 1055–7 (2012).

16. Brown, S. B., Brown, E. A. & Walker, I. The present and future role of photodynamic therapy in cancer treatment photodynamic therapy. *Lancet Oncol.* **5,** 497–508 (2004).

17. Stockert, J. C. *et al.* Porphycenes: Facts and prospects in photodynamic therapy of cancer. *Curr. Med. Chem.* **14,** 997–1026 (2007).

18. Rello-Varona, S., Stockert, J. C., Cañete, M., Acedo, P. & Villanueva, A. Mitotic catastrophe induced in HeLa cells by photodynamic treatment with Zn(II)-phthalocyanine. *Int. J. Oncol.* **32,** 1189–1196 (2008).

19. Jiang, Z., Shao, J., Yang, T., Wang, J. & Jia, L. Pharmaceutical development, composition and quantitative analysis of phthalocyanine as the photosensitizer for cancer photodynamic therapy. *J. Pharm. Biomed. Anal.* **87,** 98–104 (2014).

20. Juarranz, A., Villanueva, A., Díaz, V. & Cañete, M. Photodynamic effects of the cationic porphyrin, mesotetra(4N-methylpyridyl)porphine, on microtubules of HeLa cells. *J. Photochem. Photobiol. B.* **27,** 47–53 (1995).

21. Wu, L. *et al.* Cationic ester porphyrins cause high levels of phototoxicity in tumor cells and induction of apoptosis in HeLa cells. *Chem Biodiver.* **6,** 1066–1076 (2009).

22. Pampaloni, F., Reynaud, E. G. & Stelzer, E. H. K. The third dimension bridges the gap between cell culture and live tissue. *Nat. Rev. Mol. Cell Biol.* **8,** 839–845 (2007).

23. Yamada, K. M. & Cukierman, E. Modeling tissue morphogenesis and cancer in 3D. *Cell* **130,** 601–610 (2007).

24. Griffith, L. G. & Swartz, M. A. Capturing complex 3D tissue physiology in vitro. *Nat. Rev. Mol. Cell Biol.* **7,** 211–224 (2006).

25. Mehta, G., Hsiao, A. Y., Ingram, M., Luker, G. D. & Takayama, S. Opportunities and challenges for use of tumor spheroids as models to test drug delivery and efficacy. *J. Control. release* **164,** 192–204 (2012).

26. Sutherland, R. M., McCredie, J. A. & Inch, W. R. Growth of multicell spheroids in tissue culture as a model of nodular carcinomas. *J. Natl. Cancer Inst.* **46,** 113–120 (1971).

27. Sutherland, R. M., Sordat, B., Bamat, J., Gabbert, H. & Bourrat, B. Oxygenation and differentiation in multicellular spheroids of human colon carcinoma. *Cancer Res.* **46,** 5320–5329 (1986).

28. Huygens, A. *et al.* Accumulation and Photocytotoxicity of Hypericin and Analogs in Two- and Three-Dimensional Cultures of Transitional Cell Carcinoma Cells. *Photochem. Photobiol.* **78,** 607–614 (2003).

29. Roelants, M., Van Cleynenbreugel, B., Lerut, E., Van Poppel, H. & Witte, P. A. M. De. Human serum albumin as key mediator of the differential accumulation of hypericin in normal urothelial cell spheroids versus urothelial cell carcinoma spheroids. *Photochem. Photobiol. Sci.* **10,** 151–159 (2011).

30. Huygens, A. *et al.* Differential accumulation of hypericin in spheroids composed of T-24 transitional cell carcinoma cells expressing different levels of E-cadherin. *J. Urol.* **179,** 2014–2019 (2008).

31. Huygens, A. *et al.* Permeation of hypericin in spheroids composed of different grade transitional cell carcinoma cell lines and normal human urothelial cells. *J. Urol.* **174,** 69–72 (2005).

32. Evans, C. L. *et al.* Killing hypoxic cell populations in a 3D tumor model with EtNBS-PDT. *PLoS One* **6,** e23434 (2011).

33. Albrecht, D. R., Underhill, G. H., Wassermann, T. B., Sah, R. L. & Bhatia, S. N. Probing the role of multicellular organization in three-dimensional microenvironments. *Nat. Methods* **3,** 369–375 (2006).

34. Petersen, O. W., Rønnov-Jessen, L., Howlett, A. R. & Bissell, M. J. Interaction with basement membrane serves to rapidly distinguish growth and differentiation pattern of normal and malignant human breast epithelial cells. *Proc. Natl. Acad. Sci. U. S. A.* **89,** 9064–9068 (1992).

35. Lee, G. Y., Kenny, P. A., Lee, E. H. & Bissell, M. J. Three-dimensional culture models of normal and malignant breast epithelial cells. *Nat. Methods* **4,** 359–365 (2007).

36. I. Rizvi *et al.* Modeling stromal determinants of 3D tumor growth to inform PDT-mediated combination treatments. *SPIE Proc.* **85680H,** (2013).

37. Rizvi, I. *et al.* Synergistic enhancement of carboplatin efficacy with photodynamic therapy in a three-dimensional model for micrometastatic ovarian cancer. *Cancer Res.* **70,** 9319–28 (2010).

38. Xu, F. *et al.* A three-dimensional in vitro ovarian cancer coculture model using a high-throughput cell patterning platform. *Biotechnol. J.* **6,** 204–212 (2011).

39. Hanahan, D. & Weinberg, R. A. Hallmarks of cancer: The next generation. *Cell* **144,** 646–674 (2011).

40. Kim, J. Bin. Three-dimensional tissue culture models in cancer biology. *Semin. Cancer Biol.* **15,** 365–377 (2005).

41. Bhowmick, N. A., Neilson, E. G. & Moses, H. L. Stromal fibroblasts in cancer initiation and progression. *Nat. Rev. Cancer* **432,** 332–337 (2004).

42. Byun, J. Y., Lee, G. Y., Choi, H. Y., Myung, K. B. & Choi, Y. W. The expressions of TGF-beta(1) and IL-10 in cultured fibroblasts after ALA-IPL photodynamic treatment. *Ann Dermatol* **23,** 19 (2011).

43. Mendoza, J. *et al.* Differential cytotoxic response in keloid fibroblasts exposed to photodynamic therapy is dependent on photosensitiser precursor, fluence and location of fibroblasts within the lesion. *Arch Dermatol Res* **304,** 549-562 (2012).

44. Patito, I. A., Rothmann, C. & Malik, Z. Nuclear transport of photosensitizers during photosensitization and oxidative stress. *Biol cell* **93,** 285-291 (2001).

45. Marti, H. H. & Risau, W. Systemic hypoxia changes the organ-specific distribution of vascular endothelial growth factor and its receptors. *Proc. Natl Acad. Sci. USA* **95,** 15809-15814 (1998).

46. Rubio, N., Fleury, S. P. & Redmond, R. W. Spatial and temporal dynamics of in vitro photodynamic cell killing: extracellular hydrogen peroxide mediates neighbouring cell death. *Photochem. Photobiol.* **8,** 457-464 (2009).

47. Jimenez-Banzo, A., Ragas, X., Kapusta, P. & Nonell, S. Time-resolved methods in biophysics. Photon counting vs. analog time-resolved singlet oxygen phosphorescence detection. *Photochem. Photobiol. Sci.* **7,** 1003–1010 (2008).

48. Paoli, V. M. D., Paoli, S. H. D., Borissevitch, L. E. & Tedesco, A. C. Fluorescence lifetime and quantum yield of TMPyPH2 associated with micelles and DNA. *J All Comp* **344**, 27-31 (2002).

49. Chirvony, V. S. Primary photoprocesses in cationic 5,10,15,20-meso-tetrakis(4-N methylpyridiniumyl) porphyrin and its transition metal complexes bound with nucleic acids. *J Porphyrins Phthalocyanines* **7,** 766-774 (2003).

50. Snyder, J. W., Lambert, J. D. C. & Ogilby, P. R. 5,10,15,20- tetrakis(N-methyl-4-pyridyl)-21H,23H-porphine (TMPyP) as a sensitizer for singlet oxygen imaging in cells: characterizing the irradiation-dependent behavior of TMPyP in a single cell. *Photochem Photobiol* **82,** 177-184 (2006).

51. Juarranz, A. *et al.* Photodamage induced by Zinc(II)-phthalocyanine to microtubules, actin, alpha-actinin and keratin of HeLa cells. *Photochem Photobiol* **73,** 283–289 (2001).

52. Dolznig, H. *et al.* Modeling colon adenocarcinomas in vitro: A 3D co-culture system induces cancer-relevant pathways upon tumor cell and stromal fibroblast interaction. *Am. J. Pathol.* **179,** 487–501 (2011).

53. Acedo, P., Stockert, J. C., Cañete, M. & Villanueva, A. Two combined photosensitizers: a goal for more effective photodynamic therapy of cancer. *Cell Death Dis.* **5**, e1122 (2014).

54. Acedo, P. *et al.* Optimizing photodynamic therapy: in vitro and in vivo effects of two combined photosensitizers on murine malignant melanoma. (under submission) (2014).

55. Versluis, A. J., Rensen, P. C. N., Taylor, P. W., Kuipers, M. E. & Love, W. G. Interaction between zinc (II) - phthalocyanine-containing and human low density lipoprotein liposomes. *J. Photochem. Photobiol. B*. **23,** 141–148 (1994).

56. Konan, Y. N., Gurny, R. & Allémann, E. State of the art in the delivery of photosensitizers for photodynamic therapy. *J. Photochem. Photobiol. B.* **66,** 89–106 (2002).

57. Cho, K., Wang, X., Nie, S., Chen, Z. G. & Shin, D. M. Therapeutic nanoparticles for drug delivery in cancer. *Clin. Cancer Res.* **14,** 1310–1326 (2008).

58. Peer, D. *et al.* Nanocarriers as an emerging platform for cancer therapy. *Nat. Nanotechnol.* **2,** 751–760 (2007).

59. Alemany-Ribes, M., García-Díaz, M., Busom, M., Nonell, S. & Semino, C. E. Toward a 3D cellular model for studying in vitro the outcome of photodynamic treatments: Accounting for the effects of tissue complexity. *Tissue Eng. Part A* **19,** 1665–1674 (2013).

60. Gao, M.-Q. *et al.* Stromal fibroblasts from the interface zone of human breast carcinomas induce an epithelial-mesenchymal transition-like state in breast cancer cells in vitro. *J. Cell Sci.* **123,** 3507–3514 (2010).

CHAPTER 5

DEVELOPMENT OF 3D MODELS TO STUDY CANCER DRUG RESISTANCE

5.1 BACKGROUND

5.1.1 CANCER THERAPEUTICS AND RESISTANCE

Chemotherapeutic agents are designed to inhibit specific hallmark capabilities of cancer cells. In particular, they are directed towards cancer signaling pathways, including abnormal proliferation, evasion from growth suppressors, resistance to cell death, replicative immortality, angiogenesis or metastasis[1] (**Figure 5.1**). However, most patients show inefficient clinical response accompanied by almost-inevitable relapses. This outcome can be explained though drug resistance phenomena.

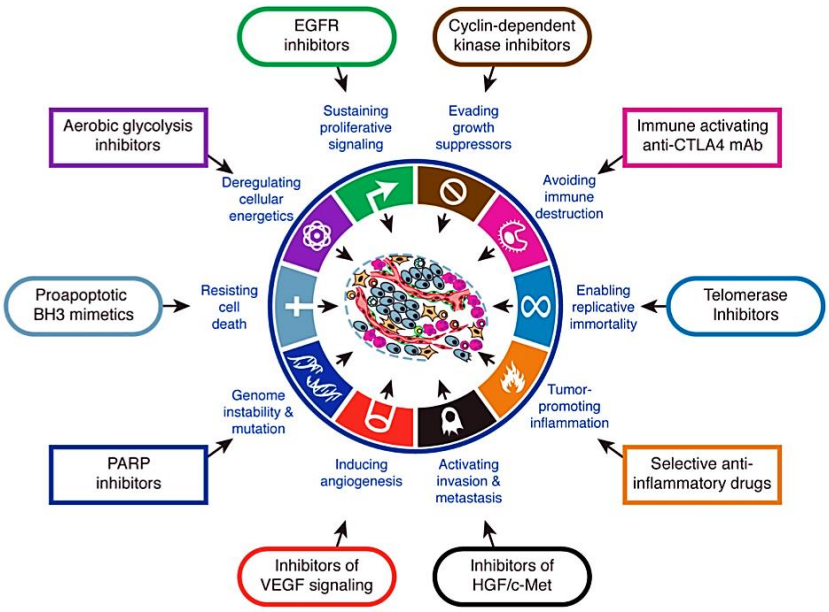

Figure 5.1. Therapeutic targets for cancer research. The diversity and complexity of cancer is rationalized by organizing this disease in different biological capabilities, including sustained proliferative signaling, growth suppressors evasion, cell death resistance, immortal replication, angiogenesis induction and invasion and metastasis activation. Different drug candidates are designed to interfere with these specific capabilities, as exemplified with telomerase inhibitors, cyclin-dependent kinase inhibitors and vascular endothelial growth factor (VEGF) signaling inhibitors. From Hanahan *et al.*[1]

Research on drug resistance is commonly performed at the intracellular level. Cells are exposed to chemotherapeutic agents and the survival clones are selected in order to identify the altered genes by molecular biology techniques[2,3]. These studies reveal the existence of three major mechanisms that account for drug resistance: (*i*) decrease in water-soluble drugs uptake through modulation of transporters expression; (*ii*) increase in energy-dependent efflux of hydrophobic drugs that can easily enter the cells by diffusion through the plasma membrane and (*iii*) changes in intracellular signaling pathways that affect the potential of drugs to kill cells, including the activation of DNA repair, the reduction of apoptosis, the alteration of drug metabolism and detoxification[2,4].

The most used cellular strategy to evade drugs is the increased efflux of a broad class of hydrophobic agents. This action is mediated through a family of energy-dependent transporters known as adenosine triphosphate (ATP)-binding cassette (ABC) transporters. They are transmembrane proteins that use the energy of ATP hydrolysis to catalyze the translocation of substrates across cell membranes against a concentration gradient. Therefore, they act as intricate molecular pumps. The human genome contains 49 ABC genes, arranged in eight subfamilies based on the sequence and organization of their ATP-binding domain[5] (**Figure 5.2**).

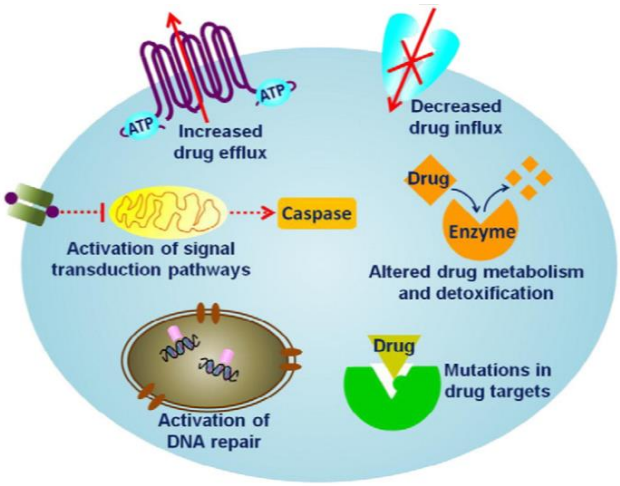

Figure 5.2. Intracellular mechanisms of cancer drug resistance. Cells are able to evade drugs action using different strategies. The most important include decreased drug influx, increased drug efflux predominantly via ATP-driven extrusion pumps, activation of DNA repair, altered drug metabolism, secondary mutations in drug targets or/and activation of downstream or parallel signal transduction pathways. The discovery of these cellular mechanisms constitute a genome-centered model for drug resistance. From Yin *et al.*[4]

5.1.1.1 Tumor Microenvironment: A Therapeutic Target

Cancer biologists have largely disregarded the contribution of tumor microenvironment to drug resistance. During the 2000s, pioneering experiments by Valerie M. Weaver group demonstrated that extracellular signaling mediated cell adhesion and organization, modifying cell responsiveness to chemotherapeutics[6,7]. In particular, different 3D models of normal and cancer breast cells were resistant to cytotoxic agents were they were arranged in polarized structures. However, the same cells were sensitive to the treatment when their polarity was disrupted through anti-E-cadherin antibody (focal adhesions). Further experiments revealed that apoptosis resistance was activated through α6β4 integrins and nuclear factor kB (NFkB) transcription factor signaling (**Figure 5.3**)[8]. These data reinforced the relevance of recapitulating tumor milieu and cellular context during drug screening processes in order to obtain reliable biomedical data.

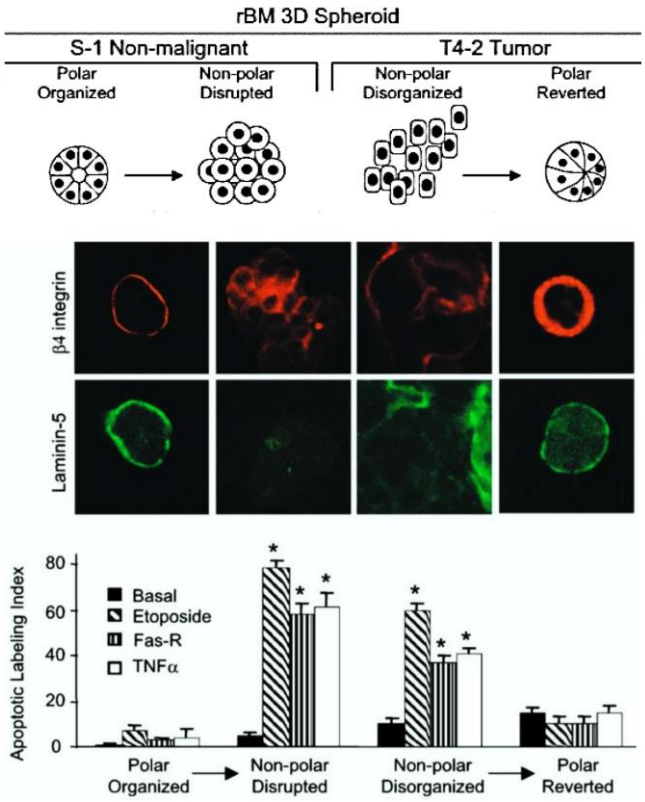

Figure 5.3. Cell adhesion and organization within extracellular matrix mediate drug resistance. Normal S-1 acini were treated with E-cadherin blocking antibody to perturb polarity. Conversely, tumorigenic T4-2 colonies were treated with β1-integrin blocking antibody to restore polarity. Immunofluorescence of β4 integrin (Texas Red) and laminin-5 (FITC) showed that polar organized S-1 and reverted T4-2 had basally localized integrins and basally secreted laminin in contrast with disrupted S-1 and disorganized T4-2 structures. Apoptotic labeling indices calculated for cells incubated with etoposide (50 μM), TNF-α (100 nM), anti-FAS antibody (2 μg/mL) or nothing (basal). Results revealed that polarized mammary structures were resistant to apoptosis. From Weaver *et al*.[8]

As previously mentioned, tumor progression is envisioned as a plastic process due to the changing environmental pressures[9]. Cancer cells continuously release cytokines, growth factors and proteases that induce inflammation and a reactive tumor stroma. In parallel, stromal cells remodel the structure and composition of the extracellular matrix (ECM) and secret more paracrine signaling molecules that enhance tumor growth, impose metabolic stress and drive disease progression[10]. Therefore, cancer cells co-evolve in order to adapt to diverse structural and molecular ECM conditions, re-defining cell adhesion complexes, cytoskeletal dynamics and motility programs. Over time, these changes drive cell heterogeneity and allow them to gain access to different signaling pathways of the microenvironment, having multiple consequences on chemotherapy[1,9,10].

First, microenvironment provides cells with access to multiple, redundant and overlapping signaling pathways. In particular, the presence of different receptors available for cell-matrix adhesion, the divergent degree of ECM remodeling capability and the range of invasion-guiding framework lead to combinatorial states or possibilities that allow flexible modes of disease progression[11,12].

As a result, the therapeutic inhibition of a specific pathway can trigger the activation of alternative and parallel mechanisms in order to reestablish the targeted biological capability[1]. For instance, breast cancers overexpress human epidermal growth factor receptor (HER)-2 in 20% of clinical cases. Two drugs for the treatment of these tumors are the monoclonal antibody trastuzumab (T) and the HER2 tyrosine kinase inhibitor lapatinib (L) that inhibit this receptor. However, both compounds show a limited efficacy due to the development of resistance. Experiments demonstrate that survival cells activate a signaling pathway that drives growth alternatively to HER tyrosine kinase. In particular, they increase the levels of β1 integrin phosphorylation, which signals downstream kinases as Focal Adhesion Kinase (FAK) and Src kinase[13].

Cancer cells can also reduce their dependence on a specific biological capability and become dependent on another[1]. For instance, tumors activate invasion and local metastasis as a response of anti-angiogenic therapies. Thus, initial hypoxic cancer cells gain access to normal and pre-existing vasculature[14].

The second contribution of the microenvironment to drug resistance arises from the phenotypical and functional heterogeneity among cancer cells. The environmental differences within a tumor drives adaptive cellular programs as epithelial to mesenchymal transition (EMT)[15]. Recent data interrelates EMT with the emergence of dedifferentiated cells with stem cell (SC)-like properties[1,15].

Cancer SCs (CSCs) show resistance to chemotherapy due to their intrinsic properties: (*i*) quiescence; (*ii*) ABC-transporter expression; (*iii*) self-renewal retaining mutations and (*iv*) capacity to differentiate and generate the cellular heterogeneity of the originating tumors. Therefore, tumors are organized into a hierarchy of subpopulations harboring diverse genetic backgrounds[5,15]. CSC population have been identified in several cancer types, including neuroblastoma, breast cancer, lung cancer, pancreatic cancer and glioblastoma[16]. However, many questions remain unanswered concerning their origin. For instance, do CSCs arise from normal SCs or from adult cells that dedifferentiate to acquire the capacity for self-renewal? Intensive research is focused on the CSC field (**Figure 5.4**).

The connection between EMT program, CSCs and drug resistance has been reported. For instance, cancer cells characterized by the expression of EMT markers and the loss of their epithelial phenotype are more resistant to chemotherapeutics (e.g. oxaliplatin and paclitaxel) than epithelial cancer cells[17].

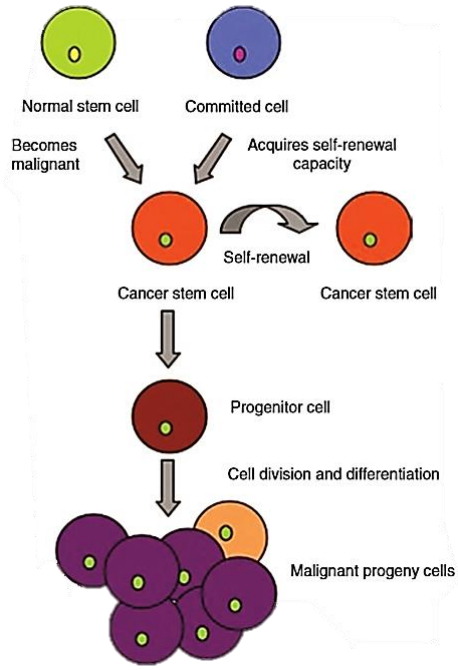

Figure 5.4. Models of cancer drug resistance. The presence of cancer stem cells (SCs) can explained the resistance of tumors to chemotherapy and radiotherapy. Cancer SCs can arise from normal SCs or normal adult cells that suffer a dedifferentiation process. This process has been interrelated with reminiscent developmental programs such as epithelial-mesenchymal transition (EMT). EMT is triggered by the evolving tumor microenvironment in order to drive cellular adaptation. Consequently, cells can acquire SC features as self-renewal and differentiation capacity. From Moitra *et al*.[5]

Models of cancer drug resistance require continuous adjustments and refinements. To summarize, data suggests that new pharmacological agents should target multiple core hallmark capabilities. Moreover, they should disrupt microenvironment-guided signaling pathways to inhibit the EMT program and cancer SC maintenance, which means the differentiation state of the tumor.

During the present thesis, the contribution of tumor microenvironment on drug resistance has been examined using tyrosine kinase inhibitors as anticancer therapeutics.

5.1.2 TYROSINE KINASES INHIBITORS

Tyrosine kinases (TKs) are enzymes that catalyze the transfer of the γ-phosphate group from adenosine triphosphate (ATP) to tyrosine residues of the target proteins. Phosphorylation of tyrosine residues modulates enzymatic activity, since it stabilizes the receptor conformation in an active state and creates binding sites for the recruitment of downstream signaling proteins (e.g. growth proteins, cytokines and hormones). Therefore, they are critical components of signal transduction and cellular regulation. There are two classes of TKs: non-receptor tyrosine kinases (NRTKs) and receptor tyrosine kinases (RTKs)[18,19].

NRTKs, also termed cellular TKs, are located in the cytoplasm, nucleus or intracellular side of the plasma membrane. They are components of the signaling cascades triggered by RTKs or by other cell surface receptors, such as the G protein-coupled receptors and immune system receptors. Examples of NRTK include Src, the Janus kinases (Jaks) and Abl[18,20].

On the other hand, RTKs are transmembrane glycoproteins that transduce extracellular signals to the cytoplasm. Activation of RTKs is typically accomplished through ligand-binding to their extracellular domain, inducing homo/heterodimerization and auto-phosphorylation of tyrosine residues. RTKs mediate numerous signaling pathways within cells, leading to cell proliferation, differentiation, migration or metabolic changes (**Figure 5.5**). Of the 90 unique TK genes identified in the human genome, 58 encode RTKs[21,19].

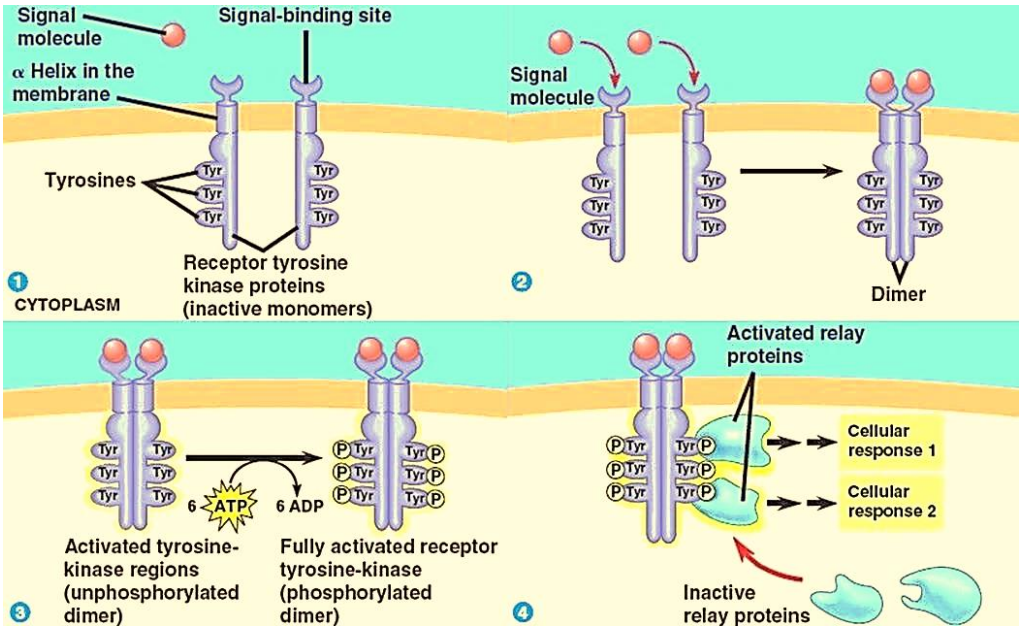

Figure 5.5. Mechanism of action of receptor tyrosine kinases. RTKs are composed of an extracellular ligand binding domain, a transmembrane domain, an intracellular tyrosine kinase domain and additional amino acid sequences that function as regulatory domains. Ligand binding induces receptor dimerization and auto-phosphorylation, meaning one subunit of the dimer phosphorylates the opposite subunit. Phosphorylated tyrosines function to recruit intracellular signaling proteins, many via their SH2 domains.

RTKs have been identified as oncogenes. During tumor progression, their hyperactivation leads to the continuous functioning of downstream signaling cascades that block cellular apoptosis, promote cellular proliferation and enhance angiogenesis. This RTKs dysregulation is achieved through (*i*) overexpression of the enzymes that increases the dynamics of the receptor homo/heterodimerization in the absence of the ligand; (*ii*) autocrine stimulation or (*iii*) activating mutations that stabilize the receptor active conformation[22]. Some relevant RTKs in the cancer field are vascular endothelial growth factor receptor (VEGFR), insulin-like growth factor receptor (IGFR) and fibroblast growth factor receptor (FGFR).

5.1.2.1 Vascular Endothelial Growth Factor Receptor

VEGFR is a class III transmembrane protein tyrosine kinase, which possesses seven immunoglobulin-like (Ig) sequences in the extracellular domain and a kinase insert in the intracellular domain[23]. There are three types of VEGFR, VEGFR2 is overexpressed with a frequency of approximately 93% in pancreatic cancer, also known as pancreatic ductal adenocarcinomas (PDAC)[24]. VEGFR2 plays a central role in the regulation of pathologic blood vessel growth and maintenance. Indeed, blockade of the VEGFR2 signaling pathway by a TKI significantly inhibits angiogenesis and lymphatic metastasis of PDAC as shown in the pancreas of nude mice. It also induces a phenotypic shift from a highly malignant to a premalignant, non-invasive tumor phenotype[25,26]. VEGF expression is regulated by hypoxia, an aggressive microenvironmental condition found in most cancer cases.

5.1.2.2 Insulin-Like Growth Factor Receptor

IGFR is a class II transmembrane protein tyrosine kinase, which is comprised of two extracellular α-subunits, ligand-binding domains and two transmembrane tyrosine kinase β-subunits. There are two types of IGFR, IGFR1 activates intracellular signaling cascades responsible for cell survival, proliferation and motility: mitogen activated protein kinase (MAPK) and phosphoinositide-3-kinase (PI3K) pathways. As a result, its dysregulation leads to an abnormal cell growth[27–29]. Moreover, IGFR1 expression is usually associated with abundant stroma. These findings suggest that its signaling system might be correlated with the hallmark desmoplastic reaction characteristic of PDAC[30].

5.1.2.3 Fibroblast Growth Factor Receptor

FGFR is a class V transmembrane protein tyrosine kinase. Four FGF receptor genes have been identified in mammals (FGFR1 to FGFR4), which comprise an extracellular domain composed of two or three Ig loops, a transmembrane segment and an intracellular tyrosine kinase. Ligand-binding specificity of the receptor is mediated by the second and third Ig-loop. For FGFR1-FGFR3, the third Ig loop is encoded by two exons, an invariant exon termed IIIa and one of two exons, termed IIIb and IIIc respectively, to which the IIIa exon is spliced (alternative splicing of C-terminal). This generates two receptor isoforms with quite different ligand-binding specificities[31]. A genetic linkage analysis has associated these three members of the FGFR gene family as the underlying cause of several diseases, including cancer[32]. The isoform FGFR2(IIIb) is found mainly in epithelia and is activated by four known ligands, which are synthesized predominantly in the tissue mesenchyme. Its dysregulation correlates with increased venous invasion[33–35].

5.1.2.4 Tyrosine Kinase Inhibitors

Constitutive activation of TKs in cancer cells can be blocked by selective tyrosine kinases inhibitors (TKIs). Several classes of TKIs have been developed as promising cancer drugs, such as heat shock proteins, immunoconjugates, antisense RNAs, peptide drugs, small molecule inhibitors and monoclonal antibodies (mAbs), being the last two the most relevant agents. mAbs bind with high affinity to the extracellular domain of the RTK to avoid the binding of the ligand and, therefore, the activation of the intracellular signal transduction pathway.

Small molecules TKIs block the phosphorylation reaction mediated by these kinases. They show two different mechanisms of action: (*i*) binding of the ATP-binding site within the intracellular catalytic domain of the kinase; (*ii*) binding outside of the ATP-binding site, modifying the tridimensional structure of the receptor and disrupting the interaction between the ATP and the kinase pocket in an allosteric manner[22,36]. They can target both receptor and non-receptor TKS. The main drawback of TKIs is that they generate cellular resistance[20].

In the present thesis, we have tested the effect of three small TKIs molecules based on the pyrido[2,3-*d*]pyrimidine scaffold[37,38] within 3D cultures of pancreatic cancer. In particular, their activity was assessed by analyzing cellular viability together with the expression levels of the RTKs that act as therapeutic targets and are known to be deregulated in pancreatic cancer[24,35] (**Figure 5.6**).

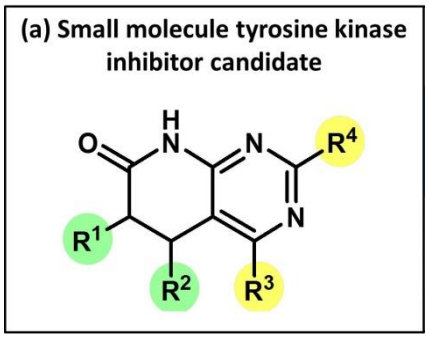

Figure 5.6. Novel drug candidates for pancreatic cancer. Small molecule tyrosine kinases inhibit the phosphorylation of tyrosine residues and, therefore, are designed as anti-cancer drugs. An example of TKIs consists in pyrido[2,3-*d*]pyrimidine scaffold. These molecules are kindly provided by Dr. José Ignacio Borrell (IQS School of Engineering).

5.2 HYPOTHESIS AND SPECIFIC AIMS

The main motivation of this chapter was to study the contribution of tumor microenvironment on drug resistance using *in vitro* models of pancreatic cancer cells.

Our working hypothesis was that three-dimensional (3D) cultures could allow us to study the ability of different extracellular cues in triggering survival strategies for cancer and stromal cells after drug treatment. In particular, the comparison between synthetic and natural scaffolds helped us to unravel the critical role of extracellular matrix (ECM)-mediated signaling pathways in these processes. The specific aims for this chapter were the following:

(1) To characterize the efficacy of cancer drugs as tyrosine kinases inhibitors in 3D cultures.

(2) To study the resistance mechanisms triggered by cancer and stromal cells depending on the received microenvironmental signals through 3D cultures.

5.3 RESULTS AND DISCUSSION

5.3.1 MORPHOLOGICAL ASSESSMENT OF 3D CANCER MODELS

A major challenge in cancer research is the development of resistance to drugs as tyrosine kinases inhibitors (TKIs). During this project, the contribution of the microenvironment to this cellular program was studied through three-dimensional (3D) cultures, using different tissue engineering scaffolds.

Pancreatic ductal adenocarcinoma cells (PANC-1) and human normal dermal fibroblasts (hNDF) were selected to evaluate the direct effect of TKIs to a cancer and stromal cell line respectively. Both models have been previously developed and characterized in detail in chapter 3 section 3.3.3. CELL PHENOTYPE AND PLASTICITY IN 3D CANCER MODELS and chapter 4 section 4.3.1 DEVELOPMENT OF 3D CELL MODELS FOR DRUG TESTING. Cells were encapsulated in collagen type I and self-assembling peptide RAD16-I. First of all, the macroscopic morphology of 3D cultures was characterized with a stereoscopic microcope (**Figure 5.7**).

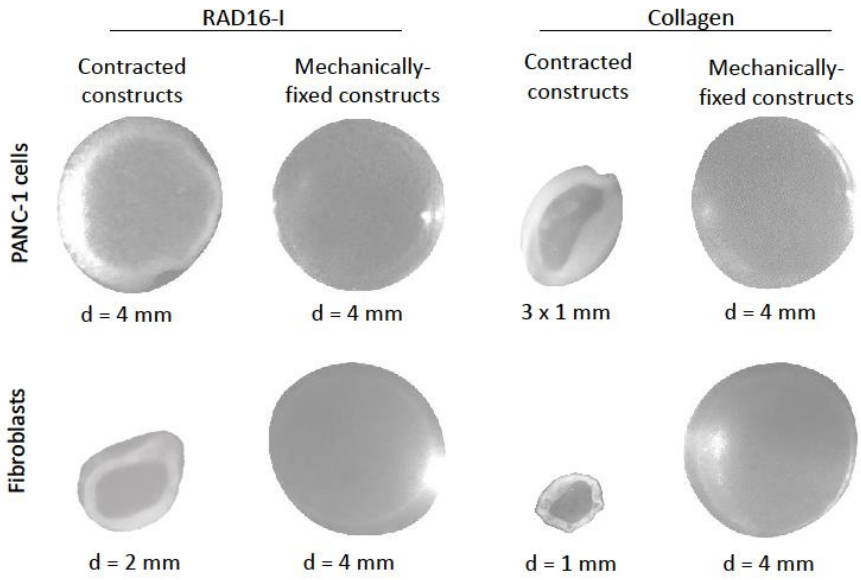

Figure 5.7. Morphologic assessment of 3D cultures at macroscopic level. Cells were encapsulated in RAD16-I and collagen scaffolds. All 3D cultures should have the same dimensions to avoid differences in drug diffusion. For this reason, the spontaneous contraction of the cultures was mechanically blocked and the resulting geometry was a disk of 4 mm of diameter and 500 µm of thickness.

At the macroscopic level, all 3D models should have the same dimensions since the efficacy of TKIs strongly depends on mass transport effects. Fibroblasts and PANC-1 cells grown in collagen scaffolds were able to contract these biomaterials spontaneously, diminishing their diameter. Cultures were performed on top of a Teflon membrane of a culture insert in order to block this process mechanically. In this way, the hydrogels underwent self-assembling in the

surface of the membrane and, therefore, they could not contract over culture time. They formed a dense disk with approximately 4 mm of diameter and 0.5 mm of thickness.

Next, cellular morpholy and organization in 3D cultures (RAD16-I and collagen scaffolds) were examined by nuclei and actin filaments staining (**Figure 5.8**).

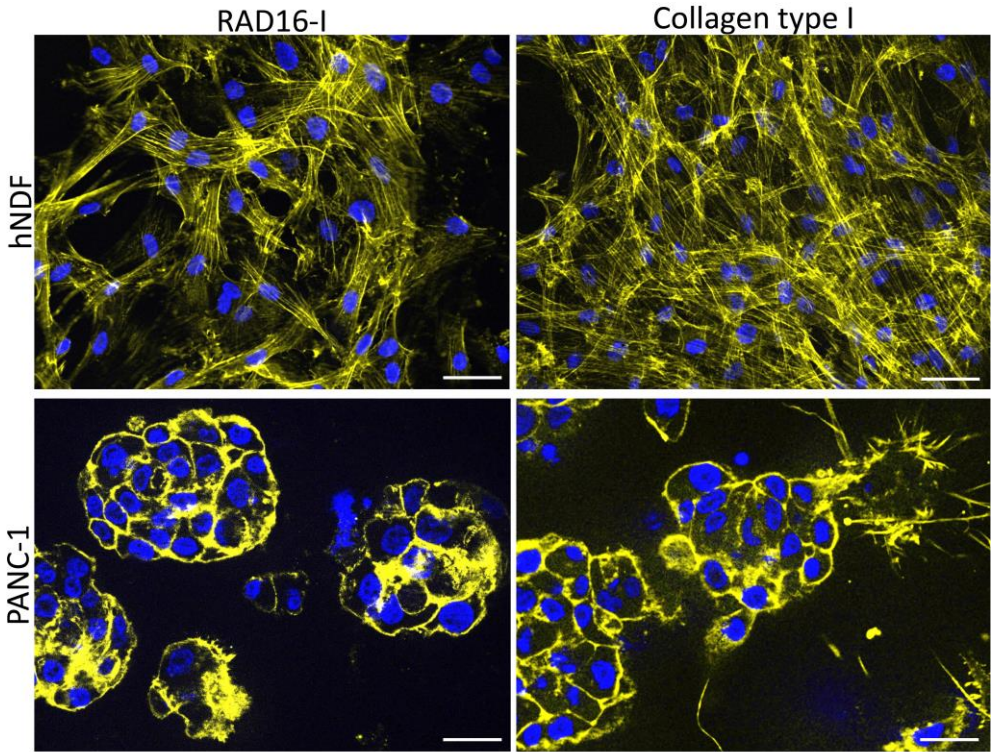

Figure 5.8. Cell morphology and organization of 3D cultures of cancer cells and fibroblasts. Cancer cells (PANC-1) and fibroblasts (hNDF) were grown in the synthetic self-assembling RAD16-I and the natural collagen type I hydrogels. After 7-day culture, samples were fixed and stained for actin microfilaments (phalloidin, pseudo-colored in yellow) and nuclei (DAPI, blue). Scale bar of 50 µm.

Fibroblasts showed an *in vivo*-like elongated morphology. Furthermore, the 3D microenvironment promoted continuous intercellular interactions that evolved during culture, in contrast to conventional monolayers, better mimicking fibroblasts architecture in connective tissues. Phenotipically, no significant differences were detected between collagen and RAD16-I scaffolds.

Cancer cells had prominent and irregular nuclei, characteristic of abnormal divisions. Actin filaments were organized in both cortical thin bundles and stress fibers filling the internal cellular area. Therefore, cells showed a cytoskeletal architecture that resembled some aspects of a mesenchymal-like phenotype. Indeed, actin remodeling emerges as the primary mechanism responsible for confering phenotypic plasticity and enabling processes as epithelial-mesenchymal transition (EMT) and metastasis. Cells cultured in collagen scaffolds adopted a more elongated and spindle-shape morphology than in RAD16-I scaffolds.

Cells remained alive during the whole 3D culture period in both collagen and RAD16-I scaffolds. Therefore, cells were grown in suitable conditions when trying to recreate the *in vivo* cellular milieu. Further experiments directed to unravel the molecular mechanism of TKIs resistance could be performed.

5.3.2 CELLULAR RESPONSE TO TYROSINE KINASES INHIBITORS

Three TKIs and a placebo were kindly provided by the group of Dr. José Ignacio Borrell (Grup d'Enginyeria Molecular, IQS School of Engineering, Ramon Llull University). All the experiments were performed under blind conditions, without previous knowledge of the identity or the activity of these molecules.

First, the effect of the four TKIs was assessed by cellular viability in 2D cultures of cancer cells (PANC-1) and stromal cells (hNDF). In particular, MTT assay was performed 24h and 48h after treatment (**Figure 5.9**).

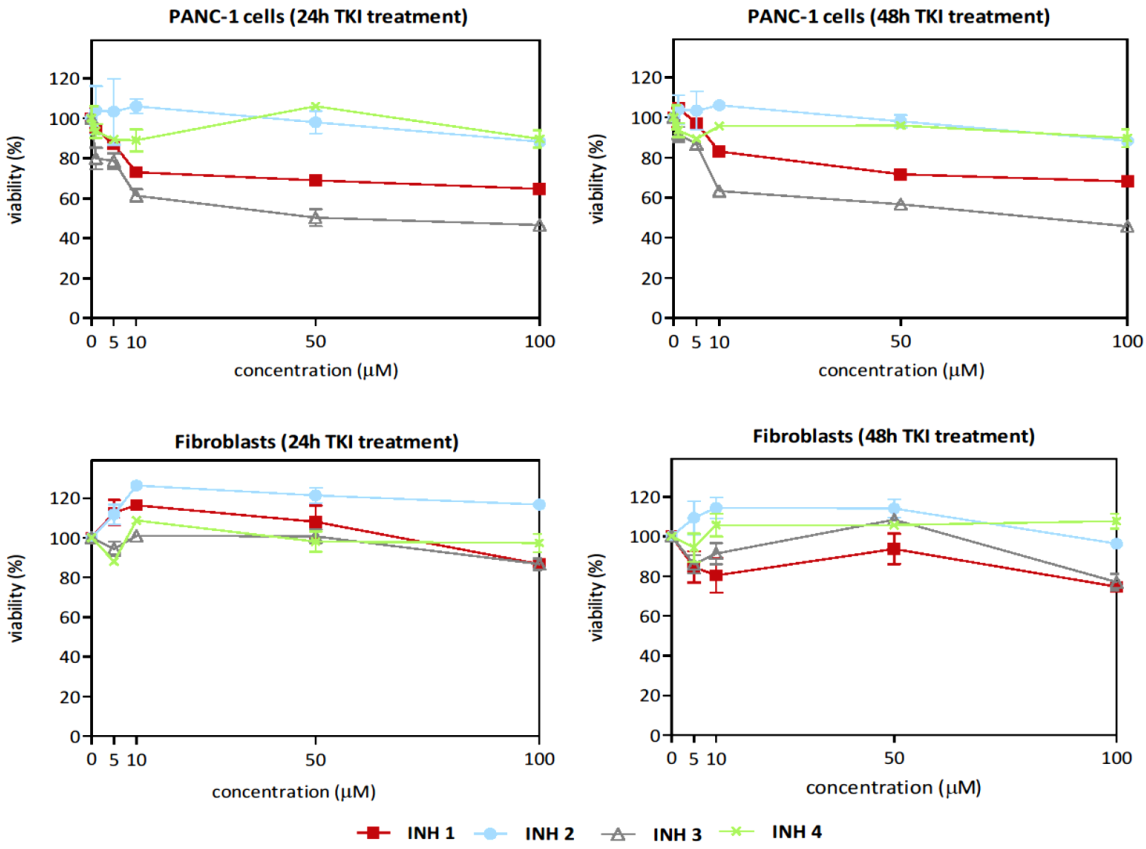

Figure 5.9. Assessment of the activity of tyrosine kinases inhibitors in 2D cultures. PANC-1 cells and fibroblasts were grown on conventional monolayers and treated with different drug concentrations, ranging from 1 µM to 100 µM during 24 and 48 hours. The resulting cellular viability was analyzed by MTT assay (*N*=2, *n*=6).

Results suggested that TKI3 (grey colour) was the most effective inhibitor against PANC-1 cells, showing a viability rate around 40% in both 24h and 48h experiments. TKI1 (red colour) gave similar results as TKI3, but the viability rate of PANC-1 was slightly higher (around 60%). However, TKI2 (blue colour) and TKI4 (green colour) did not have a significant effect against PANC-1 cells. Importantly, these experiments suggested that any of the studied TKIs did not induce cell death to fibroblasts, since they mantained a cellular population between 80-100% after drug treatment.

The cellular effect of TKIs was compared to their kinase inhibition profile obtained through a radiometric protein kinase assay (33PanQinase® Assay from Proqinase™ company, http://www.proqinase.com). This test was based on incubating the compounds at a concentration of 10 µM in front of a panel of tyrosine kinases. Briefly, these enzymes transfer a γ-phosphate group from ATP to their substrate (e.g. protein, peptide), generating phosphorylated protein/peptide and ADP as products. In this case, the chemical reaction was monitored using ATP molecules that contained a radiolabelled phosphate (^{33}P-ATP). The phosphorylated and non-phosphorylated substrates were distinguished by counting radioactivity. **Table 5.1** shows the obtained data, kindly provided by Dr. José Ignacio Borrell (Grup d'Enginyeria Molecular, IQS School of Engineering, Ramon Llull University).

Compound ID	ALK C1156Y (GST-HIS-tag)	ALK F1174L (GST-HIS-tag)	ALK F1174S (GST-HIS-tag)	ALK L1196M (GST-HIS-tag)	ALK R1275Q (GST-HIS-tag)	ALK wt (GST-HIS-tag)	AXL	DDR2	EGF-R L858R
INH 1	23	28	25	22	18	18	40	0	14
INH 2	13	10	14	7	7	9	32	24	21
INH 3	10	6	11	3	4	4	23	73	43
INH 4	92	108	107	105	99	85	102	103	110

Compound ID	EGF-R T790M	EGF-R T790M/L 858R	EPHA2	ERBB2	ERBB4	FGF-R1 wt	FGF-R2	FGF-R3 wt	FGF-R4
INH 1	36	31	0	40	21	-2	0	8	26
INH 2	31	22	7	41	16	11	9	34	28
INH 3	30	34	19	34	29	12	3	31	20
INH 4	110	118	86	85	106	104	97	114	103

Compound ID	IGF1-R	MET wt	MKNK1	MKNK2	RET wt	ROS	VEGF-R1	VEGF-R2	VEGF-R3
INH 1	21	62	83	84	2	62	15	2	32
INH 2	15	51	26	56	23	41	39	18	40
INH 3	6	47	91	116	23	70	19	8	40
INH 4	114	101	92	91	159	104	81	101	109

Table 5.1. Evaluation of the inhibitory potential of the four selected drugs. The effect of the TKIs was determined by a radiometric protein kinase assay (33PanQinase® Assay from ProqinaseTM company, http://www.proqinase.com) and classified in function of their efficacy (green, yellow and red).

TKI4 was identified as the placebo. This behaviour was consistent with viability assays (**Figure 5.9**) and ELISA-based assays (**Table 5.1**). On the other hand, TKI3 was selected as the best candidate to continue experiments of viability and drug resistance with 3D cultures since it triggered the most effective cell response with 2D cultures.

PANC-1 and hNDF cells were cultured independently in RAD16-I and collagen scaffolds, previously characterized at the morphological level. Cellular viability was assessed by MTT assay in order to evaluate TKI3 activity in a 3D milieu and compare it to the results of 2D cultures (**Figure 5.10**). It is convenient to note that MTT assay depends on the mitochondrial activity of cells, since this chemical reagent is reduced to formazan salt by the dehidrogenase enzymes present in the mitochondria. To analyze viability results, 2D and 3D cultures were normalized with intrisnic controls, not assuming that these microenvironments were equivalent.

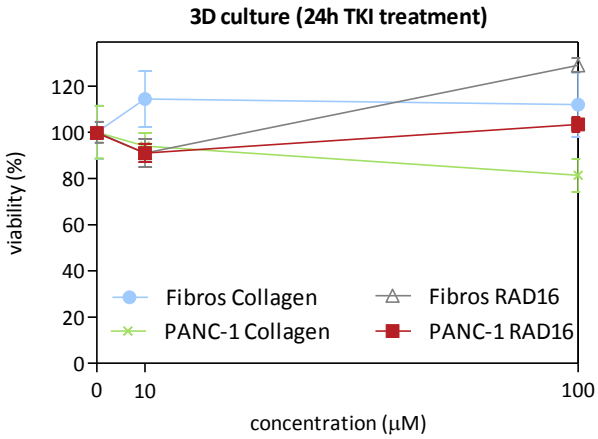

Figure 5.10. Assessment of the activity of tyrosine kinases inhibitors in 3D cultures. PANC-1 cells were grown within collagen and RAD16-I scaffolds and treated with different concentrations of the TKI 3, ranging from 1 µM to 100 µM during 24 hours. The resulting cellular viability was analyzed by MTT assay. The side effects of the TKIs were studied with a 3D culture of normal fibroblasts, as a model of the cellular population that compose the connective tissue. (*N*=2, *n*=6).

Results showed that none of the 3D cultures were affected by TKI3, using the same experimental conditions as 2D cultures (concentrations ranging from 1-100 µM). This behaviour was independent of the cell type (PANC-1 and hNDF) and the scaffold (collagen and RAD16-I biomaterials). Different hypotheses could explain the therapeutic inefficacy obtained in 3D cultures: mass transport limitations (previously studied in chapter 4) and extracellular signaling from the tumor microenvironment.

First, 2D cultures are characterized by artificial rich oxygenation and nutrition. In contrast, 3D cultures have the capacity to modulate the molecular gradients that exist for any soluble component (e.g. oxygen, nutrients, and drugs). They can mimic tumor architecture, in which the external cells are more exposed to soluble effector molecules and the inner cells remain buried, creating a protective microenvironment.

Second, 3D cultures are able to integrate multiple signals (biochemical, biomechanical and biophysical) that arise from the extracellular matrix (ECM) and neighbouring cells and are partially lost in 2D cultures. Thus, the expresion of key genes involved in disease progression (oncogenes and tumor supressor genes) can show similar levels as the *in vivo* scenario, giving cells a more aggressive nature than 2D cultures[39,40]. Furthermore, tumor microenvironment can trigger redudancy in signaling pathways and phenotypical plasticity throughout the activation of reminiscent developmental programs like EMT[1].

5.3.3 EFFECT OF INHIBITORS ON RECEPTOR TYROSINE KINASES EXPRESSION

To understand the difference of viability between 2D and 3D models after TKIs treatment, the gene expression of the target receptor tyrosine kinases (RTKs) was assessed. For this reason, three receptors were selected based on their role during tumor progression as well as their sensitivity to drug treatment (**Table 5.1**). These receptors were: the vascular endothelial growth factor receptor 2 (VEGFR2), the fibroblast growth factor receptor 2 (FGFR2) and the insulin-like growth factor receptor 1 (IGF1R). The expression of these three RTKs was quantified through Real Time RT-PCR in the different experimental models (RAD16-I with hNDF, RAD16-I with PANC-1, type I collagen with hNDF and type I collagen with PANC-1).

5.3.3.1 Receptor Tyrosine Kinases Expression on PANC-1 Cells

The RTKs expression within PANC-1 cell line was examined. Two different comparisons were done: 3D against 2D cultures and presence against absence of drugs. First of all, the effect of the microenvironment on the expression of the target RTKs was quantified through Real Time RT-PCR (**Figure 5.11**).

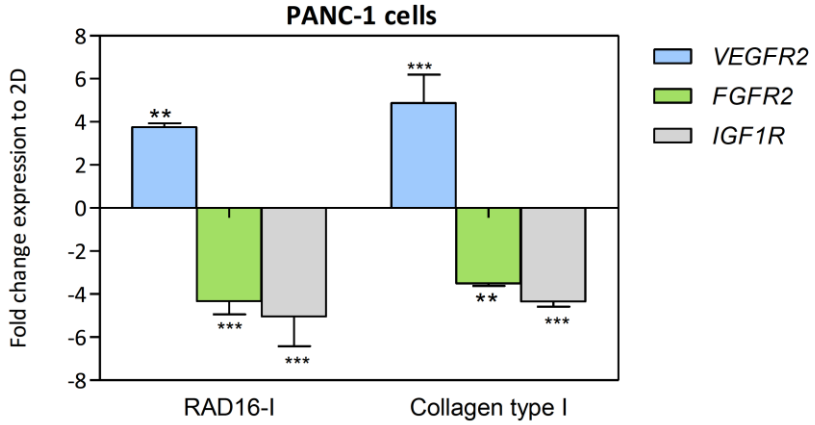

Figure 5.11. Effect of the microenvironment on receptor tyrosine kinases expression in PANC-1 cells. Cells were grown in 2D and 3D (RAD16-I and collagen type I) cultures and the expression of *VEGFR2*, *FGFR2* and *IGF1R* genes was assessed by Real Time RT-PCR. Results showed the role of microenvironmental signals on tumor gene expression. (*N*=2, *n*=6).

Results from Real Time RT-PCR experiments showed an overexpression of the *VEGFR2* gene when cells were cultured in 3D cultures compared to conventional monolayers. In particular, the fold induction increased by a relative factor of about 4 times. This pattern expression was consistent with the involvement of the *VEGFR2* gene in the process of angiogenesis. Briefly, angiogenesis is the formation of new blood vessels from pre-existing ones in order to supply oxygen and nutrients to the tumor and enable its growth beyond a critical size (1-2 mm). It has been largely reported that hypoxia is one of the major factors triggering this process[41,42]. When cells were embedded within collagen and RAD16-I scaffolds, oxygen was not uniformly distributed across the whole culture. Therefore, results suggested the development of hypoxia and the overexpression of the *VEGFR2* gene in 3D cultures.

The *FGFR2* gene was downregulated between 3-4 folds in 3D samples relative to 2D. This receptor is present in normal epithelia, contributing to the differentiation and maintenance of this phenotype. Indeed, it has been reported that most established carcinoma lines have lost the expression of FGFR2[43,44]. The downregulation of this gene suggested that PANC-1 cells began to lose their epithelial phenotype in order to acquire mesenchymal characteristics, such as migration and invasion capabilities. Thus, 3D cultures could mimic some mechanisms involved in the EMT process, consistent with morphological assessment (**Figure 5.8**). On the other hand, cells grown in monolayers were artificially polarized, resembling epithelial organization and being limited to 2D space movement.

Finally, the *IGF1R* gene was downregulated between 4-5 folds in 3D cultures relative to 2D. IGFR and epithelial growth factor receptor (EGFR) belong to E-cadherin/β-catenin complexes that form the cell-cell interactions known as adherens junctions. Data support the crosstalk between IGFR and EGFR for activating the invasive phenotype of cancer cells during metastatic progression. In particular, IGFR expression decreases, while EGFR increases to cause the destabilization of E-cadherin/β-catenin complexes[45–47]. Thus, RTKs have a different expression pattern depending on the specific cancer stage in which they are involved. Being consistent with *VEGFR2* and *FGFR2* results, the *IGF1R* gene expression suggested that the culture of cancer cells within a 3D milieu triggered the loss of the epithelial phenotype and the activation of some EMT features.

There were no significant differences between RAD16-I and collagen scaffolds. Data indicated that the RTKs expression pattern was caused by the 3D cellular organization that increased the communication network between cells and ECM rather than the chemical signaling that arose from collagen.

Next, cancer cells were incubated with TKI3 and the survival population was collected in order to characterize the expression of the target receptors. Therefore, the mechanisms that cancer cells developed to escape from drug action were studied (**Figure 5.12**).

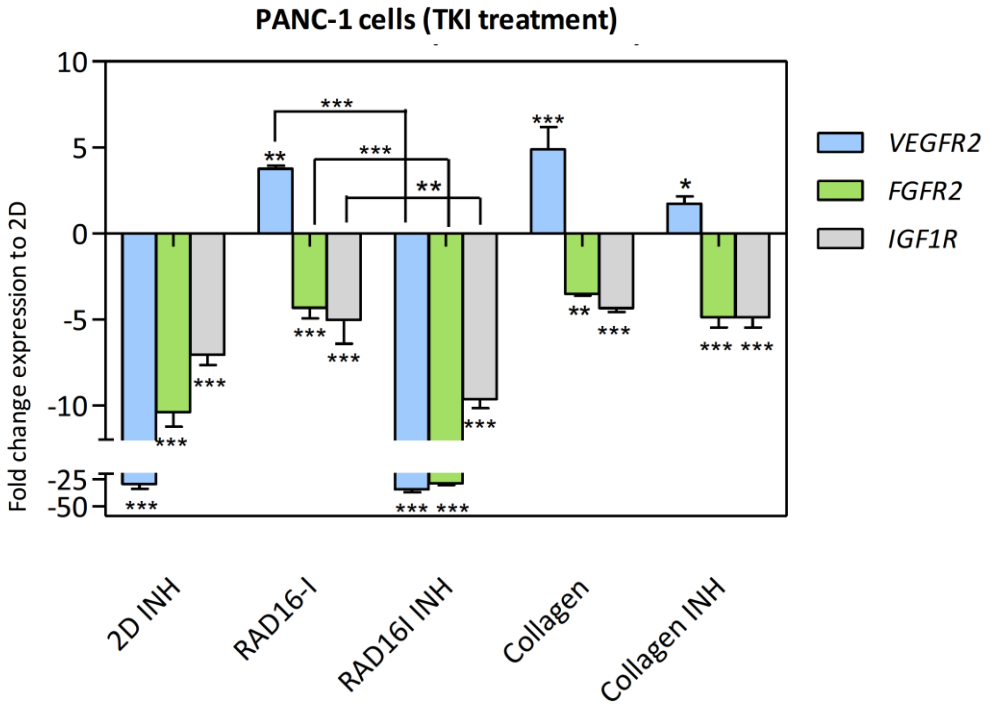

Figure 5.12. Effect of inhibitors on receptor tyrosine kinases expression in the survival PANC-1 population. Cells were grown in 2D and 3D (RAD16-I and collagen) cultures and were incubated with TKIs. The cell survival fraction was collected to study expression of *VEGFR2*, *FGFR2* and *IGF1R* genes by Real Time RT-PCR. Results showed the diversity of mechanisms that cells used to resist or escape from TKIs effect in cancer treatment. (*N*=2, *n*=6).

2D and RAD16-I cultures suffered a significant downregulation of the RTKs expression. Particularly, the *VEGFR2* mRNA expression decreased by a factor of approximately 40, *FGFR2* of 10-20 and *IGF1R* of 5 relative to non-treated samples. Conversely, collagen did not show any significant modification of the expression pattern of the analyzed kinases.

PANC-1 cells grown in 2D and RAD16-I cultures responded to drug action by stopping the transcription machinery engaged in the synthesis of the blocked receptors. We hypothesized that cells began to express alternative receptors that participated in similar signaling cascades. However, cells grown in collagen cultures resisted or escaped from drug action by regulating other survival strategies independently of the silencing of the target receptors. Collagen had a wide range of cell-matrix receptors (e.g. integrins-recognition sequences) that could create a redundant network of proteins triggering similar signaling pathways (**Figure 5.13**). Therefore, results suggested that cells did not need to begin synthesizing other receptors.

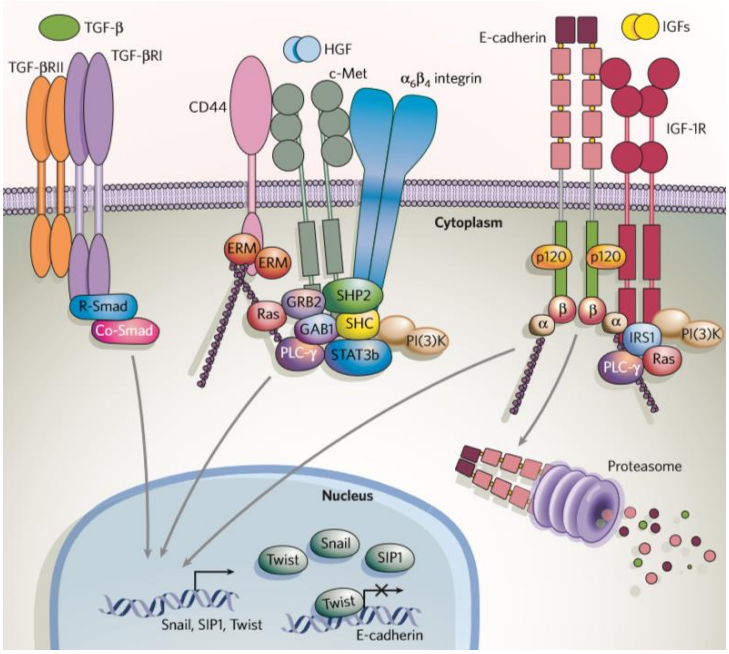

Figure 5.13. Redundant network of cellular receptors that complement similar signaling pathways. Collagen has a wide range of binding domains of cell-matrix receptors that activate a redundant signaling network o to ensure cell function when some RTKs are blocked. This figure shows the complementary role of IGFR and $\alpha_6\beta_4$ integrin receptor. Therefore, collagen reflect the mechanisms that cells use to resist or escape from cancer treatments more precisely than RAD16-I scaffold, which lacks important microenvironmental cues (e.g. cell adhesion sites and proteolytic degrading sites). From Christofori[48].

5.3.3.2 Receptor Tyrosine Kinases Expression in Fibroblasts

The RTKs expression in fibroblasts was examined. It is important to take into account that the role of these receptors depends on the cell type. Therefore, it was expected to obtain different expression patterns between PANC-1 and hNDF cells (**Figure 5.14**).

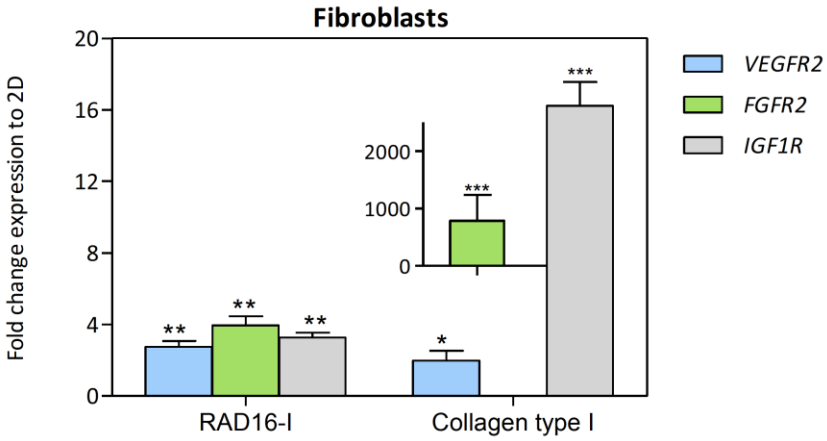

Figure 5.14. Effect of the microenvironment on receptor tyrosine kinases expression in fibroblasts. Cells were grown in 2D and 3D (RAD16-I and collagen type I) cultures and the expression of *VEGFR2*, *FGFR2* and *IGF1R* genes was assessed by Real Time RT-PCR. Results showed the role of microenvironmental signals on fibroblasts gene expression. (*N*=2, *n*=6).

The *VEGFR2* gene was upregulated between 2-4 relative folds in a 3D than a 2D milieu. This receptor is required for angiogenesis, either in physiological or pathophysiological processes (e.g. embryonic development and tumor progression). Multiple cell types and soluble effector molecules are engaged in the complex formation of new blood vessels from pre-existing ones. In particular, endothelial cells actively recruit fibroblasts for paracrine signaling[49,50]. Considering that 3D cultures induced hypoxia, it was expected that they upregulated the *VEGFR2* gene in order to activate angiogenesis and, therefore, the supply of oxygen and nutrients.

The FGFR pathway regulates cell growth in fibroblasts, since FGFs act as transforming factors, mitogens and survival factors. However, FGFRs regulate adhesion and differentiation in cancer cells accordingly to published data[43,44] and the obtained Real Time RT-PCR results of this work. Thus, the role of these receptors depends on the cell type. In the case of fibroblasts, RAD16-I cultures induced 4 folds overexpression of *FGFR2* gene compared to 2D cultures. This receptor was highly overexpressed in collagen cultures, obtaining values that were out of PCR margins and were represented separately. It would be necessary to perform a Western Blot in order to determine whether this overexpression also occurred at the protein level. These results could be explained because the culture of fibroblasts from a 2D to a 3D milieu favored cell-cell and cell-ECM interactions and enabled an extensive communication network. This situation could mimic the *in vivo* milieu, promoting ECM synthesis (e.g. glycosaminoglycans and proteoglycans) and, in turn, activating cellular growth. In fact, it was previously reported that 3D cultures upregulated the FGFRs expression in the fibroblasts population[51–53].

Finally, the *IGF1R* gene was upregulated approximately 4 folds in RAD16-I scaffolds and 15 folds in collagen scaffolds relative to 2D cultures. This expression pattern was in agreement with the mitogenic capability of the receptor, acting in a synergic manner with VEGFR and FGFR[54,55]. Therefore, results also suggested that the 3D communication network that established fibroblasts in collagen and RAD16-I biomaterials activated cellular growth.

Next, fibroblasts were incubated with TKI3 and the survival population was collected in order to characterize the expression of the target receptors. The experiment was performed as previously detailed (**Figure 5.15**).

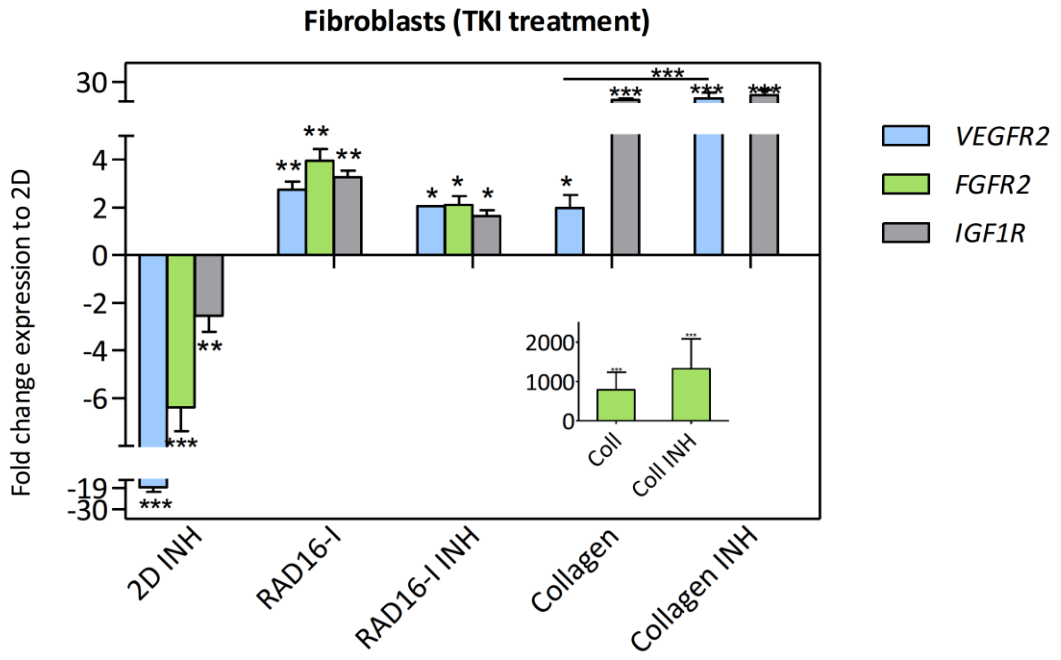

Figure 5.15. Effect of inhibitors on receptor tyrosine kinases expression in the survival fibroblasts population. Cells were grown in 2D and 3D (RAD16-I and collagen) cultures and were incubated with TKIs. The cell survival fraction was collected to study expression of *VEGFR2*, *FGFR2* and *IGF1R* genes by Real Time RT-PCR. Results showed the diversity of mechanisms that stroma cells used to resist or escape from TKIs effect in cancer treatment. (*N*=2, *n*=6).

After the TKIs treatment, 2D cultures showed a downregulation of the *VEGFR2*, *FGFR2* and *IGF1R* genes at levels of approximately 20, 6 and 3 folds relative to non-treated samples. Conversely, RAD16-I and collagen cultures maintained similar expression levels of RTKs.

Significantly, results suggested that cells embedded both in collagen and RAD16-I biomaterials acquired an equivalent mechanism of drug resistance, maintaining the expression pattern of the target receptors. We hypothesized that survival cells probably activated complementary ECM receptors to trigger similar signaling pathways in order to evade drug action. Fibroblasts are responsible for collagen synthesis, deposition and remodeling. Thus, cells could produce their own physiological matrix and mask the initial contribution of the chemical signaling that arose from collagen, mainly due to the presence of integrins-recognition sequences.

Therefore, RAD16-I scaffold emerged as a reproducible and flexible platform for drug screening processes in the case of fibroblasts population, having a similar predictive capacity as collagen. Therefore, the development of co-cultures between cancer cells and fibroblasts could facilitate the use of synthetic scaffolds since fibroblasts could synthesize their own physiologic matrix and contribute to the integration of microenvironmental signaling in these platforms.

5.3.4 FUTURE DIRECTIONS

More research is needed to unravel the contribution of tumor microenvironment on cancer drug resistance. Experiments are performed to continue studying the hypothesis that evolving extracellular pressures can trigger phenotypic plasticity and signal redundancy in cancer cells, causing inefficacy of TKIs molecules.

First, experiments are focused on the functionalization of RAD16-I scaffolds with integrin-binding domains in order to study their specific role on drug resistance. For this reason, RTKs expression before and after the treatment should be quantified. Advantageously, synthetic scaffolds provide both a reproducible and flexible microenvironment in order to study chemical or mechanical cues in an individual manner and unravel their role in cancer progression and treatment cellular response.

The synergism between drugs is also studied in 3D cultures as possible cancer treatment. The finding that tumor microenvironment triggers redundancy in cell signaling cascades has revealed it as a possible pharmacological target. In particular, the combination of TKIs with blebbistatin (BB) is under investigation (**Figure 5.16**). BB is a small molecule inhibitor of myosin II ATPase activity[56], a key regulator of the formation and maturation of integrin-mediated adhesions through actin fiber contractility[57]. Therefore, it blocks cell interactions with the extracellular milieu.

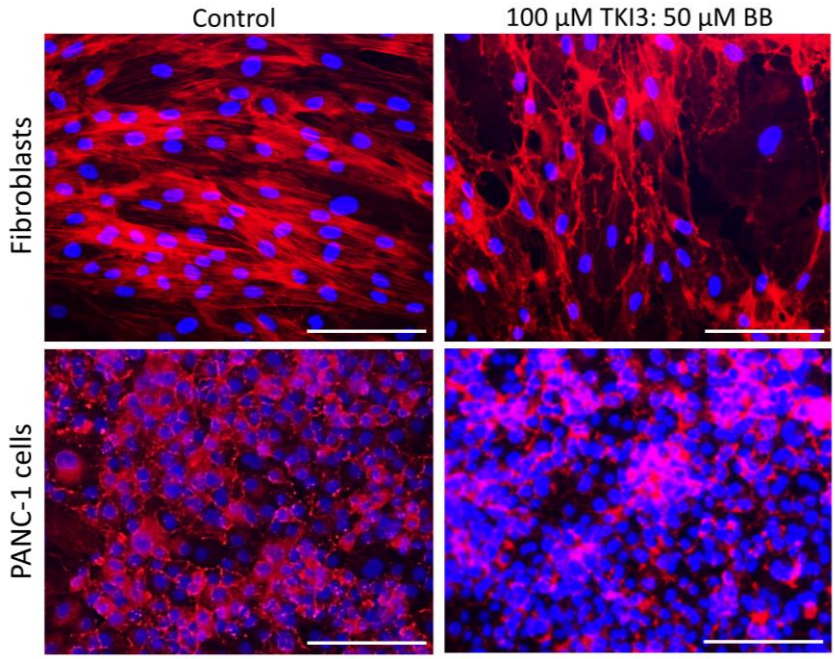

Figure 5.16. Morphological assessment of the activity of synergic tyrosine kinases- and myosin II ATPase- inhibitors. PANC-1 cells and fibroblasts were treated with 100 µM of TKI3 and 50 µM BB. Samples were fixed, stained for actin microfilaments (phalloidin, red) and nuclei (DAPI, blue) and compared with controls of non-treated cultures. Scale bar of 50 µm

In terms of cancer cells and fibroblasts, genome-centered studies are also under performance. The expression of adenosine triphosphate (ATP)-binding cassette (ABC) transporters as efflux pump of TKIs is quantified before and after treatment in 3D cultures. Therefore, the interaction between genomic and environmental changes in drug resistance can be assessed using 3D cultures.

5.4 CONCLUDING REMARKS

A major challenge in cancer research is the acquisition of drug resistance, which causes patient relapse. Traditionally, efforts have been focused on single-cell studies to identify genetic and epigenetic alterations such as upregulation of efflux pumps (ABC transporters)[36]. However, the development of three-dimensional (3D) cultures can help to study the contribution of tumor microenvironment on this cellular program. Consequently, the arsenal of cancer therapeutics could strongly increase due to the better characterization of signaling pathways triggered by extracellular matrix (ECM) and stromal cells. During this project, different 3D models of pancreatic cancer cells and fibroblasts were developed in order to study the resistance of tyrosine kinases inhibitors (TKIs).

First, the expression of the target receptor tyrosine kinases (RTKs) was studied in 3D cultures. Cancer cells downregulated epithelial markers as the fibroblast growth factor receptor II (*FGFR2*) and insulin-like growth factor receptor I (*IGF1R*) genes, which are involved in the formation of E-cadherin complexes and maintenance of this phenotype. Therefore, results suggested a transition from an epithelial to a mesenchymal-like morphology. On the other hand, fibroblasts upregulated *IGF1R* and *FGFR2* genes as mitogens and transforming factors receptors. This expression pattern could indicate that 3D models favor the formation of an extensive cell network that increased cell growth and communication. These results were consistent with publications that reported a receptors function depending on cell type.

TKIs were evaluated as cancer drugs in 2D and 3D cultures. In the present thesis, the used inhibitors was based on a pyrido[2,3-*d*]pyrimidine scaffold and were synthesized by the group of Dr. José Ignacio Borrell (IQS School of Engineering). Significantly, the most effective TKI induced a cell death of approximately 60% of cancer cell population in 2D cultures, but remained inactive in 3D ones (RAD16-I and collagen systems).

The next step consisted in analyzing the mechanisms that survival cancer cells and fibroblasts triggered in order to resist drug action. Interestingly, strategies depended on the surrounding milieu and, therefore, the extracellular cues received by cells.

Cancer cells grown in both two-dimensional (2D) and RAD16-I cultures downregulated the expression of target receptors after TKIs treatment. RAD16-I biomaterial provided a non-instructive milieu, suggesting that cells needed to express alternative receptors to re-establish similar signaling pathways. Conversely, cells grown in collagen cultures showed a different behavior and maintained RTKs expression pattern. Collagen biomaterial provided ECM bioactive sequences that were recognized by cell receptors (e.g. integrins), which probably induced signaling pathways that could complement the inhibited RTKs. Therefore, this scaffold could confer redundancy in transduction cascades, enabling phenotypic plasticity when a cancer hallmark capability was therapeutic inhibited.

Significantly, fibroblasts showed a different therapeutic response to TKIs. Cells grown in RAD16-I and collagen cultures did not change the RTKs expression pattern in contrast to 2D cultures. Thus, both 3D models showed an equivalent mechanism of drug resistance. Fibroblasts are responsible for the synthesis, deposition and remodeling of ECM components. The obtained data suggested that they were able to produce their own physiological matrix and decorate RAD16-I scaffolds. More research is needed to investigate whether co-cultures with fibroblasts and cancer cells could help to integrate the environmental signaling required for tumor progression in synthetic scaffolds, emerging as physiological relevant platforms for drug screening processes.

3D models could help to understand the mechanisms that confer multidrug resistance at both genomic and environmental level. In this case, redundancy in signaling pathways was reported through the comparison between natural collagen and synthetic RAD16-I scaffolds. Consequently, the microenvironment could emerge as an important therapeutic target that should be incorporated in drug screening processes.

5.5 REFERENCES

1. Hanahan, D. & Weinberg, R. A. Hallmarks of cancer: The next generation. *Cell* **144,** 646–674 (2011).

2. Szakács, G., Paterson, J. K., Ludwig, J. A., Booth-Genthe, C. & Gottesman, M. M. Targeting multidrug resistance in cancer. *Nat. Rev. Drug Discov.* **5,** 219–234 (2006).

3. Correia, A. L. & Bissell, M. J. The tumor microenvironment is a dominant force in multidrug resistance. *Drug Resist. Updat.* **15,** 39–49 (2012).

4. Yin, Q., Shen, J., Zhang, Z., Yu, H. & Li, Y. Reversal of multidrug resistance by stimuli-responsive drug delivery systems for therapy of tumor. *Adv. Drug Deliv. Rev.* **65,** 1699–1715 (2013).

5. Moitra, K., Lou, H. & Dean, M. Multidrug efflux pumps and cancer stem cells: Insights into multidrug resistance and therapeutic development. *Clin. Pharmacol. Ther.* **89,** 491–502 (2011).

6. Damiano, J. S., Cress, A. E., Hazlehurst, L. A., Shtil, A. A. & Dalton, W. S. Cell adhesion mediated drug resistance (CAM-DR): Role of integrins and resistance to apoptosis in human myeloma cell lines. *Blood* **93,** 1658– 1667 (1999).

7. Sethi, T. *et al.* Extracellular matrix proteins protect small cell lung cancer cells against apoptosis: A mechanism for small cell lung cancer growth and drug resistance in vivo. *Nat. Med.* **5,** 662–668 (1999).

8. Weaver, V. M. *et al.* Beta4 integrin-dependent formation of polarized three-dimensional architecture confers resistance to apoptosis in normal and malignant mammary epithelium. *Cancer Cell* **2,** 205–216 (2002).

9. Friedl, P. & Alexander, S. Cancer invasion and the microenvironment: plasticity and reciprocity. *Cell* **147,** 992–1009 (2011).

10. Bhowmick, N. A., Neilson, E. G. & Moses, H. L. Stromal fibroblasts in cancer initiation and progression. *Nat. Rev. Cancer* **432,** 332–337 (2004).

11. Wolf, K. *et al.* Multi-step pericellular proteolysis controls the transition from individual to collective cancer cell invasion. *Nat. Cell Biol.* **9,** 893–904 (2007).

12. Friedl Peter & Wolf Katarina. Tumour-cell invasion and migration: Diversity and escape mechanisms. *Nat. Rev. Cancer* **3,** 362–374 (2003).

13. Huang, C. *et al.* B1 integrin mediates an alternative survival pathway in breast cancer cells resistant to lapatinib. *Breast Cancer Res.* **13,** R84 (2011).

14. Norden, A. D., Drappatz, J. & Wen, P. Y. Antiangiogenic therapies for high-grade glioma. *Nat Rev Neurol* **5,** 610–620 (2009).

15. Singh, a & Settleman, J. EMT, cancer stem cells and drug resistance: an emerging axis of evil in the war on cancer. *Oncogene* **29,** 4741–4751 (2010).

16. Dean, M., Fojo, T. & Bates, S. Tumour stem cells and drug resistance. *Nat. Rev. Cancer* **5,** 275–284 (2005).

17. Thiery, J. P., Acloque, H., Huang, R. Y. J. & Nieto, M. A. Epithelial-mesenchymal transitions in development and disease. *Cell* **139,** 871–890 (2009).

18. Arora, A. & Scholar, E. M. Role of tyrosine kinase inhibitors in cancer therapy. *J. Pharmacol. Exp. Ther.* **315,** 971–979 (2005).

19. Hubbard, S. R. & Till, J. H. Protein tyrosine kinase structure and function. *Annu. Rev. Biochem.* **69,** 373–398 (2000).

20. Steeghs, N., Nortier, J. W. R. & Gelderblom, H. Small molecule tyrosine kinase inhibitors in the treatment of solid tumors: an update of recent developments. *Ann. Surg. Oncol.* **14,** 942–953 (2007).

21. Robinson, D. R., Wu, Y. M. & Lin, S. F. The protein tyrosine kinase family of the human genome. *Oncogene* **19,** 5548–5557 (2000).

22. Sierra, J. R., Cepero, V. & Giordano, S. Molecular mechanisms of acquired resistance to tyrosine kinase targeted therapy. *Mol. Cancer* **9,** 1–13 (2010).

23. Shibuya, M. Structure and function of VEGF/VEGF-receptor system involved in angiogenesis. *Cell Struct. Funct.* **26,** 25–35 (2001).

24. Wong, H. H. & Nicholas, R. L. Pancreatic cancer: Molecular pathogenesis and new therapeutic targets. *Nat. Rev. Gastroenterol. Hepatol.* **6,** 412–422 (2009).

25. Mueller, M. M. & Fusenig, N. E. Friends or foes - Bipolar effects of the tumour stroma in cancer. *Nat. Rev. Cancer* **4,** 839–849 (2004).

26. Bruns, C. J. *et al.* Effect of the vascular endothelial growth factor receptor-2 antibody DC101 plus gemcitabine on growth, metastasis and angiogenesis of human pancreatic cancer growing orthotopically in nude mice. *Int. J. Cancer.* **102,** 101–108 (2002).

27. Massoner, P., Ladurner-Rennau, M., Eder, I. E. & Klocker, H. Insulin-like growth factors and insulin control a multifunctional signalling network of significant importance in cancer. *Br. J. Cancer* **103,** 1479–1484 (2010).

28. Tomizawa, M. Insulin-like growth factor-I receptor in proliferation and motility of pancreatic cancer. *World J. Gastroenterol.* **16,** 1854–1858 (2010).

29. Appleman, V. A., Ahronian, L. G., Cai, J., Klimstra, D. S. & Lewis, B. C. KRAS(G12D)- and BRAF(V600E)-induced transformation of murine pancreatic epithelial cells requires MEK/ERK-stimulated IGF1R signaling. *Mol. cancer Res.* **10,** 1228–1239 (2012).

30. Pollak, M. N., Schernhammer, E. S. & Hankinson, S. E. Insulin-like growth factors and neoplasia. *Nat. Rev. Cancer* **4,** 505–518 (2004).

31. Kornmann, M., Lopez, M., Beger, H. & Korc, M. Expression of the IIIc variant of FGF receptor-1 confers mitogenic responsiveness to heparin and FGF-5 in TAKA-1 pancreatic ductal cells. *Int. J. Pancreatol.* **29,** 85–92 (2001).

32. De Moerlooze, L. *et al.* An important role for the IIIb isoform of fibroblast growth factor receptor 2 (FGFR2) in mesenchymal-epithelial signalling during mouse organogenesis. *Development* **127,** 483–492 (2000).

33. Berg, T. *et al.* Fibroblast growth factor 10 is critical for liver growth during embryogenesis and controls hepatoblast survival via beta-catenin activation. *Hepatology* **46,** 1187–1197 (2007).

34. Xu, J. Receptor Specificity of the Fibroblast Growth Factor Family. *J. Biol. Chem.* **271,** 15292–15297 (1996).

35. Ishiwata, T. *et al.* Enhanced expression of fibroblast growth factor receptor 2 IIIc promotes human pancreatic cancer cell proliferation. *Am. J. Pathol.* **180,** 1928–1941 (2012).

36. Shukla, S., Chen, Z.-S. & Ambudkar, S. V. Tyrosine kinase inhibitors as modulators of ABC transporter-mediated drug resistance. *Drug Resist. Updat.* **15,** 70–80 (2012).

37. Galve, I. *et al.* Synthesis of 2-arylamino substituted 5,6-dihydropyrido[2,3-d]pyrimidine-7(8H)-ones from arylguanidines. *Mol. Divers.* **16,** 639–649 (2012).

38. Mont, N., Teixidó, J., Kappe, C. O. & Borrell J I. A one-pot microwave-assisted synthesis of pyrido[2,3-d]pyrimidines. *Mol. Divers.* **7,** 153–159 (2003).

39. Weaver, V. M. *et al.* Reversion of the malignant phenotype of human breast cells in three-dimensional culture and in vivo by integrin blocking antibodies. *J. Cell Biol.* **137,** 231–245 (1997).

40. Bissell, M. J. & Radisky, D. Putting tumours in context. *Nat. Rev. Cancer* **1,** 46–54 (2001).

41. Folkman, J. Tumor angiogenesis. *Cancer Med.* 132–152 (2000).

42. Semino, C. E., Kamm, R. D. & Lauffenburger, D. A. Autocrine EGF receptor activation mediates endothelial cell migration and vascular morphogenesis induced by VEGF under interstitial flow. *Exp. Cell Res.* **312,** 289–298 (2006).

43. De Medina, S. G.-D. *et al.* Relationship between E-cadherin and fibroblast growth factor receptor 2b expression in bladder carcinomas. *Oncogene* **18,** 5722–5726 (1999).

44. Thiery, J. P. Epithelial-mesenchymal transitions in tumour progression. *Nat. Rev. Cancer* **2,** 442–454 (2002).

45. Ueda, S., Hatsuse, K., Tsuda, H., Ogata, S. & Kawarabayashi, N. Potential crosstalk between insulin-like growth factor receptor type 1 and epidermal growth factor receptor in progression and metastasis of pancreatic cancer. *Mod. Pathol.* **19,** 788–796 (2006).

46. Pennisi, P. A., Barr, V., Nunez, N. P., Stannard, B. & Le Roith, D. Reduced expression of insulin-like growth factor I receptors in MCF-7 breast cancer cells leads to a more metastatic phenotype. *Cancer Res.* **62,** 6529–6537 (2002).

47. Damon, S. E. *et al.* Transcriptional regulation of insulin-like growth factor-I receptor gene expression in prostate cancer cells. *Endocrinology* **142,** 21–27 (2001).

48. Christofori, G. New signals from the invasive front. *Nature* **441,** 444–450 (2006).

49. Hata, Y., Rook, S. L. & Aiello, L. P. Basic fibroblast growth factor induces expression of VEGF receptor KDR through a protein kinase C and p44/p42 mitogen-activated protein kinase-dependent pathway. *Diabetes* **48,** 1145–1155 (1999).

50. Berthaut, A. *et al.* Vascular endothelial growth factor receptor-1 (VEGFR-1) expression in human corneal fibroblast decreased with age. *Mol. Vis.* **15,** 1997–2007 (2009).

51. Xian, W., Schwertfeger, K. L. & Rosen, J. M. Distinct roles of fibroblast growth factor receptor 1 and 2 in regulating cell survival and epithelial-mesenchymal transition. *Mol. Endocrinol.* **21,** 987–1000 (2007).

52. Gospodarowicz, D. Localisation of a fibroblast growth factor and its effect alone and with hydrocortisone on 3T3 cell growth. *Nature* **249,** 123–127 (1974).

53. Olsen, C. J., Moreira, J., Lukanidin, E. M. & Ambartsumian, N. S. Human mammary fibroblasts stimulate invasion of breast cancer cells in a three-dimensional culture and increase stroma development in mouse xenografts. *BMC Cancer* **10,** 444 (2010).

54. Eckardt, K., May, C., Koenen, M. & Eckel, J. IGF-1 receptor signalling determines the mitogenic potency of insulin analogues in human smooth muscle cells and fibroblasts. *Diabetologia* **50,** 2534–243 (2007).

55. Sell, C. *et al.* IGF-1 receptor levels and the proliferation of young and senescent human fibroblasts. *Biochem. Biophys. Res. Commun.* **194,** 259–265 (1993).

56. Kovács, M., Tóth, J., Hetényi, C., Málnási-Csizmadia, A. & Sellers, J. R. Mechanism of blebbistatin inhibition of myosin II. *J. Biol. Chem.* **279,** 35557–63 (2004).

57. Vicente-Manzanares, M., Ma, X., Adelstein, R. S. & Horwitz, A. R. Non-muscle myosin II takes centre stage in cell adhesion and migration. *Nat Rev Moll Cell Biol.* **10,** 778–790 (2009).

CONCLUSIONS

Three-dimensional models for pancreatic cancer were developed in order to study the contribution of microenvironment on early stages of epithelial-mesenchymal transition (EMT) during tumor progression:

- ✓ Pancreatic cancer cells showed different phenotypes depending on the composition and stiffness of tissue engineering scaffolds. Therefore, results revealed their plasticity to adapt to different surrounding milieus. The increase in matrix storage modulus could disrupt epithelial morphogenesis through changes in cytoskeletal dynamics. The presence of extracellular matrix (ECM) signaling sequences caused the cellular scattering and the acquisition of protrusions. All these events promoted a more mesenchymal-like phenotype of cancer cells.

- ✓ Downregulation of E-cadherin was reported in all 3D cancer models. Therefore, the transition from a 2D to a 3D milieu could induce the disruption of epithelial cell-cell adhesions and the activation of some early stages of the EMT program as observed in RAD16-I scaffolds. However, this process was more pronounced in collagen scaffolds, revealing the critical role of ECM signaling sequences in terms of both presence and concentration.

- ✓ The mechanisms that account for dynamic regulation of E-cadherin expression were also analyzed. No significant hypermethylation of E-cadherin gene promoter was detected in any 3D model of pancreatic cancer. On the other hand, the upregulation of SNAI1 and ZEB2 transcriptional repressors was observed.

Three-dimensional models for cervical cancer and stromal fibroblasts were developed in order to study the contribution of microenvironment on photodynamic therapy (PDT) outcome:

- ✓ 3D cultures were able to recreate the *in vivo* limitation of drug and oxygen diffusion, creating a protective microenvironment for cells located in the core of the scaffold. Experiments demonstrated that mass transfer effects accounted for the lower PDT therapeutic efficacy in 3D cultures relative to 2D. For the first time, the production and decay of singlet oxygen (reactive oxygen specie and main PDT cytotoxic agent) was observed in a 3D culture.

- ✓ The cytotoxic outcome of PDT did not strongly depend on the presence of ECM binding sequences. These results were explained because the therapy is based on an acute and general stress effect to cells and does not target specific signaling cascades.

- ✓ Co-culture models revealed that fibroblasts could induce the scattering of cancer cells, promoting their presence along fibroblasts network and compromising epithelial morphology. In collagen scaffolds, fibroblasts in co-cultures were more resistant to PDT treatment than individual ones. These finding suggested a crosstalk between tumor microenvironment and cancer cells, increasing the aggressiveness of stromal cells.

The contribution of tumor microenvironment on drug resistance was studied through 3D models of pancreatic cancer and stromal fibroblasts.

- ✓ The effect of tyrosine kinases inhibitors (TKIs) as cancer drugs was evaluated in 2D and 3D cultures. The most effective TKI caused a cell death of approximately 60% of cancer cells population in 2D cultures, but remained inactive in 3D cultures.

- ✓ After drug treatment, survival cancer cells grown in 2D and RAD16-I cultures downregulated the expression of the blocked receptor tyrosine kinases, suggesting that the transcription machinery did engage in the synthesis of receptors that could trigger complementary signaling pathways. On the other hand, cancer cells grown in collagen cultures did not change receptor expression pattern. Collagen has a wide range of cell-matrix binding receptors, which could create redundancy in signaling pathways.

- ✓ Fibroblasts showed the same behavior in RAD16-I and collagen scaffolds after drug treatment, maintaining their receptor expression levels. Results suggested that fibroblasts were able to produce their own physiological matrix and decorate RAD16-I biomaterial.

CONCLUSIONES

Se han desarrollado modelos tridimensionales de cáncer de páncreas para estudiar la contribución del microambiente durante las primeras etapas de la transición epitelial-mesenquimal (EMT) en la progresión tumoral:

- ✓ Las células pancreáticas tumorales mostraban diferentes fenotipos dependiendo de la composición y rigidez de las matrices donde se cultivaban. Por lo tanto, los resultados revelaban su plasticidad para adaptarse a diferentes entornos. En concreto, un aumento del módulo de almacenamiento de la matriz provocó la perturbación de la morfogénesis epitelial a través de cambios en la configuración del citoesqueleto. La presencia de secuencias de señalización de la matriz extracelular (ECM) causó la dispersión de las células de las colonias tumorales y la adquisición de protrusiones. Este conjunto de eventos promovieron un fenotipo más mesenquimal de las células cancerígenas.

- ✓ Todos los modelos 3D de cáncer de páncreas mostraron una disminución en la expresión de la E-cadherina. Por lo tanto, la transición de un microambiente 2D a uno 3D pudo inducir la disociación de las adhesiones epiteliales célula-célula y la activación de las primeras etapas del programa EMT tal y como se observó en las matrices sintéticas de RAD16-I. Este proceso fue más pronunciado en las matrices naturales de colágeno, revelando el papel crítico de las secuencias de señalización de la ECM en términos de presencia y concentración.

- ✓ Los mecanismos que regulan la expresión dinámica de la E-cadherina también se analizaron. No se detectó la hipermetilación del promotor de la E-cadherina en ninguno de los modelos 3D de cáncer de páncreas. En cambio, se observó la sobre-expresión de represores transcripcionales como los genes SNAI1 y ZEB2.

Se han desarrollado modelos tridimensionales de cáncer de cérvix y fibroblastos del estroma para estudiar la contribución del microambiente en la respuesta celular de la terapia fotodinámica (PDT):

- ✓ Los cultivos 3D pudieron recrear la limitación de difusión de fármaco y oxígeno que experimentan las células *in vivo*, creando un ambiente protector para las células localizadas en el centro de la matriz. Los experimentos demostraron que los efectos de transferencia de masa eran la principal causa de la menor eficacia terapéutica de la PDT en los cultivos 3D respeto los 2D. Por primera vez, se detectó la formación y el decaimiento del oxígeno singlete (especie reactiva del oxígeno y principal agente citotóxico de PDT) en un cultivo 3D.

- ✓ La respuesta citotóxica de la PDT no mostraba una dependencia fuerte a la presencia de secuencias de señalización de la ECM. Estos resultados se podían explicar por el hecho que la terapia se basa en un efecto de estrés agudo y general a las células y no está dirigida a cascadas de señalización específicas.

- ✓ Los modelos de co-cultivos revelaron que los fibroblastos podían inducir una mayor dispersión de las células cancerígenas, promoviendo su presencia a lo largo de la red celular que forman los mismos fibroblastos y comprometiendo la morfología epitelial. En la matriz de colágeno, los fibroblastos de co-cultivos eran más resistentes al tratamiento de la PDT que la población individual. Estos datos sugirieron que había una comunicación bidireccional entre el microambiente tumoral y las células cancerígenas, aumentando la agresividad de las células del estroma.

La contribución del microambiente en el fenómeno de la resistencia de fármacos se estudió a través de los modelos tridimensionales de cáncer de páncreas y fibroblastos del estroma:

- ✓ El efecto de inhibidores de tirosina quinasas (TKIs) como fármacos anticancerígenos se evaluó en cultivos 2D y 3D. El TKI más potente causó una muerte celular de aproximadamente el 60% de las células cancerígenas de los cultivos 2D, mientras que se mantuvieron inactivos en los cultivos 3D.

- ✓ Después del tratamiento con fármaco, las células cancerígenas supervivientes cultivadas en 2D y en matrices de RAD16-I disminuyeron la expresión de los receptores bloqueados, sugiriendo que la maquinaria de transcripción se dedicó a la síntesis de receptores alternativos que desencadenaban rutas de señalización similares. Por otro lado, las células cancerígenas cultivadas en matrices de colágeno no cambiaron su patrón de expresión de los receptores bloqueados. Los datos sugerían que el colágeno podía proporcionar una red de receptores redundantes a nivel de cascadas de señalización debido a la presencia de múltiples motivos de unión célula-matriz.

- ✓ Después del tratamiento de fármaco, los fibroblastos mostraron el mismo comportamiento en las matrices de RAD16-I y colágeno, manteniendo su patrón de expresión de receptores diana. Los resultados sugirieron que los fibroblastos podían producir su propia matriz fisiológica y decorar el RAD16-I.

CONCLUSIONS

S'han desenvolupat models tridimensionals de càncer de pàncrees per estudiar la contribució del microambient durant les primeres etapes de la transició epitelial-mesenquimal (EMT) en la progressió tumoral:

- ✓ Les cèl·lules pancreàtiques tumorals van mostrar diferents fenotips depenent de la composició i rigidesa de la matriu on es cultiven. Per tant, els resultats van revelar la seva plasticitat per adaptar-se a diferents entorns. En concret, un augment en el mòdul d'emmagatzematge de la matriu va provocar la pertorbació de la morfogènesis epitelial a través de canvis de la configuració del citoesquelet. La presencia de seqüències de senyalització de la matriu extracel·lular (ECM) va causar la dispersió de les cèl·lules de les colònies tumorals i l'adquisició de protrusions. Aquest conjunt d'esdeveniments va promoure un fenotip més mesenquimal a les cèl·lules cancerígenes.

- ✓ Tots els models 3D de càncer de pàncrees van mostrar una disminució en l'expressió de l'E-cadherina. Per tant, la transició d'un microambient 2D a un 3D va poder induir la dissociació de les adhesions epitelials cèl·lula-cèl·lula i l'activació de les primeres etapes del programa EMT tal i com es va observar en les matrius sintètiques de RAD16-I. Aquest procés va ser més pronunciat en les matrius de col·lagen, revelant el paper crític de les seqüències de senyalització de la ECM en termes de presència i concentració.

- ✓ Els mecanismes que regulen l'expressió dinàmica de l'E-cadherina també es van analitzar. No es va detectar l'hipermetilació del promotor de l'E-cadherina en cap dels models 3D de càncer de pàncrees desenvolupat. En canvi, es va observar la sobre-expressió de repressors transcripcionals com els gens *SNAI1* i *ZEB2*.

S'han desenvolupat models tridimensionals de càncer de cèrvix i fibroblasts de l'estroma per estudiar la contribució del microambient en el resultat de la teràpia fotodinàmica (PDT):

- ✓ Els cultius 3D van ser capaços de recrear la limitació de difusió de fàrmac i oxigen que experimenten les cèl·lules *in vivo*, creant un ambient protector per les cèl·lules que estan localitzades a la part interior central de la matriu. Els experiments van demostrar que els efectes de transferència de massa eren la principal causa de la menor eficàcia terapèutica de la PDT en els cultius 3D respecte els 2D. Per primera vegada, es va detectar la formació i el decaïment d'oxigen singlet (espècie reactiva de l'oxigen i principal agent citotòxic de la PDT) en un cultiu 3D.

- ✓ La resposta citotòxica de la PDT no mostrava una dependència forta a la presència de les seqüències de senyalització de la ECM. Aquests resultats es podien explicar pel fet que la teràpia es basa en un efecte d'estrès agut i general a les cèl·lules, sense estar dirigida a cascades de senyalització específiques.

- ✓ Els models de co-cultius van revelar que els fibroblasts podien induir una major dispersió de les cèl·lules cancerígenes, promovent la seva presència al llarg de la xarxa cel·lular que creen els mateixos fibroblasts i comprometent la morfologia epitelial. En la matriu de col·lagen, els fibroblasts de co-cultius eren més residents a la PDT que la població individual. Aquestes dades suggerien que hi havia una comunicació bidireccional entre el microambient tumoral i les cèl·lules cancerígenes, augmentant l'agressivitat de les cèl·lules de l'estroma.

La contribució del microambient en el fenomen de resistència de fàrmacs es va estudiar a través dels models tridimensionals de càncer de pàncrees i de fibroblasts de l'estroma:

- ✓ L'efecte d'inhibidors de tirosina quinases (TKIs) com fàrmacs anti-cancerígens es va avaluar en cultius 2D i 3D. El TKI més potent va causar una mort cel·lular d'aproximadament 60% de la població cel·lular dels cultius 2D, però es va mantenir inactiu en els cultius 3D.

- ✓ Després del tractament de fàrmac, les cèl·lules cancerígenes supervivents cultivades en 2D i en les matrius de RAD16-I van disminuir l'expressió dels receptors de tirosina quinases bloquejats, suggerint que la maquinaria de transcripció va dedicar-se a la síntesis de receptors alternatius que poguessin desencadenar rutes de senyalització similars. Per una altra banda, les cèl·lules cancerígenes cultivades en les matrius de col·lagen no van canviar el seu patró d'expressió dels receptors bloquejats. Aquestes dades podrien indicar que el col·lagen proporcionava una xarxa de receptors redundants a nivell de cascades de senyalització, degut a la presència de múltiples motius d'unió cèl·lula-matriu.

- ✓ Després del tractament amb el fàrmac, els fibroblasts van mostrar el mateix comportament en les matrius de RAD16-I i col·lagen, mantenint el seu patró d'expressió de receptors diana. Els resultats van suggerir que els fibroblasts podien produir la seva pròpia matriu fisiològica i decorar el RAD16-I.

PUBLICATIONS

RESEARCH PAPERS FROM THIS THESIS:

Alemany-Ribes, M.*, García-Díaz, M.*, Busom, M., Nonell, S., Semino, C.E., *Toward a 3D cellular model for studying in vitro the outcome of photodynamic treatments: Accounting for the effects of tissue complexity. Tissue Engineering Part A,* **19**, 1665-1674 (2013). *Equal contribution.

Alemany-Ribes, M.*, Castells-Sala, C.*, Caballero-Camino, J., Aloy-Reverté, C., Semino, C.E., *Contribution of the microenvironment on E-cadherin regulation in pancreatic cancer* (In preparation) *Equal contribution.

Alemany-Ribes, M., Márquez-Gil, A., López-Chicón, P., Borrell, J.I., Semino, C.E., *Mechanisms of cellular resistance to tyrosine kinases inhibitors (In preparation).*

Acedo, P.*, **Alemany-Ribes, M.*,** Boix-Garriga, E., Nonell, S., Stockert, J.C., Cañete, M., Villanueva, A., Semino, C.E., *Assessing the therapeutic efficiency of photodynamic therapy with two combined photosensitizers on an in vitro 3D tumor model (In preparation).*

REVIEWS FROM THIS THESIS:

Alemany-Ribes, M., García-Díaz, M., Acedo, P., Agut, M., Nonell, S., Sagristá, M.L., Mora, M., Cañete, M., Villanueva, A., Stockert, J.C., Semino, C.E., *Why not introducing the third dimension in photodynamic therapy? Analytical & Bioanalytical Techniques,* S1: 004 (2013) doi:10.4172/2155-9872.S1-004.

Castells-Sala, C.*, **Alemany-Ribes, M.*,** Fernández-Muiños, T., Recha-Sancho, L., López- Chicón, P., Aloy-Reverté, C., Caballero-Camino, J., Márquez-Gil, A., Semino, C.E., *Current applications of tissue engineering in biomedicine. Biochips and Tissue Chips*, S2: 004 (2013) doi: 10.4172/2153-0777.S2-004. *Equal contribution.

Alemany-Ribes, M., Semino, C.E., *Bioengineering 3D environments for cancer models. Advanced Drug Delivery Reviews* (Accepted July 1th 2014).

OTHER RESEARCH PAPERS

Rezusta, A., Lopez-Chicón, P., Paz-Cristobal, M.P., **Alemany-Ribes, M.,** Royo-Díez, D., Agut, M., Semino, C.E., Nonell, S., Revillo, M.J., Aspiroz, C., Gilaberte, Y., *In vitro fungicidal photodynamic effect of hypericin on Candida Species. Photochemistry and Photobiology*, **88**, 613-619 (2012).